Design, Modelling, and Seismic Performance of Outrigger Braced Frame Steel Buildings Subjected to Crustal and Subduction Earthquakes

Aid Jnaid

A Thesis

in

The Department

of

Building, Civil and Environmental Engineering

Presented in Partial Fulfilment of the Requirements

For the Degree of

Doctor of Philosophy (Civil Engineering) at

Concordia University

Montreal, Quebec, Canada

December 2017

CONCORDIA UNIVERSITY

School of Graduate Studies

This is to certify that the thesis prepared

By: Aid Jnaid

Entitled: Design, Modelling, and Seismic Performance of Outrigger Braced Frame Steel Buildings Subjected to Crustal and Subduction Earthquakes

and submitted in partial fulfillment of the requirements for the degree of

Doctor of Philosophy (Civil Engineering)

Complies with the regulations of the University and meets the accepted standard with respect to originality and quality.

Signed by the final Examining Committee:

_____ Chair

Dr.Subhash Rakheja

_____ External Examiner

Dr.Solomon Tesfamariam

_____ External to Program

Dr. Sivakumar Narayanswamy

_____ Examiner

Dr. Michelle Nokken

_____ Examiner

Dr. Anjan Bhowmick

_____ Thesis supervisors

Dr. A. Bagchi

_____

Dr. L. Tirca

Approved by _____

Dr. Fariborz Haghighat Graduate Program Director

26 -01- 2018

Date of Defence

_____

Dr. Amir Asif, Dean, Faculty of Engineering and Computer Science

ABSTRACT

Design, Modelling, and Seismic Performance of Outrigger Braced Frame Steel Buildings Subjected to Crustal and Subduction Earthquakes

Aid Jnaid, Ph.D.

Concordia University, 2018

Concentrically braced frames (CBFs) are widely used in North America. The CBFs possess high stiffness and moderate ductility, while braces are designed to buckle in compression and yield in tension. However, after a brace experiences buckling, its compression strength diminishes and the system undergoes asymmetrical response, while the distribution of internal forces and deformations is influenced by the frequency content of ground motions. Despite the system's stiffness, CBFs are prone to concentrate damage within a floor which leads to the formation of storey mechanism. To preserve the stability of the system during the nonlinear seismic response, the National Building Code of Canada (NBCC) imposes limits on a building's height which depends on the selected ductility-related force modification factor, R_d. Thus, the height limit for buildings with moderately ductile concentrically braced frames, MD-CBFs, is 40 m and for limited ductility concentrically braced frames, LD-CBFs, is 60 m.

To safely increase the height limit of ductile braced frame buildings, a system labelled Outrigger Braced Frame, OBF, is proposed and developed in this study. According to the Council on Tall Buildings and Urban Habitat (CTBUH), a building with more than 14 stories or more than 50 meters in height may be considered a high-rise building. The aim of this research is to develop, design, model, and study the seismic performance of mid-rise (e.g. tweleve-storey) and high-rise (e.g., sixteen-storey) OBF buildings subjected to dynamic loads. It is noted that the outrigger system functions by tying together a core system and a perimeter system. Herein, the core system is made of MD-CBFs and the perimeter system is made of gravity columns. Furthermore, only the core braces are designed to dissipate energy, while the outrigger's diagonals are designed to respond in the elastic range. The performance of OBF system is controlled by the amount of added stiffness and optimum location of outriggers across the building's height, the number of levels with outriggers and the intensity of seismic zone. All multi-storey buildings are located in high-risk seismic zone of Victoria, B.C. Canada, on Site Class C. The selection of ground motions was made to capture the seismic characteristics at

buildings location. Herein, two sets of crustal and subduction ground motions were considered such as California records and the mega-thrust magnitude 9 Tohoku records, respectively. The nonlinear time-history dynamic analyses were conducted using the OpenSees software.

The main objectives of this thesis are three-fold: i) to identify the effect of subduction versus crustal ground motions on the seismic response of low-rise, mid-rise and high-rise MD-CBF buildings and to study their seismic performance from yielding to failure, ii) to provide design method and optimum location for outriggers of OBF steel buildings, iii) to assess the collapse safety of the proposed mid-rise and high-rise OBF steel buildings using FEMA P695 procedure and to compare their seismic performance against that resulted for MD-CBF buildings.

It is concluded that the OBF buildings are slightly stiffer than the corresponding MD-CBF buildings, and they experienced lower interstorey drift and residual interstorey drift than the MD-CBF buildings. In all case studies considered here, the collapse margin ratio (CMR) is greater for buildings subjected to crustal ground motions than subduction ground motions. Evaluation of seismic performance of sample 12-storey and 16-storey OBF buildings shows that these buildings are able to pass the collapse safety acceptance criteria, $ACMR \geq ACMR_{10\%}$, when subjected to both sets of ground motions. On the other hand, the corresponding MD-CBF buildings are not able to pass the collapse safety acceptance criteria when subjected to subduction records set. Hence, special attention should be given when designing buildings in seismic regions which are prone to both types of earthquakes.

ACKNOWLEDMENTS

Completion of this research thesis at Concordia University could not be accomplished without the support received from my supervisors and my family.

First, I want to express my sincere and deepest gratitude to my supervisors Professor Ashutosh Bagchi and Professor Lucia Tirca for their continued encouragement and their expert guidance. Their help and support for this research project will never be forgotten, their continuous help and support let this thesis to come to the end.

Second, my deepest thanks is to my wife and my kids for their help and support by giving me the time I need even in the weekends to continue my work in my thesis research, the time that should be for them and their enjoyments and activities, so this research and the works behind it cannot be done without the support of them. At the same time I thank my parents overseas for their moral support all the time.

I would also thank my colleagues Liang Chen, Masaaki Ohira and Ovidiu Serbam for sharing our experience gained using the software OpenSees.

Table of Contents

List of Figures

List of Tables

Chapter 1. Introduction

1.1. Background

Concentrically braced frames (CBF) are widely used in seismic areas due to their high stiffness and moderate ductility. The CBF system can be designed with tension – compression or tension only braces. The tension-compression braces are proportioned to buckle in compression and yield in tension in order to dissipate the input energy. The hysteretic response of a typical tension-compression brace is asymmetrical, because the buckling strength is much lower than the tensile strength. Then, after a brace buckles, its compressive capacity diminishes to the post-buckling strength. The main drawback of the CBF system is its tendency to concentrate damage within a floor which leads to weak-storey mechanism followed by system failure. As depicted in Fig. 1-1, the storey mechanism may be triggered at ground floor or an upper floor. When the former occur, the CBF system may be driven to complete failure. In the other case it leads to partial failure.

The National Building Code of Canada (NBCC, 2010) specified limits for building heights (expressed in meters) in function of system ductility and the level of seismic zone. Thus, in medium-to-high seismic zones, moderately ductile CBFs with tension-compression braces (R_d = 3 and R_0 = 1.3) and ductile buckling-restrained braced frames (R_d = 4.0, R_0 = 1.2) are limited to 40 m height, while the limited ductility CBFs with tension-compression braces (R_d = 2.0 and R_0 = 1.3) are limited to 60 m height. It is noted that conventional construction braced frames are limited to 40 m height where $I_E F_a S_a(0.2) > 0.75$, but those for assembly occupancy type to 15 m height. Herein, I_E is the earthquake importance factor of the structure, F_a is the acceleration-based site coefficient and $S_a(0.2)$ is the spectral response acceleration value of uniform hazard spectrum at period T = 0.2 s. To account for building irregularities, more critical design requirements were adopted. For example, verifications for stiffness irregularity (Type 1), weak-story irregularity (Type 6) and torsional sensitivity (Type 7) are among them. For instance, dynamic analysis is required even for low-rise buildings showing irregularity Type 7, or for buildings with other irregularity types that have the fundamental period > 0.5 s. In spite of reinforced code provisions, the likelihood of weak-storey response in CBFs and even EBFs (eccentrically braced frame) systems may still occur due to the lack of lateral force redistribution.

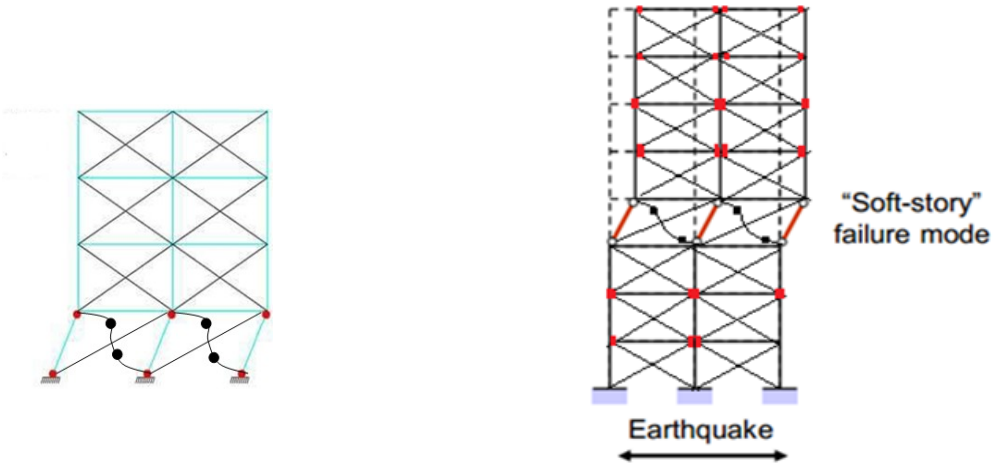

Figure 1-1 Weak-story mechanism

Hence, for buildings taller than 60 m or even 40 m height another type of earthquake resistant braced frame system is required. Since 1970, researchers found that adding horizontal outrigger trusses that tie the earthquake resistant core system to exterior columns, the efficiency of the building system improves by about 30% (Schueller, 1977). Important number of studies conducted have considered the reinforced concrete shear walls as being the core system, while the outrigger trusses were fixed to the core and pinned to perimeter columns. Different types of core systems and outrigger floors are depicted in Fig. 1-2. In general, this system was proposed with the aim to reduce the lateral inter-storey drift, as well as, to reduce the overturning moment developed in the shear walls and in consequence the size of shear walls foundation. It was concluded that the benefit of employing outriggers was to reduce the building construction cost. In addition, if belt truss systems are employed, the lateral drift of the building is reduced by 30% to 40% in comparison with the free cantilever system.

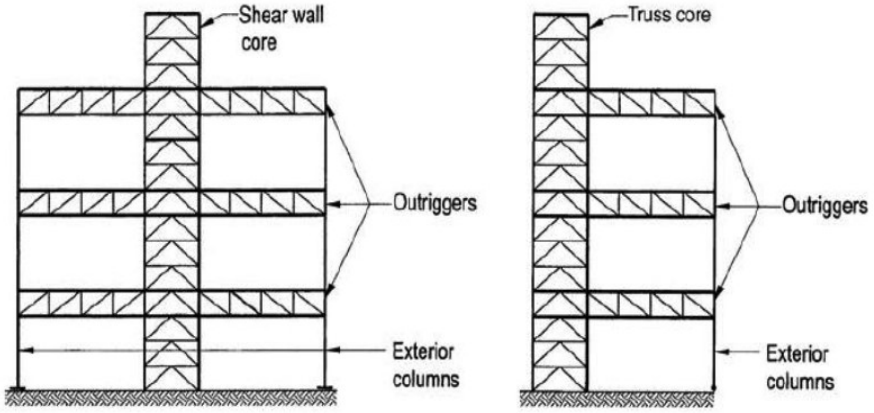

Figure 1-2 Different types of outrigger system (Krem, 2012)

Theoretical and experimental studies were conducted on lateral load resisting systems to reduce the effect of earthquakes and respectively the damage and number of causalities that lead to economic losses. The knowledge and experience grow after each earthquake event lead to the improvement of design regulations. According to the Insurance Information Institute Munich Re the cost of losses resulted from the most 10 damaging earthquakes ranked Tohoku earthquake in the first place and Northridge earthquake in the 3rd place as shown in the table below.

Table 1-1 Northridge and Tohoku earthquake loss (Insurance Information Institute, 2017)

Rank	Date	Location	Losses in US$ m		Fatalities
			Overall	Insured	
1	Mar. 11, 2011	Japan: Aomori, Chiba, Fukushima, lbaraki, lwate, Miyagi, Tochigi, Tokyo, Yamagata. Includes tsunami	210,000	40,000	15580
3	Jan. 17, 1994	USA (CA): Northridge, Los Angeles, San FernandoValley,Ventura, Orange	44,000	15,300	61

2017 Munich Re, Geo Risks Research, NatCatSERVICE; Wikipedia
https://www.iii.org/

1.2. Problem statement and recent development

Nowadays, cities expend vertically to accommodate growing population. The Council on Tall Buildings and Urban Habitat (CTBUH-2010) defines tall buildings as those higher than 50 m or taller than 14 or more stories. Due to faster construction time, CBFs are good candidates for the

core system of taller buildings. However, the system used in the past to resist mostly wind loads was not studied for high-rize applications designed in high-risk seismic areas.

Although outriggers are used in several high-rise buildings since 1970, there are not sufficient studies leading to a design method for earthquake resistant braced frames with outrigger trusses. Since that time, significant advances have been made in nonlinear analytical capability and in the definition of ground motions to be used in performance based design. This need was underlined in the Guideline for Seismic Based Design of Tall Buildings developed by PEER as part of Tall Building Initiative (PEER, 2010). As illustrated in Fig. 1-3, the main motivation of this study is to develop a design method proposing the computation of outrigger system capacity.

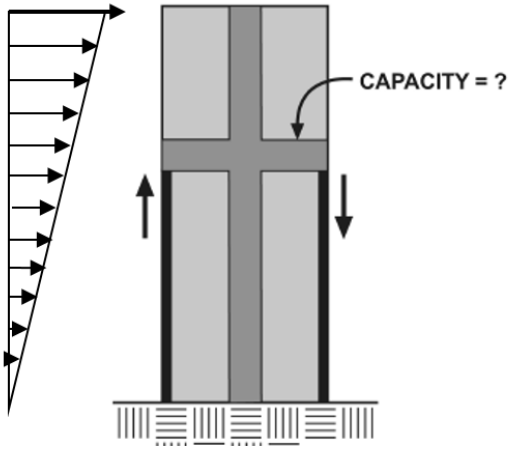

Figure 1-3 Searching for outrigger capacity assessment (adapted from PEER, 2010)

Recently, Dardis (AISC, 2017) highlighted the importance of outriggers added to a structure's core system in order to reduce the lateral drift and increase the shear capacity. He also advanced the term "virtual belt trusses" that can be added to connect the perimeter columns of the building as illustrated in Fig. 1-4.

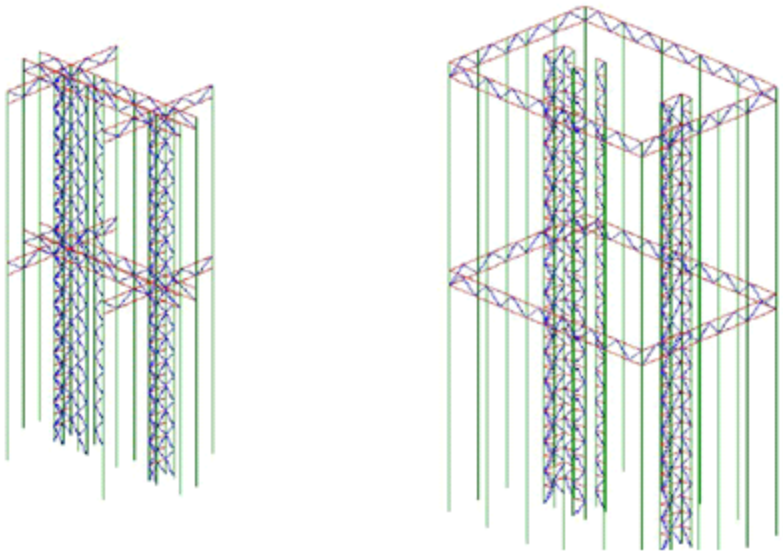

a) b)

Figure 1-4 Steel truss outrigger system: a) a conventional outrigger system, b) a virtual outrigger system incorporating a hat truss and a belt truss (Dardis, 2017).

1.3. Objectives

The main objectives of this thesis are:

(i) To identify the effect of long duration ground motions that characterizes subduction earthquakes versus crustal ground motions on the seismic response of low-rise, middle-rise and high-rise moderately ductile concentrically braced frames (MD-CBF) buildings;

(ii) To develop a design method for a floor outrigger system, its optimum geometry, stiffness, and location as part of the proposed Outrigger Braced Frame System (OBF) for tall buildings;

(iii) To study the effect of long duration ground motions on the seismic response of tall OBF steel buildings and to validate their response against the pair MD-CBF building response; and

(iv) To assess the seismic performance of low-rise, middle-rise, and high-rise MD-CBF buildings and OBF buildings using the FEMA P695 proceedure.

Here the following building configurations have been consided for the present study: (i) a 2-storey and 4-storey buildings representing low-rise buildings; (i) an 8-storey building

representing middle-rise buildings; and (iii) a 12-storey and a 16-storey buildings represing high-rise buildings. All buildings have the same floor plan and are located in Victoria, B.C., Canada. For Victoria, B.C., the important contributions to seismic hazard are moderate-to-large crustal earthquakes of magnitudes M 7.0 – M 7.5, as well as, the megathrust subduction earthquake of magnitudes M 8.0 – M 9.0 that may occur along the Cascadia subduction fault. According to NBCC 2010, the uniform hazard spectrum, UHS, for Victoria is defined based on the probabilistic crustal hazard for 2% probability of exceedance in 50 years. The Cascadia subduction source contribution was not considered in the UHS given in the 2010 edition of NBCC. As proxy subduction ground motions compatible to study the seismic response of buildings in Victoria, the ground motion records from the megathrust M9 Tohoku earthquake in Japan (March 2011) have been selected for the present study.

1.4. The thesis layout

The present thesis includes six chapters that linked to each other. The first chapter preents the introduction where the problem is stated and objectives are formulated. The second chapter covers the literature review. The third chapter presents the design and nonlinear dynamic analysis of low-rise, middle-rise and high-rise MD-CBF buildings using the OpenSees software. These buildings were designed and subjected to two sets of seven scaled crustal and seven scaled subduction records. The effect of accidental torsion and P-Δ was considered in design. All buildings were verified to respond in the elastic range to wind loads. A detailed numerical model that is able to simulate the MD-CBF response from yield to failure was developed in OpenSees. The fourth chapter contains the design method for the Outrigger Braced Frame (OBF) system with conventional outrigger and ductile core system. The nonlinear seismic response of the 12-storey and 16-storey OBF buildings subjected to both sets of crustal and subduction records were investigated. A detailed numerical model developed in OpenSees was used. The fifth chapter presents the computations required to verify if the studied buildings subjected to crustal records and to subduction records are able to pass the collapse safety acceptance criteria defined in FEMA P695 (2009) provisions. Fragility curves associated to immediate occupancy limit state, design limit state and collapse prevention limit state are provided. The sixth chapter presents conclusions and future work. Due to large amount of analysis and computations some work is given in Appendices.

Chapter 2. Literature review

The outrigger and belt truss systems, as well as advances in numerical modeling developed for steel braced frames in the OpenSees environment (Open System for Earthquake Engineering Simulation) are described in this chapter, as well as the methodology presented in FEMA P695 for the computation of collapse safety acceptance criteria is also presented. An example of using outriggers and belt truss system in high-rise buildings is illustrated in Fig. 2-1.

Figure 2-1 Shanghai Tower (Modern Steel Construction, 2013)

2.1. Outrigger and belt truss system

2.1.1. Background

According to NBCC 2010, the CBF system cannot be considered for buildings taller than 60 m height. However, by adding horizontal outriggers and/ or belt trusses the performance of buildings improve by about 30% (Schueller, 1977). It is worth noting that the exisiting codes do not have any provisions for outriggers as an earthquake resistant system (Choi and Joseph, 2012). The outrigger trusses tie the central core to perimeter columns and the belt trusses tied all the perimeter columns. Thus, the middle core is free to deflect laterally between two floors where outriggers are installed. This is schematically illustrated in Fig. 2-2.

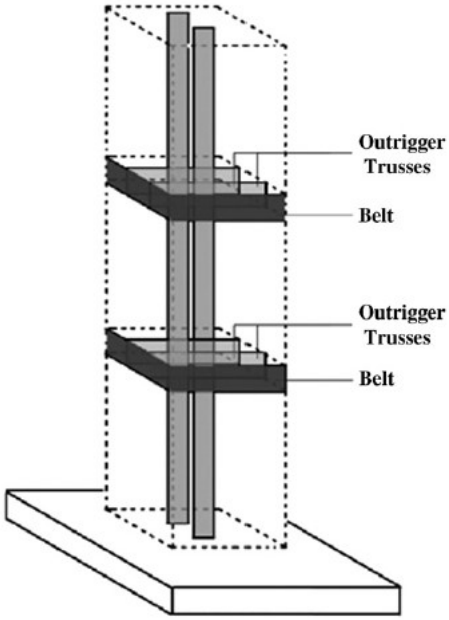

Figure 2-2 Multi-level floors of belt truss and outriggers (Fawazia and Fatima, 2010)

An example of a building with outriggers and belt trusses is the 53-storey Chifley tower in Sydney, Australia, constructed in 1992. The building system has a steel braced frame core and two levels of outrigger systems. It is noted that in a study about the evaluation of earthquake resistant systems for tall buildings, Gunel and Elgin (2006) stated that outriggers and belt trusses is an evolution of braced frame system. Furthermore, Taranath (1998) stated that adding outriggers it reduces the foundation cost of the core system.

In 1998, Nair stated that storey shear forces can be transferred from the core system through the rigid floor diaphragms to a system composed of trusses that are not directly connected to the core. This truss system was labelled “virtual” outrigger system. In general, the belt truss system is used as the virtual outrigger system.

On the basis of connectivity of the middle core system to perimeter columns, the outrigger truss system may be classified as: i) conventional outrigger and ii) virtual outrigger. An example of a structural system made of a core and conventional outriggers is illustrated in Fig. 2-3a and a structural system composed of a core system and virtual outriggers is shown in Fig. 2-3b. As depicted, the outrigger system is developed along the height of a floor or several floors. It is noted that the exterior columns strength and stiffness should provide resistance to overturning

moment caused by lateral forces. This is mostly the case when the core consists of a reinforced concrete shear wall. The transfer of forces from the core to perimeter columns using conventional outriggers is illustrated in Fig. 2-4 and using virtual outriggers in Fig. 2-5.

Nair (1998) pointed out some drawbacks regarding conventional outrigger trusses in high-rise buildings:

- Space occupied by outrigger trusses implies functional limits at floors where they are located.
- Outrigger trusses installed in one or several floors may affect the building's architecture.
- Connections between outrigger trusses and core need special design mechanism which is different if the core is made of reinforced concrete shear walls or braced frames.
- Under gravity loads, the shortening of the core and exterior columns are not equal. When the truss is pinned connected to exterior column the above phenomenon does not affect. Typically, the gravity columns supporting outriggers are at the outer edge of the building.

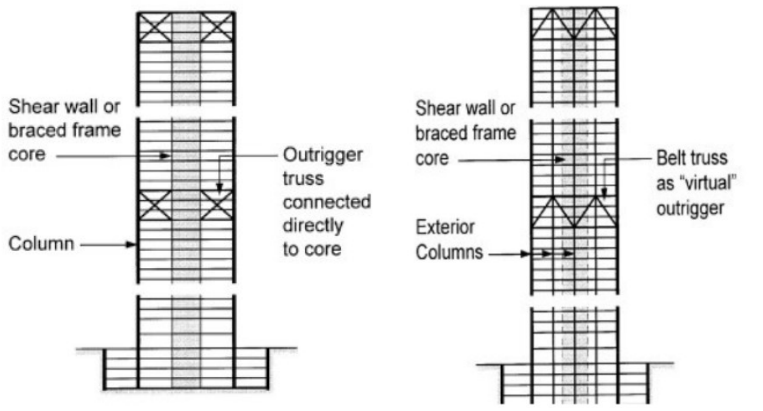

(a) (b)

Figure 2-3 Outrigger system outrigger (Nair, 1998)

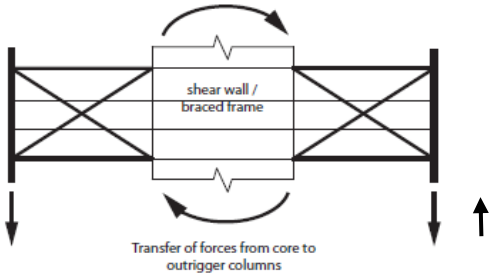

Figure 2-4 Transfer forces from core to perimeter columns using conventional outriggers (Nair, 1998)

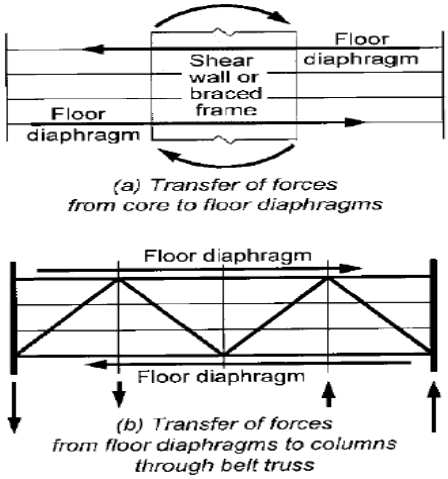

Figure 2-5 Transfer forces from core to perimeter columns using virtual outriggers (Nair, 1998)

The belt truss can be hinged to the exterior columns rather than using rigid connections. When the truss is connected to the perimeter columns by rigid connections the system works as a rigid body and the overturning moment initially resisted only by the core is reduced by the counteracting moment generated by the axial force developed in the perimeter columns times the lever arm (Fig. 2-6). On the other hand, when the truss is cantilevered from the core and hinged to the perimeter columns, there is no bending moment induced in these columns. Hence, the capacity of perimeter columns increases because it carries only axial force instead of axial force plus bending moment resulted in the previous case. Then, in Fig. 2-7b and Fig. 2-7c is schematically showed the effect of adding one-floor outrigger and two-floor outrigger, respectively, on the distribution of overturning moment along the building height against the bare core system Fig. 2-7a). As depicted, outriggers act as restrainers for the cantilevered core system. To enhance the lateral resistance of structure, the core has to possess enough stiffness which can

be achieved by minimizing the overturning moment caused by lateral loads as illustrated in Fig. 2-7

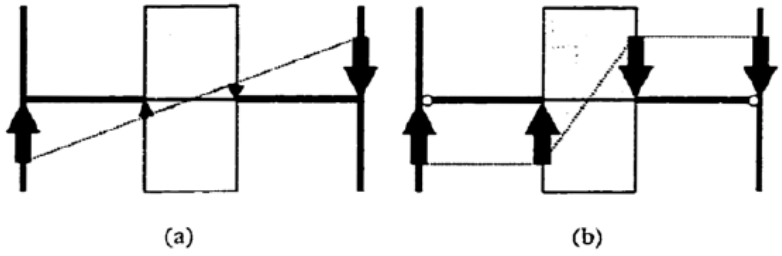

Figure 2-6 Shear distribution in the shear wall system a) rigid connection b) pin connection to exterior columns. (Bayati et al., 2008)

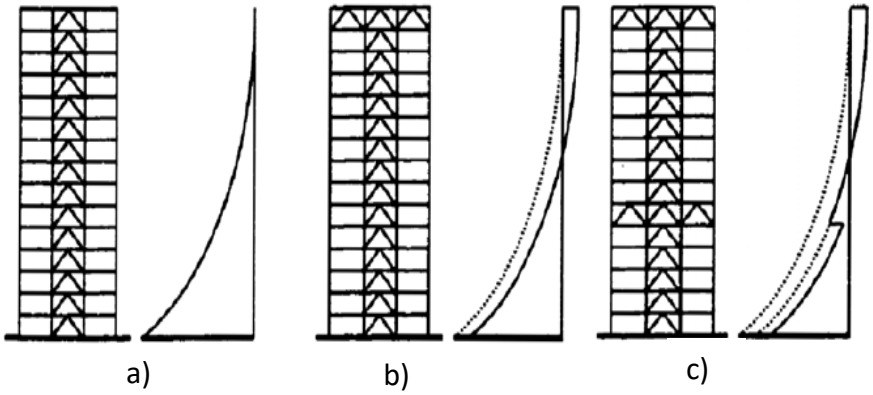

Figure 2-7 Effect of outriggers on the distribution of overturning moment: a) CBF system, b) CBF system with top outrigger, c) CBF system with top and middle outriggers (Bayati et al., 2008)

When braced frames deflect under lateral loads (e.g. earthquake loads) there is a bending deformation and a shear deformation (Fig. 2-8a). However, this occurs if the columns of braced frame are continuous over the building height. In case that these columns are continuous over two stories, as recommended in the CAN/S16 standard, the bending deformation is reduced and the shear deformation is predominant. The mechanism of forces transferred from the braced frame core to perimeter columns is plotted in Fig. 2-8b. It is noted that in Fig. 2-8b, columns of the core system are continuous over the building height.

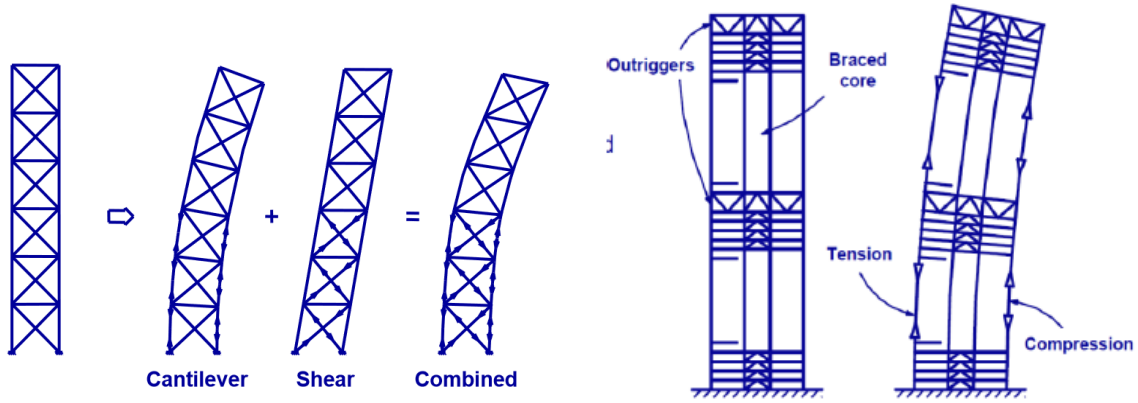

(a) (b)

Figure 2-8 Deformed shapes under lateral forces: a) braced frame, b) braced frame core and outrigger trusses system (Buyukozturk and Gunes, 2004)

2.1.2. Optimum location of outrigger trusses

Taranath (1974) concluded that the location of outrigger trusses has a big impact on the structure's response to lateral loads. In light of this, Taranath proposed a simplified method in order to recommend the location of outriggers along the building height. He assumed that outriggers are installed in one floor and they have infinite stiffness, columns are continuous with constant cross-section along the building height and the core has constant moment of inertia. In the analytical model given in Fig. 2-9, it is shown that the model is subjected to wind load with uniform distribution along the height and the outrigger system is arbitrary located at a distance x measured from the top. It was also assumed that the outriggers are rigidly connected to the core and pinned connected to perimeter columns, which are pinned connected at the base. Using three stiffness parameters representing the stiffness of the core, outrigger and perimeter columns, it was possible to combine them as a single dimension parameter. This method allows for a rapid procedure to find the optimum location of outriggers in order to cause the largest reduction in the lateral deflection measured at the top of building.

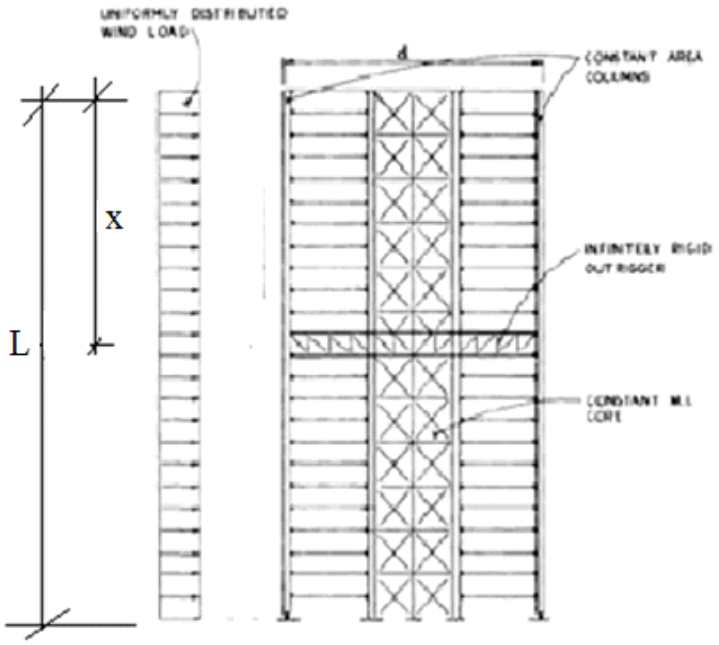

Figure 2-9 Analytical model for founding the optimum location of one-floor outrigger (Taranath,1974)

It is noted that Taranath's method depends on matching the rotation of lateral resisting core with the rotation of outriggers. The restoring moment M_x at the location of outrigger is evaluated, and the deflection of core at the top level due to restoring moment is maximized. The mathematical derivation gives the optimum location of single outrigger in terms of drift control. The optimum location was found to be at x = 0.445L measured from the top of the building, where L is the building height as illustrated in Fig. 2-9.

Verification of Taranath's procedure on the case study considering two-floor outriggers was conducted by Mc Nabb et al. (1975). They found that the optimum location of two-floor outriggers is at 0.312H and 0.685H measured from the top of a structure, where H is the building height. However, Rutenberg et al. (1987) stated that real buildings equipped with outrigger trusses do not fulfill the simplified assumptions considered by Taranath (e.g. Fig. 2-9).

Meanwhile, Moudarres et al. (1985) used dynamic analysis to investigate the free vibration of high-rise buildings taking into account the inertia of the outrigger, shear deformation, and moment of inertia of the building core.

Simple approximate guidelines to determine the location of outrigger location was also proposed by Smith et al. (1991).

To find the optimum location of outriggers with or without belt trusses, Stafford (1981) proposed a graphical method. According to Smith and Coull (1991) the number of computability equations is equal to the degree of redundancy. Thus, he developed a set of non-dimensional parameters $\alpha = \frac{EI}{(EA)_c(d^2/2)}$ and $\beta = \frac{\mathrm{EI}}{(\mathrm{EI})\mathrm{o}}\frac{\mathrm{d}}{\mathrm{H}}$ which expressed the rigidity of core-to-column and core-to-outrigger respectively, while the above non-dimensional parameters are combined into one non-dimensional parameter $\omega = \frac{\beta}{12(1+\alpha)}$ which represent a structural parameter for a uniform structure with flexible outriggers. Herein, EI is the flexural rigidity of the core, $(EA)_c$ is the axial rigidity of the exterior columns, $(EI)_o$ is the flexural rigidity of the outrigger, d is the distance between center of the core to the exterior column and H is the height of the building.

It is stated that the the value of ω reduces when the flexural stiffness of the outrigger increased, and it increases when the axial stiffness of columns increases. Therefore, for a range of ω values, the optimum location of outrigger can be graphically plotted. From ω value, the optimum location of outrigger can be determined in term of minimizing the lateral drift. In Fig. 2-10 is shown the ω parameter versus the outrigger location, x, normalized to H for different number of outriggers as reported in Smith and Coull (1991).

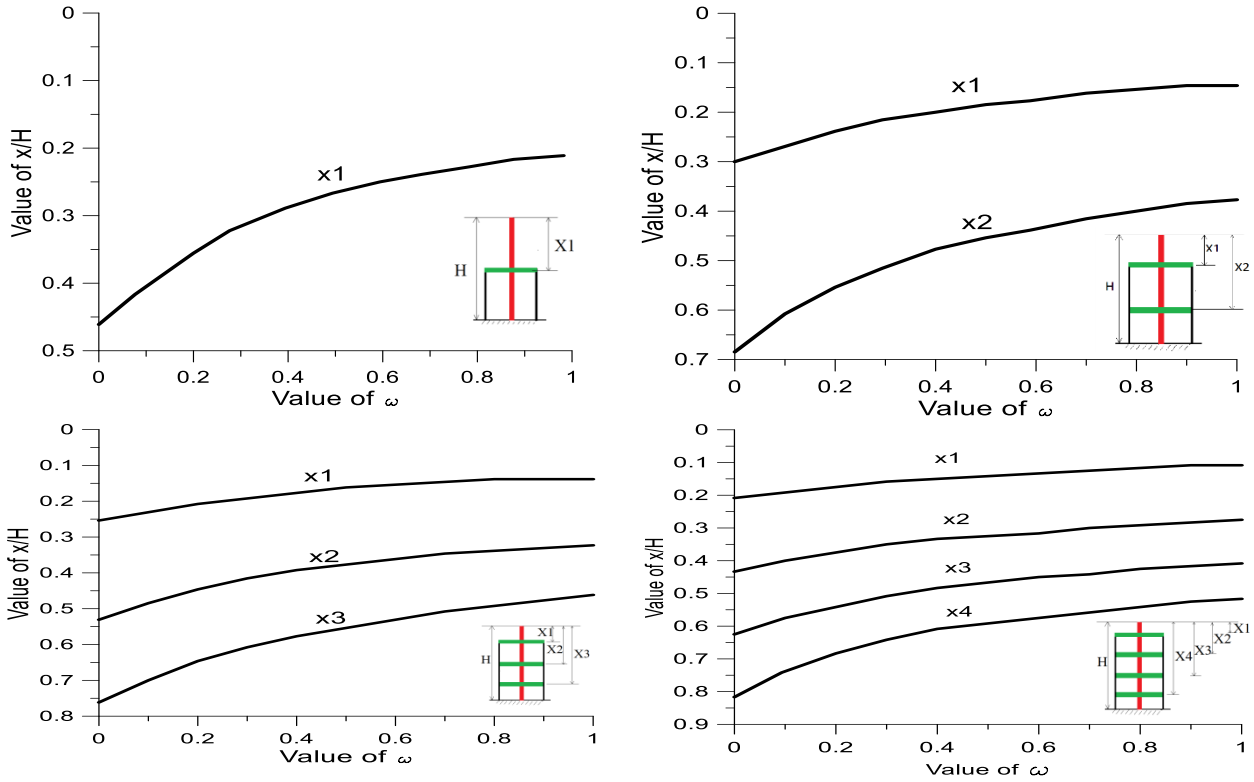

Figure 2-10 Optimum location of outrigger Smith and Coull (1991)

Using the method proposed by Taranath (1974), Hoenderkamp et al. (2003) presented a method of analysis to be used for preliminary design of high-rise braced frames with outriggers under lateral loads. The studied system is illustrated in Fig. 2-11. Later on, Hoenderkamp et al. (2008) investigated the location of the second-floor outrigger with the building having an outrigger at the roof level.

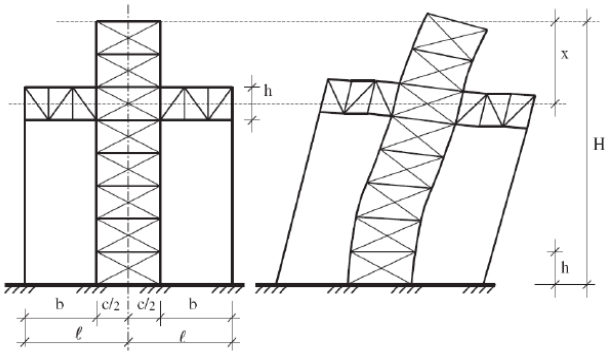

Figure 2-11 Braced frame with outrigger system (Hoenderkamp et al., 2003)

Recommendations for the optimum location of single-floor or multi-floor outriggers were proposed by Taranath (2012) and are illustrated in Fig. 2-12.

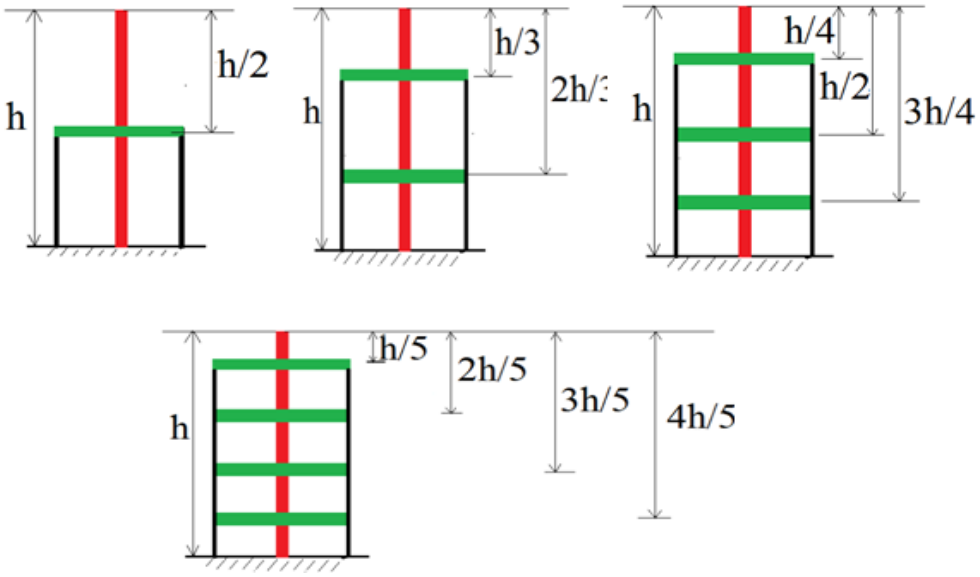

Figure 2-12 Optimum location of outrigger trusses (Taranath, 2012)

Taranth (2012) did not recommend placing outriggers at the top floor level because they are not fully efficient, while placing the outriggers at mid-height it may reduce the interstorey drift by 75%. In addition, he summarized that the theoretical optimum location for two-floor outriggers is:

1/3 and 2/3 of the building height. In the case of a high-rise building requiring three-floor outriggers, the theoretical optimum locations are at ¼, ½, and ¾ of the building height. Generally, it was recommended to place outriggers at: (1/n+1), (2/n+1), (3/n+1), (4/n+1),….(n/n+1) etc., where *n* is the number of outrigger trusses. For outriggers at two-floor or more, the drift reduction could be achieved when adding outriggers at different locations other than the theoretical optimum locations mentioned above, therefore the engineers and architects may have alternative locations for outriggers.

Herath et al. (2009) investigated the required number of outriggers to be placed in outrigger braced building subjected to earthquake and concluded the following:

- The behavior of the building is different from one earthquake ground motion to another; this can be conducted from lateral displacement result.
- Location of outrigger has a critical influence on the lateral behavior of the structure, thus the location of the outrigger should be chosen carefully.

From all the above studies, it is clear that the location of outrigger trusses and its design procedure it is an important research topic for steel high-rise buildings subjected to earthquake loads. It is important to determine the adequate number of outrigger trusses required to control the lateral deflection of a building. It should be noted that presently, there is no comprehensive design method for outrigger braced frame buildings, that is validated against nonlinear time-history analysis by using detailed numerical models and real subduction ground motions.

2.2. Characteristics of Concentrically Braced Frames

2.2.1. Background

Concentrically braced frames, CBFs, are widely used seismic force resisting systems in North America. The CBF system designed according to the current Canadian code (NBCC) and Steel design standard (CSA/S16) is able to dissipate energy through braces yielding in tension and buckling in compression. The repeated number of loading/ unloading energy cycles input into the system by ground motion accelerograms is released by hysteresis loops of brace deformations, while preserving the remaining structural members in elastic range. The hysteresis response of braces subjected to cyclic displacement is asymmetrical as the brace tensile strength is about two times greater than the compression strength, while the brace post-buckling strength is about 20% of its tensile strength. However, previous studies e.g., Black et al. (1980), Ikeda and Mahin

(1984), Remnikov and Walpole (1997), Lee and Bruneau (2002), Tremblay (2002), Haddad (2004) and others have revealed that braces are able to dissipate the input energy. Researchers stated that braces with low slenderness ratios leads to lower fracture life of braces in comparison with more slender braces.

Lacerte and Tremblay (2006) studied the inelastic response of 2-storey, 4-storey, 8-storey, and 12-storey CBF buildings with Split-X braces located in Eastern and Western Canada. The study showed that the CBF system with Split-X braces taller than 8-storey that were designed for Western Canada may experience significant concentration of inelastic deformation within a floor across the building height. This phenomenon is more pronounced if the gravity load transferred to CBF columns has been increased.

Due to the changes in seismic hazards and seismic hazard maps, the base shear values significantly increased since 1970 when the first probabilistic map was released. The seismic hazard evolved from 50% in 50 years probability of exceedance (NBCC, 1970), to 10% in 50 years probability of exceedance (NBCC 1985) and 2% in 50 years probability of exceedance (NBCC 2005). It is noted that in Canada the capacity design method was introduced in the 1989 edition of CSA/S16 standard. This means that non-ductile members are designed to carry increased seismic induced forces that correspond to the probable resistance of braces in the case of CBFs. Meanwhile, braces designed to comply compressive strength criteria may be subject to increase size in order to verify the code limitation on brace slenderness and width-to-thickness ratio.

The advantages of using CBFs in seismic areas are:

- Concentrically braced frame system is effective to provide lateral strength and stiffness to buildings subjected to lateral loads (earthquake and wind).
- The CBF system dissipates energy through tension yielding and inelastic buckling of braces.
- Simple pin connections of beams to columns and gusset plate connection used to connect braces to the frame are cost efficient in comparison to rigid connections used for moment resisting frames (MRF). This makes the construction process fast and easy as complexity.

The main drawbacks of this seismic force resisting system are:

- Asymmetrical behavior of CBFs after braces have buckled and their buckling strength is consumed.

- Concentration of deformation within a floor may leads to weak-storey mechanism and increase residual interstorey drift;
- Due to its large stiffness, the system is subjected to large base shear demand;
- Replacement of braces after buckling may be costly and time consuming.

2.3. Behavior of braces

The brace hysteresis behavior was also studied by Diclelic and Calik (2008). The main parameters are: the axial load, P, the axial displacement δ, and a transverse mid-span displacement Δ. The cyclic behaviour of a brace is illustrated in Fig. 2-13. To study the inelastic cyclic behavior of steel braces, the axial force deformation hysteresis can be broken into six main zones as shown in Fig. 2-13b.

Zone 1: represented in segment O–A, shows the brace behaving in compression in the linearly elastic range. Due to the initial imperfections within the brace, the second-order moments are generated under the applied axial load and the brace deflects transversely as demonstrated in Fig. 2-13a.

Zone 2: represented in segment A–B, shows that the brace behavior is dominated by the inelastic bending of the brace due to the P x Δ moment induced by the compressive axial load P. Additional increase in the axial displacement of the brace will lead to larger transverse displacement Δ, which lead to larger second order moment at the mid length of the brace. This results in a drop in the axial force resistance of the brace along A-B segment due to the moment axial force interaction effects. This stage is characterized by big lateral deflection and by plastic hinge at the brace mid-span length.

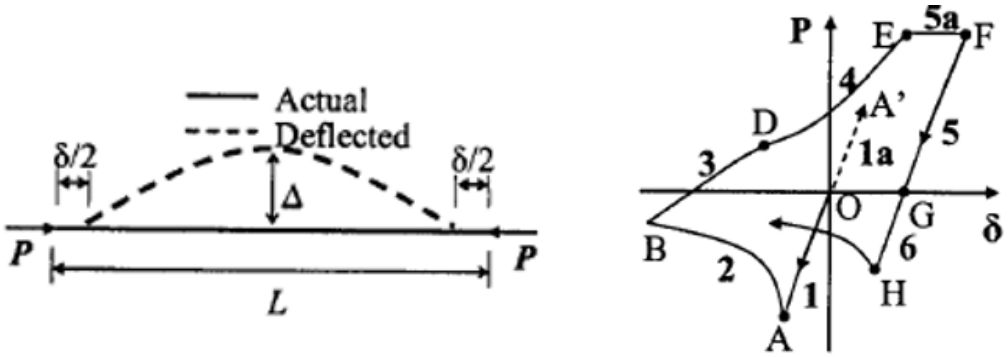

a) b)

Figure 2-13 Inelastic behaviour of brace under axial load (Diclelic and Calik, 2008)

Zone 3: is represented in segment B-D. This zone corresponds to elastic unloading and tension loading of the brace. The slope of this zone is much smaller than that of Zone 1 due to the large permanent lateral deflection at the mid-span length of the brace.

Zone 4: is represented in segment D-E. At the starting point of this zone, a plastic hinge at the mid-span length of the brace is produced. However, within Zone 4, the plastic hinge rotations act in the reverse direction of that of Zone 2.

Zone 5a: is represented in segment E–F which shows a purely plastic axial elongation.

Zone 5: is represented in segment F-G. This zone consists of elastic unloading where the brace elongation decreases linearly with decreasing tensile load within the region beyond Point G.

Zone 6: is represented in segment G-H. The brace is compressed by axial force and buckled again at Point H.

It knows that braces buckle at small interstorey drift. When a brace reaches its compressive capacity, the brace member buckles, and a plastic hinge is developed at the mid-span length of the brace. After plastic hinge occurred at hinge location, a large displacement occurs and the axial capacity of brace reduces to accommodate the bending moment developed at the plastic hinge location. The amount of inelastic rotation to the plastic hinge increased at every cycle. When acting in tension, the brace develops strain hardening after it reached the tensile yield resistance, and the brace accumulated permanent elongation.

2.4. Weak-story mechanism

When a first brace consumed its plastic capacity in a floor, suddenly, all braces at that given floor are on the verge of losing their strength. The damage is concentrated at that floor and the

cyclic deflection remains in one side without being able to return to its initial equilibrium position. At this given floor, the weak storey mechanism is formed. When this phenomenon happens, the CBF columns are excessively loaded and tilted, while bending moment is developed. The peak values of bending moments occur at floors above and under the weak-storey, while plastic hinges may develop in columns as shown in Fig. 2-14. It is noted that in Fig. 2-14 both CBF columns and gravity columns are continuous along the building height, while braces are designed to yield in tension and buckle in compression.

In the case showed in Fig. 2-14, the lateral displacement of the top floor is approximately equal to that of the floor below where the weak-storey occurred. Furthermore, the plastic capacity of the whole building is only the plastic capacity of one floor, while the capacity of the rest of the building is unused. The formation of weak-story mechanism leads to initiation of floor failure and the occurrence of partial building collapse. In the case that weak-storey is triggered at the bottom floor, the partial failure of this floor leads to building collapse. Therefore, mitigating the weak-storey formation increases the safety of the whole building.

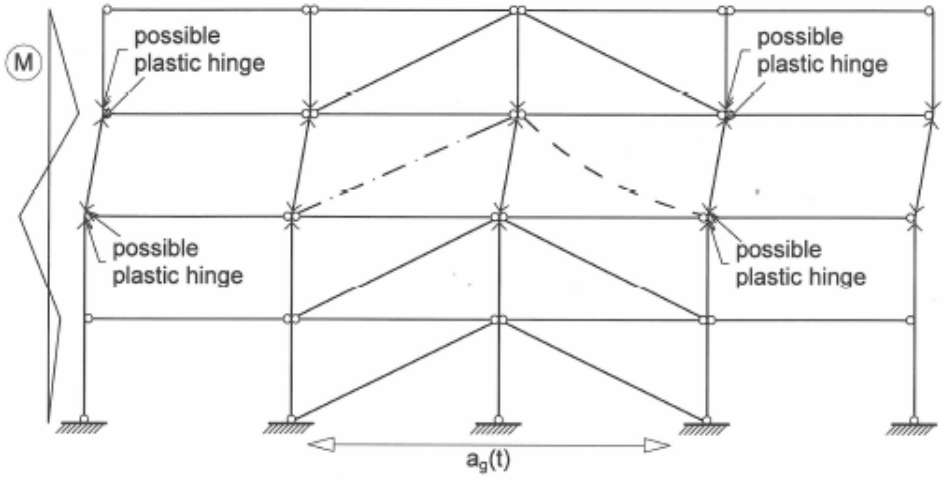

Figure 2-14 Weak story mechanism (Merczel, 2010)

2.5. Consideration of torsion in seismic design

Torsion is an important part of sesmic design consideration. Torsion occurs when the center of mass and the center of rigidity of a structure do not match and the torsion calculated as the lateral sesmic force multiplied by the distance between the two centers as shown in Fig 2-15.

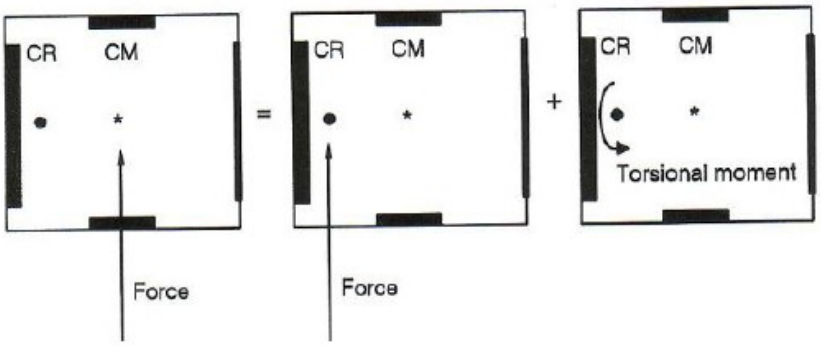

Figure 2-15 Torsion consideration (Filiatrault, 2002)

To preserve the building safety when subjected to seismic load, the Canadian building code, NBCC 2010, requires to account on the accidental torsional effect caused by accidental eccentricity equal to $0.1D_n$. Herein, D_n is the distance perperdecular to the direction of the force application when the static method is considered as depicted in Fig 2-16.

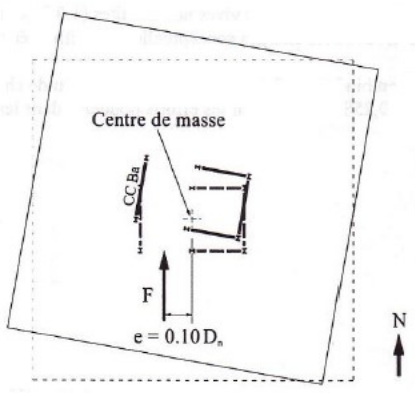

Figure 2-16 Effect of accidental torsion (Filiatrault, 2002).

Considering torsion in 3D models is very important to get accurate results specially if the building is irregular and has a special shape like L-shape, where the torsion causes an increase in the stress in the inner angle of the building (Ahmed et al. 2016).

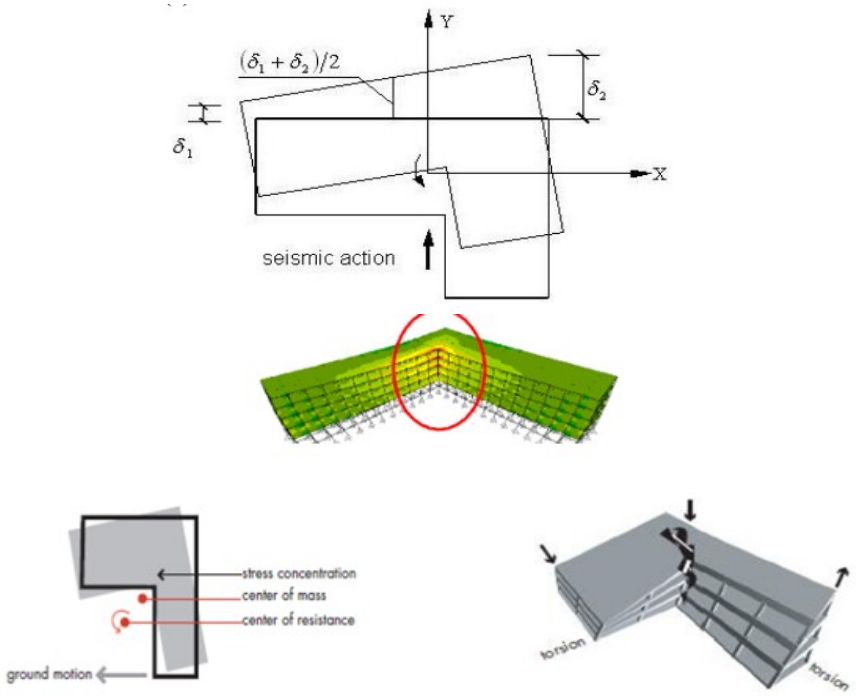

Figure 2-17 Effect of torsion in on 3D model (Ahmed et al., 2016)

2.6. Experimental test on concentrically braced frames

There are several experimental tests conducted on HSS braces to identify their behaviour from yielding to failure under symmetrical and asymmetrical quasi-static cyclic loading (e.g. Lee and Goel, 1987, Archambault, 1995, Termblay et al., 2003, Shaback, 2001, Shaback and Brown, 2003). From these studies it was concluded that square HSS braces buckle out-of-plane, after braces experienced buckling their compression capacity diminishes to the post-buckling capacity, HSS braces are able to yield in tension, stocky braces are able to experience reduced number of life cycles than slender braces, when plastic hinge is formed at HSS brace mid-span a crack is initiated when is loaded in compression which opens when is reloaded in tension.

Experimental tests on full scale 2-storey CBF with split-X HSS braces were conducted and reported by Tsai et al. (2008). The detailed dimension of the CBF specimen designed according to a balanced design procedure relying on cyclic yielding of braces is shown in Fig. 2-18. The CBF specimen was tested under cyclically increasing story displacements, and the test loading protocol is shown in Fig. 2-19. Results from experimental tests are shown in Fig. 2-20. As depicted, HSS braces buckle out-of-plane and failure occurs caused by low-cycle fatigue.

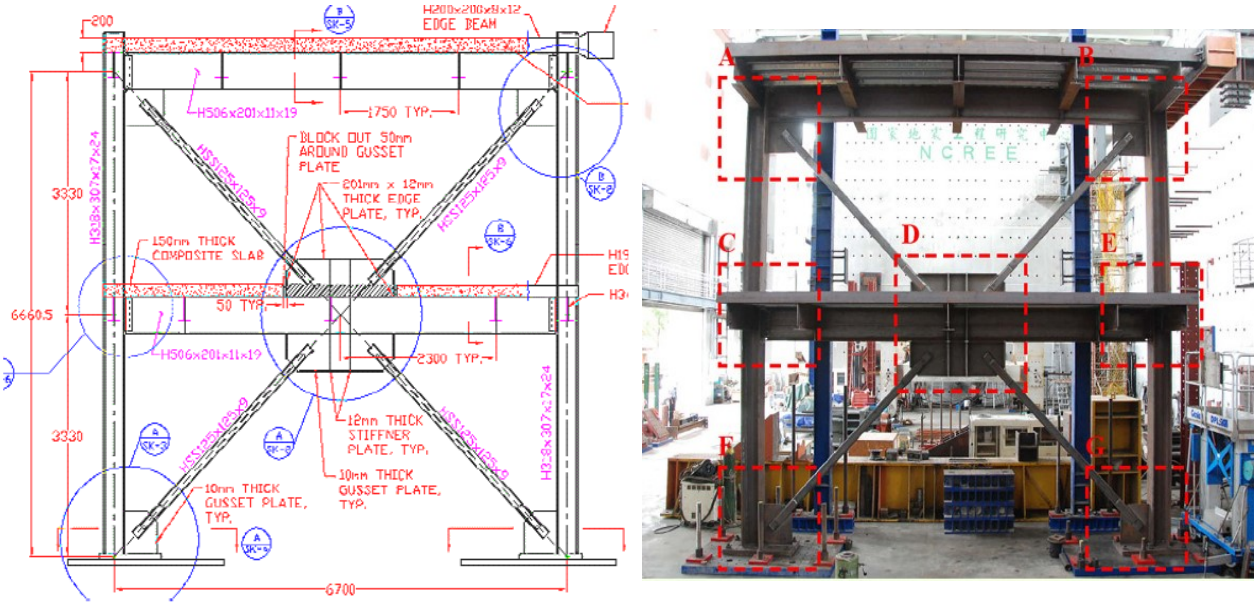

a) b)

Figure 2-18 The 2-storey CBF tested: a) Detail sketch, b) Specimen (Tsai et al. 2008, http://exp.ncree.org/cbf)

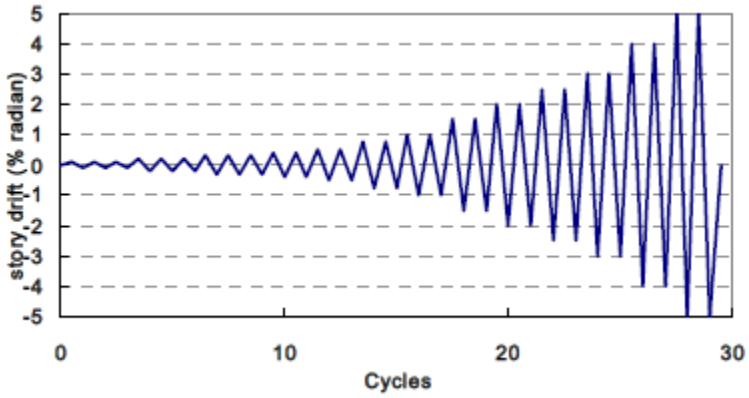

Figure 2-19 Loading protocol (Tsai et al.2008)

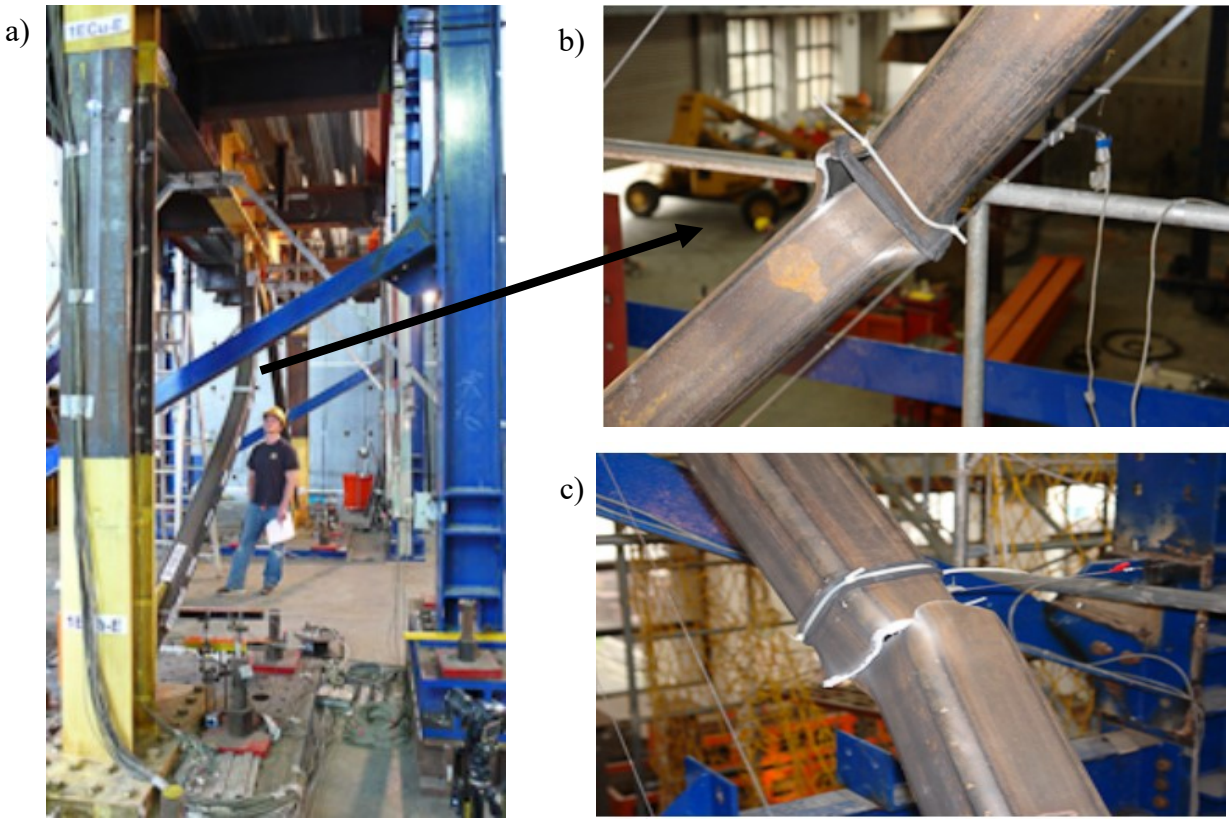

Figure 2-20 Response of tested CBF specimen: a) HSS brace buckle out-of-plane, b) HSS brace initiates fracture at mid-span, c) Fracture of HSS brace (http://exp.ncree.org/cbf)

To allow square HSS braces to buckle out-of-plane and to dissipate the input energy, the brace-to-frame gusset plate connection has to be designed to carry the brace capacity and in the same time to deflect out-of-plane as shown in Fig. 2-21. No fracture was noticed in the beams or columns.

Figure 2-21 Response of brace to frame connections of tested CBF specimen (http://exp.ncree.org/cbf)

The results of the test were as follow: a) the split-X braces of CBFs have good energy dissipation characteristics (Fig. 2-22) up to a story drift equal to 0.03 radians under the cyclically lateral displacements; b) the 2t-linear clearance of the gussets provide satisfactory ductility at each test (Fig. 2-21); c) the fracture was initiated in compression in the compression side of HSS as showed in Fig. 2-20b.

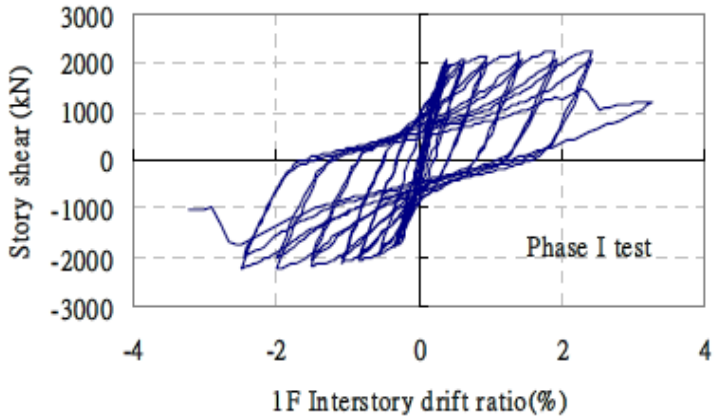

Figure 2-22 Shear force verses inter-storey drift (Tsai et al. 2008)

Hsiao at al. (2012) tested a single story specimen shown in Fig. 2-23a. From the test, the hysteresis loops given in term of force-deformation is shown in Fig. 2-23d. The OpenSees model developed for this CBF specimen was calibrated against the experimental test results. Line-element was used to model all the braces, beams, and columns as indicated in Fig. 2-23b. Fiber-type of sections are used for the beams, columns, and braces. Rigid links are used to simulate the rigid part of the gusset-to-beam, and gusset-to-column connections.

The behavior of the brace to frame gusset plate connection was modelled as shown in Fig. 2-23c. As illustrated, nonlinear rotational springs were inserted in the Zero-length element. The rotational spring simulating the out-of-plane flexure of gusset plate is based on the gusset plate material and geometry. The hysteresis loops obtained from the OpenSees model are able to match that resulted from experimental response of HSS brace resulted under cyclic loading (Fig. 2-23d).

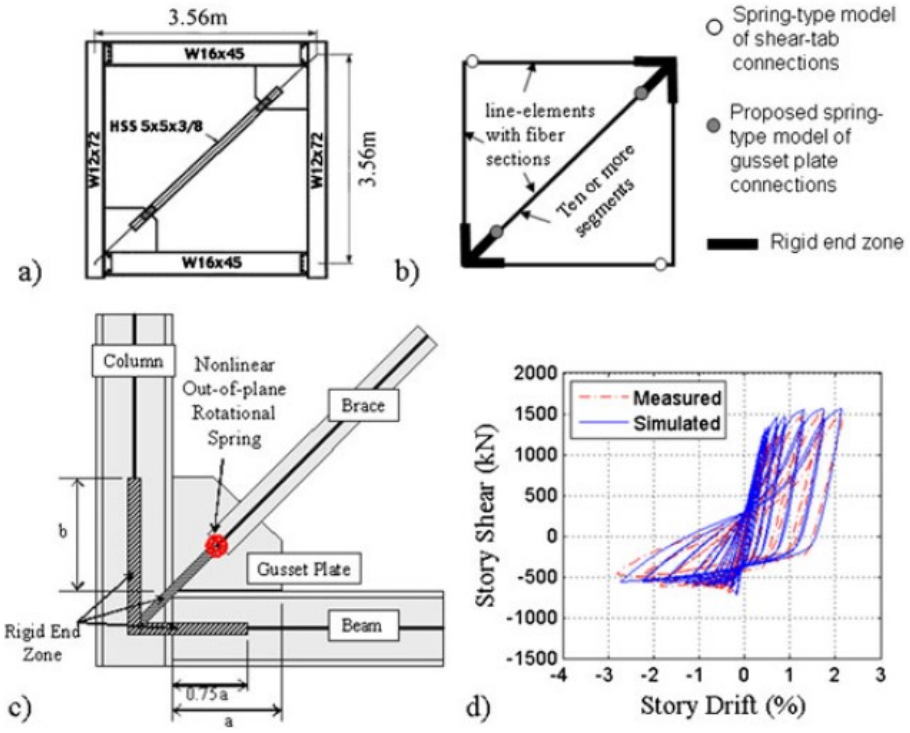

Figure 2-23 Single-storey CBF: a) test specimen; b) modeling approach; c) gusset plate simulation; d) experimental versus numerical results (Hsiao et al. 2012).

2.7. OpenSees framework

Open System for Earthquake Engineering Simulation (OpenSees) is an open source finite element framework method to develop applications for the simulation of the performance of structural system under earthquake loads. This software was developed at the University of California at Berkeley by Frank McKenna in 1997 (McKenna, 1997). The OpenSees has been sponsored by the National Science Foundation (NSF), the Pacific Earthquake Engineering Research Center (PEER) and George E. Brown, Jr. Network for Earthquake Engineering Simulation (NEES).

The capabilities of OpenSees were supported by analytical and experimental studies that make this software a versatile tool for analyzing the nonlinear response of structural systems. The OpenSees software is a research tool which is free for use. The software can be downloaded from: http://opensees.berkeley.edu/wiki/index.php/Main_Page. Furthermore, the OpenSees is an object-oriented software framework written in C++ with several interpreters reading input information written in the Tcl programming language. The modeling process including nonlinearities at the level of the cross-section and members are summarized in Fig. 2-24.

2.7.1. Modeling of CBFs using OpenSees

Uriz (2005) and Uriz and Mahin (2008) showed for the first time the inelastic cyclic response of steel bracing members with fiber cross-sections discretization and large displacements buckling formulation.

To simulate the inelastic response of brace member in OpenSees, the brace member is divided into *n* force-based nonlinear beam-column elements with fiber cross-section discretization and distributed plasticity. Each nonlinear beam-column element has at least three Gauss-Lobatto integration points. Uriz and Mahin (2008) proposed that each HSS brace to be made of minimum 20 elements. To allow the deformation of HSS brace out-of-plane, an out-of-straightness parameter (i.e., geometric imperfection) of L/500 is recommended to be applied in the out-of-plan direction of brace deflection. Herein, L is the length of the brace. The geometric transformation is considered to be corotational transformation. To simulate the gusset plate connection between the HSS brace and frame, two rotational springs and one torsional spring were defined and inserted in the Zero-length element that connect the brace to the rigid element as shown on Fig. 2-25.

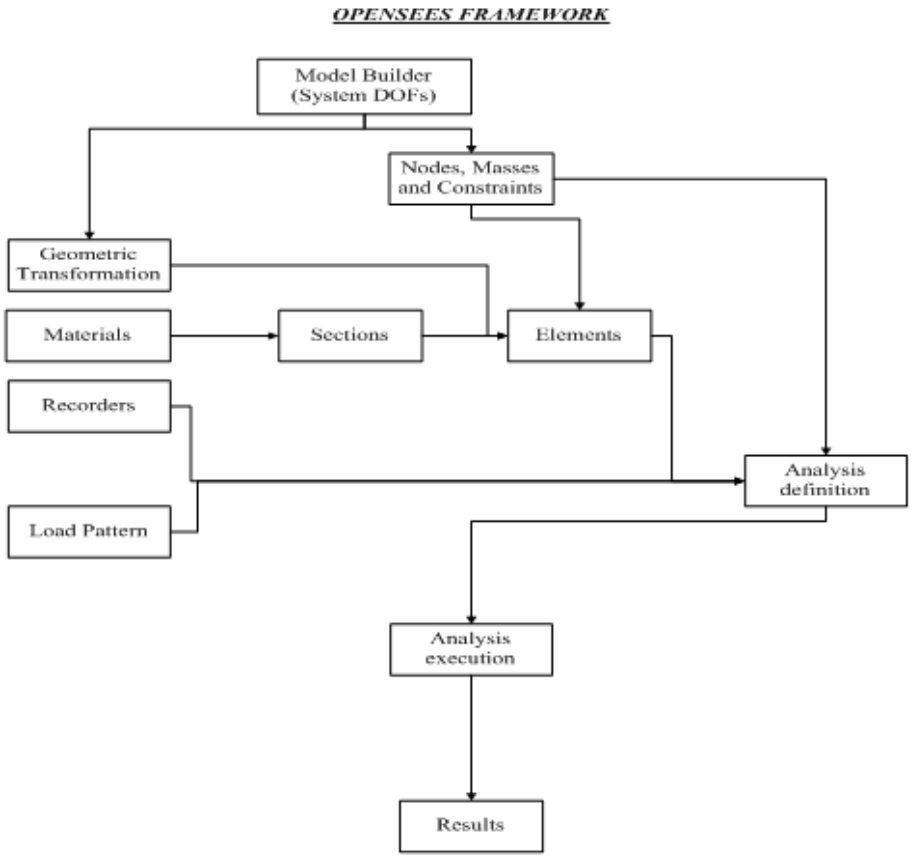

Figure 2-24 Modeling process in OpenSees software (Morales 2011)

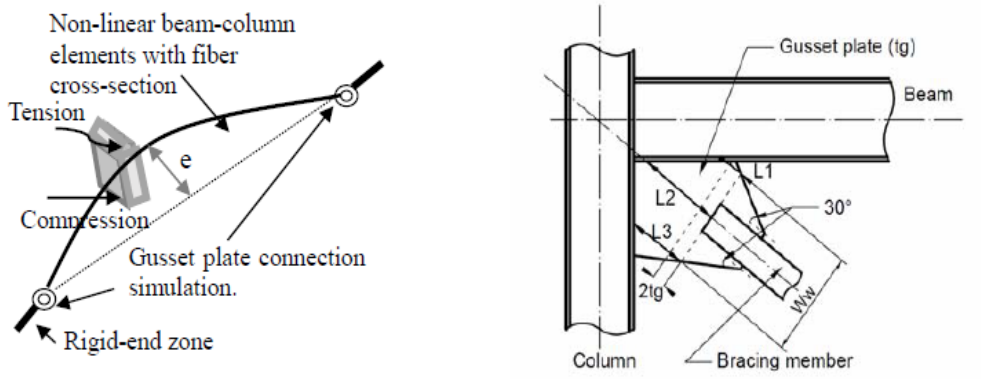

Figure 2-25 Model of HSS brace with end gusset plate connections (Tirca and Chen, 2014)

2.7.1.1. Brace element modeling

The brace member is simulated using 20 elements of force-based nonlinear beam-column elements with distributed plasticity and fiber-based cross-sections. The nonlinearity is assigned

by using the Giuffre-Menegotto-Pinto steel material with isotropic strain hardening, where the stress is expressed as a function of strain. This steel material is designated in OpenSees as *Steel02* material.

$$\sigma^* = b\varepsilon^* + \frac{(1-b)\varepsilon^*}{(1+\varepsilon^{*R})^{\frac{1}{R}}} \qquad 2\text{-}1$$

In Eq. (2-1), $\sigma^* and\ \varepsilon^*$ are the effective stress and strain depending on unload/reload interval, b is the ratio of final to initial stiffness, and R is the material parameter dependent on the shape of the unload curve. The same values for R as proposed by Aguiro et al. (2006) was considered.

2.7.1.2. Out-of-straightness assigned to HSS brace

Tirca and Chen (2014) considered different ratios for defining the out-of-straightness parameter assigned to a HSS brace deflecting in its out-of-plane direction. The brace consists of eight non linear beam-column elements with distributed plasticity, four integration points per each element and fiber-based cross-sections. The influence of the out-of-straightness parameter, *e,* on the brace hysteresis response is depicted in Fig. 2-26. The out-of-straightness was considered L/100, L/300, L/400, L/500 and L/1000, where L is the brace length. It was concluded that for small values (e.g. L/1000), the buckling force increases significantly, while the post–buckling force remains

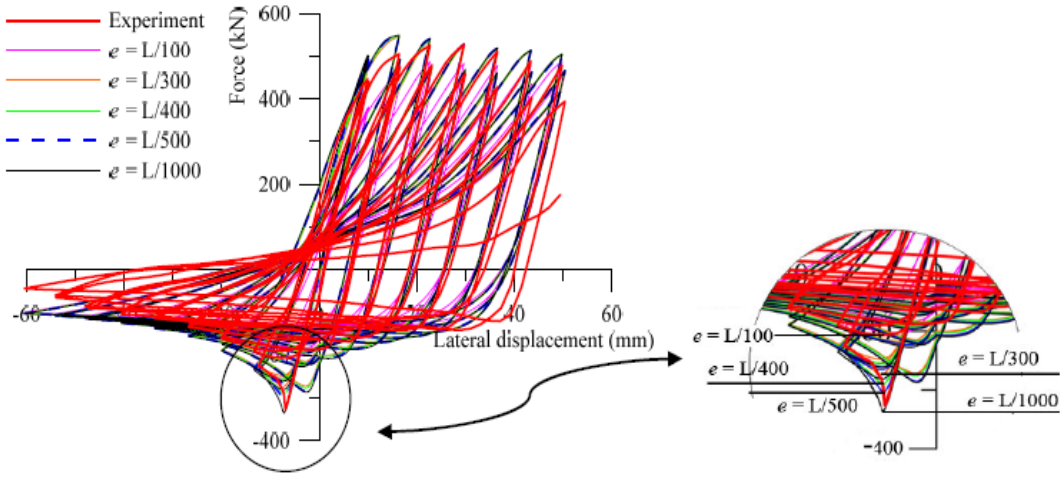

Figure 2-26 The effect of out-of-straightness on the HSS brace response (Tirca and Chen, 2014)

unchanged. When the out-of-straightness is between L/500 and L/300, the difference in buckling force is small. However, e = L/500 is recommended. It is noted that Ziemian (2010) recommended the same L/500 out-of-straightness value for HSS braces.

2.7.1.3. Number of fibers

The number of fibers within a brace cross-section has an important parameter on the response of a HSS brace. Three models of meshing technique as shown in Fig. 2-27 were assigned to discretize the HSS brace cross-sections. As per above, the brace member is made of 8 nonlinear beam-column elements with distributed plasticity, four integration points per each element, and e = L/500. Although the cross-sections have the same area, the brace response is different.

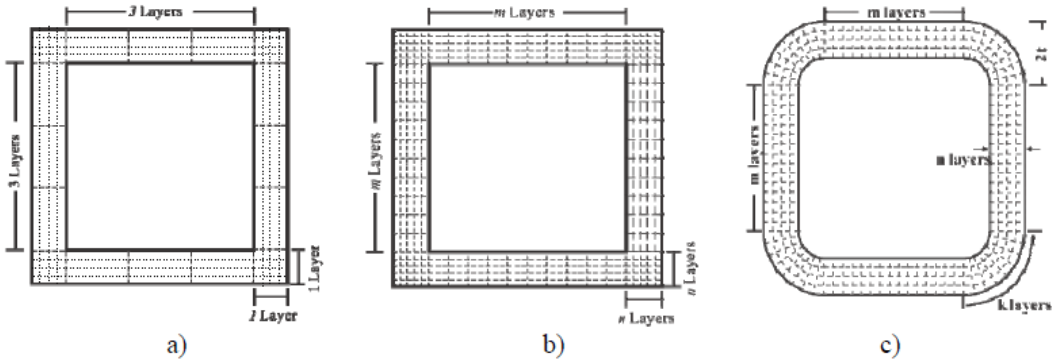

Figure 2-27 Fiber cross-section discretization models: a) model A, b) model B, c) model C (Tirca and Chen, 2014)

As depicted in Fig. 2-28, using the model A of discretization for brace cross-section, the tensile force is underestimated; using model B, the tensile force is overestimated and the compressive force is larger than that in the experimental test; and using model C meshing, the best matching for the results is obtained. It is noted that 240 fibers were considered for the HSS brace cross-section.

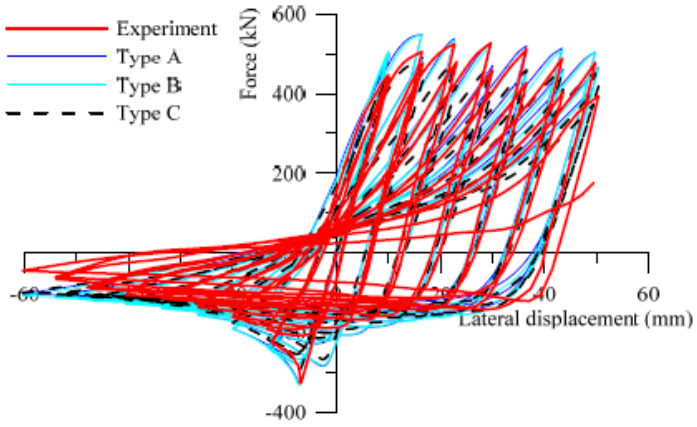

Figure 2-28 Effect of meshing cross-sections on the response of HSS brace (Tirca and Chen, 2014)

2.7.1.4. Number of element and integration points

A parametric study was conducted by Tirca and Chen (2014) to emphasize the importance of number of nonlinear beam-column elements with distributed plasticity used to simulate the nonlinear response of a HSS brace. In this study, various numbers of beam-column elements i.e. 4, 8, 10 and 20 with 4 integration points per each element and fiber cross-section meshing model C are considered. The out-of-straightness equal to L/500 was applied in the out-of-plane direction deflection of HSS brace. The results of this parametric study shows that a brace modeled to yield in tension and buckle in compression but no loaded up to fracture failure would require eight elements in order to fit the nonlinear response closely. If the fracture of the brace caused by low-cycle fatigue is modeled, at least 16 nonlinear beam-columns elements should be used (Hsiao et al., 2012). However, 20 beam-column elements are sufficient to capture the all modes of brace failure (Uriz and Mahin, 2008). The number of integration points does not have major impact on the brace behaviour but at least three integration points for each element is recommended. The impact of number of nonlinear beam-column elements used to simulate the nonlinear behaviour of HSS brace against an experimental test is depicted in Fig. 2-29.

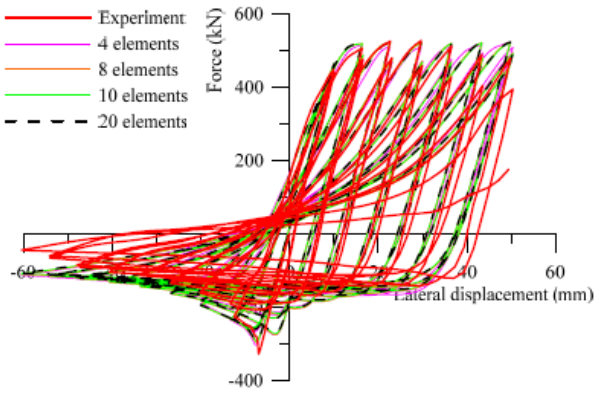

Figure 2-29 Effect of number of nonlinear beam-column elements with distributed plasticity on brace behavior (Tirca and Chen, 2014)

2.7.1.5. Definition of low-cycle fatigue material parameters

Manson (1963) and Coffin (1962) concluded that the relationship between the plastic strain amplitude ε_i, that is experienced by each cycle *i* and the number of cycles to failure N_f is linear in the log-log domain with a slop equal to m according to Eq. (2-2). Other researchers concluded this finding (ASTM 2003; Fisher et al. 1997; Glinka and Kam 1987).

$$\varepsilon_i = \varepsilon_0 (N_f)^m \qquad 2\text{-}2$$

The low-cycle fatigue model in OpenSees was first proposed by Uriz (2005). He considered constant values for fatigue material parameters: ε_0 = 0.095 and m =-0.5. Herein, *m* and ε_0 are known as fatigue ductility exponent and fatigue ductility coefficient, respectively. Replicating several experimental tests, researchers concluded that the fatigue material parameters cannot have constant values and these parameters should be dependent on the properties of brace cross-section. To solve this drawback, Lignos and Karamanci (2013) proposed the following equation to calculate the predicted fatigue ductility coefficient, ε_{0pred} for HSS braces with slenderness ratio between 27 and 85.

$$\varepsilon_{0pred} = 0.291 \left(\frac{KL}{r}\right)^{-0.484} \left(\frac{w}{t}\right)^{-0.613} \left(\frac{E}{F_y}\right)^{0.3} \qquad 2\text{-}3$$

Herein, *KL/r* is the slenderness ration, *w/t* is the width–to–thickness ratio where *w* is calculated as *(b-3t)*, F_y is the yield strength, and E is the Young modulus. It is noted that *b* is the HSS cross-section dimension and *t* is its thickness. The ductility exponent was set m = -0.3.

Later, Tirca and Chen (2014) proposed the following expression given in Eq. (2-4) to predict the failure strain at the first reversal for square HSS braces with slenderness ratio varying between 50 and 150.

$$\varepsilon_{0pred} = 0.006\left(\frac{KL}{r}\right)^{0.859}\left(\frac{w}{t}\right)^{-0.6}\left(\frac{E}{F_y}\right)^{0.1} \qquad 2\text{-}4$$

Eq. (2-4) resulted from regression analysis obtained from modeling 14 experimental tests found in the literature. The ductility exponent was set m =-0.5. A comparison between experimental hysteresis loops experienced by two HSS braces loaded up to failure caused by low-cycle fatigue and the simulated model with fatigue material parameters computed according to Eqs. (2-3) and (2-4) is depicted in Fig. 2-30. It is noted that the HSS specimen noted 2A presented in Fig. 2-25a is HSS 152x152x8 and KL/r = 53.3. The second specimen depicted in Fig. 2-25b is HSS 127x127x8 with KL/r = 65.8. In the case of specimen 2A, both Eqs. (2-3) and (2-4) yield the same results. However, in the case of specimen 3B depicted in Fig. 2-25b, Eq. (2-4) matched the experimental test, while Eq. (2-3) predicted the failure with two cycles earlier that the experimental test.

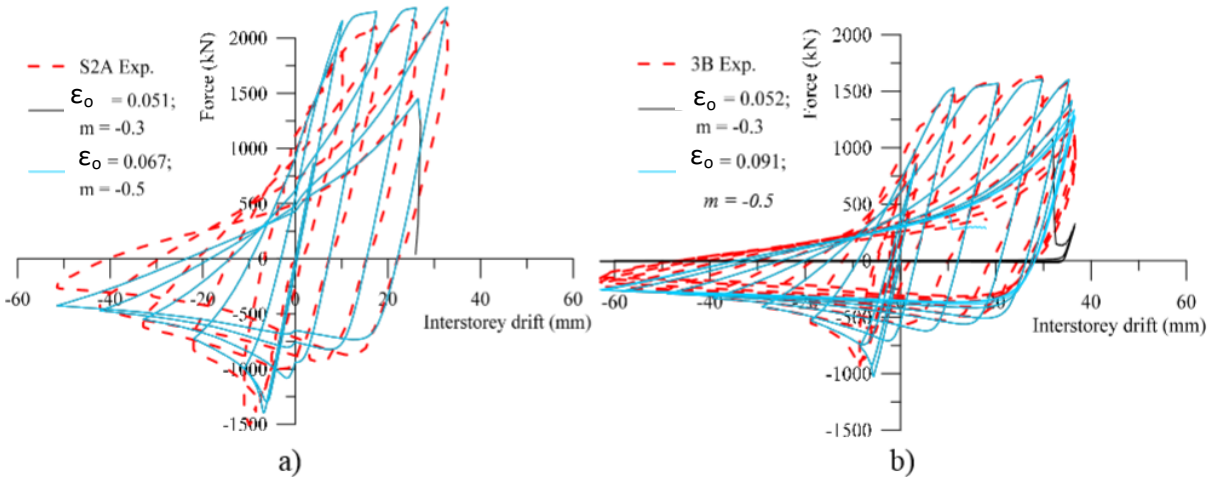

Figure 2-30 Brace fracture simulation based on strain predicted from Eq. (2-3) and Eq. (2-4) (Tirca and Chen, 2014)

2.7.1.6. Gusset plate connection

2.7.1.6.1. Brace connection

Gusset plate connection has a significant effect on stiffness, resistance and inelastic deformation capacity of CBFs. It is worth noting that these connections are neither pinned nor fixed. The first model proposed by Uriz (2005) employed concentrated springs with fiber cross-section. Later, Hsiao et al. (2012) simulated the brace-to-frame gusset plate connection by using two rotational springs and one torsional spring assigned in a zero-length element located at the physical end of brace as illustrated in Fig. 2-31. As depicted, in the OpenSees model, the rest of the gusset plate was assumed as rigid link simulated by using elastic beam-column elements with large stiffness. The first rotational spring replicates the out-of-plan bending and its stiffness is computed by using the Whitmore width (W_w) cross-section as shown on Fig. 2-31. The second rotational spring captures the in-plan bending with stiffness bigger than that of the brace. The torsional spring is made of *Steel01*elastic material. In this model, *Steel02* material was assigned to both rotational springs.

The stiffness of the first rotational spring was computed as:

$$K_{cal}^{rotational} = \frac{E}{L_{ave.}}\left(\frac{W_w {t_p}^3}{12}\right) \qquad 2\text{-}5$$

Where L_{ave} is the average value of L_1, L_2 and L_3 measured from Fig. 2-31and t_p is the thickness of gusset plate resulted from design.

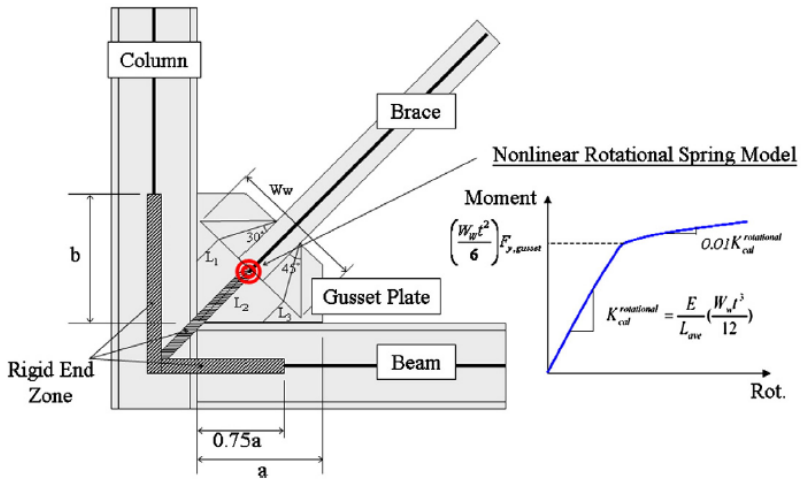

Figure 2-31 Model for brace to gusset connection (Hsiao et al., 2012)

2.7.1.6.2. Beam to column connection of CBF

Beam-to-column connection of CBFs was considered as recommended by Astaneh (2005). According to CSA/S16, the beam-to-column connection is a pinned connection. However, in Fig. 2-32, different conditions are illustrated that vary from pin connection to rigid connection represented by parameter m. According to Astaneh (2005), the stiffness of beam-to-column connection is computed with Eq. (2-6), where m = 0.2.

$$K_{conn} = \frac{m}{\frac{EI}{L}} \qquad 2\text{-}6$$

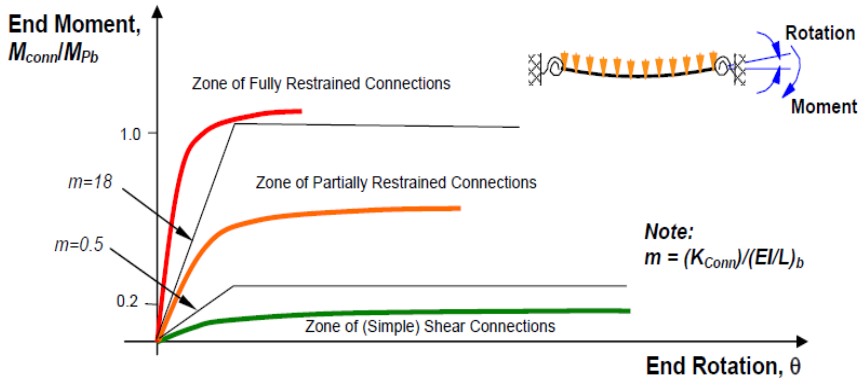

Figure 2-32 Beam to column connection (Astaneh, 2005)

2.8. Assessing the performance of CBF Buildings

2.8.1. Increament dynamic analysis

To assess the seismic performance of CBF buildings the methodology presented in FEMA P695 (2009) is employed. The steps of the method are depicted in Fig. 2-33. To obtain accurate results a detailed numerical model is required. As presented in the previous section, the CBF system behaviour can be simulated from yielding to failure. The median collapse intensity can be computed through the concept of incremental dynamic analysis (IDA) proposed by Vamvatikos and Cornell (2002).

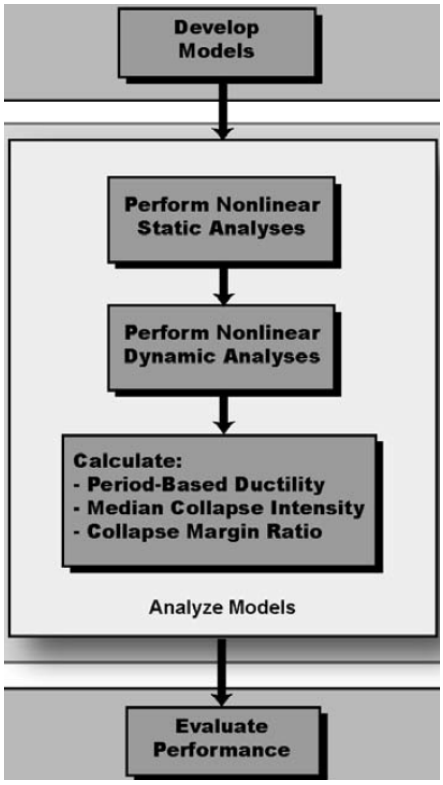

Figure 2-33 Process for performing nonlinear analysis for collapse assessment (FEMA P695, 2009)

Hence, IDA is a parametric analysis method in which individual ground motions are scaled to increasing intensities until the structure reached a collapse point due to dynamic instability. The proposed methodology is based on constructing an IDA curve that is obtained by joining points defined by two coordinates: an intensity measure parameter (IM) and an engineering demand parameter (EDP). For IM parameter, one of the following parameters can be selected: Peak ground acceleration (PGA), Peak ground velocity, the 5% damped spectral acceleration at the structure's first-mode period (S_a (T_1 , 5%)), etc. The EDP can be one of the following: maximum base shear, peak roof drift, peak interstorey drift, peak residual interstorey drift, etc.

Constructing the IDA curves of a structural model, Vamvatsikos and Cornell (2004) found that the graph exhibits an initial linear region which ends when the first non-linearity occurs. In this regard, Fig. 2-29 shows IDA curves for 5-storey braced frame building and for different ground motion records. In Fig. 2-34a, after the initiation of buckling, the graph shows sharp softening which accelerates towards large drift and eventual collapse. Other types of IDA curves show segments with softening and others with hardening, while the initial stiffness decreased or

increased with increasing IM. As depicted in Figs. 2-34c and d, a final softening segment occurs when the structure accumulates the DMs in higher rates for small increase in IM. Then, the curve flattens and the DM reaches infinity. Thus, each point of IDA shown in Fig. 2-34 corresponds to the results of one nonlinear dynamic analysis.

The median collapse capacity is defined as the spectral intensity when half of the ground motions from a set of minimum seven records cause the structure to collapse. The ratio between the median collapse intensity and the design spectrum intensity corresponding to first-mode period is known as the Collapse Margin Ratio, CMR. This parameter is primarily used to characterize the collapse safety of the structure.

To evaluate the performance, a parameter called the Adjusted Collapse Margin Ratio, ACMR should be calculated. The ACMR is computed as the product of CMR and the Spectral Shape Factor, SSF, while the SSF is obtained from tables and depends on the fundamental period, *T*, and period-based ductility, μ_T. Then, total system collapse uncertainty, β_{TOT} is calculated based on the quality ratings of the design requirements and test data, and the quality rating of index archetype models. Knowing the values of β_{TOT}, the acceptable values of adjusted collapse margin ratio, $ACMR_{10\%}$ can be selected from tables. The collapse safety acceptance criteria are verified to check if $ACMR \geq ACMR_{10\%}$.

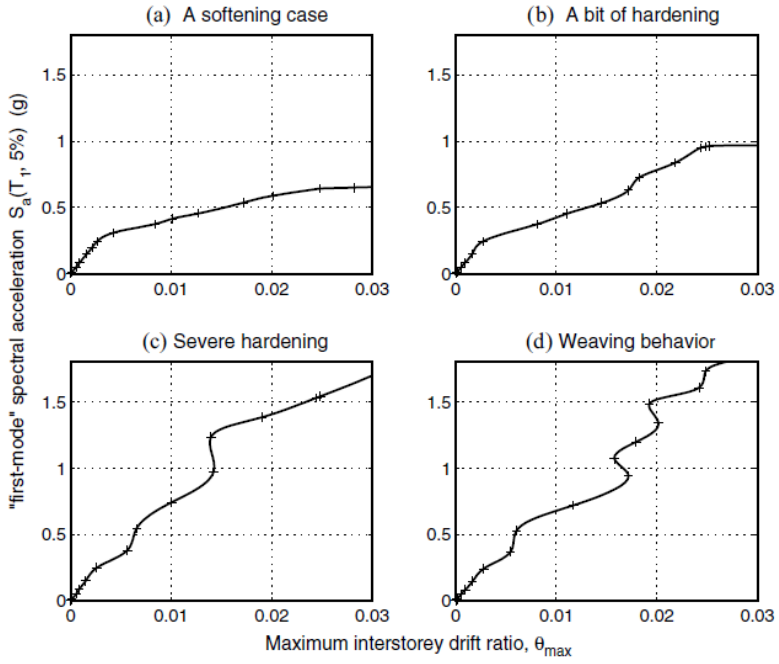

Figure 2-34 Four types of IDA curves observed from analyzing a 5-storey braced frame building (Vamvatsikos and Cornell, 2004)

To investigate the effect of subduction records on CBF buildings, Tirca et al. (2015) conducted a study on the behaviour of 4-storey, 8-storey and 12-story MD-CBF buildings located on site class C in Victoria B.C., Canada. The subduction records used in this analysis were selected from the megathrust magnitude 9 Tohoku earthquake in Japan (March 2011). These records are characterized by 300 s duration and around 100 s Trifunac duration. From this study it was found that the collapse margin ratio, CMR, and the adjusted collapse margin ratio, ACMR, is approximately 150% greater under crustal records than the subduction records. Furthermore, the 12-storey MD-CBF building subjected to subduction records failed to meet the collapse safety criterion of ACMR $\geq$ $ACMR_{10\%}$. Thus, the strength and implicitly the stiffness of the 12-storey MD-CBF building should be increase although the building was designed according to NBCC 2010 and CSA/S16-09 provisions.

2.8.2. Fragility analysis

The probability of collapse for any structure is quantified by using fragility curves, which are also used to find the probability of exceeding some limit states that are required to assess the structural performance when a structure is subjected to hazard intensity measure IM. Fragility curves were studied by several researchers using different methods (Kennedy and Ravindra, 1984, Masanobu et. al., 2000, Baker and Cornell, 2005, and others). They used the analytical fragility function method considering the lognormal distribution to estimate fragility of structure derived from the results from the IDA curves as:

$$P(C|IM = x) = \Phi\left(\frac{\ln(x/\theta}{\beta}\right) \qquad 2\text{-}7$$

Where: $P(C|IM = x)$ is the probability of ground motion with IM=x will casue the structure to collapse, Φ ( ) is the standard normal distribution function, θ is the median of fragility function, and β is the standard deviation of ln (IM).

Epistemic and aleatoric uncertainties were considered by Ellingwood et al. (2007) and the fragility was described as:

$$F_R(x) = \Phi[\ln(x/m_R)/\beta_R] \qquad 2\text{-}8$$

Where: $m_R$is the median capacity of the damage level under consideration, β_R is the logarithmic standard deviation , and $\Phi( )$ is the normal cumulative distribution function (CDF).

To include both aleatoric and epistemic uncertainties, the value of β_R in the Eq. (2-8) is replaced the following equation:

$$\beta_R = \sqrt{\beta^2{}_{RR} + \beta^2{}_{RU}} \qquad 2\text{-}9$$

where B_{RR} is the aleatoric uncertainty and B_{RU} is the epistemic uncertainty. To calculate the aleatoric uncertainty the following equation can be used:

$$\beta_{RR} = \sqrt{\beta^2{}_{D|Sa} + \beta^2{}_{C}} \qquad 2\text{-}10$$

Herein: $\beta_{D|Sa}$ represents the seismic demand uncertainty, and β_C is uncertainity in capacity and depends on performance level.

The seismic demand uncertainty can be expressed as recommended by Wen et al. (2004):

$$\beta_{D|Sa} = \sqrt{\ln(1 + s^2)} \qquad 2\text{-}11$$

where s is conditional slandered deviation. Luco and Cornell (2007) mentioned that because of record to record large scatter, a non linear regression analysis of the power–law form given in Eq. (2-12) can be used.

$$\delta_{max} = aS_a^b \qquad 2\text{-}12$$

Above equation is reduced to linear form by a logarithmic transform:

$$ln\ \delta_{max} = \ln a + b\ ln\ S_a \qquad 2\text{-}13$$

where the EDP represents the engineering demand parameter used to build the IDA curve and where *a* and *b* are constants which are determined using a simple linear regression analysis.

2.8.3. Scaling of ground motions

The nonlinear time history analysis reproduces the actual behavior of a structure under a ground motion by considering the material properties and the geometry of a structure. Therefore, an adequate set of ground motion records is very essential to get the real structural performance. There are two main sources of ground motions: Synthetic ground motions which can be generated from numerical models (Boore, 2003, Vanmarcke et al., 1990), or real ground motions

which obtained from real records. There are many methods to scale the ground motions as mentioned in (Oyarzo-vera and Chouw, 2008).

In Eurocode 8 (EC8), the average spectrum of the scaled records should be larger than 90% of the target spectrum between 0.2T1 and 2.0T1, where T1 is the fundamental period of the structure in the direction of the ground motion. At least a set of three scaled records should be used in the time history analysis. When less than seven records are used the maximum response of the structure should be used, and when seven records or more are used the average response of the structure should be considered in design.

In the U.S Standard (ASCE), the average spectrum of the scaled records should be equal to the target spectrum in the period between 0.2T1 and 1.5T1 where T1 is the fundamental period of the structure in the direction of the ground motion. At least a set of three scaled records should be used in the time history analysis, when less than seven records are used the maximum response of the structure should be used, and when seven records are used the average response of the structure should be used in design.

In the New Zealand standard (NZS), the scaling method is the most elaborated among the building codes, and recommends of using at least three records scaled by two scaling factors: a) the records scaling factor (k1), and b) the family scaling factor (k2). By using k1, the response spectrum of the scaled records fit the target spectrum in a way that the function log(k1) is minimized over the period 0.4T1 to 1.3T1. The parameter, k2 is applied to check that the energy of at least one record of the set exceeds the energy of the target spectrum, while the recommended values are: $0.33 < k1 < 3.0$, and $1.0 < k2 < 1.3$. In all cases the maximum response should be considered in design.

2.9. Summary

From the literature review, it is concluded that the number and location of outrigger trusses and their design procedure is an important research topic for high-rise steel buildings subjected to earthquake loads. Finding an adequate number of outrigger trusses is required to control the lateral deflection of buildings, as well as, their optimum location along the building height. Presently, no comprehensive design method for outrigger braced frame buildings that is

validated against nonlinear time-history analysis using detailed numerical models and real subduction ground motions is available.

The review of the literature on optimum location of the outrigger, analysis of braced frame behavior under nonlinear seismic loads, and modeling the concentrically braced frames in OpenSees software were presented in this chapter. Beside the above main topics, the literature review provides the evaluation of safety of structures under FEMA P695 (2009) procedure. Theoretical background of fragility curves was presented in this chapter. The effect of torsion and type of scaling ground motions were also described herein.

Detailed numerical models for steel braced frame buildings developed using the OpenSees software are available in the literature. Furthermore, it was found that the effect of long duration earthquakes induces more damage into high-rise steel braced framed buildings than the typical crustal earthquakes. To complete the work proposed in the stated objectives, the designed outrigger braced frame buildings should be verified against the collapse safety acceptance criteria after the design method is developed.

Chapter 3. Design, Modelling and Nonlinear Dynamic Analysis of Low-rise, Middle-rise and High-rise MD-CBF Buildings

The design, modeling and nonlinear seismic response of low-rise (2-storey and 4-storey), middle-rise (8-storey), and high-rise (12-storey and 16-storey) prototype steel buildings were studied. All these buildings are braced with moderately ductile concentrically braced frames (MD-CBF). The same floor plan geometry was used for all buildings. These buildings are located in Victoria, B.C., Canada on Site Class C (firm soil) and are designed according to NBCC 2010 and CSA/S16 2009 standard. It is noted that Victoria is located in the vicinity of Cascadia subduction fault, this type of subduction earthquake has a return period of 500 years, and the last event was in 1700. The dynamic analysis by means of the numerical integration nonlinear time-history method was conducted on detailed building models using OpenSees. The purpose of studying the nonlinear seismic response of multi-storey MD-CBF buildings is two-fold: i) to identify the difference in the seismic response of MD-CBF buildings subjected to crustal versus subduction ground motions and ii) to validate the response of the proposed Outrigger Braced Frame system presented in Chapter 4 against a traditional braced frame as the MD-CBF.

3.1. Building description

The building occupancy type is an office which leads to normal importance category. The building has two identical lateral force resisting systems in each direction (MD-CBF). The floor plan of prototype building is shown in Fig.3-1a and the multi-storey building elevations in Fig. 3-1b. Loads applied of these buildings are also summarized in Fig. 3-1b.

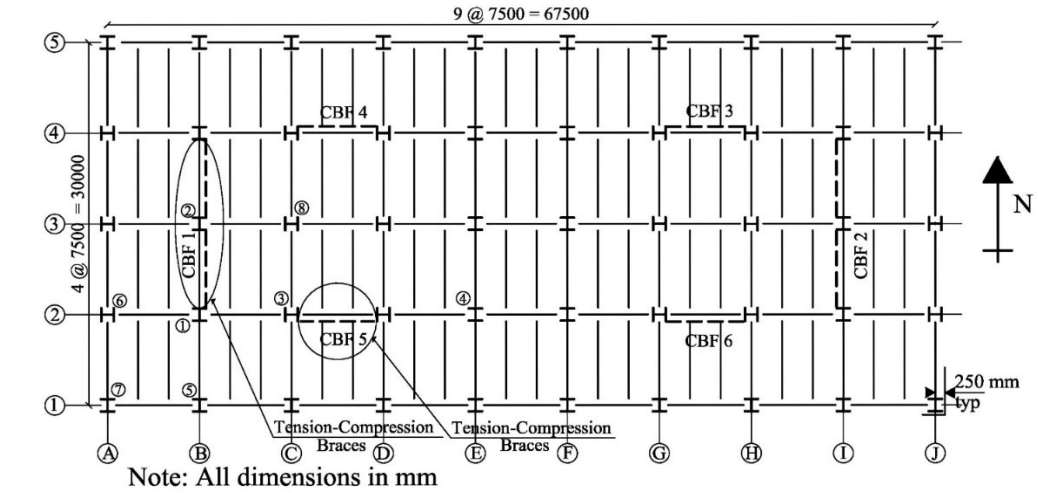

(a)

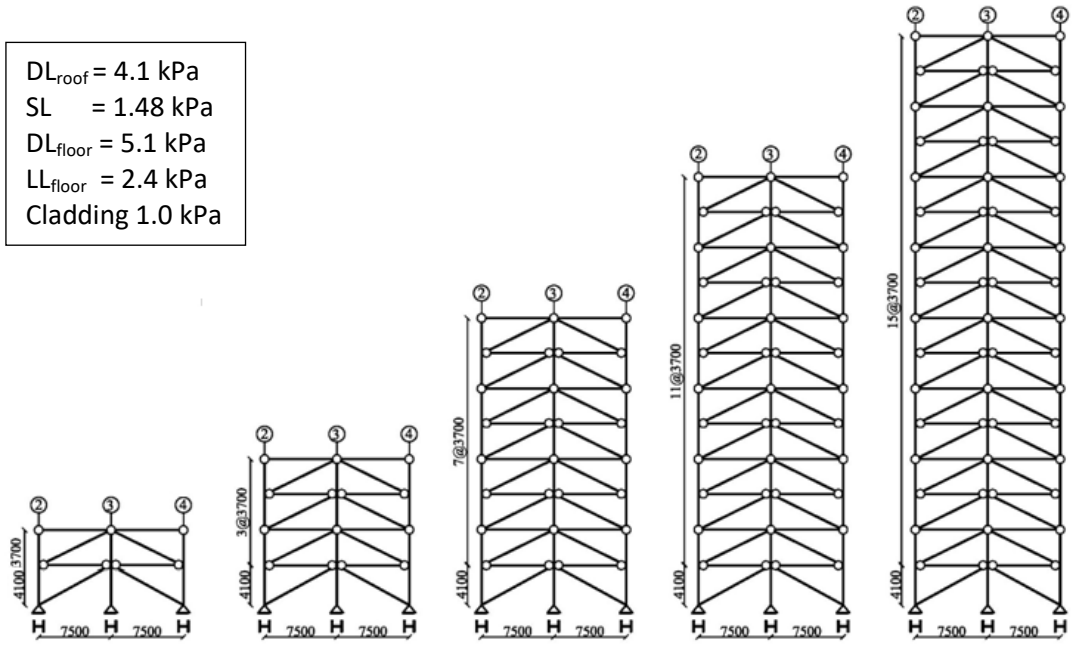

(b)

Figure 3-1 Building plan and CBF1 elevation of the 2-, 4-, 8-, 12- and 16-storey buildings

3.2. Design of Buildings

Buildings are designed according to National Building Code of Canada, NBCC 2010 edition. The load combinations are given in Table 3-1 where DL is the dead laod, LL is the live load, SL is the snow load, W is the wind load and E is the earthquake load.

Table 3-1 Load combinations as per NBCC 2010

Case	Load combination
1	1.4DL
2	1.25DL+1.5LL
3	1.25DL+1.5SL
4	1.25DL+1.4WL
5	1.0DL+0.5LL+0.25SL+1.0E

The minimum lateral earthquake force V, is computed according to the equivalent static force procedure using the following equation.

$$V = \frac{S(T_a)M_v I_E W}{R_d R_0} \quad 3\text{-}1$$

where: $S(T_a)$ is the design spectral acceleration corresponding to the fundamental period T_a, M_v is the higher mode factor on base shear, R_d is the ductility related-force modification factor, R_0 is the over strength related-force modification factor, W is the seismic weight and I_E is the importance factor for earthquake load.

Hence, V shall not be less than V_{min} as obtained from Eq. (3-2) and no greater than V_{max} as per Eq. (3-3).

$$V_{min} = \frac{S(2.0)M_v I_E W}{R_d R_0} \quad 3\text{-}2$$

$$V_{max} = \frac{\left(\frac{2}{3}\right)S(0.2)M_v I_E W}{R_d R_0} \quad 3\text{-}3$$

For concentrically braced frame, the equation for T_a is $T_a = 0.025h_n$ where h_n is the height of the building in meter. When dynamic analysis is employed a value of $2T_a$ can be considered. For all buildings, the height of ground floor is 4.1 m and that of typical floors is 3.7 m. The fundamental period of all MD-CBF buildings, as well as the seismic weight W is provided in Table 3-2. For the MD-CBF system, R_d is 3.0 and R_0 is 1.3. For Victoria, the uniform hazard spectrum ordinates at 0.2 s, 0.5 s, 1.0 s and 2.0 s are 1.2 g, 0.82 g, 0.38 g and 0.18 g, while the peak ground acceleration, PGA is 0.61. For the 4.0 s period, the spectral acceleration is 0.09 g which is half of S(2.0). It is worth noting that for Site Class C, the site coefficients F_a and F_v required for design spectral acceleration at the above periods are equal to 1.0. According to Eq. (3-3), the maximum spectral ordinate is 2/3S(0.2) = 0.8 g. In Table 3-2 the calculation is conducted for $T_a = 0.05\ h_n$.

Because S(0.2)/S(2.0) < 8 it results M_v =1.0. In the case of 2-storey MD-CBF building, V computed with Eq. (3-1) resulted greater than V_{max} shown in Eq. (3-3). Hence, in Table 3-2 it is provided the base shear for the 2-storey building, V_{max}. The base shear provided for the 12-storey and 16-storey building in Table 3-2 is computed for V_{min} given in Eq. (3-2). In the preliminary design it is allowed to consider $0.8V_{min}$ in the case that the building is regular and has less than 60 m height. As depicted in Fig. 3-1, this building does not have the vertical stiffness irregularity, mass irregularity, nor discontinuity in capacity, out-of-plane offsets or in-plane discontinuity in vertical lateral-force-resisting element irregularity.

Torsional sensitivity irregularity exists when the ratio B computed for each level exceeds 1.7 at least at one floor. This ratio is computed as: $B_x = \delta_{max}/ \delta_{ave}$ where δ_{max} is the maximum storey displacement at the extreme points of the structure at level *x* in the direction of the earthquake induced by the equivalent static forces acting at a distance equal to $\pm 0.1D_{nx}$ from the centres of mass at each floor and δ_{ave} is the average of storey displacements at these extreme points. Herein, D_{nx} is the plan dimension of the building perpendicular to the direction of seismic loading. The maximum value of B_x resulted among floors is given in Table 3-2. As resulted, the building is not torsional sensitive. In Table 3-2 it is also provided the value of 0.8V for all buildings.

Table 3-2 Buildings characteristics according to the equivalent static force procedure

Building	h_n [m]	$T_a=0.025h_n$ [s]	$T_a=0.05h_n$ [s]	W [kN]	B_x	V [kN]	0.8V [kN]
2-storey	7.8	0.195	0.39	19537	1.153	4008	3206
4-storey	15.2	0.38	0.76	40812	1.313	6488	5190
8-storey	30	0.75	1.50	81904	1.317	5880	4704
12-storey	44.8	1.12	2.24	124137	1.319	5729	4583
16-storey	59.6	1.49	2.98	167388	1.307	7788	6230

Both the torsional effect and the P-Δ effect were considered in design. As depicted in Fig. 3-1, the building is symmetric in both orthogonal directions and the location of center of mass and resistance is the same. The torsion is caused by accidental eccentricity considered as $\pm 0.1D_{nx.}$ The shear amplification factor U_2 caused by P-Δ effects it amplifies the translational load.

$$U_2 = 1 + \frac{\Sigma C_f R_d \Delta_f}{\Sigma V_f h} \qquad 3\text{-}4$$

where, ΣV_f is the design shear force resulted from earthquake loads at the calculation level, ΣC_f is the tributary axial force associated to the gravity component (DL+0.5LL+0.25SL) of the earthquake load combination at the calculation level, h is the storey height and Δ_f is the interstorey drift. If U_2 is less than 1.1, the P-Δ effect is not considered. When $U_2 > 1.4$ the structure is not stable and the stiffness should be increased. When $1.1 \leq U_2 < 1.4$, the base shear is amplified with the resulted coefficient.

The design of MD-CBF members was performed in accordance with CSA/S16-2009 standard. Thus, braces made of HSS-shape sections were selected to be Class 1 and beams and columns selected as W-shape were designed as Class 1 or Class 2. The nominal yield strength of all structural sections is F_y = 350MPa and the tensile strength F_u = 450MPa.

The diagonal brace members of braced frames were designed as tension-compression members such that the axial factored load to be less or equal to the axial compression resistance C_r:

$$C_r = \Phi A F_y (1 + \lambda^{2n})^{-1/n} \qquad 3.5$$

where Φ = 0.9, λ is the slenderness computed as: $\lambda = \frac{KL}{r}\sqrt{\frac{F_y}{\pi^2 E}}$, KL is the effective brace length, r is the radius of gyration in the direction of brace buckling, A is the area of brace cross-section and E is the elastic modus of elasticity of steel. For members acting in tension-compression, the slenderness ratio KL/r is limited to 200. The tensile resistance T_r is calculated from Eq. (3-6).

$$T_r = \Phi A_g F_y \qquad 3\text{-}6$$

The probable tensile strength is $T_u = A_g R_y F_y$ where RyFy is the probable yield stress. The product $R_y F_y$ shall be taken 385 MPa for W-shape members where R_y = 1.1 and not less than 460 MPa for HSS sections. However, same experimental tests on HSS sections showed $R_y F_y$ less than 460 MPa. For this reason, a value of 385 MPa was considered for HSS members, as well. The probable compressive resistance of HSS brace C_u is equal to $min\left(A_g R_y F_y, \frac{1.2 R_y C_r}{\Phi}\right)$ and the probable post-buckling compressive resistance of braces C_u' is computed as $min\left(0.2 A_g R_y F_y, \frac{R_y C_r}{\Phi}\right)$. Beams of MD-CBFs are designed by considering the following two loading conditions: i) the compression acting braces attaining their probable compressive resistance C_u in conjunction with the tension acting brace developing the probable tensile resistance T_u, ii) the compression acting braces attaining their probable post-buckling

compressive resistance C_u' in conjunction with the tension acting brace developing its probable tensile resistance T_u. Columns in braced bays are designed as beam-columns and are continuous with constant cross-section over a minimum of two storeys. Columns are designed to carry the gravity load component of earthquake loading combination in addition to axial forces triggered from braces capacity C_u and T_u but no greater than the verical projection of factored forces developed in braces that are associated to $R_d = 1.5$ and $R_0 = 1.3$. An additional bending moment of $0.2ZF_y$ is applied in the direction of the braced bay. The capacity of beam-column members is computed and examined for: a) cross-sectional member strength where C_r is calculated with $\lambda = 0$, b) overall member strength calculated with C_r computed for the axis of bending, c) lateral torsional buckling computed with C_r corresponding to weak-axis. Members of Class 1 and Class 2 sections of I-shaped members required to resist bending moments and axial compressive force are proportioned as:

$$\frac{C_f}{C_r} + \frac{0.085 U_{1x} M_{fx}}{M_{rx}} \leq 1.0 \qquad 3\text{-}7$$

where $U_1 = [\frac{\omega_1}{1-\frac{C_f}{C_e}}]$ and $c_e = \frac{\pi^2 EI}{L^2}$. For column members which are not subjected to transverse loads between supports, $\omega_1 = 0.6 - 0.4k \geq 0.4$ where k is the ratio of the smaller factored moment to the larger factored moment at opposite ends of the member length. Because the bending moment is zero at one end it leads to $\omega_1 = 0.6$. In case of bending moment and axial tension force the interaction equation is:

$$\frac{T_f}{T_r} + \frac{M_x}{M_r} \leq 1.0 \qquad 3\text{-}8$$

From preliminary design associated to the equivalent static force procedure, the MD-CBF member cross-sections of the 2-storey, 4-storey, and 8-storey buildings are shown Table 3-3 and those of the 12-storey and 16-storey building in Table 3-4. Cross-sections for HSS braces, W-shape columns and W-shape beams provided in Tables 3-3 and 3-4 were selected to comply with forces resulted from seismic load combination, as well as, the wind load combination.

To verify the dynamic response, firstly, all buildings were analysed using the dynamic analysis procedure by means of modal response spectrum method using the ETABS software. The results in terms of first-mode period and base shear from earthquake loads are provided in Table 3-5. The accidental torsion effect was also considered in the ETABS model, as well as the P-Δ effect. As resulted, there is about 20% torsion caused by accidental eccentricity added to the shear force.

It is noted that forces resulted from ETABS where scaled up to match at least 0.8V resulted from the static equivalent procedure.

Table 3-3 Members sections for the 2-storey, 4-storey and 8-storey buildings

Floor	Brace	Beam	Middle column	Side column
2-storey building				
2	HSS 254x254x13	W360x72	W360x122	W310x91
1	HSS 203x203x9.5	W360x110	W360x122	W310x91
4-storey building				
4	HSS 178x178x13	W360x79	W360x110	W360x91
3	HSS 203x203x13	W360x79	W360x110	W360x91
2	HSS 254x254x13	W360x110	W360x179	W360x179
1	HSS 254x254x13	W360x110	W360x179	W360x179
8-storey building				
8	HSS 152x152x9.5	W360x64	W360x122	W360x79
7	HSS 178x178x13	W360x106	W360x122	W360x79
6	HSS 203x203x13	W360x106	W360x237	W360x147
5	HSS 203x203x13	W360x128	W360x237	W360x147
4	HSS 228x228x13	W360x128	W360x382	W360x262
3	HSS 228x228x13	W360x144	W360x382	W360x262
2	HSS 254x254x13	W360x144	W360x551	W360x347
1	HSS 254x254x13	W360x144	W360x551	W360x347

Table 3-4 Members sections for the 12-storey and 16-storey buildings

Floor	Brace	Beam	Middle column	Side column
12-storey building				
12	HSS 152x152x8	W360x64	W360x122	W360x110
11	HSS128x128x9.5	W360x91	W360x122	W360x110
10	HSS203x203x9.5	W460x106	W360x216	W360x134
9	HSS203x203x9.5	W360x110	W360x216	W360x134
8	HSS203x203x9.5	W360x110	W360x347	W360x347
7	HSS203x203x13	W360x128	W360x347	W360x347
6	HSS203x203x13	W360x128	W360x509	W360x463
5	HSS203x203x13	W360x128	W360x509	W360x463
4	HSS228x228x13	W360x128	W360x634	W360x592
3	HSS228x228x13	W360x128	W360x634	W360x592
2	HSS254x254x13	W460x144	W360x818	W360x634
1	HSS254x254x13	W460x144	W360x818	W360x634
16-storey building				
16	HSS178x178x8	W360x64	W360x122	W360x110
15	HSS178x178x8	W360x110	W360x122	W360x110
14	HSS203x203x9.5	W360x110	W360x216	W360x134
13	HSS203x203x9.5	W460x106	W360x216	W360x134
12	HSS203x203x9.5	W460x106	W360x347	W360x237
11	HSS203x203x9.5	W460x106	W360x347	W360x237
10	HSS203x203x13	W460x128	W360x509	W360x347
9	HSS203x203x13	W460x128	W360x509	W360x347
8	HSS203x203x13	W460x128	W360x634	W360x463
7	HSS228x228x13	W460x144	W360x634	W360x463
6	HSS228x228x13	W460x144	W360x744	W360x634
5	HSS228x228x13	W460x144	W360x744	W360x634
4	HSS228x228x13	W460x144	W360x900	W360x744
3	HSS254x254x13	W460x144	W360x900	W360x744
2	HSS254x254x13	W460x158	W360x1086	W360x990
1	HSS254x254x13	W460x158	W360x1086	W360x990

Table 3-5 Buildings characteristics according to linear dynamic analysis (ETABS)

Parameter	2-storey	4-storey	8-storey	12-storey	16-storey
T_1 (s)	0.41	0.74	1.38	2.24	3.04
T_2 (s)	0.18	0.28	0.48	0.78	1.03
V (kN)	4008	6488	5880	5729	6230

3.3. Nonlinear dynamic analysis

The nonlinear response of buildings is obtained by means of nonlinear time-history analysis using the OpenSees framework. The 2-D model developed in OpenSees considers half of the building depicted in Fig. 3-1. An example developed for the 4-storey building is showed in Fig. 3- 2.

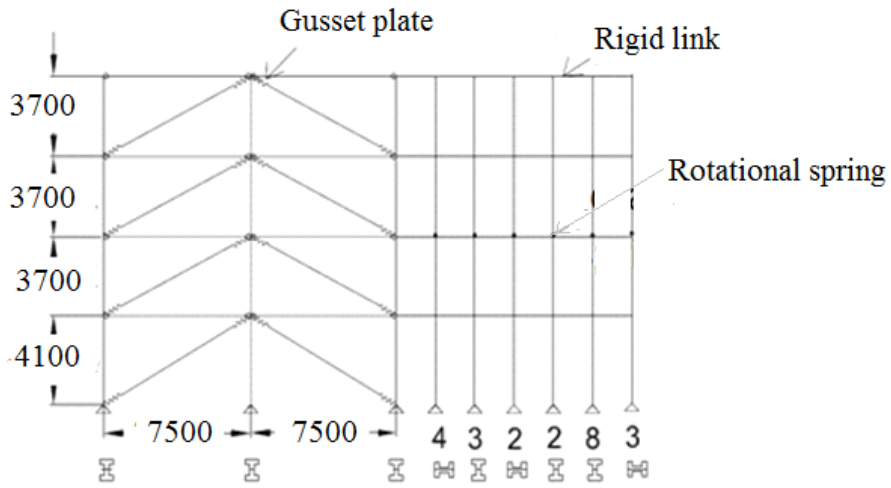

Figure 3-2 Schematic model for half of 4-storey building developed in OpenSees

The model includes two adjacent bays of MD-CBFs and the associated gravity columns connected with rigid links to simulate the effect of rigid diaphragm. Half of the building mass was assigned to nodes of MD-CBFs.

Braces of MD-CBFs are modelled as force-based nonlinear beam-column elements with distributed plasticity. Each HSS brace is made of 20 nonlinear beam-column elements with four integration points per element and fiber cross-section discretization. Each HSS cross-section simulated with rounded corners is divided in 280 fibers as shown in Fig. 3-3. The *Steel02* with isotropic strain hardening material, known as Giuffré-Menegotto-Pinto material, is assigned to all brace fibers. For considering the isotropic hardening, the parameters are: R_0 = 25, cR1 = 0.925, cR2 = 0.15; a1= a3= 0.00001, a2 = a4 = 0.00002, while the kinematic hardening parameter b was set to 0.01. Two initial cambers of L/500 were assigned to each brace (e.g. one in-plane and other out-of-plan). To simulate the effect of low-cycle fatigue, the fatigue material was wrapped around parental material *Steel02*. The low-cycle fatigue material parameters were

defined with m =-05 and $\boldsymbol{\varepsilon_{0pred} = 0.006\left(\frac{KL}{r}\right)^{0.859}\left(\frac{w}{t}\right)^{-0.6}\left(\frac{E}{F_y}\right)^{0.1}}$. These fatigue material parameters were proposed in Tirca and Chen (2014) and were calibrated against seven tests from the literature.

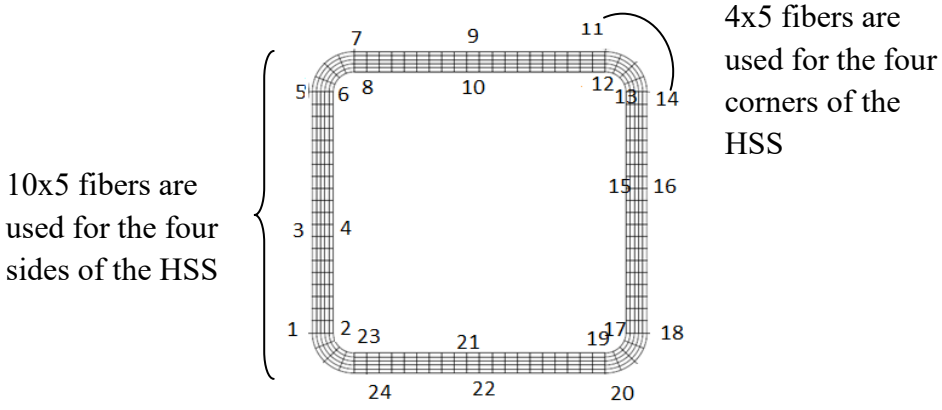

Figure 3-3 The HSS brace cross- section discretization with round corners using 280 fibers

As depicted in Fig. 3-2, braces are connected to the frame by means of gusset plate connections. The HSS brace dissipate energy when buckles in compression and yield in tension. These HSS braces are designed to buckle out-of-plane and to fracture after a plastic hinge is formed at their middle-length after its rotation capacity is consumed. To allow braces to deflect out-of-plane, the brace to frame gusset plate connections need to follow the brace deformation by deforming in bending and possible to form plastic hinge within the *2t* clearance distance of gusset plate. The rigid part of gusset plate is simulated with a rigid link attached to the brace member by means of the Zero-length element where two rotational springs and a torsional spring were inserted. One rotational spring simulates the out-of-plane bending with stiffness corresponding to the Whitmore width cross-section. The other rotational spring captures the in-plane bending and the considered stiffness is equivalent to that of HSS brace. The torsional spring captures the torsional effect with stiffness explained in Chapter 2, Eq. (2-5). The *Steel 02* material was assigned to rotational spring and elastic material to torsional spring.

Each MD-CBF column was modeled with 8 nonlinear beam-column elements with distributed plasticity and 4 integration points per element. The W-section of column is fiber based. In plan camber equal to L/1000 was assigned to each column. *Steel02 with Isotropic Strain Hardening* material was assigned to columns considered continuous for two stories. These column segments

were connected using the Zero-length elements. The splice connection between the two column segments was modeled with high rotational stiffness assigned out-of-plan and very small rotational stiffness in-plan. Beams were modeled as elastic beam-column elements. All beams are pinned connected to columns and their connection was explained in Section 2.5.1.6. Gravity columns were modeled as elastic beam-column elements. They are considered continuous for two floors and connected by shear splices with zero bending moment. The shear splice consists of two steel plates located on each side of the column web and connected together with number of bolts calculated to carry the shear force at the splice location as shown in Fig 3-4.

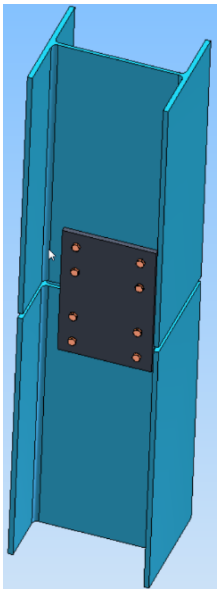

Figure 3-4 Shear splice columns connection

It is noted that the gravity load assigned to gravity columns resulted from combination (DL+0.5LL+0.25SL). To capture the higher mode contributions, the 2% Rayleigh damping was specified in the first-mode and second-mode of vibration for 2-storey building, and first-mode and third-mode of vibration for the 4-storey building and 8-storey building and the first-mode and forth-mode of vibration for the 12-storey and 16-storey buildings.
Modeling summarization for the considered 2-D model is shown on the Fig 3-5.

The reason for modeling half of the building including the associated lateral load resisting systems and corresponding gravity columns is to reduce the time of analysis. Molding the whole building will not change the results became of building's symmetrical geometry.

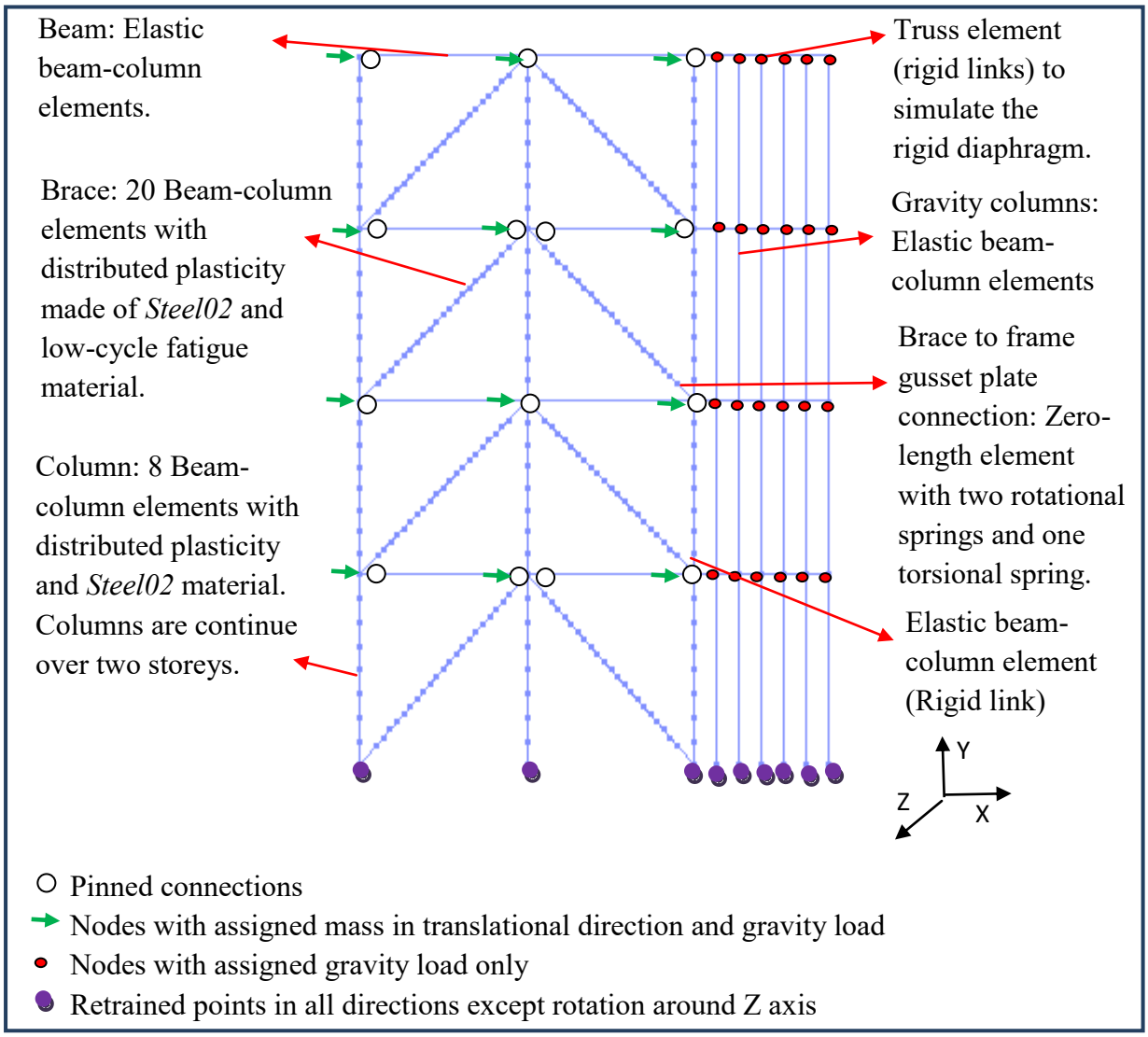

Figure 3-5 OpenSees model for 4-storey MD-CBF building

3.4. Seismic response of MD-CBF buildings

3.4.1. General

This section describes the response of low, middle, and high-rise MD-CBF buildings under selected two sets of ground motions, the crustal ground motions, and the mega-thrust subduction ground motions. Table 3-6 shows the first-mode and second-mode period resulted from OpenSees for studied MD-CBF buildings. As resulted, the period is similar with that obtained from ETABS that was provided in Table 3-5.

Table 3-6 Buildings characteristics according to nonlinear dynamic analysis (OpenSees)

Period	2-storey	4-storey	8-storey	12-storey	16-storey
T_1 (s)	0.38	0.69	1.40	2.27	3.01
T_2 (s)	0.16	0.26	0.49	0.78	1.03

3.4.2. Selected and scaled ground motions

For Victoria, B.C., the important contributions to seismic hazard are moderate to large crustal earthquakes of magnitudes M 7.0 – M 7.5, as well as, the megathrust earthquake of magnitudes M 8.0 – M 9.0 that may occur along the Cascadia subduction fault. Thus, the uniform hazard spectrum, UHS, for Victoria is a combination of the deterministic Cascadia hazard with the probabilistic crustal hazard. The Cascadia subduction source contribution to the probabilistic model increases the seismic demand. The parameters used to represent seismic hazard for Victoria are the 5% damped horizontal spectral acceleration for 0.2, 0.5, 1.0 and 2.0 s periods, S(T), the horizontal peak ground acceleration, PGA, and peak ground velocity, PGV, with values given for 2% probability of being exceeded in 50 years. The 5% damped horizontal spectral acceleration of design spectrum for the aforementioned periods is given in Table 3-7. It is noted that the UHS and the design spectrum is the same for Site Class C because the acceleration and velocity coefficients are equal to 1.0.

Table 3-7 Design spectrum ordinates for design spectrum of Victoria, Site Class C

Period (s)	0.2	0.5	1.0	2.0
$S_a(T_a)$ (g)	1.2	0.82	0.38	0.18

The selection of crustal ground motions was made such that these records to be compatible with geotechnical conditions for Victoria, Site Class C, defined when the average shear wave velocity $\overline{V}_s$ in top 30 m layer is in the range of 360 m/s < $\overline{V}_s$< 760 m/s. Thus, seven records compatible for Site Class C in Victoria were selected from the PEER Ground Motion Database Beta Version (2010).

The subduction records were selected from the megathrust M 9.0 Tohoku earthquake in Japan (March 11, 2011) as explained in Tirca and Chen (2015). The similarity between the potential Cascadia subduction earthquake and Tohoku earthquake is illustrated in Fig. 3-6. These records were selected from the website: www.k-net.bosai.go.jp.

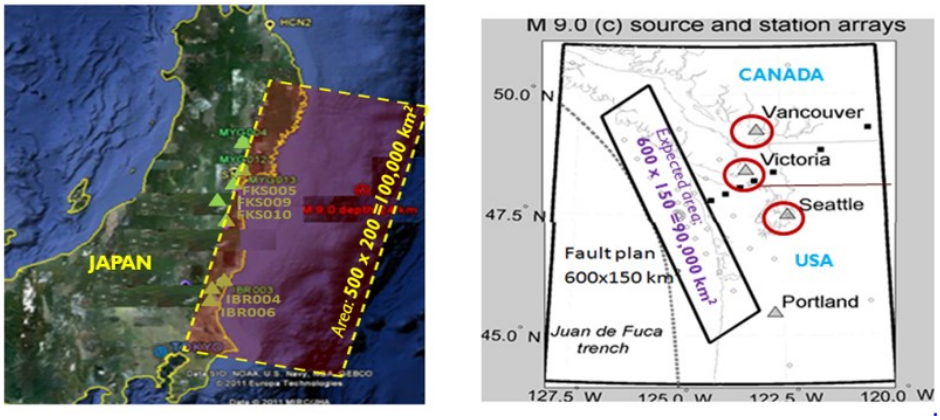

Figure 3-6 Similarities between the potential Cascadia subduction earthquake source and its proxy Tohoku earthquake

The crustal and subduction ground motions are given in Table 3-8 together with the peak ground acceleration, *PGA*, peak ground velocity, *PGV*, the *PGV/PGA* ratio, the total duration, *t,* the Trifunac duration, t_d, the predominant period of ground motions, T_p, and the main period, T_m.

Among the seven crustal ground motions, six have a total duration around 40 s and one has 60 s, while the average value of the Trifunac duration is about 11.3 s. The average shear wave velocity of the seven crustal ground motions is 424 m/s with a minimum value of 360 m/s and a maximum value of 489 m/s. The average value of PGV and PGA of selected crustal ground motions is 0.28 m/s and 0.33 g, respectively, while the average value of the predominant and mean period of selected crustal ground motions is 0.21 s and 0.53 s, respectively.

In comparison, the selected Tohoku ground motions show duration of 300 s and the average of the Trifunac duration is 67 s. These values are six times greater than those corresponding to crustal ground motions. The average shear wave velocity is in the same range with that computed for the crustal records set, while the average value of PGV and PGA is 0.39 m/s and 0.8 g, respectively. Thus, there is no great difference in the average PGA but the average PGV is about three time greater in the case of subduction records than crustal records. However, Tohoku records are characterized by high frequency with an average T_p value of 0.25 s and an average T_m value of 0.19 s. By comparison with crustal records, the predominant period is in the same range, while the mean period is about three times lower. At the same time, some Tohoku records are characterized by a combination of two wave shapes arising from the propagation of rupture along

the shore, while following a north – south axis. In this light, the S1, S2, S3 records show a double pulse wave, while the others are characterized by a single wave similar to crustal records.

Table 3-8 Characteristics of selected crustal and subduction ground motions

#	Event, M	Station	R[3]; Comp Km; Degree	PGA (g)	PGV (m/s)	t; t_d (s)	T_p; T_m (s)
Subduction ground motions[1]							
S1	Tohoku'11, M9	MYG001	155 EW	0.43	0.23	300; 83	0.27; 0.26
S2	Tohoku'11, M9	MYG004	184 EW	1.22	0.48	300; 85	0.26; 0.25
S3	Tohoku'11, M9	FKS005	175 EW	0.45	0.35	300; 92	0.32; 0.15
S4	Tohoku'11, M9	FKS010	189 EW	0.86	0.56	300; 66	0.27; 0.18
S5	Tohoku'11,M9	FKS009	216 EW	0.83	0.44	300; 74	0.20; 0.20
S6	Tohoku'11, M9	IBR004	273 EW	1.03	0.38	300; 33	0.21; 0.15
S7	Tohoku'11, M9	IBR006	283 EW	0.78	0.3	300; 36	0.25; 0.12
Crustal ground motions[2]							
C1	Northridge, M6.7	Castaic Old Ridge	44; 90	0.57	0.52	45; 9.10	0.26; 0.54
C2	Northridge, M6.7	LA, UCLA Grd.	25; 90	0.28	0.22	60; 11.3	0.22; 0.34
C3	Northridge, M6.7	Moorpark – Fire	36; 180	0.29	0.20	40; 14.2	0.26; 0.47
C4	Loma Prieta, M6.9	Gilroy Array #3	36; 0	0.56	0.36	39.9; 6.4	0.20; 0.37
C5	Loma Prieta, M6.9	Palo Alto, SLAC	54; 360	0.28	0.29	39.6;11.6	0.30; 0.65
C6	Loma Prieta, M6.9	Apeel 9 Crystal S	41; 227	0.11	0.18	40; 16.2	0.30; 0.88
C7	Loma Prieta, M6.9	Anderson Dam Ds	20; 250	0.25	0.20	40; 10.4	0.20; 0.46

[1] Subdaction ground motions were selected from: www.k-net.bosai.go.jp

[2] Crustal ground motions selected from: http://peer.berkeley.edu/peer_ground_motion_database/

[3] In this table is it illustrated the hypo central distance and not the distance to the fault.

According to ASCE/SEI 7-10 procedure, each set of seven ground motions were scaled such that their acceleration response spectrum to match or be above the design spectrum over the period of interest ranging from $0.2T_1$ to $1.5T_1$, where T_1 is the first mode period of studied building. It is noted that the scaling procedure adopted in ASCE/SEI 7-10 standard emerged from the method proposed by Reyes and Kalkan (2009). For each studied building, the scaling factor used for crustal ground motions is shown in Table 3-9, where NGA is the record identification in the

website. It is worth to note that the subduction records were selected such that their mean to match the design spectrum. Thus, a scaling factor equal to 1.0 was used for all these records.

The acceleration response spectrum of scaled crustal and seduction records are illustrated in Fig.3-7 for the 2-storey, 4-storey and 8-storey buildings and in Fig. 3-8 for the 12-storey and 16-storey buildings together with the mean value and the design spectrum for Victoria, B.C., Site Class C. The acceleration response spectrum obtained from the selected Tohoku records show very large ordinates in the short period range 0.1s - 0.35 s which mostly excite low-rise buildings. However, buildings with a fundamental period larger than 1.6 s are not exposed to increase earthquake demand. Although in the interval 0.7s - 0.8 s the average spectrum shows a slightly lower value than that required by design spectrum, the scale factor was not raised above 1.0.

Table 3-9 Scaling factors of crustal ground motions

#	Record NGA	SF (2-storey)	SF (4-storey)	SF (8-storey)	SF (12-storey)	SF (16-storey)
C1	963-90	1.20	0.86	0.85	1.2	1.00
C2	1006-90	2.50	1.95	1.35	2.3	2.20
C3	1039-180	2.50	1.90	1.50	2.3	2.20
C4	767-0	1.30	1.00	1.70	1.7	2.20
C5	787-360	1.50	1.39	1.65	1.7	1.70
C6	736-227	3.50	3.28	2.72	2.0	2.00
C7	739-250	2.50	1.70	2.20	2.5	2.50

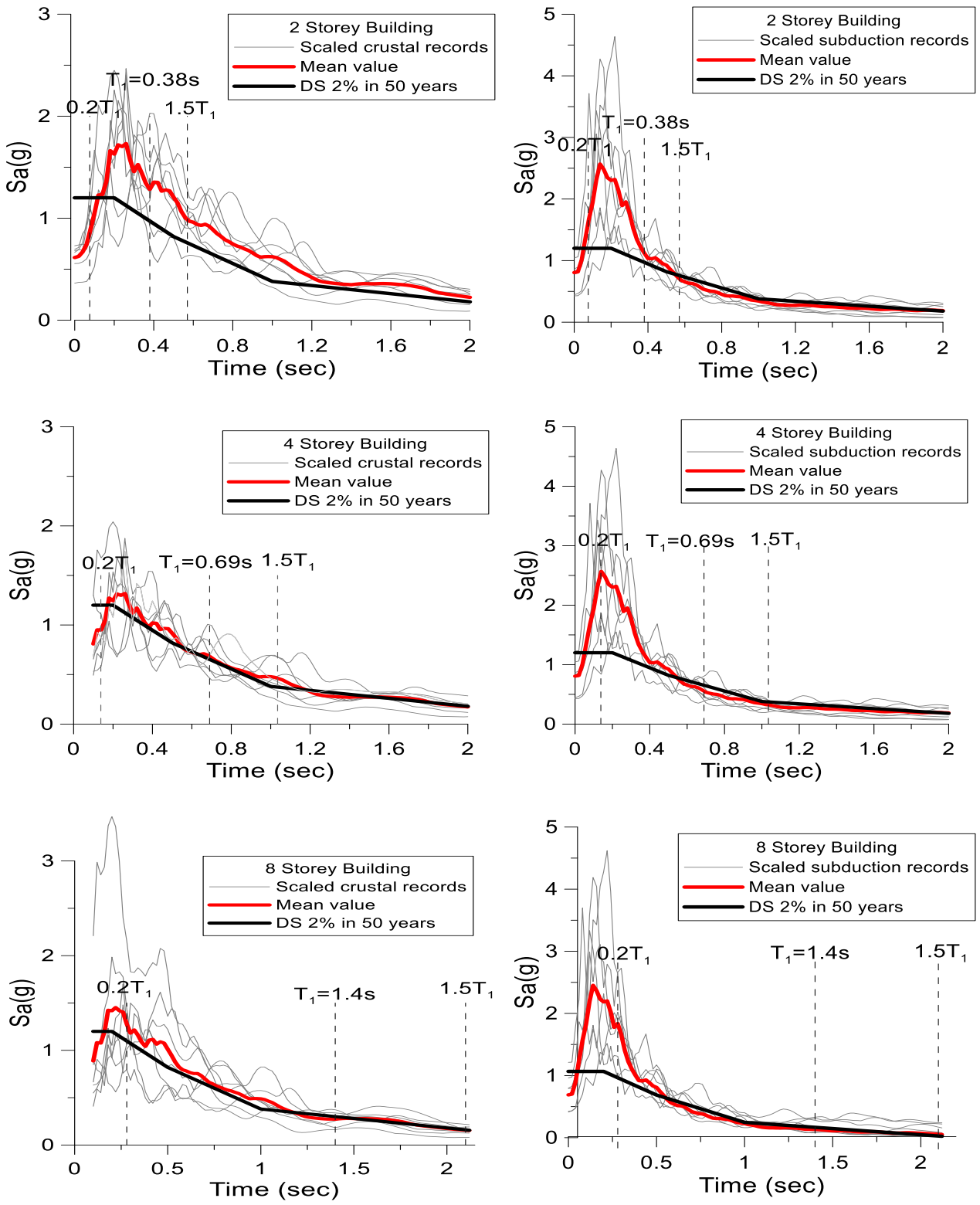

Figure 3-7 Scaled response spectra of 2-storey, 4-storey, and 8-storey buildings

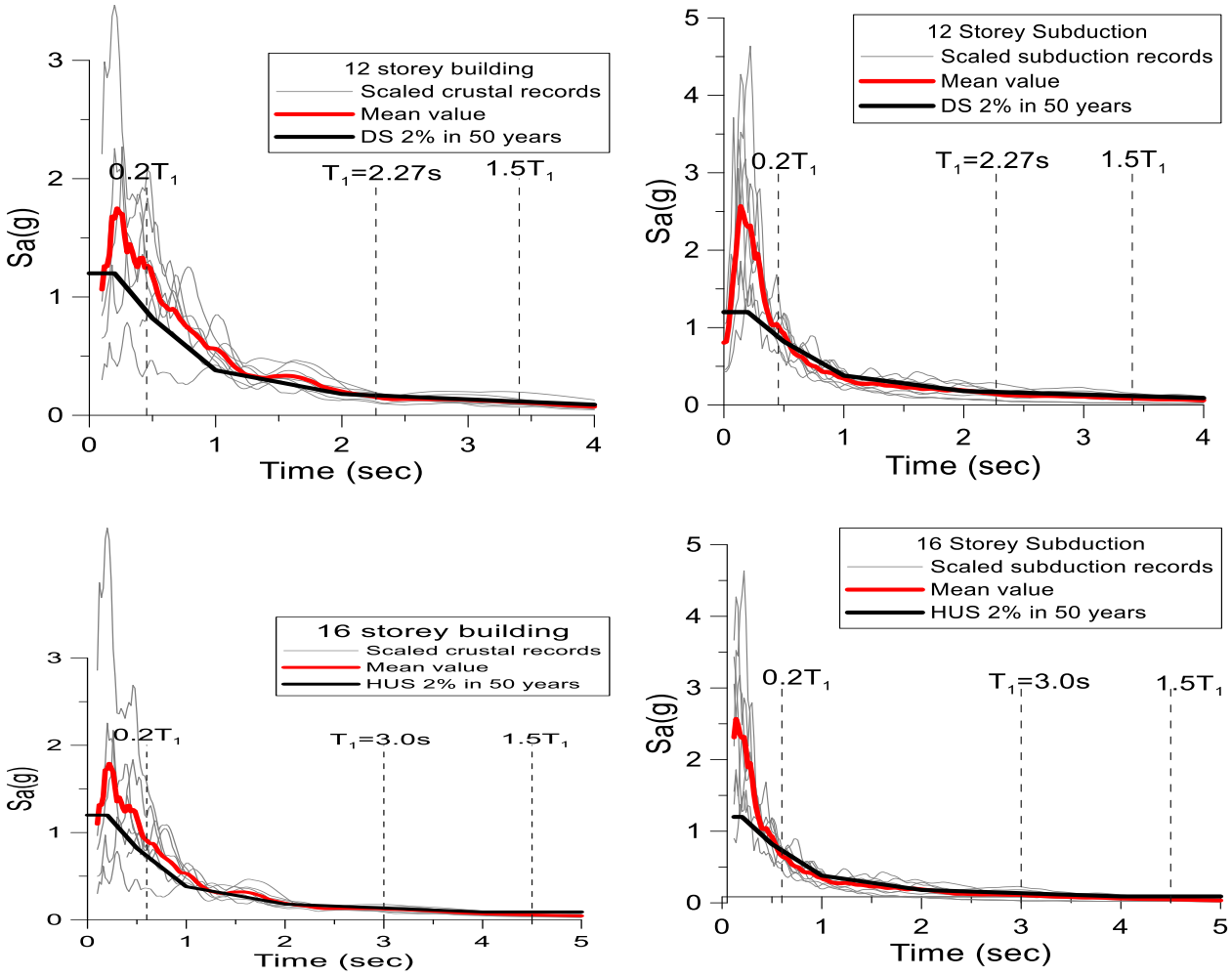

Figure 3-8 Scaled response spectra of 12-storey and 16-story buildings

3.4.3. Seismic response of MD-CBF buildings

OpenSees software was used to calculate the nonliner dynamic response of moderately ductile concentrically braced frames (MD-CBF) for low-rise, middle-rise, and high-rise buildings located in Victoria B.C. To emphasize the differences in the nonlinear response of multistory MD–CBF buildings subjected to subduction records compared to crustal records, the following response parameters were investigated: i) Interstorey drift, ii) Residual interstorey drift and iii) Damage index computed to account for strain accumulated in HSS brace cross-section fibers at the location of plastic hinge formation.

It is noted that the shear generated from torsion caused by accidental eccentricity was considered in the preliminary design in addition to the P-Δ effect and the ratio between the total base shear including the shear from torsion caused by accidental eccentricity and the base shear without the

consideration of accidental eccentricity is about 1.2 for all buildings. Thus, in order to obtain consistent results, the accelerograms of both crustal and subduction sets were re-amplified by the about 1.2 factor as presented in Table 3-10.

Table 3-10 Ratio of the torsional base shear to the total base shear resulted from static analyses for studied buildings

St.	C_f in brace from shear (kN)	C_f in brace from torsion (kN)	Shear per floor (pure shear) (kN)	Shear per floor (from torsion) (kN)	Total shear V_s (kN)	Total shear from torsion, V_t (kN)	Total shaer V (kN)	V_t/V
2-storey building								
2	773	192	1400	349	1400	349	1749	0.2
1	1238	315	2173	572	3573	920	4493	0.2
4-storey building								
4	682	171	1237	309	1237	309	1546	0.2
3	1138	281	2063	509	3299	818	4117	0.2
2	1477	372	2677	674	5976	1492	7468	0.2
1	1745	428	3062	752	9038	2244	11282	0.2
8-storey building								
8	484	116	877	211	877	211	1088	0.19
7	766	194	1389	352	2266	563	2829	0.2
6	991	243	1797	440	4062	1002	5065	0.2
5	1110	277	2011	486	6074	1488	7562	0.2
4	1283	312	2325	565	2325	565	2890	0.2
3	1425	344	2583	623	4908	1188	6096	0.19
2	1562	390	2830	706	7738	1894	9632	0.2
1	1743	422	3059	741	10798	2635	13433	0.2
12-storey building								
12	386	92	700	166	700	166	867	0.19
11	646	154	1171	280	1871	446	2318	0.19
10	773	192	1402	347	3273	793	4066	0.2
9	858	213	1555	373	4828	1167	5995	0.19
8	904	224	1639	406	1639	406	2045	0.2
7	981	248	1778	450	3417	856	4273	0.2
6	1038	262	1882	474	5300	1330	6630	0.2
5	1169	285	2119	501	7418	1831	9249	0.2
4	1262	311	2288	563	2288	563	2851	0.2
3	1387	340	2513	617	4801	1180	5981	0.2
2	1536	374	2783	677	7584	1857	9441	0.2
1	1666	411	2924	720	10508	2577	13086	0.2

St.	C_f in brace from shear (kN)	C_f in brace from torsion (kN)	Shear per floor (pure shear) (kN)	Shear per floor (from torsion) (kN)	Total shear V_s (kN)	Total shear from torsion V_t (kN)	Total shear V (kN)	V_t/V
16-storey building								
16	308	73	559	132	559	132	691	0.19
15	519	126	941	229	1500	360	1860	0.19
14	643	158	1165	286	2666	646	3312	0.2
13	721	181	1306	317	3971	963	4935	0.2
12	803	199	1455	362	1455	362	1817	0.2
11	874	219	1583	397	3038	759	3797	0.2
10	936	234	1697	424	4735	1183	5918	0.2
9	1005	254	1821	445	6556	1629	8184	0.2
8	1075	265	1948	481	1948	481	2429	0.2
7	1141	283	2067	513	4015	994	5009	0.2
6	1190	292	2156	529	6171	1523	7694	0.2
5	1261	326	2286	573	8457	2096	10553	0.2
4	1339	333	2428	604	10885	2699	13584	0.2
3	1412	356	2559	645	13444	3344	16788	0.2
2	1489	373	2699	654	16143	3998	20141	0.2
1	1633	412	2866	746	19009	4744	23753	0.2

3.4.3.1. **Interstorey drift**

The interstorey drift of studied MD-CBF buildings subjected to scaled crustal ground motions and subduction ground motions is depicted in Fig. 3-9 and Fig. 3-10, respectively. The 50 percentile and 84 percentile interstorey drift are also provided in these figures. Crustal ground motions excite mostly the upper part of buildings, while the subduction records excite mostly the lower part. This observation is not applicable for the 16-storey building where both ground motion sets excite mostly the upper floors. As depicted, the peak interstorey drift is below 2.5% h_s for all buildings but no for the16-storey building. However, the peak of 84 percentile interstorey drift of the 16-storey building is less than 2.5% h_s. In general, the amplitudes of interstorey drift resulted for studied buildings under both ground motion sets are similar.

The interstorey drifts of studied buildings under the re-scaled crustal and subduction records by 1.2 factor are plotted in Fig. 3-11 and 3-12, respectively. The trend in drift response of the studied buildings is found to be similar, while the interstorey drift is amplified as the building

height increases. In all cases, the peak of 84 percentile interstorey drift is found to be below the 2.5% h_s.

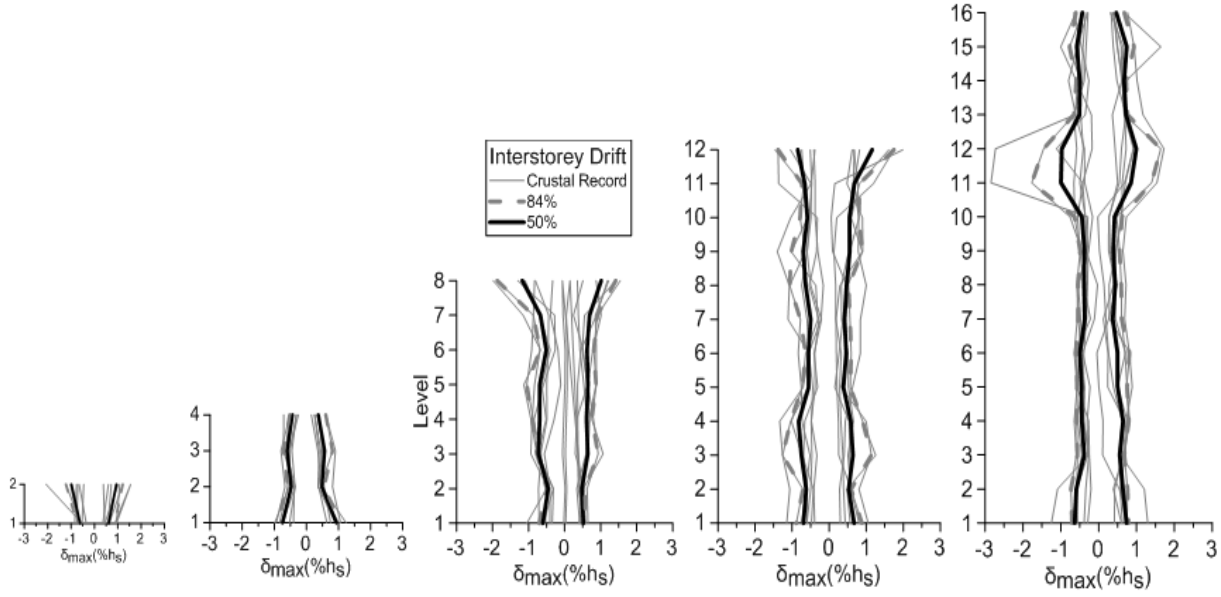

Figure 3-9 Interstorey drift of studied MD-CBF buildings under scaled crustal ground motions

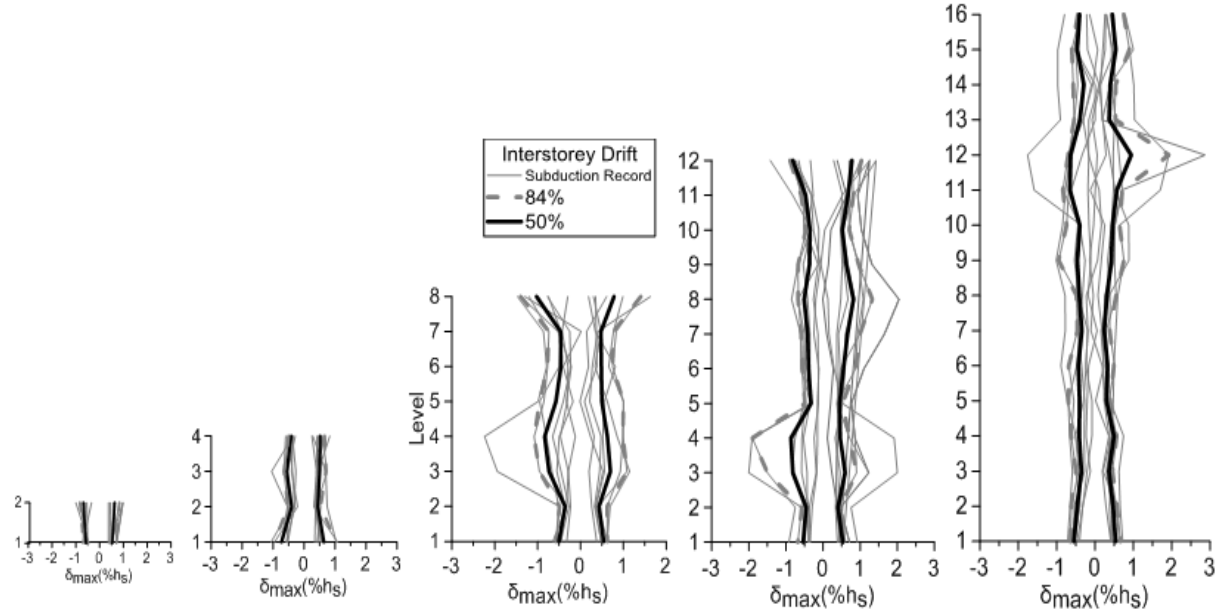

Figure 3-10 Interstorey drift of studied MD-CBF buildings under subduction ground motions

It is noted that the aforementioned interstorey drift results presented in terms of peak 84 percentile and 50 percentile interstorey drift among floor is presented in Table 3-11 and Table 3-

12 under the scaled and re-scaled crustal ground motions and subduction ground motions, respectively. It is noted that there is one re-scaled crustal record that driven the 16-storey building to experience brace fracture at the 12 floor. In the case of subduction ground motions there is one that drives the bottom floors of the low-rise and middle-rise buildings to experience brace fracture, as well as, in the case of 16-storey building is the brace of the 12 floor that reached fracture.

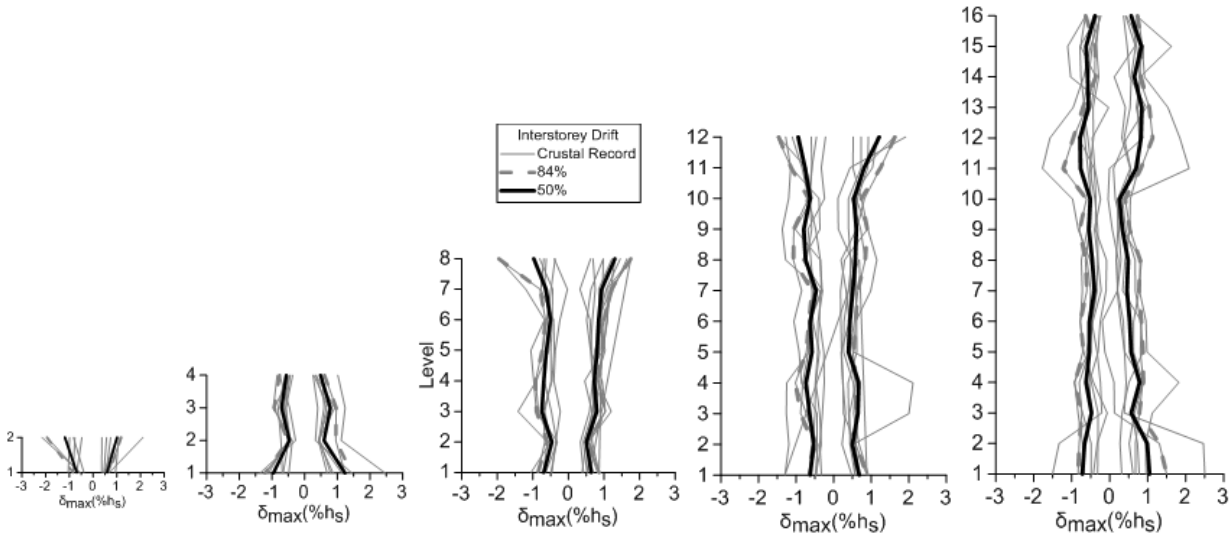

Figure 3-11 Interstorey drift of studied buildings under re-scaled crustal ground motions

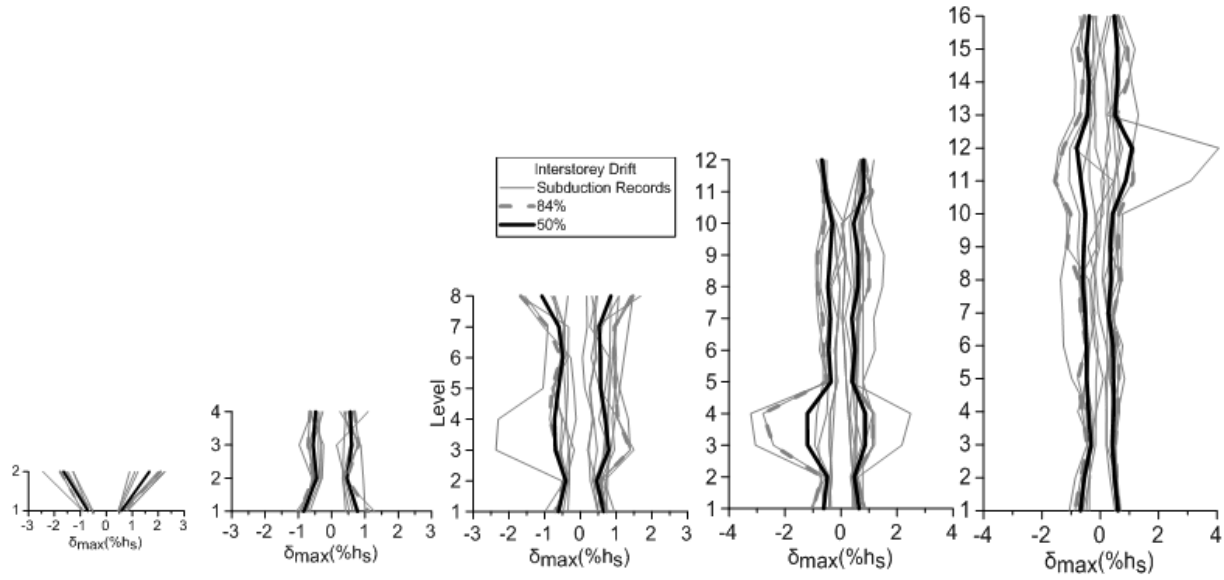

Figure 3-12 Interstorey drift of studied buildings under re-scaled subduction ground motions

Table 3-11 The 84 percentile and 50 percentile of interstorey drift and residual interstorey drift of studied buildings under scaled and re-scaled crustal ground motions

Buildings	Peak Drift (%hs)		Residual Drift (%hs)		Floor exp. collapse	Number of failed GM
	50%	84%	50%	84%		
Lateral deformations under scaled crustal ground motions						
2-Storey	0.99	1.22	0.10	0.19		0
4-Storey	0.93	1.06	0.08	0.11		0
8-Storey	1.18	1.87	0.13	0.24		0
12-Storey	1.16	1.75	0.22	0.32		0
16-Storey	**1.00**	**1.77**	0.29	0.73		0
Lateral deformations under re-scaled crustal ground motions						
2-Storey	1.20	1.95	0.22	0.41		0
4-Storey	1.24	1.45	0.17	0.13		0
8-Storey	1.31	1.96	0.82	1.75		0
12-Storey	1.21	1.63	0.71	1.60		0
16-Storey	1.05	1.50	0.55	1.19	12^{th} Floor	1

Table 3-12 The 84 percentile and 50 percentile of interstorey drift and residual interstorey drift of studied buildings under scaled and re-scaled subduction ground motions

Buildings	Peak drift (%hs)		Residual drift (%hs)		Floor exp. collapse	Number of failed GM
	50%	84%	50%	84%		
Lateral deformations under scaled subduction ground motions (SF = 1.0)						
2-Storey	0.69	0.83	0.06	0.14	2^{nd} floor	1
4-Storey	0.73	1.04	0.07	0.11		0
8-Storey	1.03	1.41	0.12	0.19		0
12-Storey	0.87	1.90	0.25	0.58		0
16-Storey	0.94	1.92	0.42	0.78		0
Lateral deformations under re-scaled subduction ground motions (SF = 1.2)						
2-Storey	1.66	2.09	0.06	0.14	2^{nd} floor	1
4-Storey	0.84	1.10	0.08	0.12	G floor	1
8-Storey	1.10	1.70	0.44	1.14	3^{rd} floor	1
12-Storey	1.20	2.80	0.62	1.70		0
16-Storey	1.10	1.60	1.03	0.58	12^{th} floor	1

3.4.3.2. **Residual interstorey drift**

The residual interstorey drift of studied buildings subjected to scaled crustal and subduction ground motions are plotted in Fig. 3-13 and 3-14, respectively. The 50 percentile and 84

percentiles of residual interstorey drift computed for each ground motion set are also presented. As can be seen from these figures, the peak of maximum residual interstorey drift of low-rise and middle-rise buildings were less than 0.5% h_s which is the upper limit recommended in the literature for reparable buildings in the aftermath of an earthquake event. For high-rise buildings subjected to scaled crustal ground motions the peak of maximum residual interstorey drift is greater than 0.5% h_s.

Thus, in case of 12-storey building, the peak of the maximum residual interstorey drift is 0.56% h_s and the peak values of 84-percentile and 50-percentile residual interstorey drift are 0.32% h_s and 0.22% h_s, respectively. In the case of the 16-storey building subjected to scaled crustal ground motions the peak of the maximum residual interstorey drift is 0.81% h_s and the peak of 84-percentile and 50-percentile residual interstorey drift are 0.72% h_s and 0.29% h_s, respectively. In the case of the 12-storey building subjected to the subduction earthquake records, the peak value of the maximum residual interstorey drift is 0.99% h_s and the peak values of 84-percentile and 50- percentile residual interstorey drift are 0.58% h_s and 0.24% h_s, respectively.

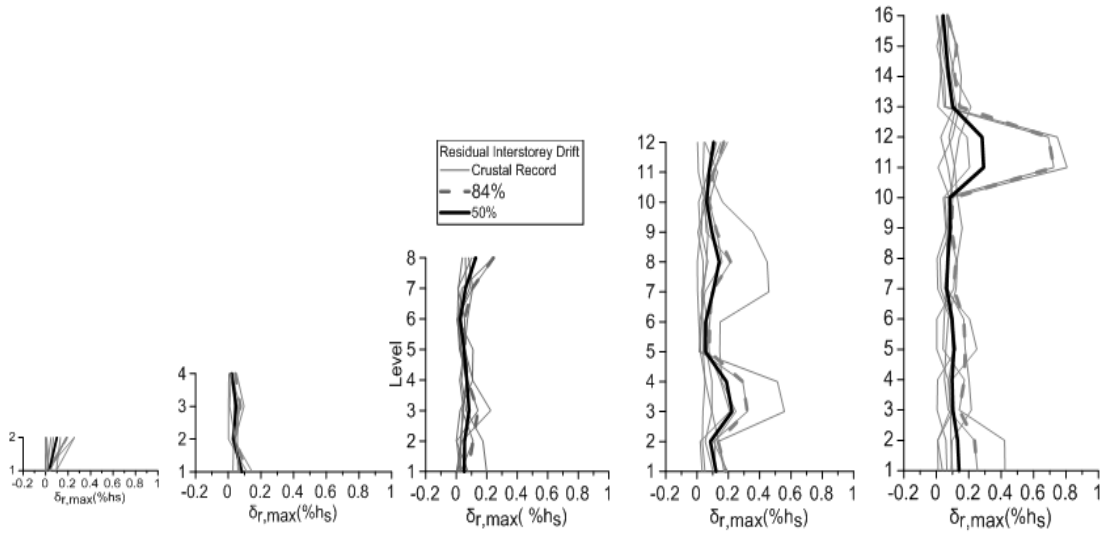

Figure 3-13 Residual Interstorey drift of studied buildings under scaled crustal ground motions

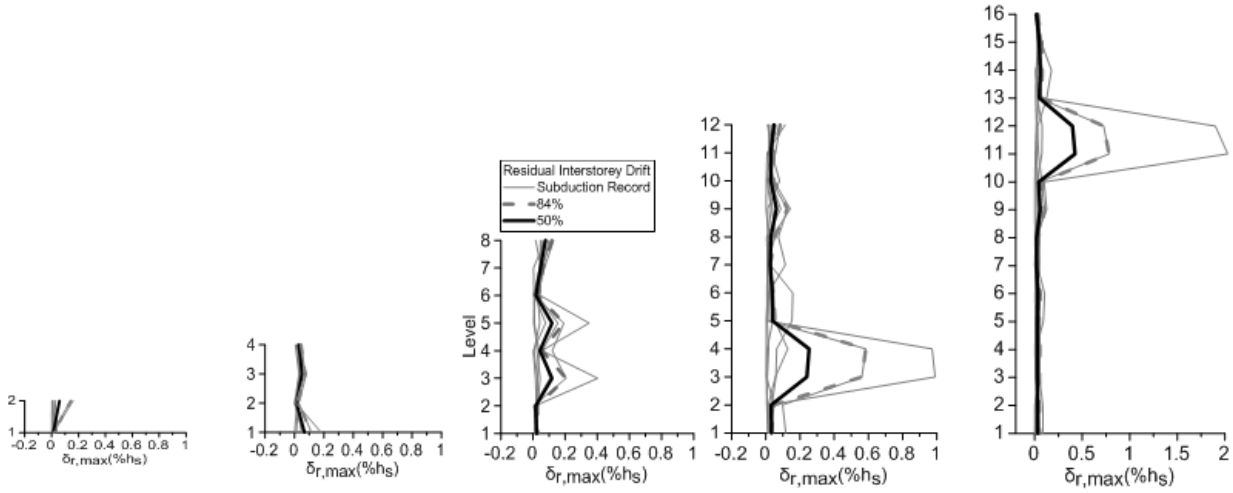

Figure 3-14 Residual Interstorey drift of studied buildings under subduction ground motions

In the case of the 16-storey building subjected to the subduction earthquake records, the peak value of the maximum residual interstorey drift is 2.03% h_s and the peak values of the 84-percentile and 50-percentile residual interstorey drift are 0.78% h_s and 0.42% h_s, respectively.

Hence, the peak value of the maximum residual interstorey drift for low-rise and middle rise buildings are lower than 0.5% h_s. For the high-rise buildings, the residual interstorey drift is greater under the subduction earthquake records than under the crustal earthquake records. For example, for the 12-storey building, the peak value of the 84-percentile of the residual interstorey drift is found to be 0.32% h_s under the crustal records and 0.58% h_s under the subduction records. Similar trend is observed for the 16-storey building as well. However, in all case studies presented here, the peak value of the 50-percentile of the residual interstorey drift is found to be less than 0.5% h_s.

The residual interstorey drift of the studied buildings resulted under the crustal and subduction ground motions re-scaled by 1.2 factor, are plotted in Fig. 3-15 and 3-16, respectively. For the low-rise and middle-rise buildings, the peak values of the 50-percentile of the residual interstorey drift for the re-scaled crustal records are found to be 0.22% h_s, 0.17% h_s and 0.82% h_s, respectively. This shows an increase of residual interstorey drift with the building height. When these buildings were subjected to re-scaled subduction ground motions it resulted lower peak of 50-percentile residual interstorey drift such as: 0.06% h_s, 0.08% h_s and 0.44% h_s, respectively. It is noted that subduction records were selected from the same earthquake event and these records are more homogenous than the crustal record set which required bigger scaling factors. In case of

12-storey building subjected to re-scaled crustal records, the peak value of the maximum residual interstorey drift is 1.58% h_s, while the peak values of the 84-percentile and 50-percentile are found to be 1.6% h_s and 0.71% h_s, respectively. When the 12-storey building is subjected to re-scaled subduction records the peak of maximum residual interstorey drift is determined as 2.32% h_s, and the peak of 84 percentile and 50 percentile are 1.7% h_s and 0.62% h_s, respectively.

For the 16-storey building the same trend is observed. Thus, the peak value of the maximum residual interstorey drift, the 84-percentile, and 50-percentile values under the re-scaled crustal ground motions are found to be 1.81% h_s, 1.15% h_s and 0.55% h_s, respectively. When the 16-storey building is subjected to the re-scaled subduction records the peak values of the 84-percentile and 50-percentile are 1.03% h_s and 0.58% h_s, respectively.

Thus, in all of the case study buildings but low-rise buildings, the peak values of the 50-percentile residual interstorey drift is greater than 0.5% h_s under both sets of crustal and subduction records re-scaled with 1.2 factor in order to account for the accidental torsion effect.

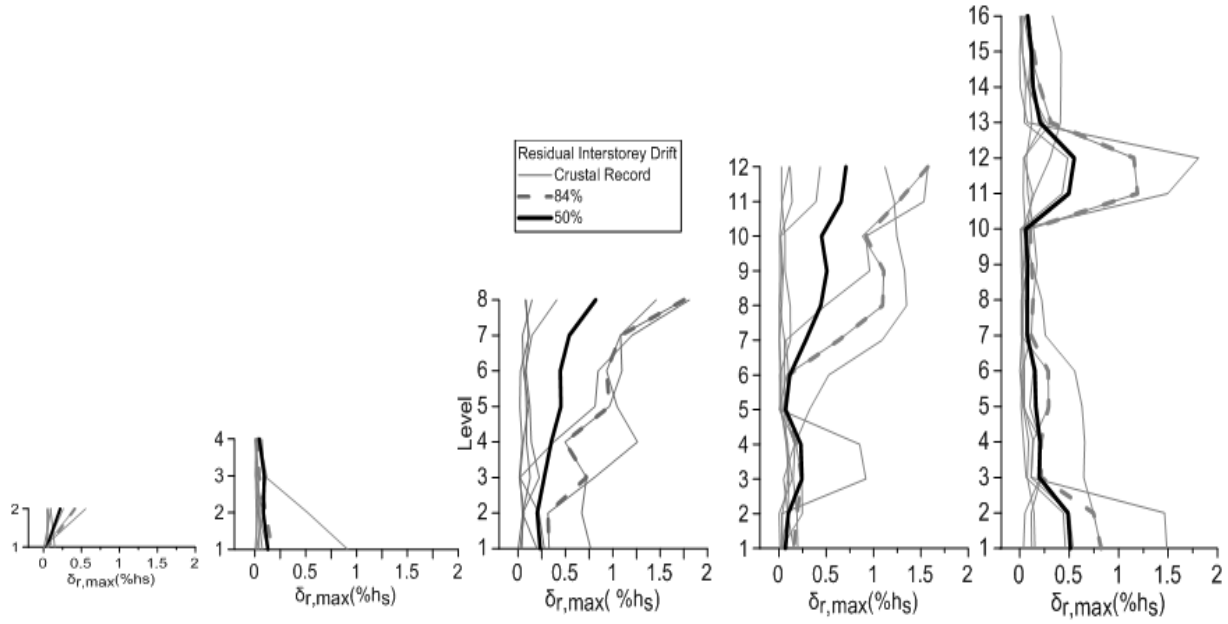

Figure 3-15 Residual Inter-storey drift of studied buildings under re-scaled crustal ground motions

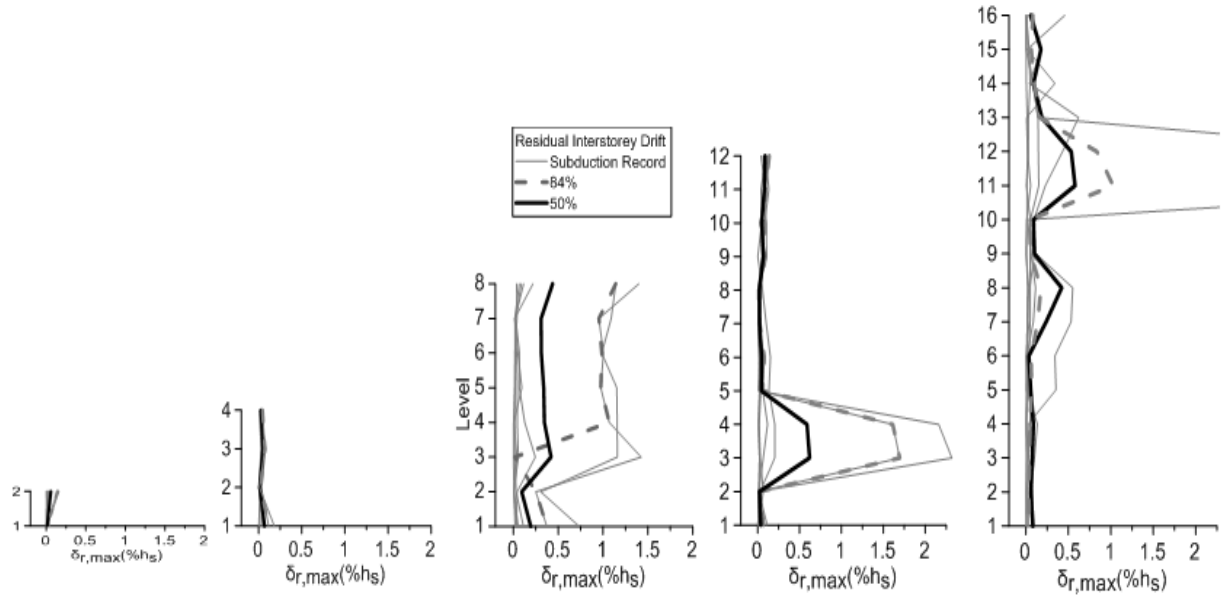

Figure 3-16 Residual Inter-storey drift of studied buildings under re-scaled subduction ground motions

3.4.3.3. **Damage index of HSS braces**

The ductile fracture of a brace due to low-cycle fatigue is the desirable failure mode for the CBF system (Hasiao et al., 2012). The time-history strain series recorded in the outermost compressive fiber of HSS cross-section located at the brace mid-span length where the plastic hinge is formed and the accumulated strain are good indicators of brace strain life. It is worth mentioning that the strain life is based on the premise that the local strain developed around stress concentration controls the fatigue life. Thus, the low-cycle fatigue damage is dependent on strain accumulation.

In OpenSees, the low-cycle fatigue material is defined by using as input the fatigue ductility exponent m and fatigue ductility coefficient $\epsilon_{0,\text{pred}}$. The value of predicting fatigue parameters was proposed by Tirca and Chen (2014) after simulating several experimental tests from the literature. Hence, m = -0.5 and $\varepsilon_{0pred} = 0.006\left(\frac{KL}{r}\right)^{0.859}\left(\frac{w}{t}\right)^{-0.6}\left(\frac{E}{F_y}\right)^{0.1}$ are recommended where kL/r is the brace slenderness ratio and w/t is the brace width-to-thickness ratio (e.g. w = (b-4t)). The low-cycle fatigue model is based on low-cycle fatigue of constant plastic strain amplitude which uses a damage accumulation model in accordance to Miner's Rule. However, under earthquake accelerogram loading the strain amplitude are not constant. Based on Coffin-Masson research it was concluded that the relationship between the plastic strain amplitude ϵ_i

experienced by a cycle *i* and the number of cycles to failure N_f is linear in the log-log domain and the slope is *m*. The expression of equation is: $\epsilon_i = \epsilon_0(N_f)^m$. Herein, the accumulation of number of cycles is used to evaluate the damage reached by the mid-span brace cross-section and the maximum number of cycles permitted by Coffin Manson's fatigue theory was considered. To accumulate damage, while preserving economic computations, the number of cycles was counted "on the go" with a modified rainflow cyclic counting algorithm. If the damage index, DI, of a fiber cross-section reaches 1.0, the fiber is disconnected by dropping its stress and stiffness to zero. Furthermore, when half of fibers at a critical brace cross-section reached DI = 1.0, the brace reached failure caused by low-cycle fatigue. Below is presented the DI of the outermost compressive fiber of a critical brace cross-section.

The DI of the outermost compression fiber of critical cross-section of HSS braces of low-rise, middle-rise and high-rise buildings under crustal and subduction records are shown in Fig. 3-17 and Fig. 3-18, respectively. As resulted, there is about two times larger DI recorded for HSS braces when studied buildings were subjected to subduction than crustal ground motions. This finding is explained by the greater number of loading-unloading cycles of subduction ground motion acceleration in comparison with crustal ground motion acceleration. The larger demand occurs at floors experiencing the peak interstorey drift. As depicted, under the subduction record MYG004, the outermost compression fiber of the top floor brace of 2-storey building reached DI =1.0. In addition, DI = 1.0 was experienced by the 12th floor brace of 16-storey building.

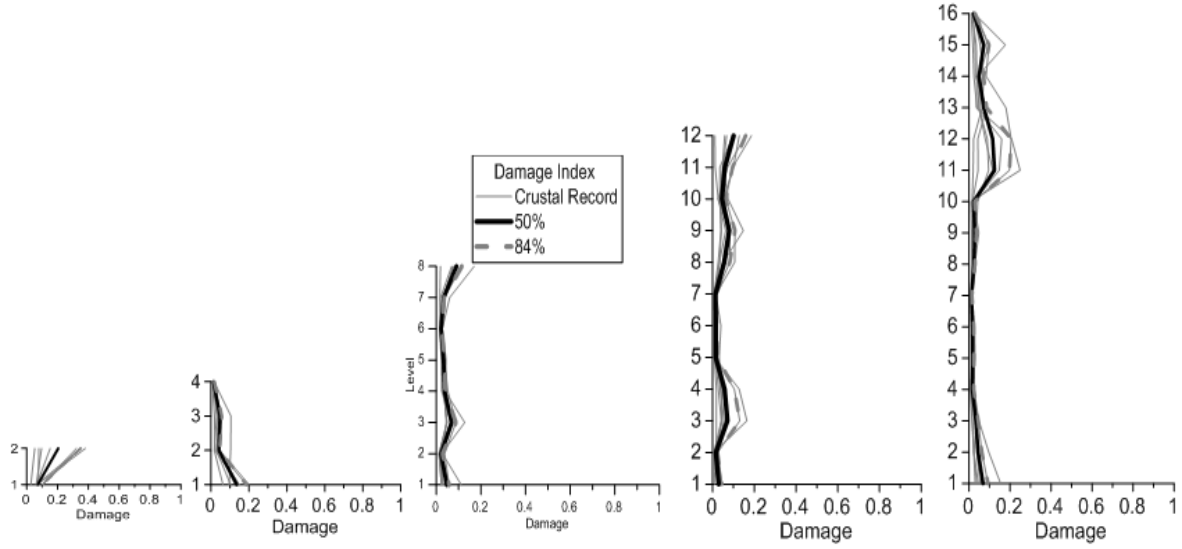

Figure 3-17 Damage index of the outermost compression fiber of critical cross section of HSS braces of studied buildings under crustal records

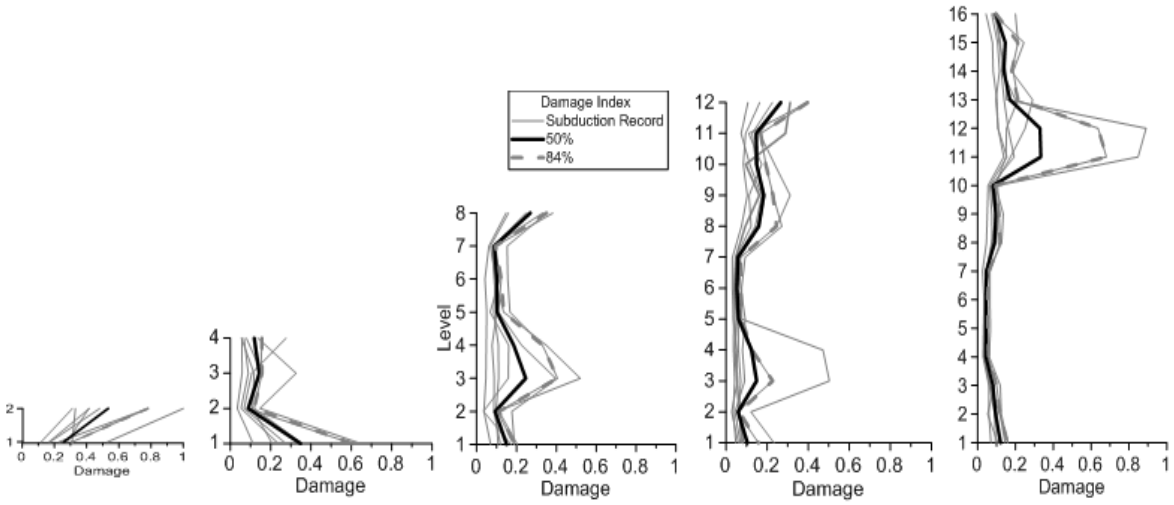

Figure 3-18 Damage index of the outermost compressive fiber of critical cross section of HSS braces of studied buildings under subduction records

The DI of the outermost compression fiber of critical cross-section of HSS braces of low-rise, middle-rise and high-rise buildings subjected to crustal and subduction records re-scaled by about 1.2 factor are shown in Fig. 3-19 and Fig. 3-20, respectively.

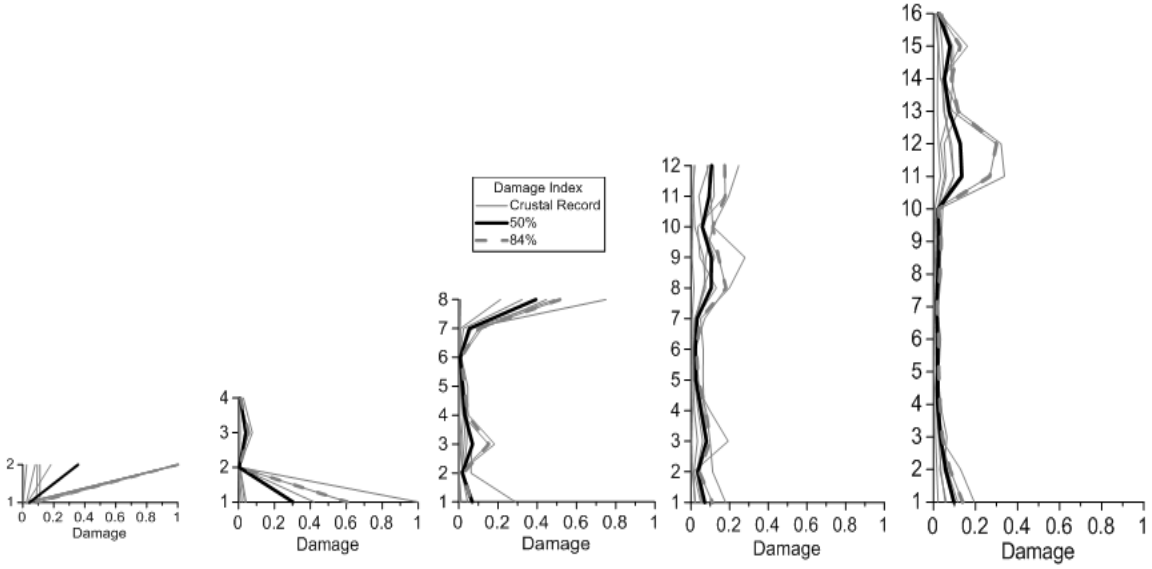

Figure 3-19 Damage index of the outermost compressive fiber of critical cross-sectionof HSS brace of studied buildings under re-scaled crustal records

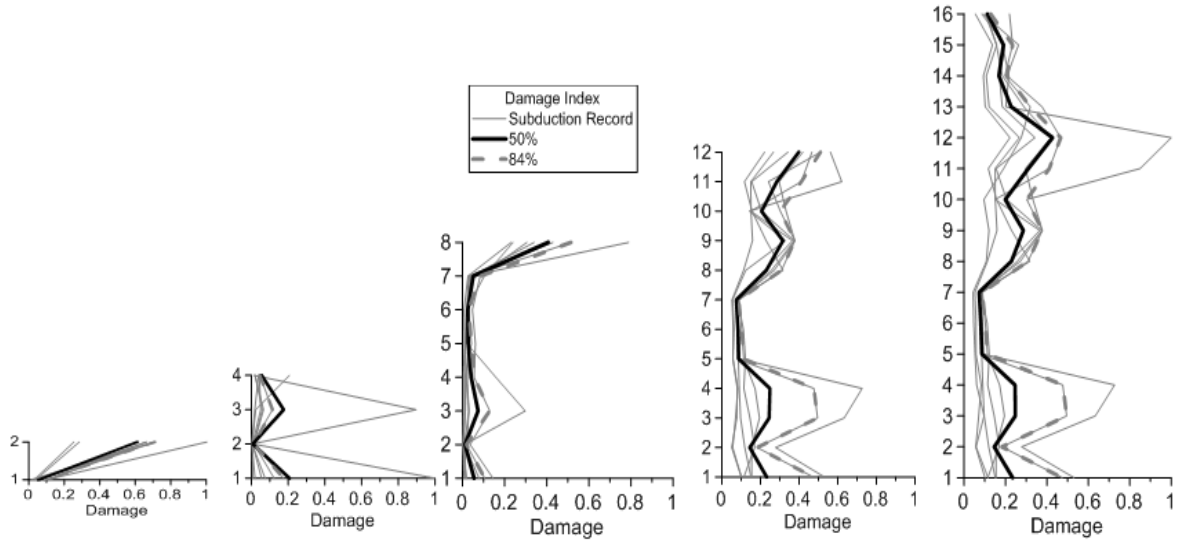

Figure 3-20 Damage index of the outermost compressive fiber of critical cross-section of HSS brace of studied buildings under re-scaled subduction records

The DI of an outermost compression fiber of the top floor brace cross-section of the 2-storey MD-CBF building reached 1.0 under one re-scaled crustal record. Similarly, the outermost compression fiber of a bottom floor brace cross-section of the 4-storey MD-CBF building experienced DI = 1.0 under one re-scaled crustal record. As depicted in Fig. 3-19, the peak value of 84 percentile of DI is less than 0.5 for all studied buildings except the 2-storey building. When studied buildings were subjected to re-scaled subduction records, the fatigue life of the outermost compressive fiber of critical cross-sections of HSS braces reduced. As depicted in Fig. 3-20, DI = 1.0 was recorded in the outermost compressive fiber of top floor brace of 2-storey building, the bottom floor brace of 4-storey building and the 12 floor brace of 16-storey building. In general, the peak value of the 84 percentile of DI is about 0.5.

Therefore, lower fatigue life reserve was recorded for HSS braces of studied MD-CBF buildings subjected to subduction ground motions than crustal ground motions.

3.5. Case Study of Dynamic Response of MD-CBF buildings

In this section, a detailed nonlinear behaviour of studied buildings under a representative crustal and subduction ground motion is presented, while the analyses are conducted using OpenSees. The investigated parameters are: i) the roof drift time-history series, ii) the interstorey drift time-

history series of the floor experiencing maximum relative displacement, iii) the hysteresis response of HSS braces located at the floor experiencing the maximum interstorey drift, iv) the time-history series of the outermost compression fiber and tensile fiber of HSS brace cross-section, and v) the accumulated DI of the fiber cross-section depicted at iv).

3.5.1. Seismic response of 2-storey MD-CBF building under crustal #1039 and subduction MYG004 record

The seismic response in terms of roof drift and peak interstorey drift time-history series of the 2-story MD-CBF building under the crustal #1039 Northridge record is plotted in Fig. 3-21 together with the scaled accelerogram. As resulted, the peak interstorey drift is 1.47% h_s which is within the code limit. The nonlinear hysteresis response of the left and right braces located at the top floor is given in Fig. 3-21a. Both braces buckle in compression and yield in tension. The hysteresis loops of braces are plotted by normalizing the forces to the probable tensile force. Fig. 3-21b shows the plot of the time-history series of strain recorded in the outermost compression fiber and tensile fiber at middle section of the braces. From the time history of compression strain, it is observed that the braces still possess strain capacity before failure because the amplitude of compressive strain diminishes toward the end of ground motion and is preserved in the negative side. Fig.3-21c illustrates the damage index of the same outermost fiber. In this case, DI = 0.4, which means that the fatigue life of these braces is not consumed yet.

Increasing the accelerogram amplitude of the #1039 record by the re-scaled factor 1.2 (to take into account the effect of shear caused by accidental torsion), in Fig. 3-23 is shown the scaled accelerogram, the time-history series of roof drift and maximum interstorey drift. As depicted, the maximum interstorey drift is 2.5% h_s which is equal to the code limit. The inelastic behavior of top floor braces, the time-history series of tensile and compressive strain as well as the brace damage index is illustrated in Fig. 3-24

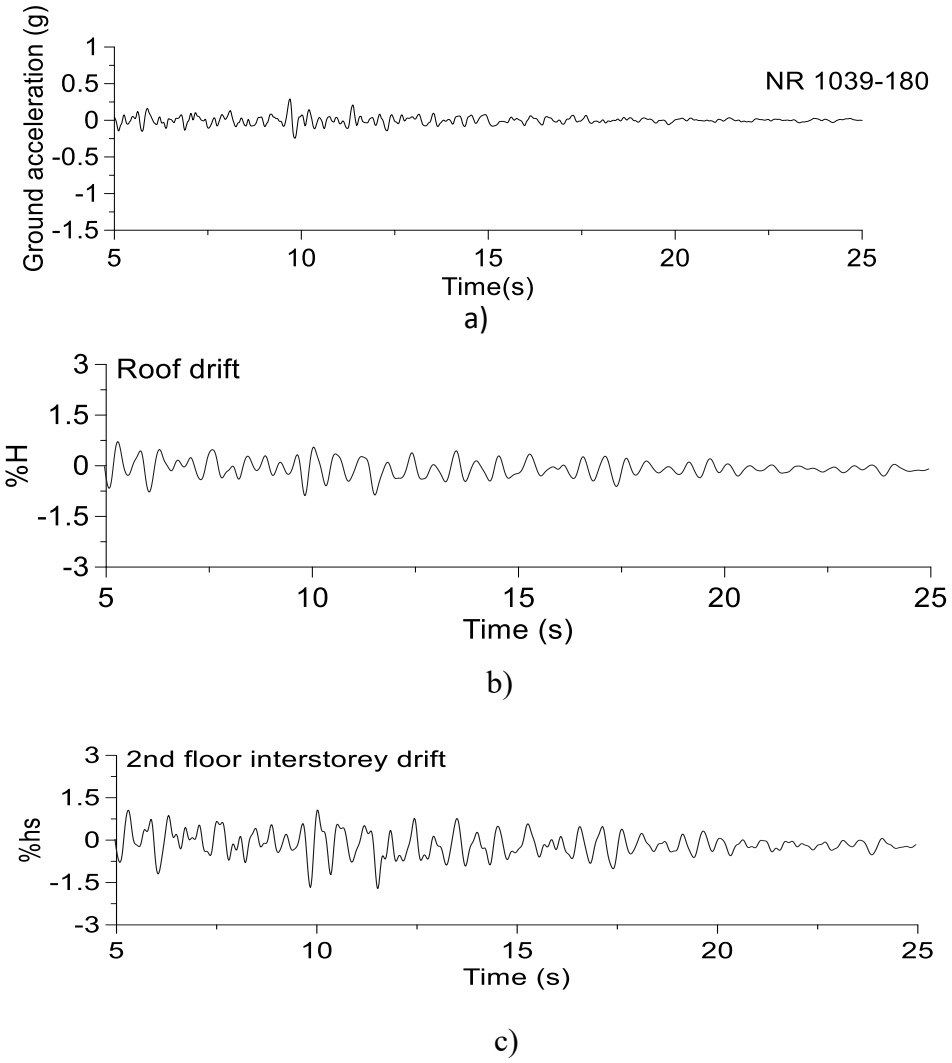

Figure 3-21 Response of 2-storey MD-CBF building under #1039 record: a) accelerogram, b) roof drift, c) interstorey drift time-history series recorded at top floor

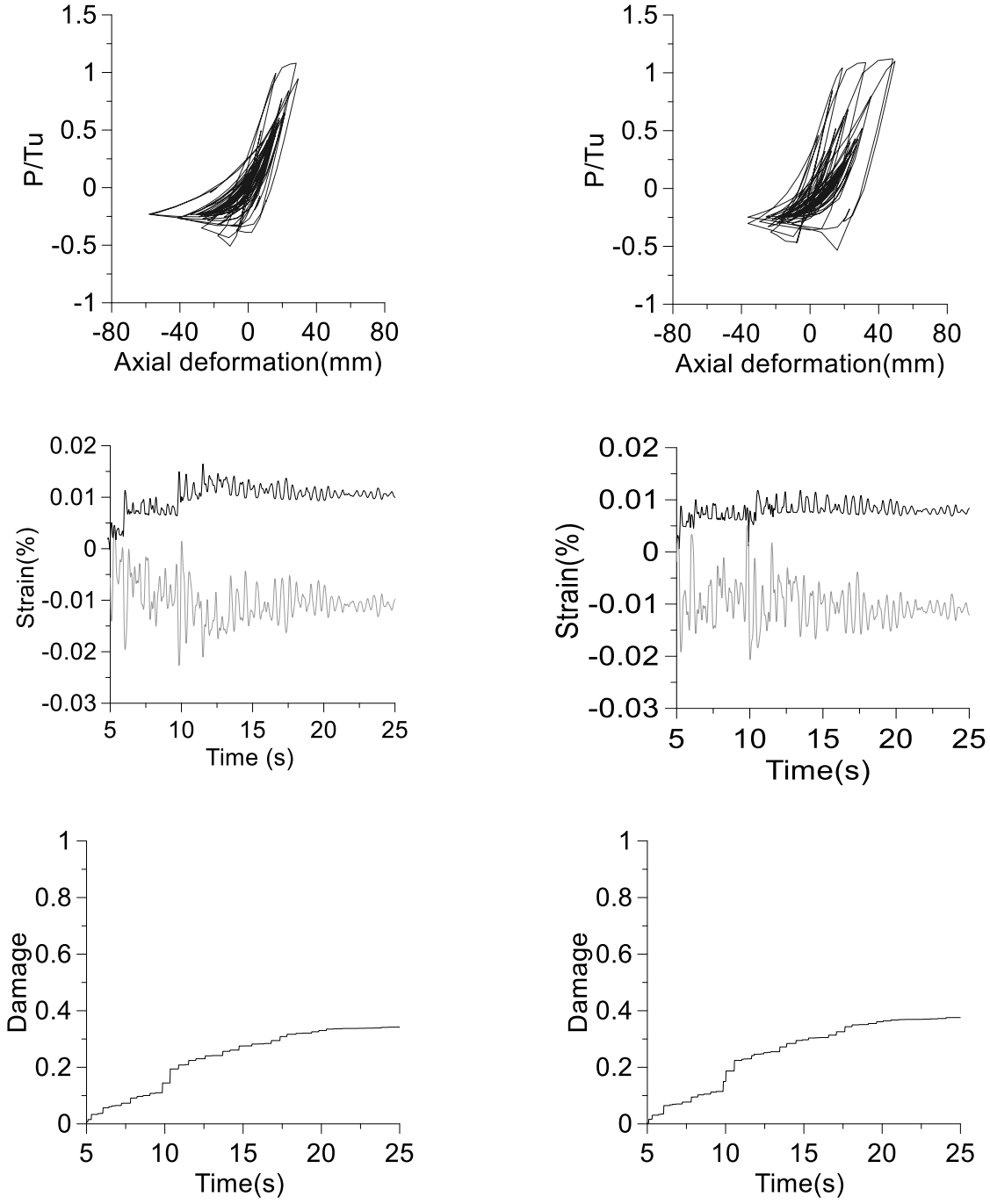

Figure 3-22 Hysteresis response of top floor braces, their strain time-history series and damage index of the outermost compressive fiber under the scaled #1039 crustal record

Comparing Figs. 3-24 and Fig. 3-22 is shown important changes in the nonlinear behaviour leading to failure (DI = 1.0) of the outermost compression fiber of critical cross-section of HSS brace (left side). Thus, the left side brace is able to carry one or two more cycles before failure.

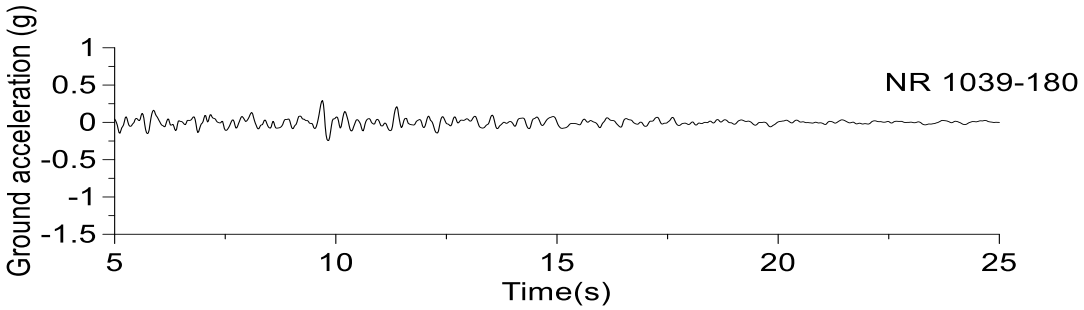

a)

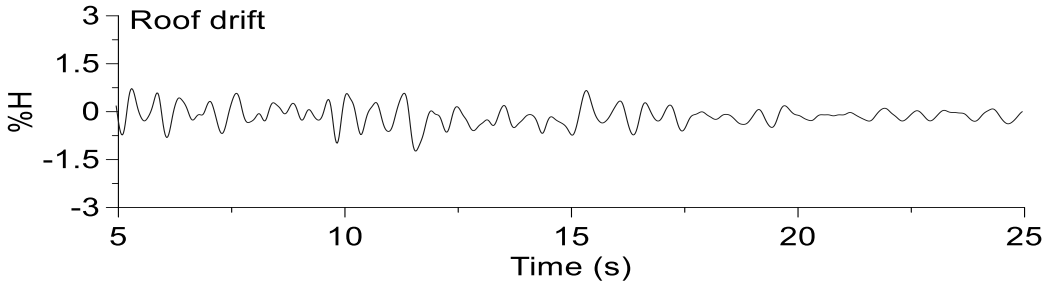

b)

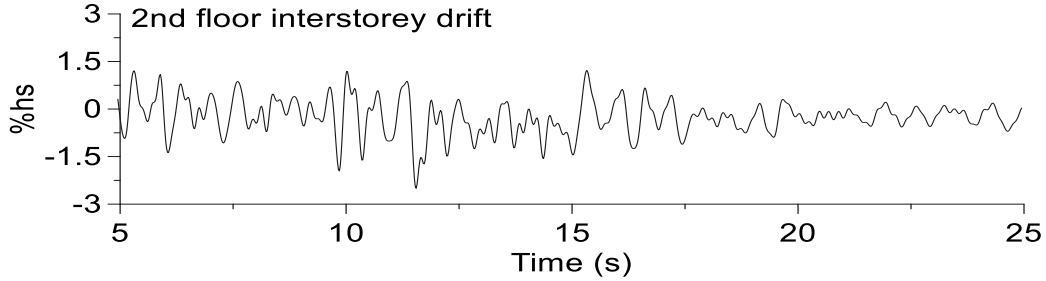

c)

Figure 3-23 Response of 2-storey MD-CBF building under re-scaled #1039 record: a) accelerogram, b) roof drift, c) interstorey drift time-history series recorded at top floor

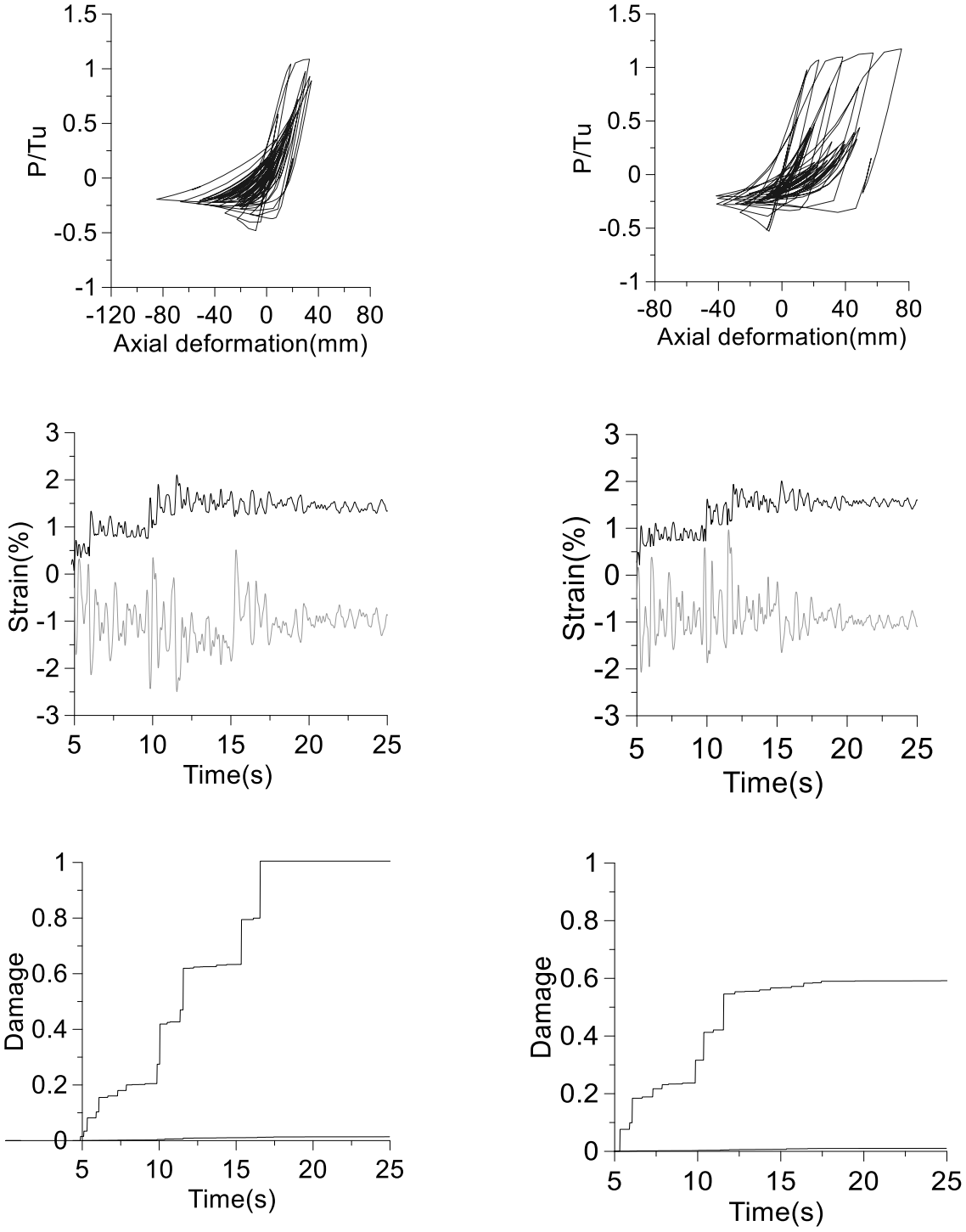

Figure 3-24 Hysteresis response of top floor braces, their strain time-history series and damage index of the outermost compressive fiber under the re-scaled #1039 crustal record

The response of the 2-storey MD-CBF building under the subduction record MYG004 is presented in Fig. 3-25 in terms of roof drift and maximum interstorey drift time-history series.

As aforementioned, the scaling factor applied is 1.0. To better emphasize the building response only that recorded between the time sequence 50 s and 150 s is presented. The peak interstorey drift is 1.72% h_s which is similar with that resulted under #1039 crustal record.

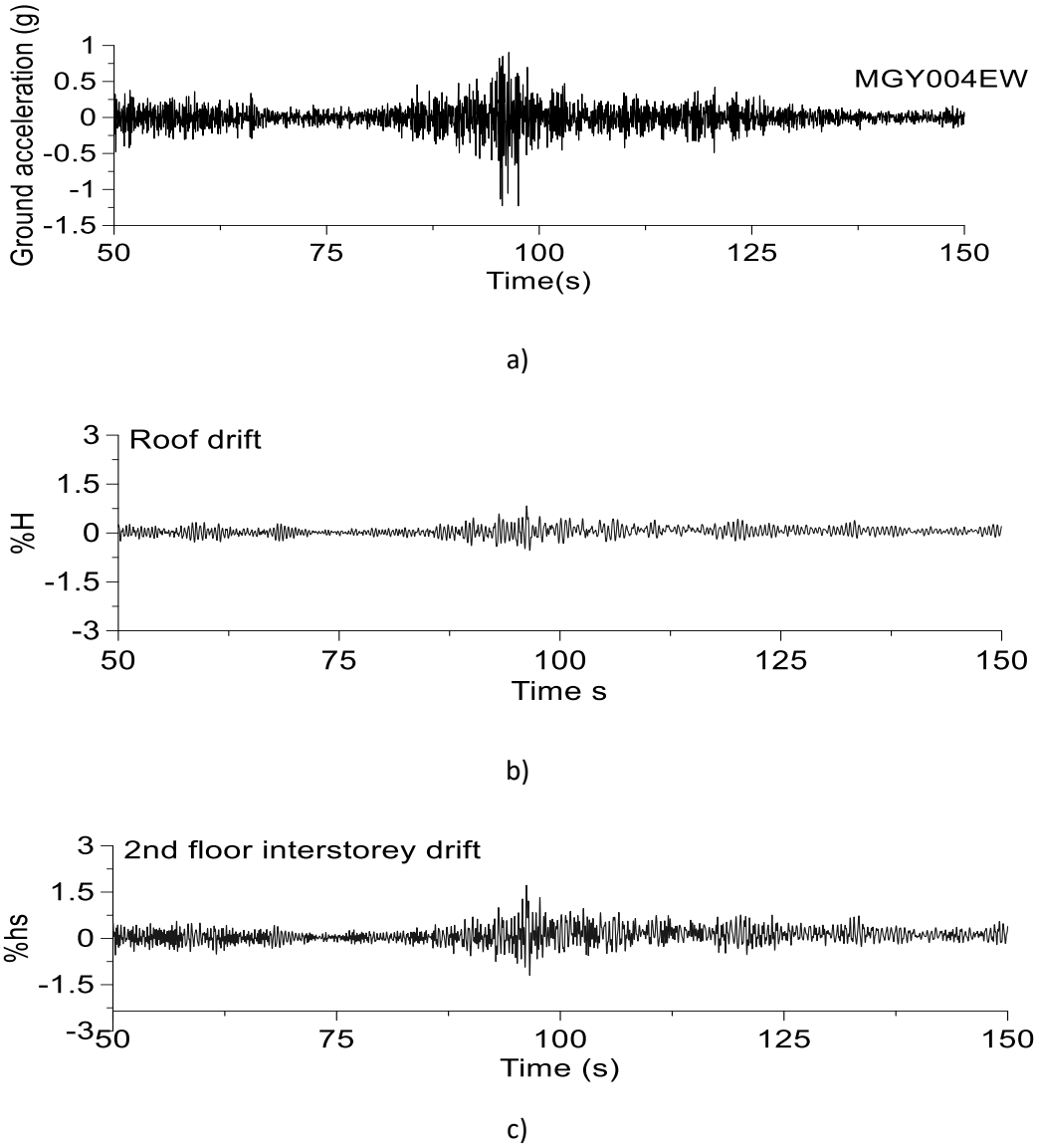

Figure 3-25 Response of 2-storey MD-CBF building under #MYG004 subduction record: a) accelerogram, b) roof drift, c) interstorey drift time-history series recorded at roof

Figure 3-26 shows the hysteresis response of the left and right braces of top floor, as well as the time-history series of the outermost compressive and tensile fiber of critical brace cross-section and its DI. Due to high spectral acceleration ordinates reported within the short period interval, both left and right braces experienced DI = 1.0. This means braces failure caused by low-cycle fatigue will occur at very small increase of seismic demand.

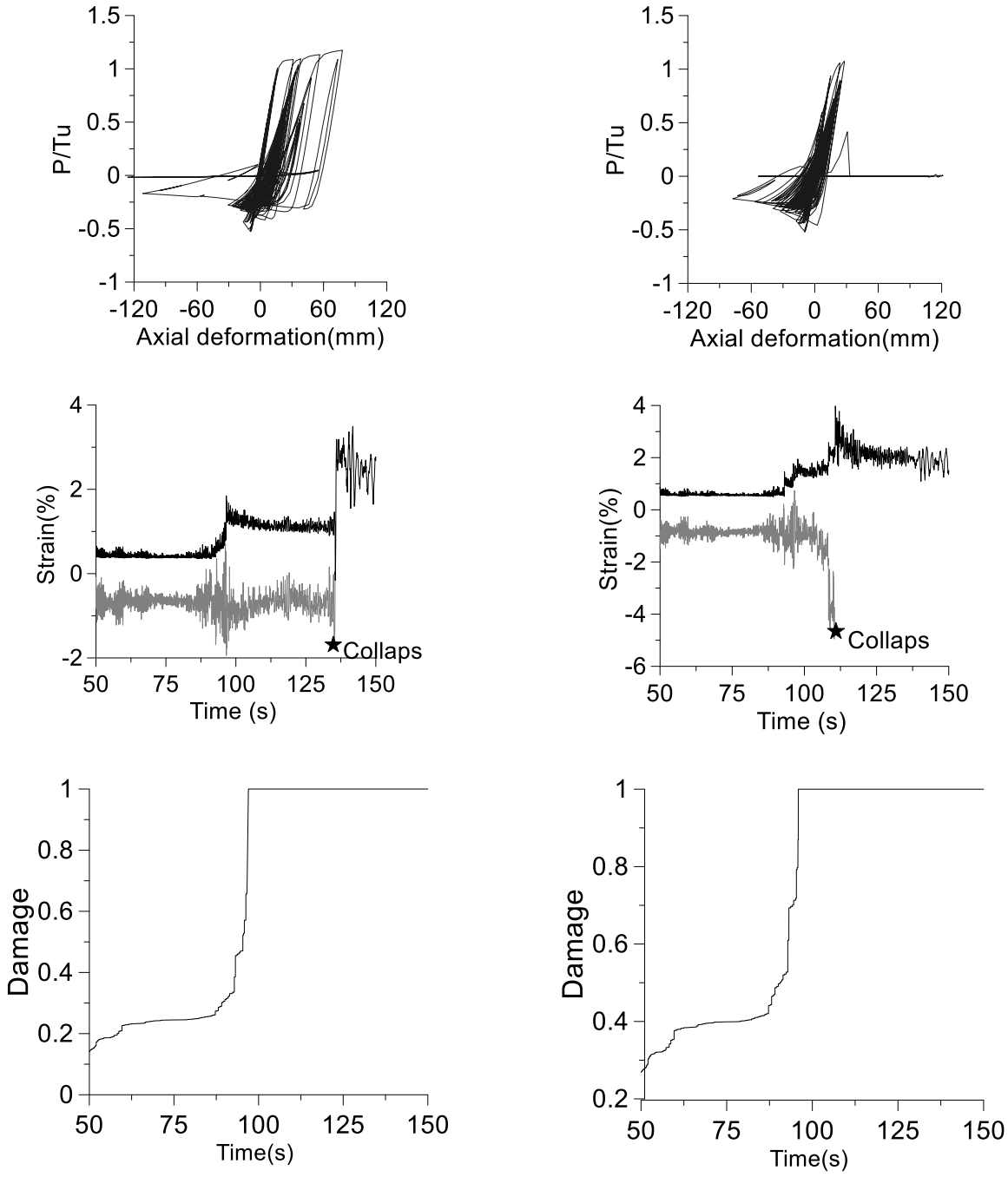

Figure 3-26 Hysteresis response of top floor braces, their strain time-history series and DI of the outermost compressive fiber under the #MYG004 subduction record

3.5.2. Seismic response of 4-st MD-CBF building under crustal #787 and subduction MYG004 record

Detailed nonlinear seismic response of the 4-storey MD-CBF building is presented under the shaking of #787 Loma Prieta crustal record. The same response parameters used for the 2-storey

MD-CBF building are considered. Hence, the time-history series of roof drift and roof interstorey drift is plotted in Fig. 3-27. As resulted, the peak interstorey drift was recorded at the bottom floor and is 0.93% h_s. As depicted, the behavior of building deflection is approximately symmetric. The nonlinear hysteresis response of the left and right brace located at the bottom floor, their time history strain series of the outermost compressive and tensile fiber of critical brace's cross-section and the associated DI are plotted in Fig. 3-28. Both braces are found to buckle in compression and yield in tension, while their DI = 0.2.

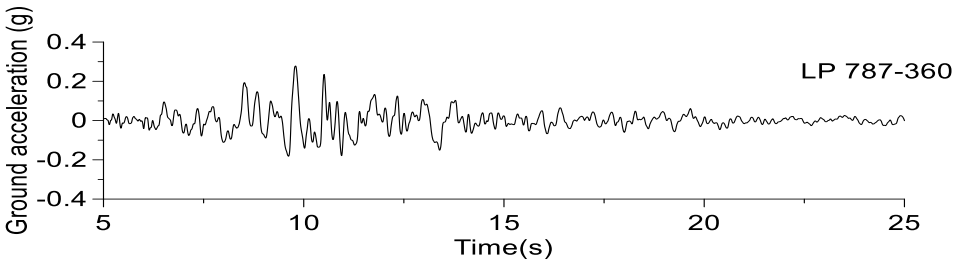

a)

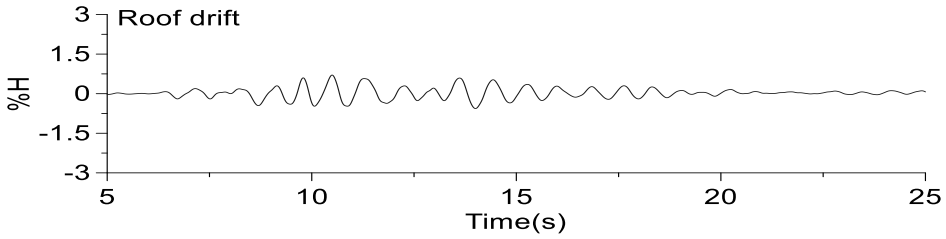

b)

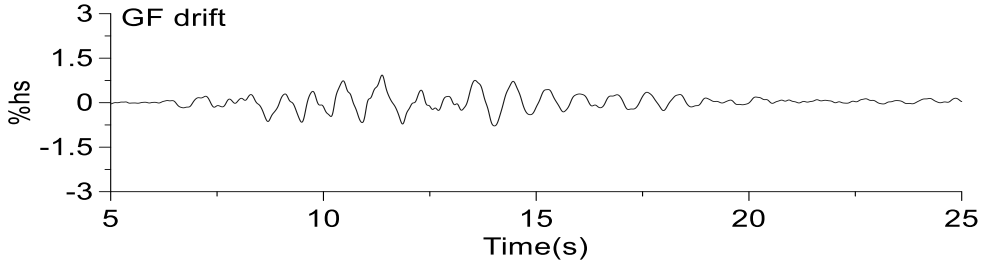

c)

Figure 3-27 Response of 4-storey MD-CBF building under #787 Loma Prieta record: a) accelerogram, b) roof drift, c) interstorey drift time-history series recorded at ground floor level

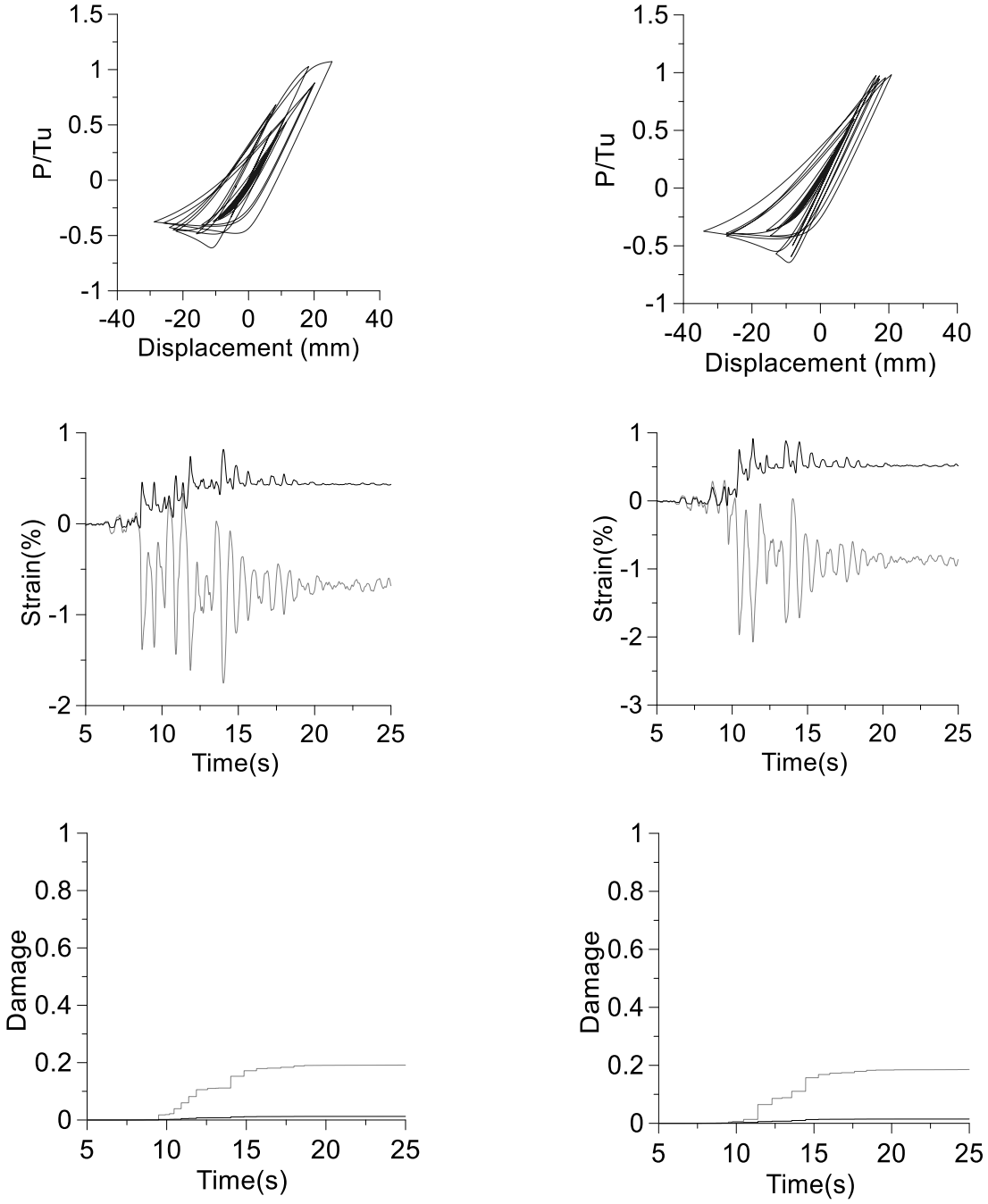

Figure 3-28 Hysteresis response of bottom floor braces, their strain time-history series and damage index of the outermost compressive fiber under the scaled #787 crustal record

Similarly, in Figs. 3-29 and 3-30 show the same parameters as above recorded for higher shaking level. To account for accidental torsion effect the #787 record was re-scaled by 1.2 factor. As depicted, the maximum interstorey drift was recorded at the bottom floor and is 1.18% h_s. The outermost compression fiber of critical cross-section of braces located at the bottom floor

experienced DI = 0.3. Comparing Figs. 3-28 and 3-30, there is no significant difference observed on the nonlinear behaviour of selected HSS braces.

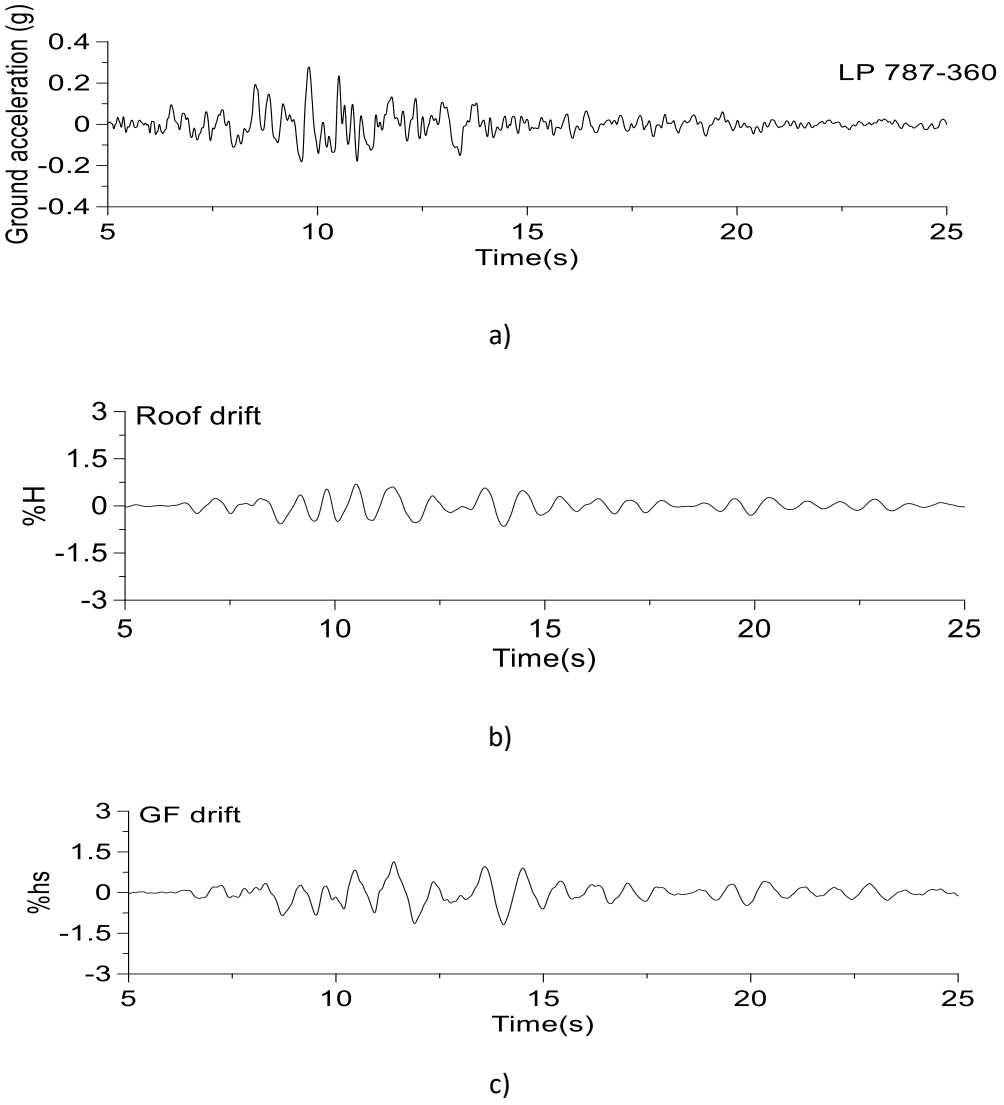

Figure 3-29 Response of 4-storey MD-CBF building under re-scaled #787 Loma Prieta record: a) accelerogram, b) roof drift, c) interstorey drift time-history series recorded at ground floor level

The response of the 4-storey MD-CBF building under the subduction record SKS010 scaled with 1.0 is presented in Figs. 3-31 and 3-32. It is noted that the peak interstorey drift was recorded at bottom floor level.

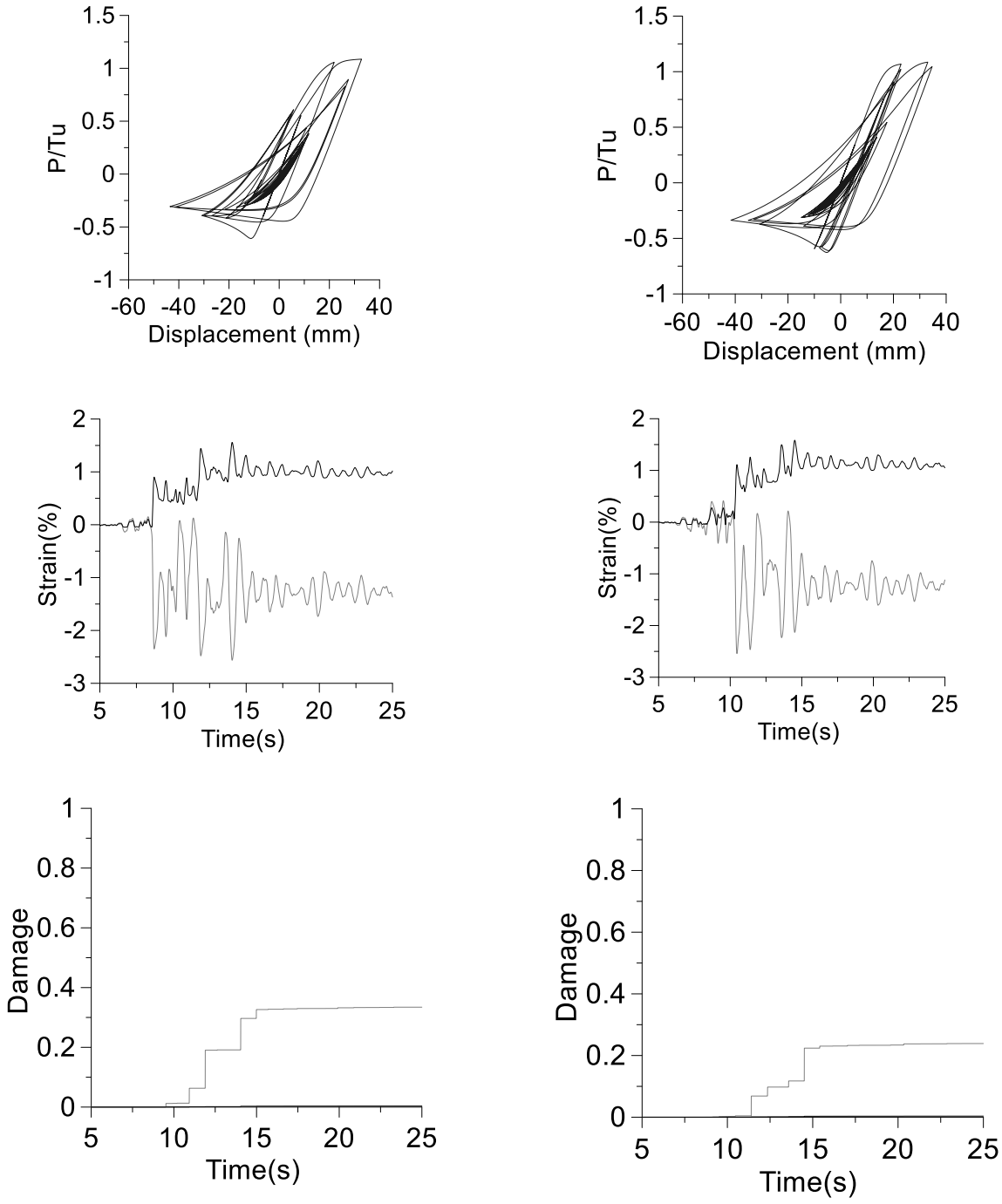

Figure 3-30 Hysteresis response of bottom floor braces, their strain time-history series and damage index of the outermost compressive fiber under the re-scaled #787 crustal record

To better emphasize the seismic response only that recorded between the time sequence 50 s and 150 s is presented. The maximum interstorey drift is 1.04% h_s. The nonlinear hysteresis response

of both left and right braces show yielding in tension and buckling in compression. The maximum compressive strain of the outermost fiber is 2.5% and DI is 60% of braces capacity.

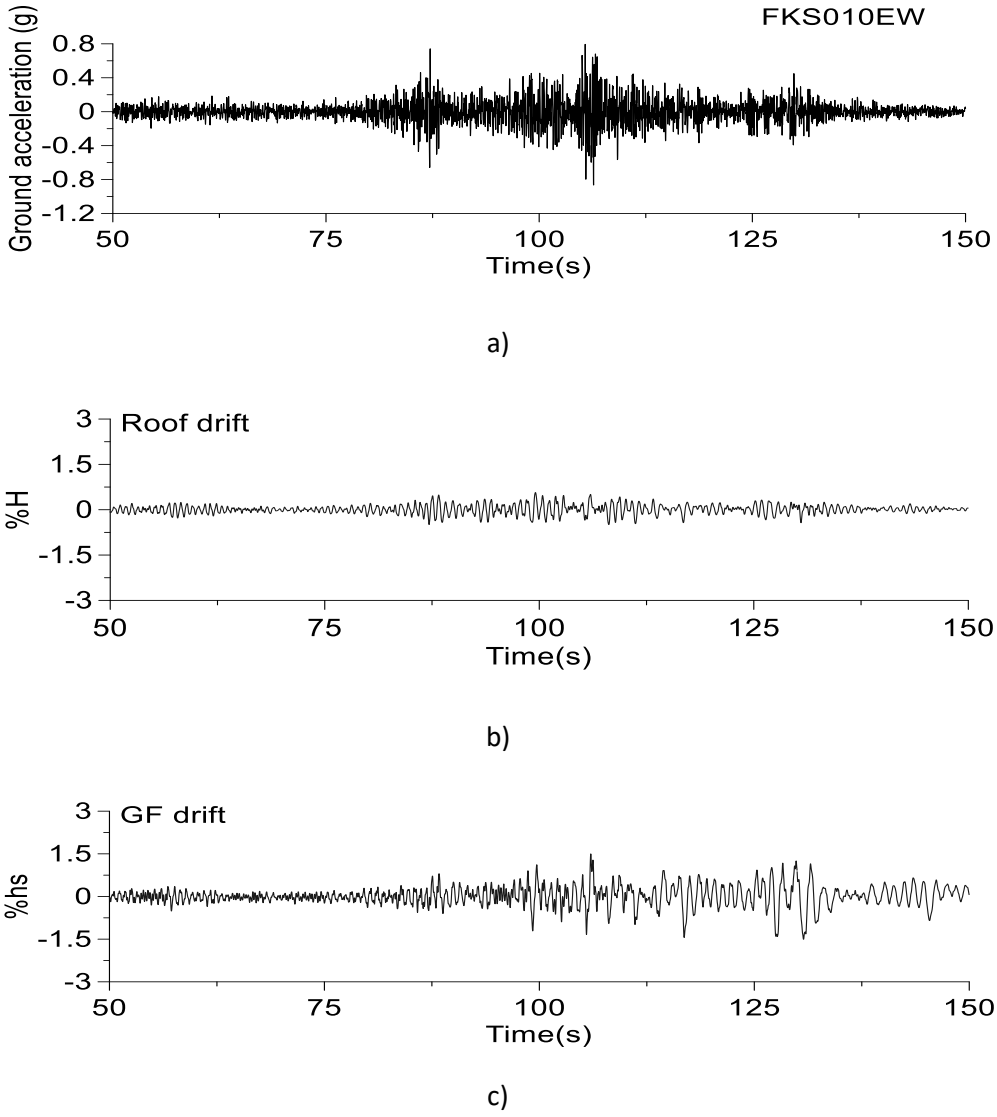

Figure 3-31 Response of 4-storey MD-CBF building under #FKS010 subduction record: a) accelerogram, b) roof drift, c) interstorey drift time-history series recorded at bottom floor level

The nonlinear seismic response of the 4-storey MD-CBF building recorded under the re-scaled subduction record #SKS010 by 1.2 scaling factor is presented in Figs. 3-32 and 3-33. As resulted, the building response is symmetrical and the recorded peak interstorey drift is 1.48% h_s. Despite reduced interstorey drift, the right side brace located at bottom floor experienced DI = 1.0 which shows that the outermost compressive fiber of critical brace cross-section attained its fatigue life at time sequence 116 s. At the same time sequence, the compressive strain moved to positive side.

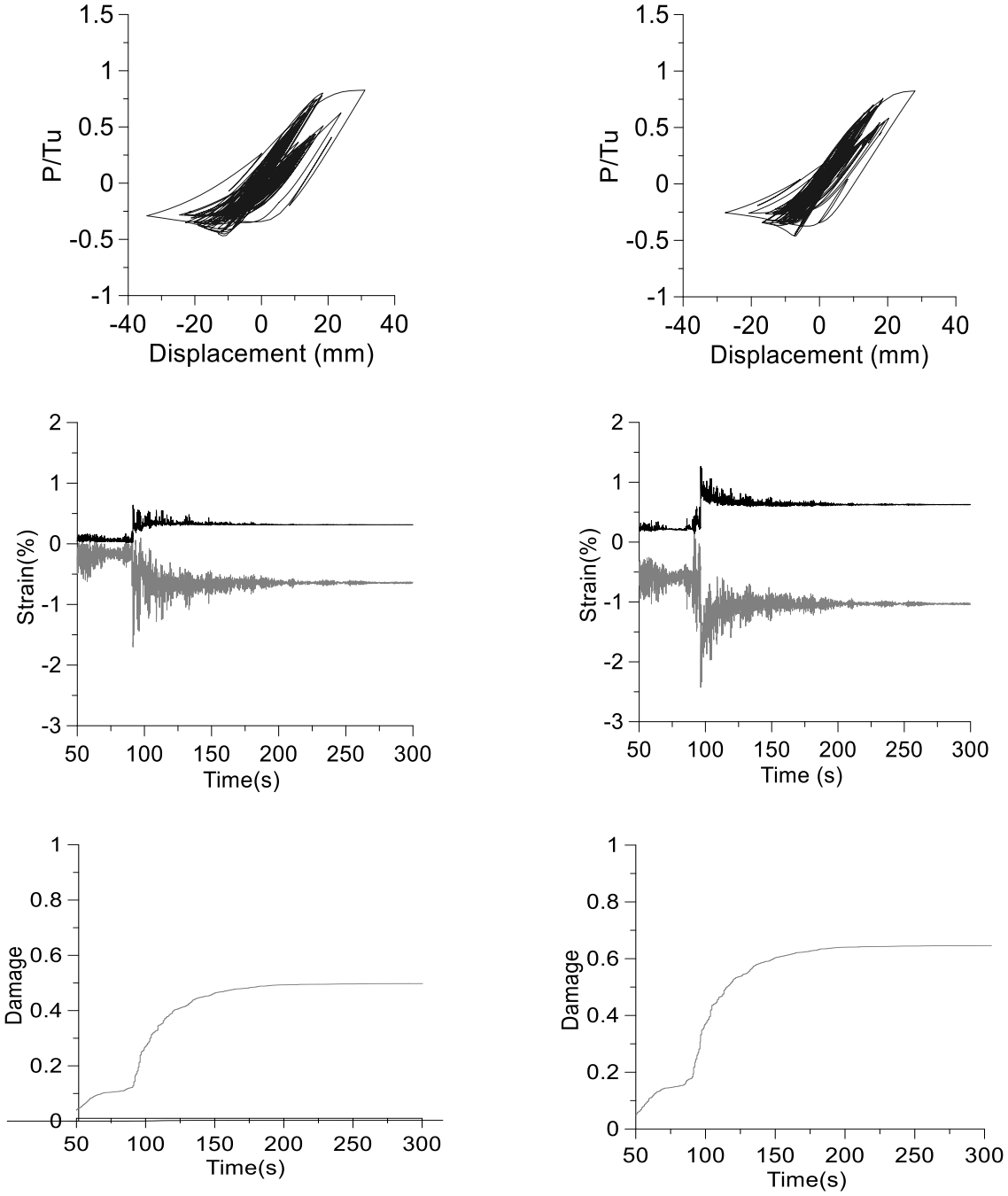

Figure 3-32 Hysteresis response of bottom floor braces, their strain time-history series and damage index of the outermost compressive fiber under the #FKS010subduction record

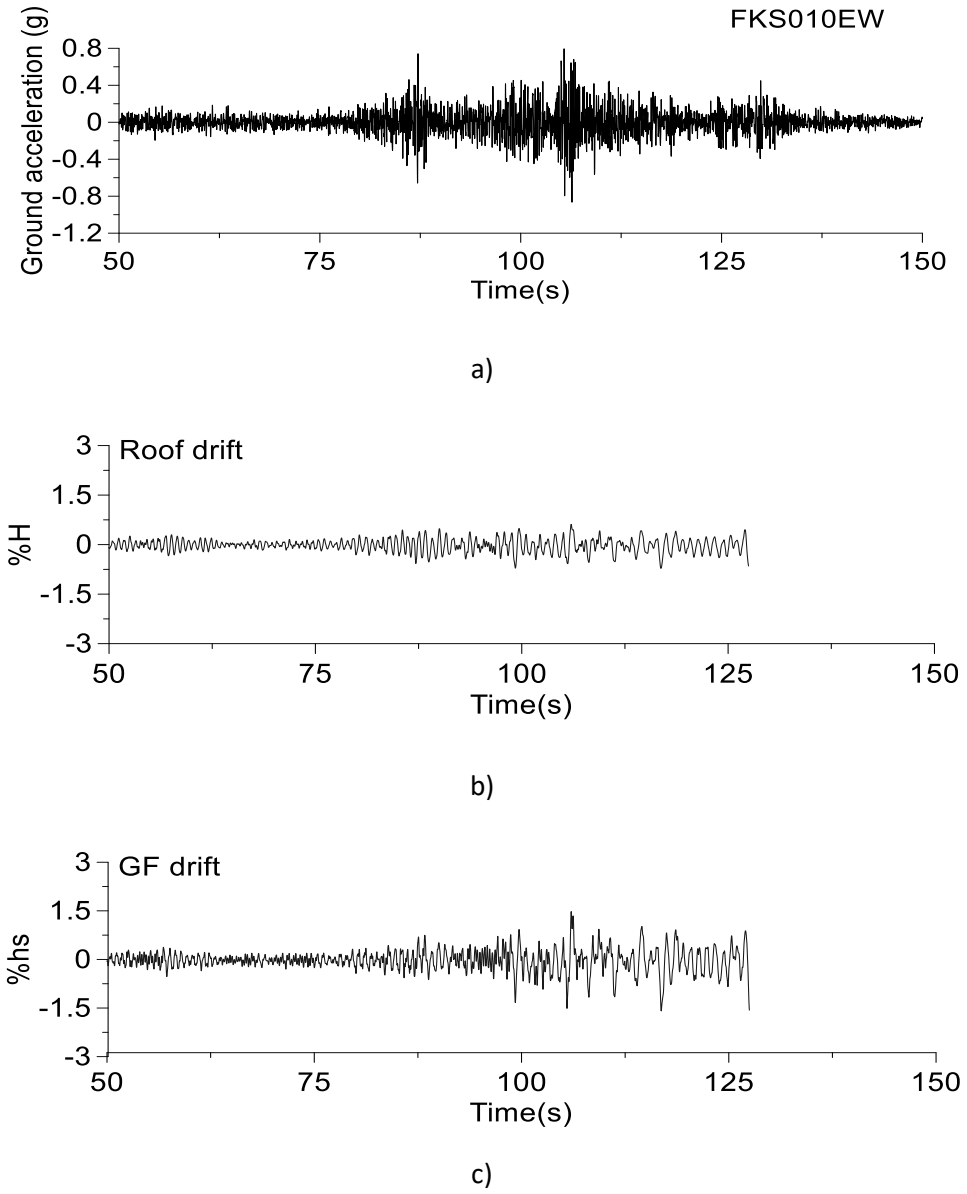

Figure 3-33 Response of 4-storey MD-CBF building under re-scaled #FKS010 subduction record: a) accelerogram, b) roof drift, c) interstorey drift time-history series recorded at bottom floor level

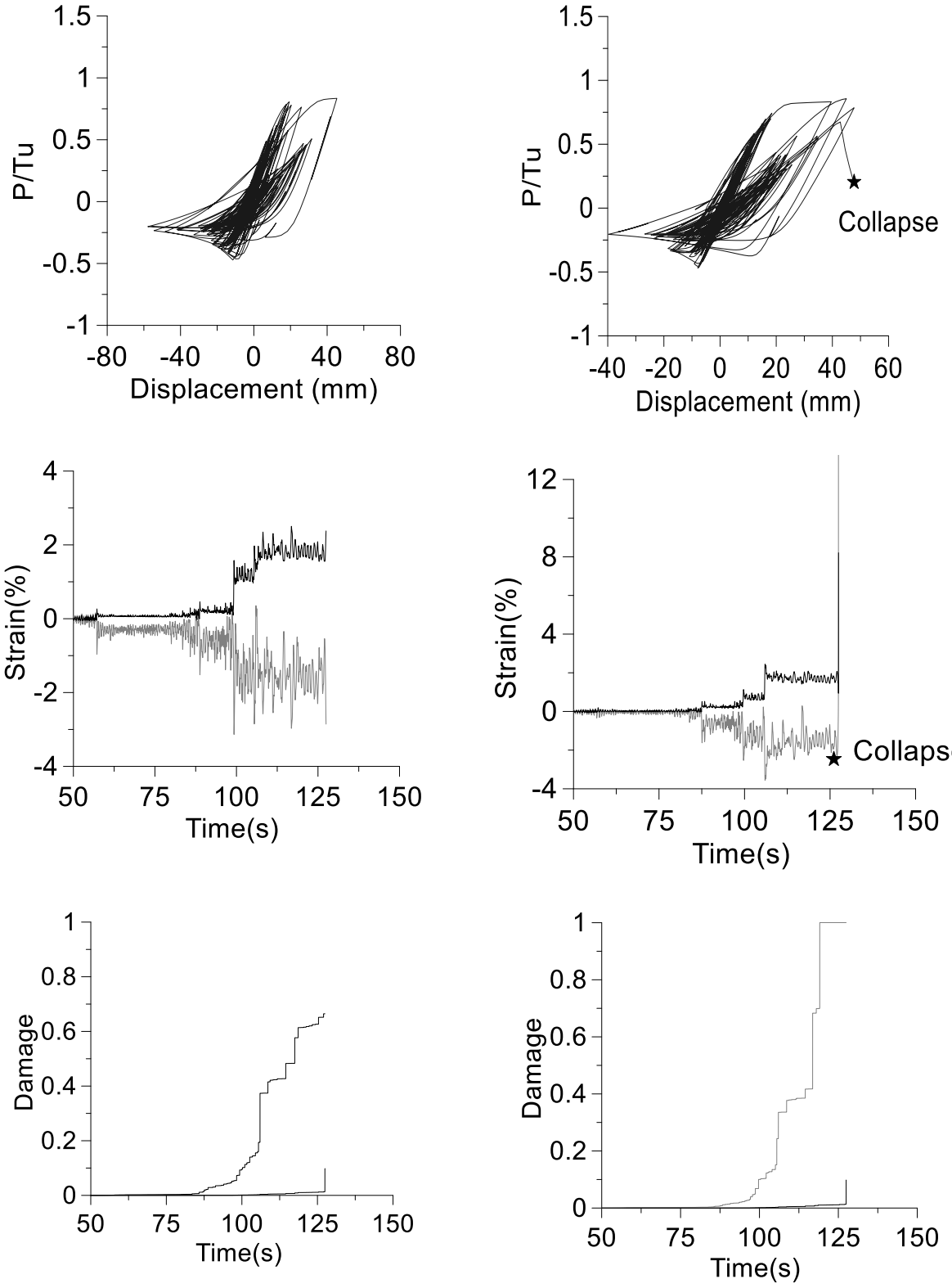

Figure 3-34 Hysteresis response of bottom floor braces, their strain time-history series and damage index of the outermost compressive fiber under re-scaled #FKS010 subduction

3.5.3. Seismic response of 8-st MD-CBF building under crustal #739 and subduction FKS005 record

To analyze the nonlinear response of the 8-storey building, two seismic ground motions were selected as input: the crustal Loma Prieta record #739 which accelerogram is depicted in Fig. 3-35a and the Tohoku subduction record #FKS005 depicted in Fig. 3-39a. When the 8-storey MD-CBF building was subjected to the crustal record, the peak interstorey drift of 2.45% h_s was recorded at the roof level. The time-history series of roof drift and roof interstorey drift are plotted in Figs. 3-36b and 3-36c. Figure 3-37 shows the nonlinear hysteresis response of the left and right braces located at the top floor. It is observd that both braces buckle in compression and yield in tension. In Fig. 3-37b the time-history series of tensile and compressive strain recorded is plotted

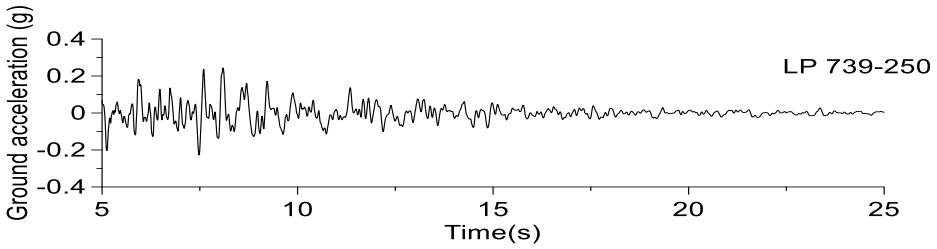

a)

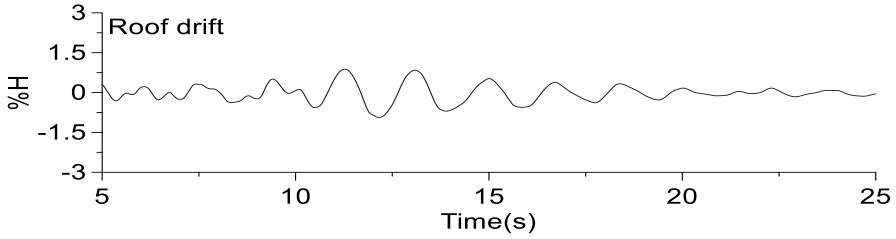

b)

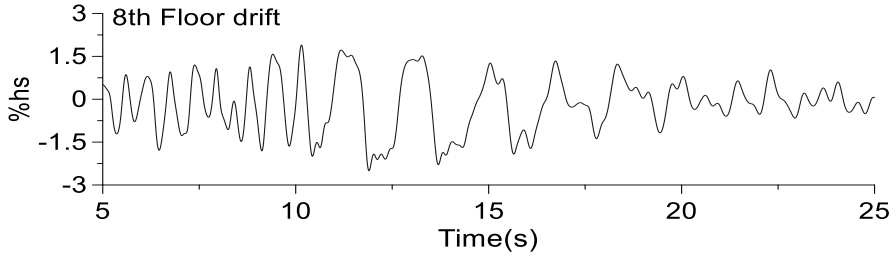

c)

Figure 3-35 Response of 8-storey MD-CBF building under #739 Loma Prieta record: a) accelerogram, b) roof drift, c) interstorey drift time-history series recorded at top floor

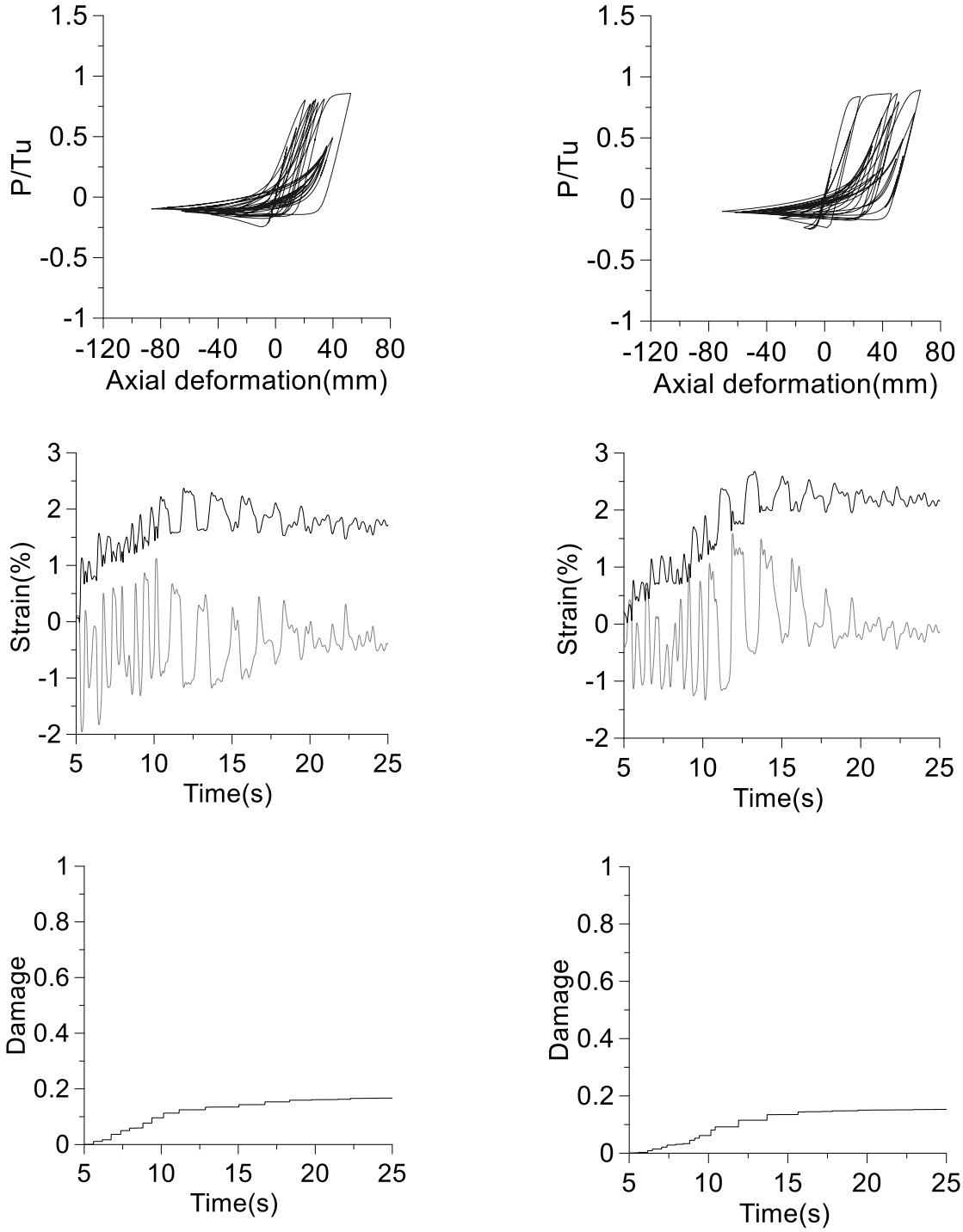

Figure 3-36 Hysteresis response of top floor braces, their strain time-history series and damage index of the outermost compressive fiber under the scaled #739 Loma Prieta crustal record

in the outermost compression fiber and tensile fiber of critical cross-section of HSS brace. Under the accumulated compression strain in the braces possess, the damage idex is DI = 0.2. The seismic respond of 8-storey MD-CBF building under the re-scaled Loma Prita record #739 is

depicted in Figs. 3-37 and 3-38. As aforementioned, the record was re-scaled by 1.2 factor to account on the accidental torsion effect. From Fig. 3-37 the maximum interstorey drift of 2.5% h_s was recorded at roof level. Therefore, it resulted a slight increase of interstorey drift when the record was re-scaled by 1.2 factor.

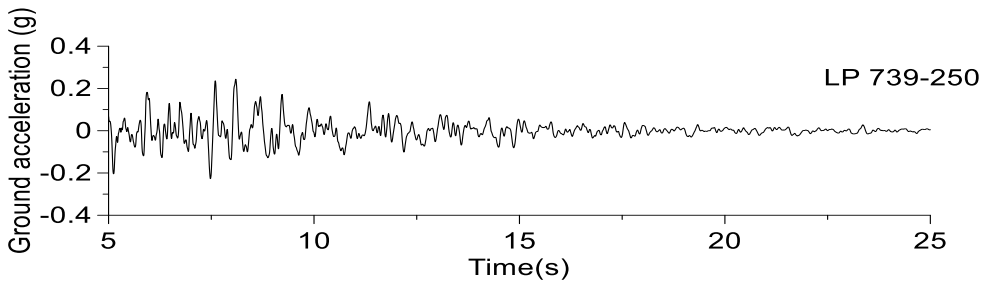

a)

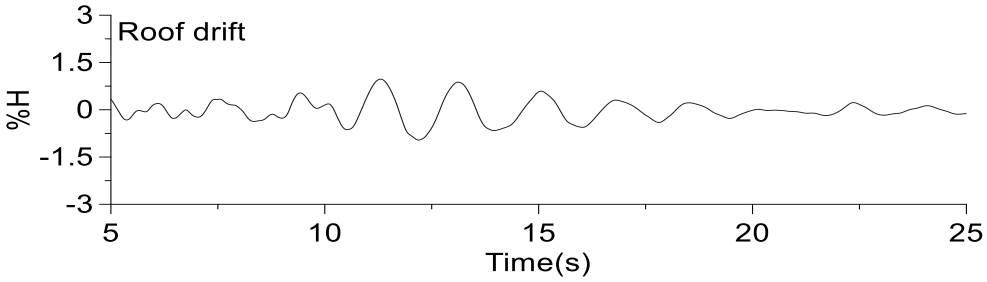

b)

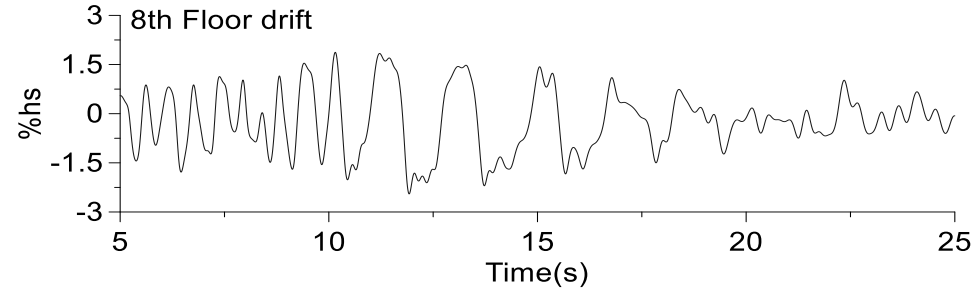

c)

Figure 3-37 Response of 8-storey MD-CBF building under #739 record amplified by correction factor: a) accelerogram, b) roof drift, c) interstorey drift time series recorded at roof roof.

The normalized hysteresis response of the left and right brace is depicted in Fig. 3-38, as well as their tensile and compressive strain time-history series experienced by the outermost compressive and tensile fiber of critical brace cross-section. Although a small increase in the

interstorey drift was observed after the record was re-scaled, the damage index of braces increased more than two times reaching 50% of brace capacity.

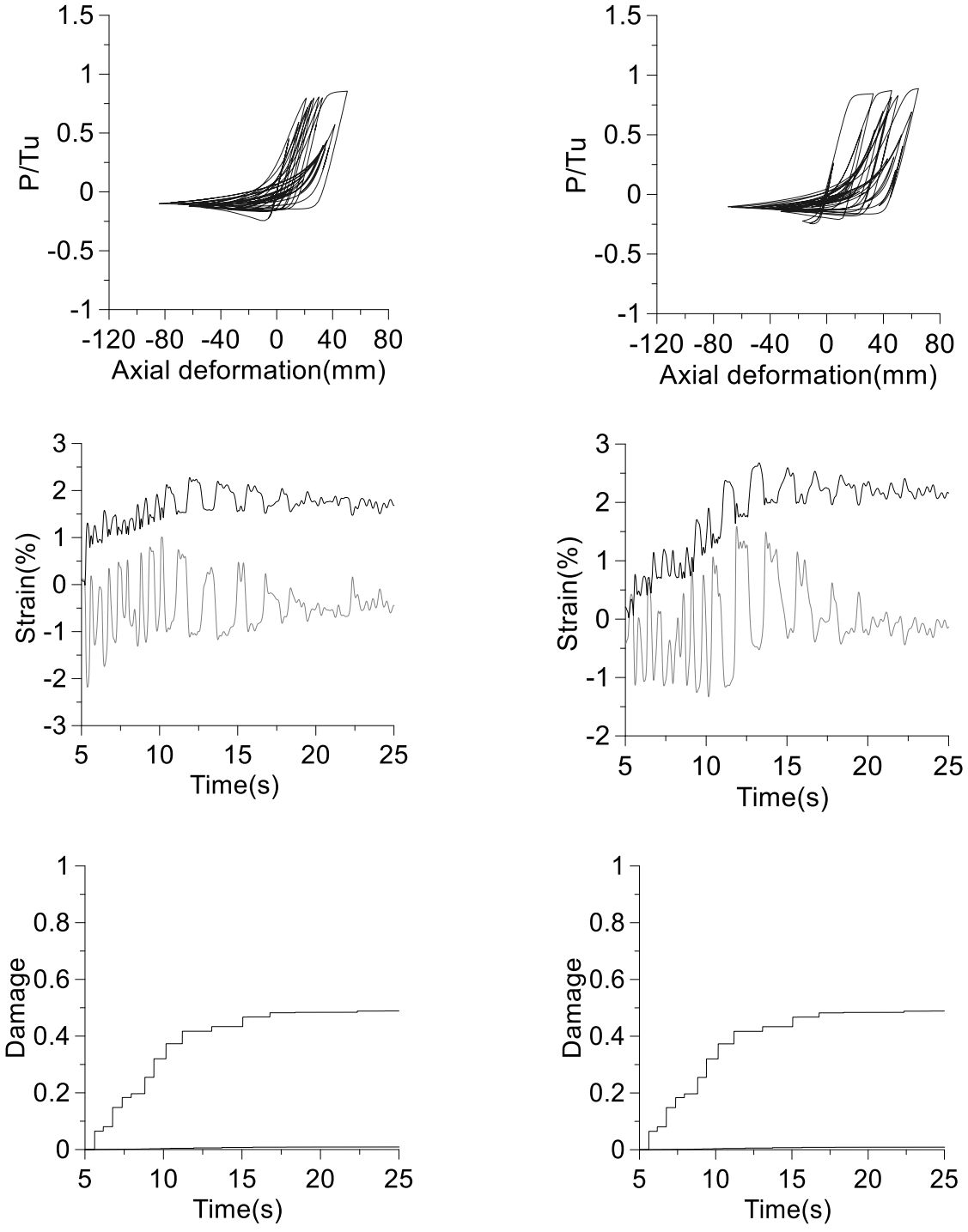

Figure 3-38 Hysteresis response of top floor braces, their strain time-history series and damage index of the outermost compressive fiber under the re-scaled #739 crustal record

The response of the 8-storey MD-CBF under the subduction record FKS005 scaled with 1.0 is presented in Figs. 3-39 and 3-40. Hence, in Figs. 3-39b and 3-39c show the time-history series of roof drift and interstorey drift recorded at the 3rd floor where the peak interstorey drift among floors was experienced. To better emphasize the building behaviour only the response between the time sequence 50 s and 150 s is presented. The maximum interstorey drift is 2.33% h_s which is within the code limits. The nonlinear hysteresis response of braces located at the 3rd floor is illustrated in Fig. 3-40. It is observed that both braces buckle in compression and yield in tension. The strain time-history series of the outermost compressive and tensile fiber of the critical brace cross-section of the 3rd floor is depicted in Fig. 3-40. The DI of these braces is 0.5.

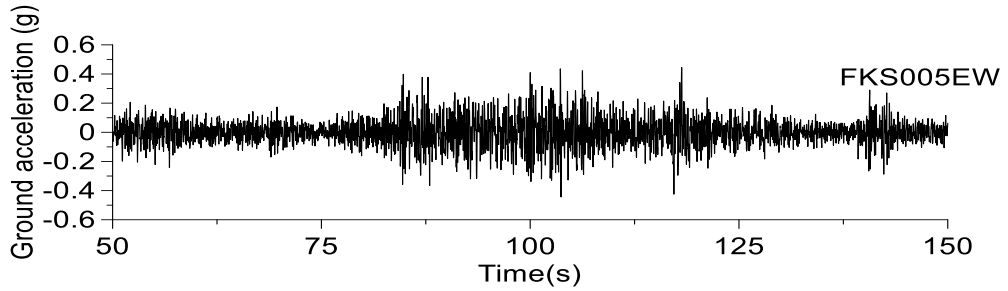

a)

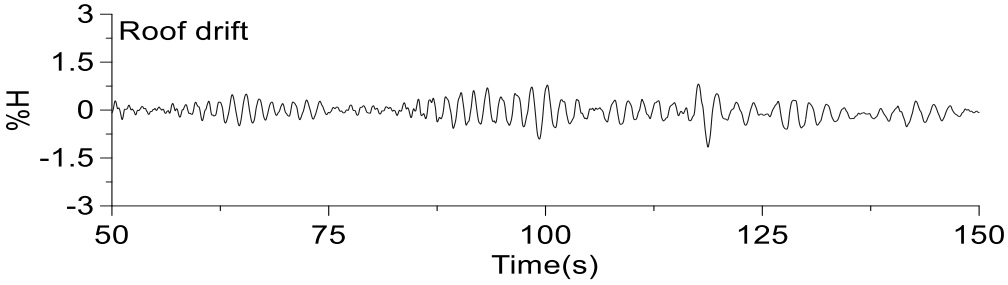

b)

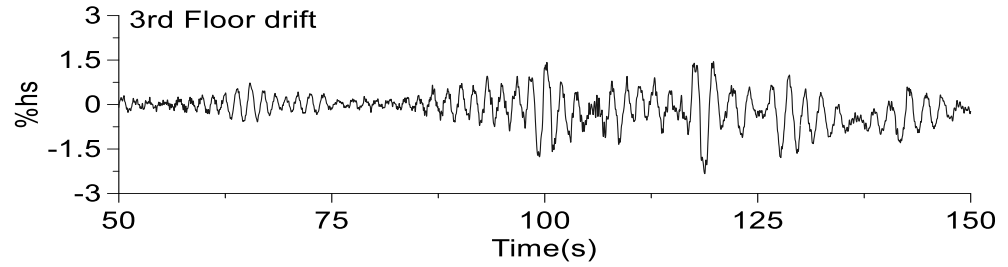

c)

Figure 3-39 Response of 8-storey MD-CBF building under #FKS005 subduction record: a) accelerogram, b) roof drift, c) interstorey drift time-history series recorded at the 3rd floor

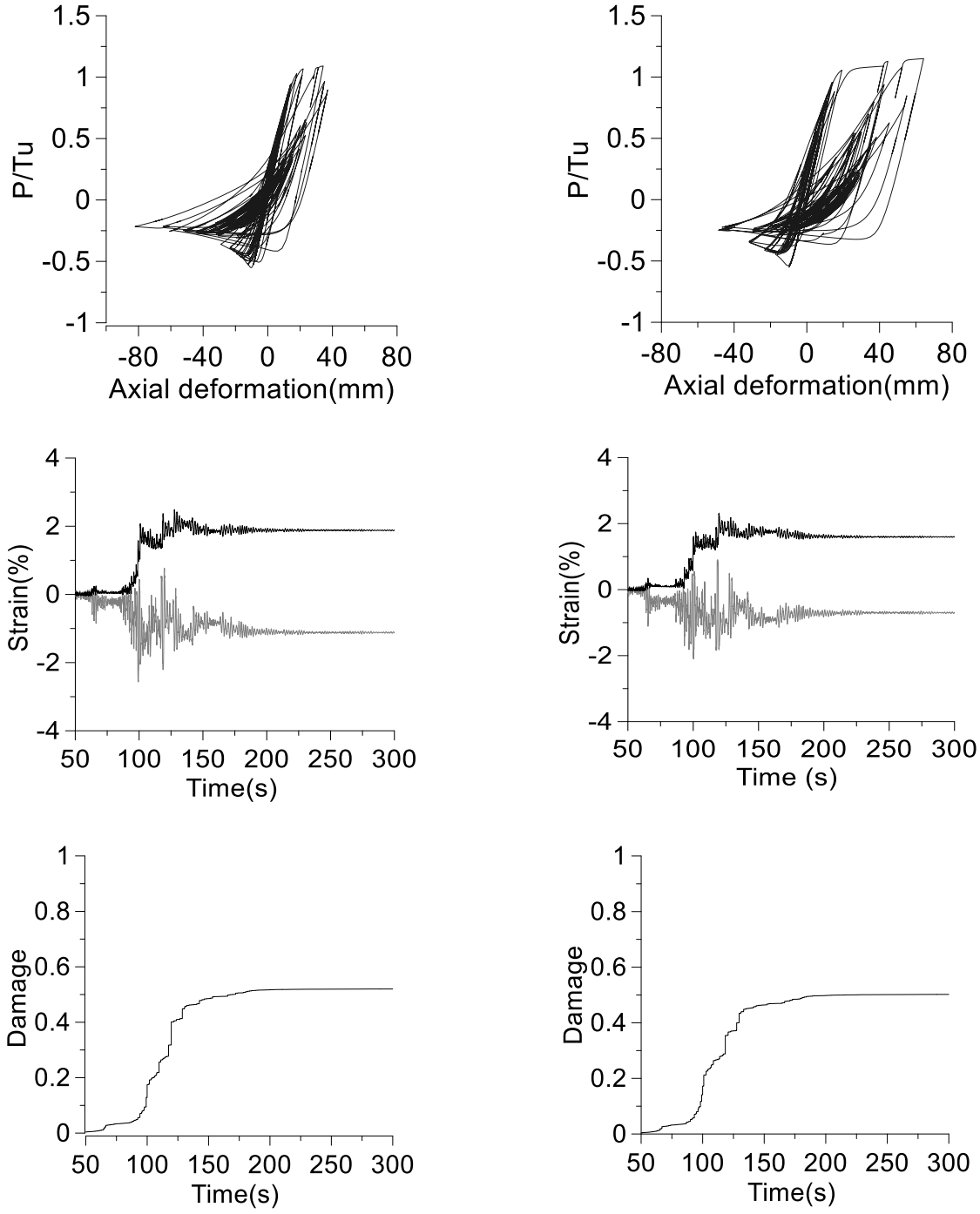

Figure 3-40 Hysteresis response of 3rd floor braces, their strain time-history series and damage index of the outermost compressive fiber under the # FKS005 subduction record

The response of the 8-storey MD-CBF building subjected to re-scaled subduction record #FKS005 using the 1.2 factor is depicted in Figs. 3-41 and 3-42. The accelerogram, the roof

drift and inter- storey drift of 3rd floor are shown in the Fig. 3-42. Herein, the maximum interstorey drift is 3.36% h_s which is greater than the code limit and occurred at 118 s. It is interesting to note that after the peak interestorey drift is recorded, the building oscillates to one side and a jump is observed in the strain time-history series, as well as, the strain accumulated in the monitored fiber accounting for higher DI. As expected, both left and right braces of 3rd floor show yielding in tension and buckling in compression. The strain in the outermost compression fiber of critical cross-section of the right side brace is found to reach 60%.

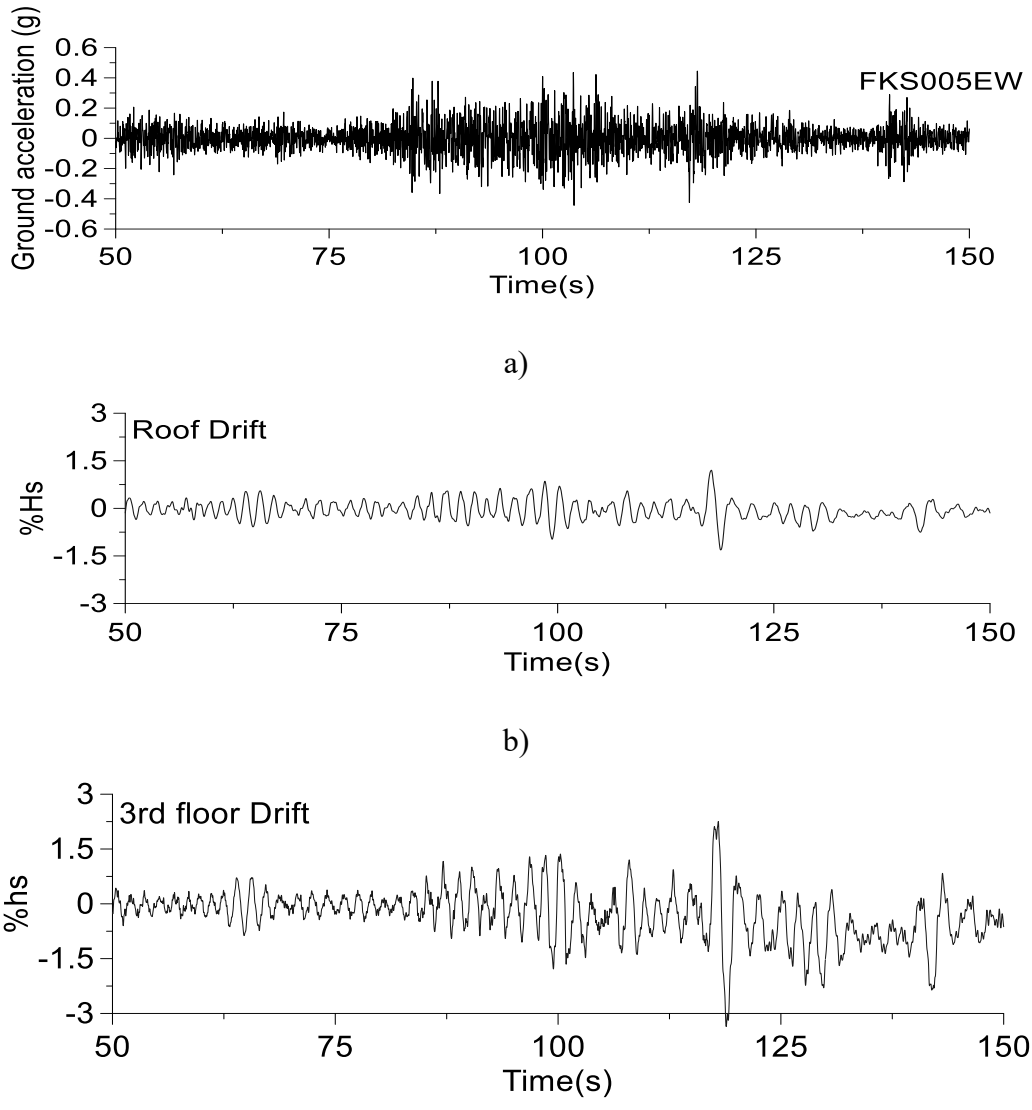

Figure 3-41 Response of 8-storey MD-CBF building under re-scaled # FKS005 subduction record: a) accelerogram, b) roof drift, c) interstorey drift time-history series at the 3rd floor

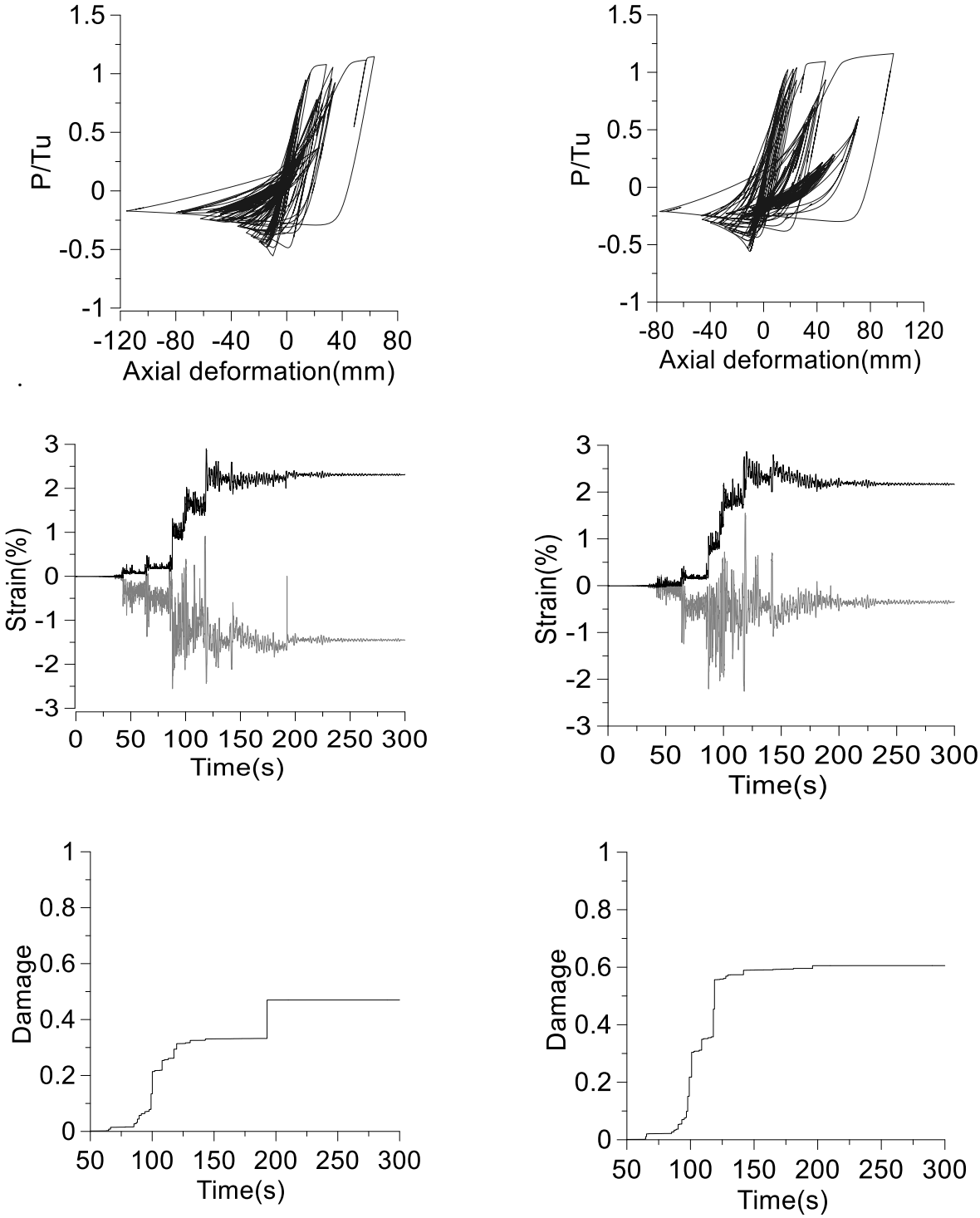

Figure 3-42 Hysteresis response of 3rd floor braces, their strain time-history series and damage index of the outermost compressive fiber under re-scaled # FKS005 subduction record.

3.5.4. Seismic response of 12-st MD-CBF building under crustal #1039 and subduction MGY004 record

To analyze the seismic response of the 12-story MD-CBF building, the selected event is Northridge, crustal record #1039 with the scaled accelerogram plotted in Fig. 3-43 together with the time-history series of roof drift and interstorey drift. It is noted that the peak interstorey drift of 1.37% h_s among floors was recorded at the top floor. As depicted, the building vibrates almost symmetrically. The nonlinear hysteresis response of the left and right braces located at the top floor is given in Fig. 3-44. As resulted both braces buckle in compression and yield in tension. In Fig. 3-44b is plotted the time-history series of strain recorded in the outermost compression fiber

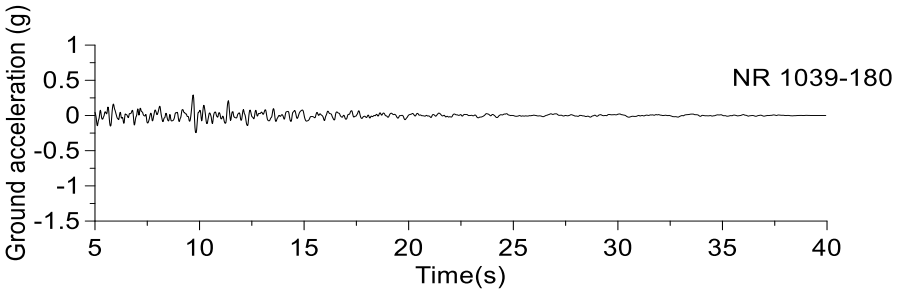

a)

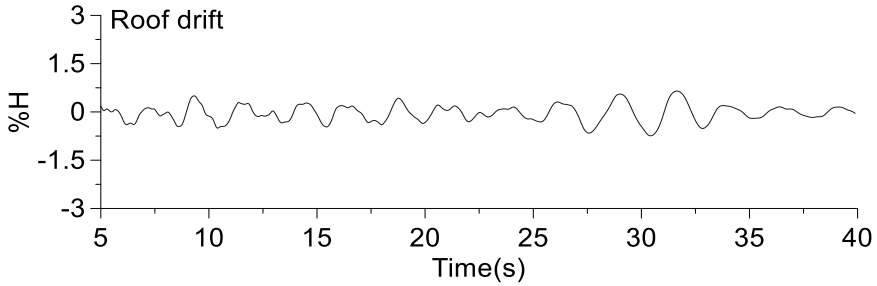

b)

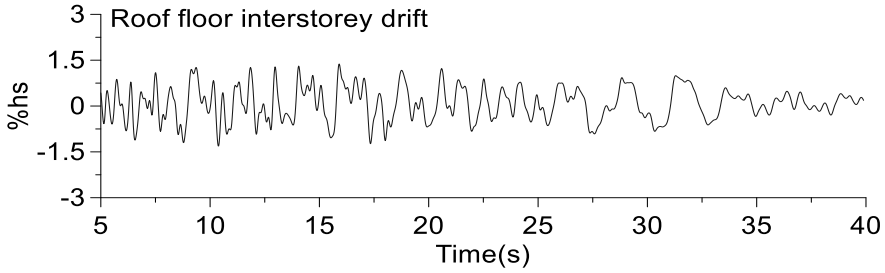

c)

Figure 3-43 Response of 12-storey MD-CBF building under scaled #1039 record: a) accelerogram, b) roof drift, c) interstorey drift time-history series recorded at top floor.

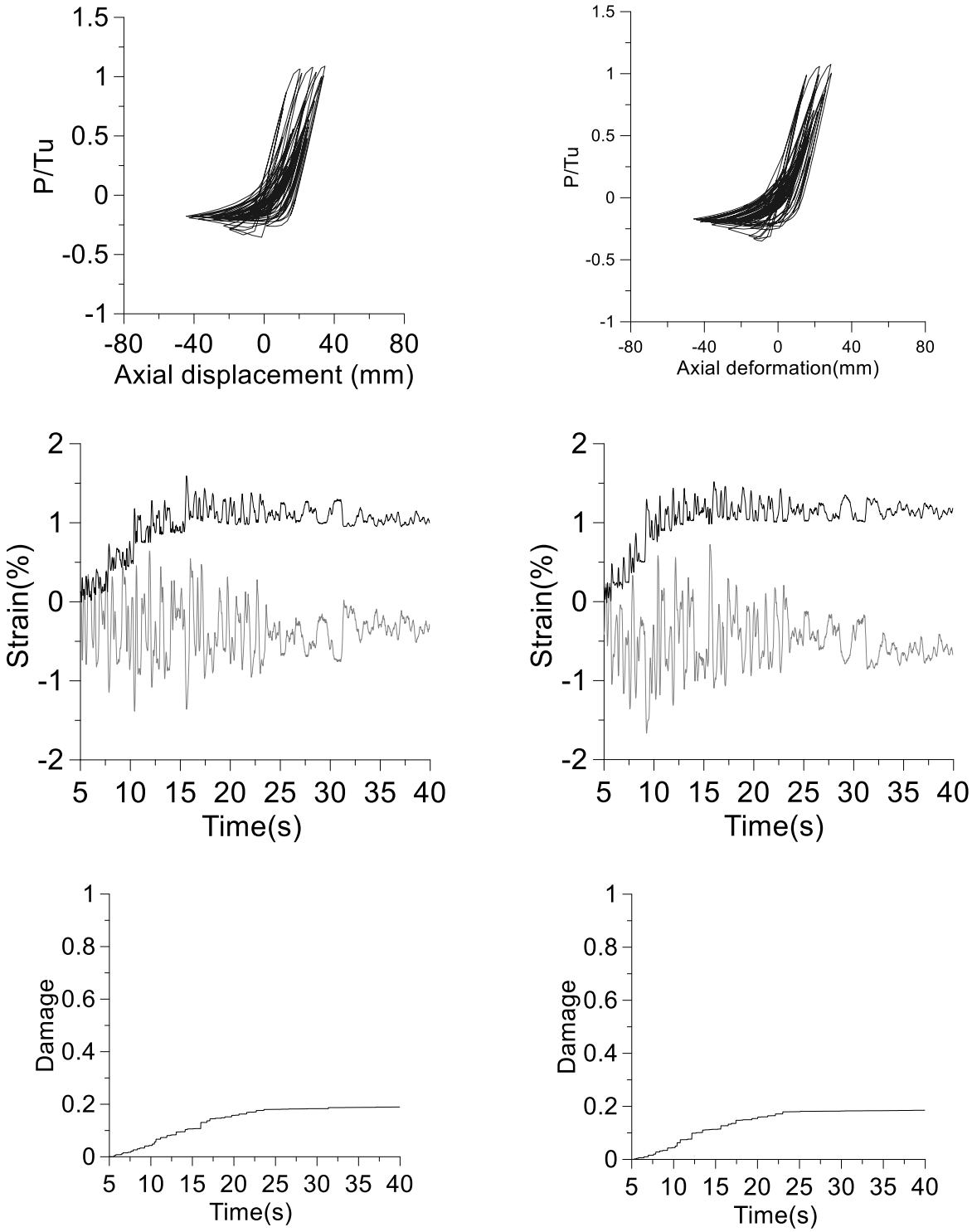

Figure 3-44 Hysteresis response of top floor braces, their strain time-history series and damage index of the outermost compressive fiber under the scaled #1039 crustal record

and tensile fiber of critical brace cross-section. From time-history of compression strain it is observed that the amplitude of compressive strain diminishes toward the end of ground motion and is preserved in the negative side. In Fig. 3-44c is illustrated DI = 0.2 for the same fiber.

Increasing the acceleration amplitude of ground motion by the scale factor of 1.2 (to take into account the effect of shear due to torsion caused by accidental eccentricity), Fig. 3-45 shows the scaled accelerogram, the time-history series of roof drift, and the interstorey drift recorded at the top floor. The response of the 12-storey MD-CBF building has the same trend as shown in Fig. 3-43 but the peak interstorey drift increases to 2.13% h_s. The hysteresis response of top floor braces, the time-history series of tensile and compressive strain of the outermost fiber of critical braces cross-sections, as well as the brace damage index (DI = 0.2) is illustrated in Fig. 3-45.

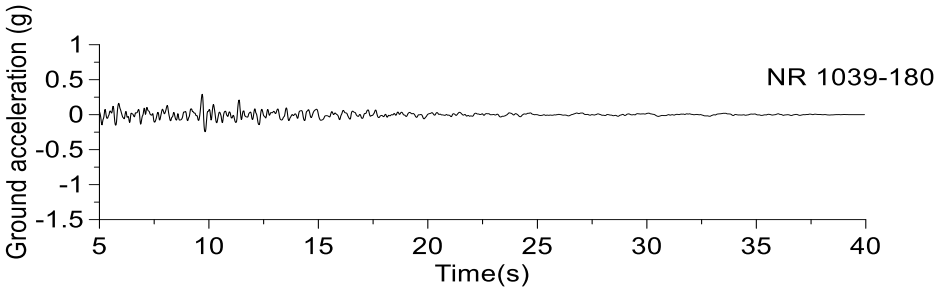

a)

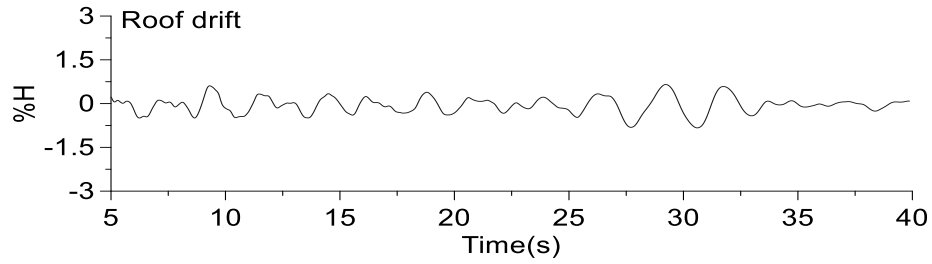

b)

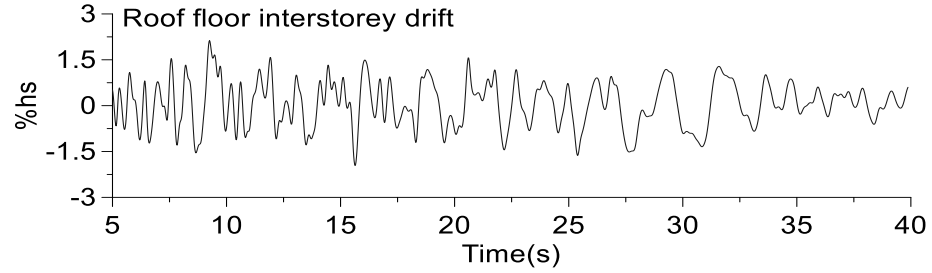

c)

Figure 3-45 Response of 12-storey MD-CBF building under re-scaled #1039 record: a) accelerogram, b) roof drift, c) interstorey drift time-history series recorded at top floor

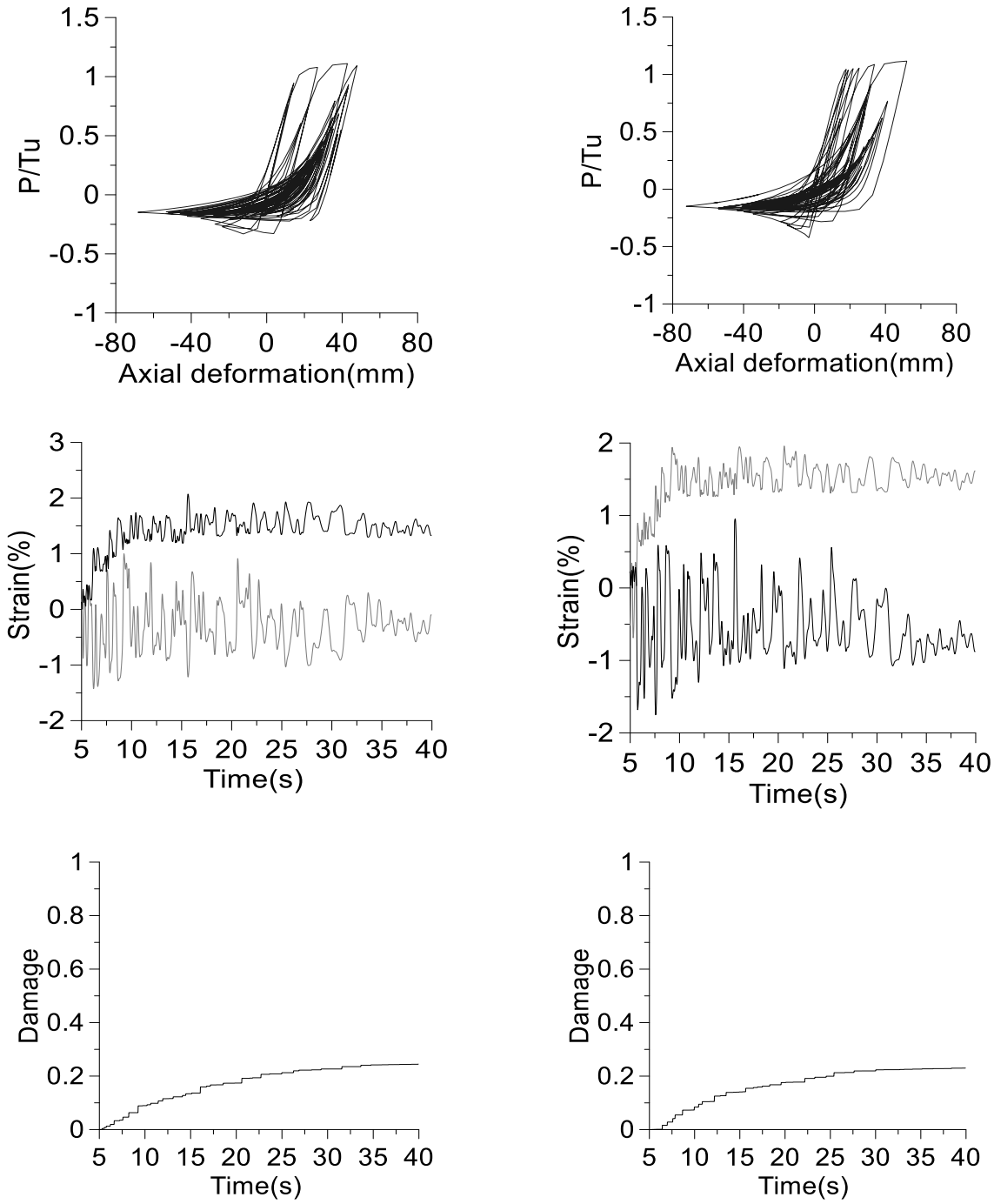

Figure 3-46 Hysteresis response of top floor braces, their strain time-history series and DI of the outermost compressive fiber under the re-scaled #1039 crustal record

Comparing Fig. 3-44 and Fig. 3-46 there is not a large difference in behavior. The response of 12-storey MD-CBF building under the subduction record #MYG004 is presented in Fig. 3-47

and Fig. 3-48. Hence, Fig. 3-47 presented the accelerogram with an applied scaling factor equal to 1.0, as well as the time-history series of roof drift and interstorey drift recorded at the 3rd floor where the peak among floors was experienced. To better emphasize the building response, only the time sequence interval 50 s and 150 s was selected. After the occurrence of the main shock at the time sequence of 96 s, the building deflected laterally in one side. The maximum interstorey drift is 2.3% h_s which is within the code limit. The hysteresis response of braces located at the 3rd floor shows that both braces buckle in compression and yield in tension (Fig. 3-48). There is an important difference in the time-history series of tensile and compression strain recorded at the outermost compressive fiber of critical brace cross-section. At the time sequence corresponding to the main shock (t = 96 s) there is a jump in the time-history series of tensile and compressive strain which means that a large amount of strain was suddenly accumulated. Meanwhile, at the same time sequence, the compressive strain recorded in the outermost compressive fiber of critical cross-section of right side brace increases in the tensile side. Meanwhile, at the same time sequence, a jump in the damage index of brace is also recorded. The DI of the outermost compressive fiber of critical section of right brace reaches 0.5.

The response of 12-storey MD-CBF building subjected to subduction record #MGY004 amplified by 1.2 scaling factor is presented in Fig. 3-49 and 3-50. Fig. 3-49 shows the re-scaled accelerogram and the time-history series of roof drift and interstorey drift of the 3rd floor, respectively. As depicted, the peak interstorey drift of 3.33% h_s is recorded at the time sequence of 96 s where the jump in strain is emphasized in Fig. 3-50. After the peak interstorey drift was experienced, the building starts oscillating to one side without being able to return to the initial position. The hysteresis response of braces is illustrated in Fig 3-50. As depicted, both braces buckle in compression and yielding in tension. Meanwhile, in Fig. 3-50 the plot of time-history series of tensile and compressive strain recorded in the outermost compressive and tensile fiber of critical braces are shown, and the damage index shows the braces reaching 60% of its capacity.

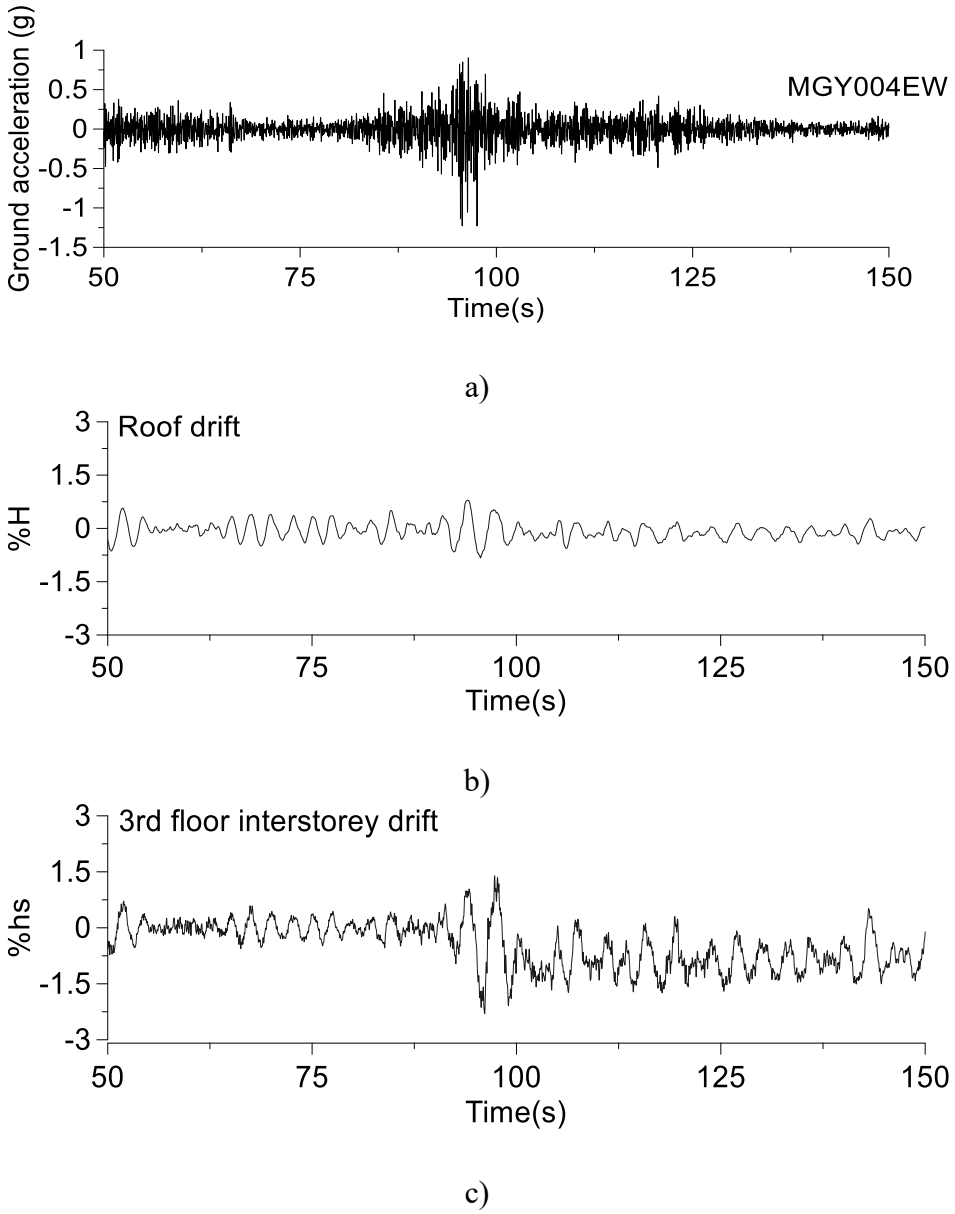

Figure 3-47 Response of 12-storey MD-CBF building under #MYG004 subduction record: a) accelerogram, b) roof drift, c) interstorey drift time series recorded at the 3rd floor

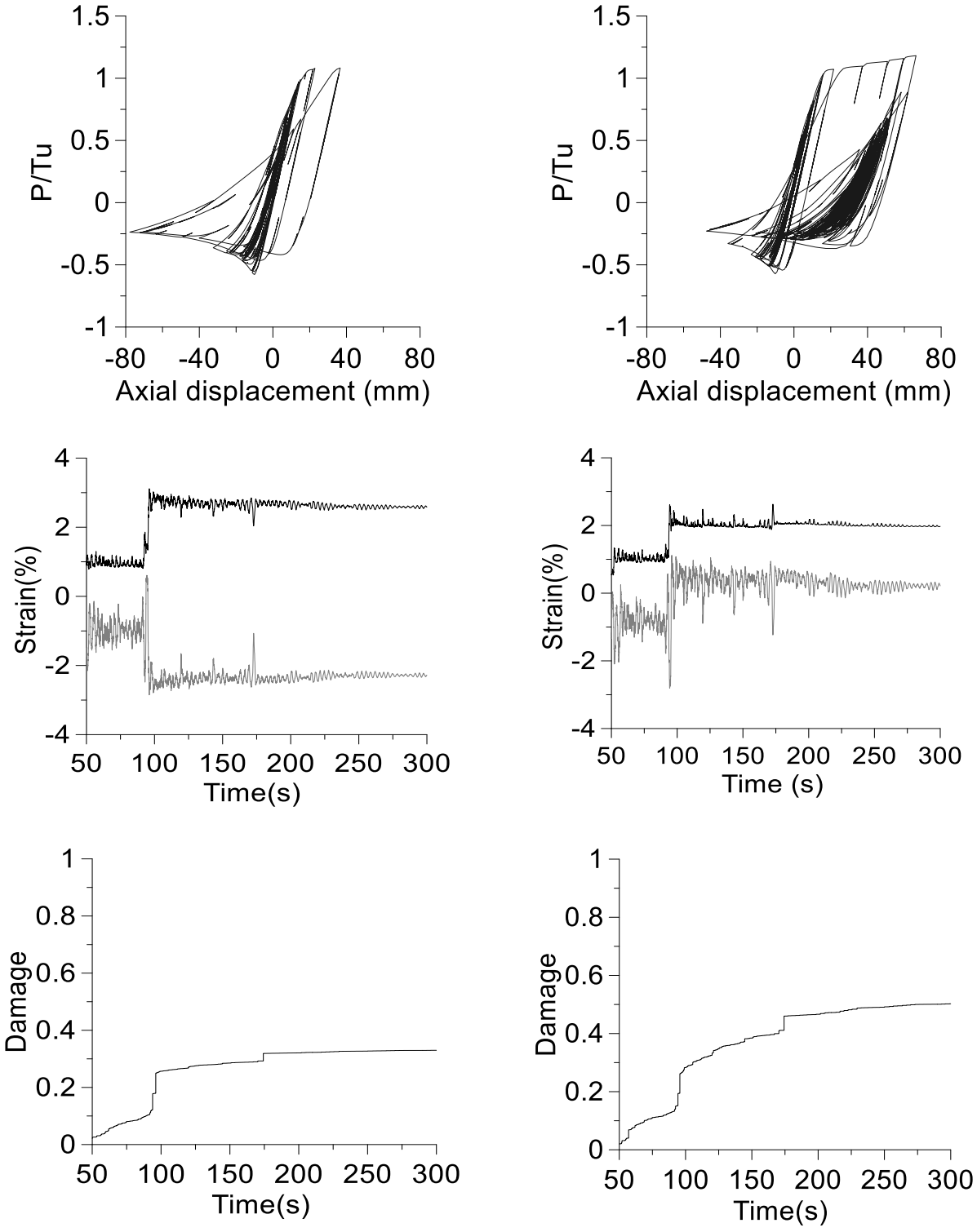

Figure 3-48 Hysteresis response, strain, and DI of both braces located at the 3rd floor under the #MYG004 subduction record

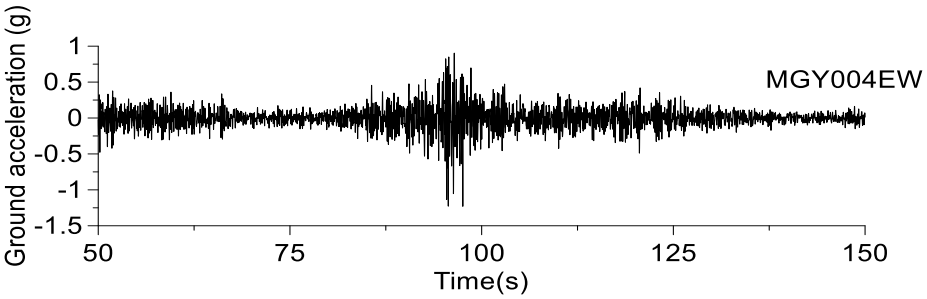

a)

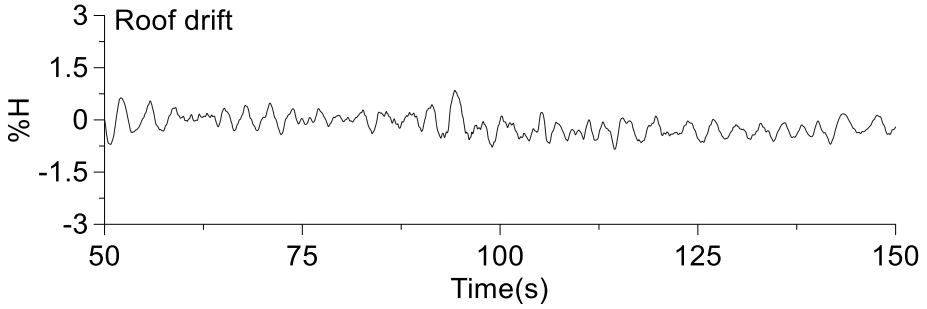

b)

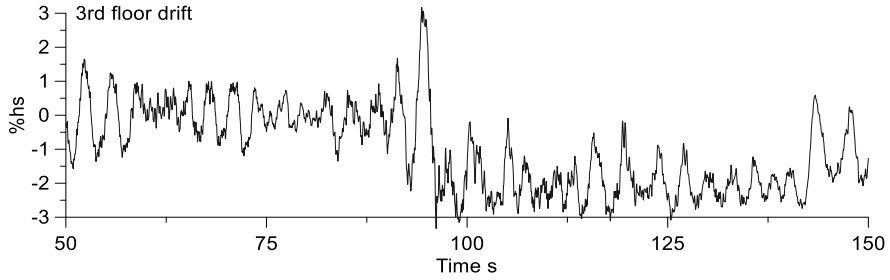

c)

Figure 3-49 Response of 12-storey MD-CBF building under #MYG004 subduction record amplified by correction factor: a) accelerogram, b) roof drift, c) interstorey drift time series at the 3rd floor.

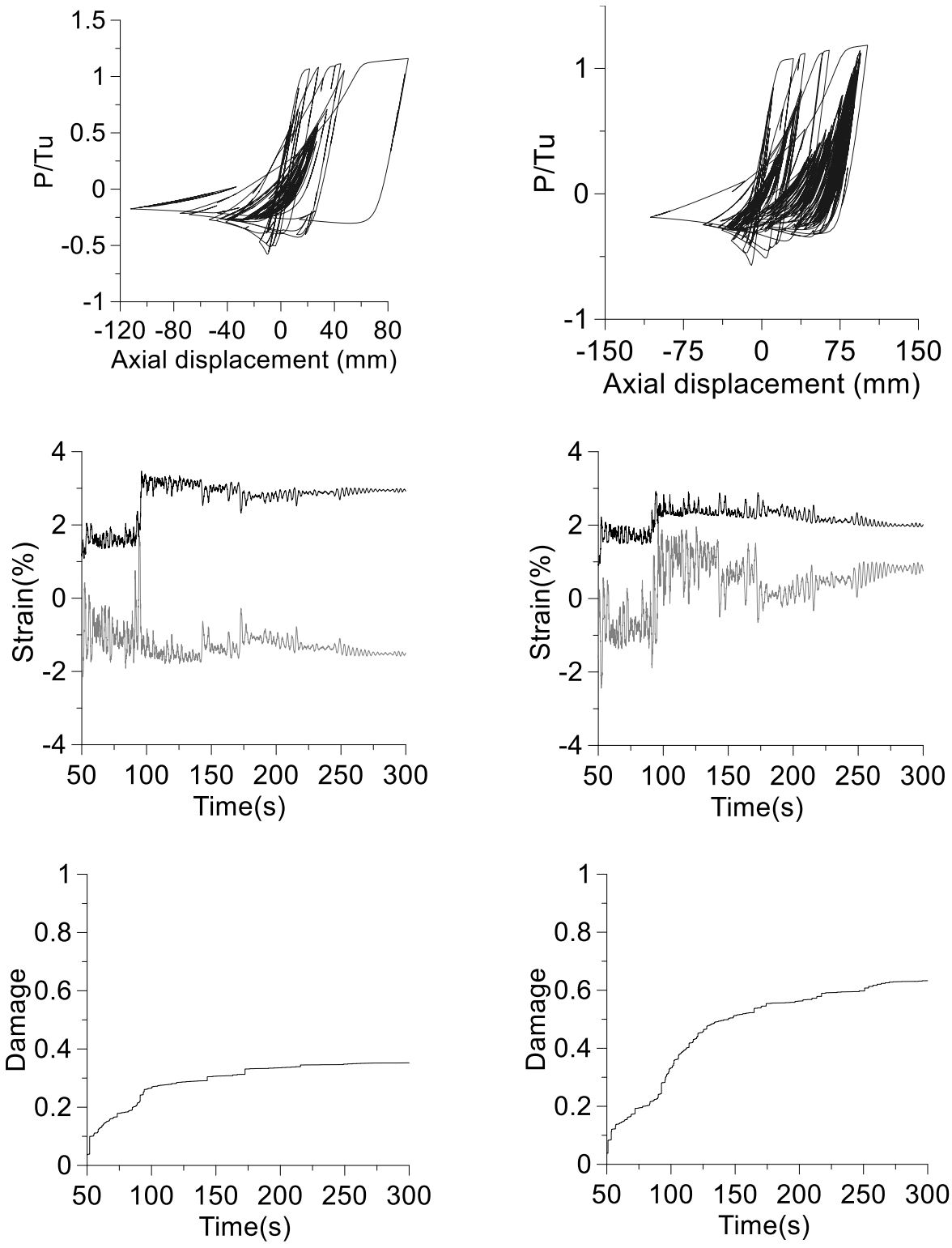

Figure 3-50 Hysteresis response, strain, and DI of both braces located at the 3rd floor under the #MYG004 subduction record amplified by correction factor

3.5.5. Seismic response of 16-st MD-CBF building under crustal #736 and subduction MGY004 record

To analyze the response of the 16-story MD-CBF building, the Loma Prieta crustal record #736 was selected. The scaled accelerogram, time-history series of roof drift and interstorey drift recorded at the 11th floor level are plotted in Fig. 3-51. The peak interstorey drift is 2.79% h_s which is slightly greater than the code limit. As depicted, the building oscillates approximately symmetric. The nonlinear hysteresis response of the left and right braces located at the top floor is given in Fig. 3-52a. Both braces buckle in compression and yield in tension. Figure 3-52b shows the plots of the time-history series of the strain recorded in the outermost compression fiber and tensile fiber of critical braces and Fig. 3-52c shows the damage index computed for the outermost

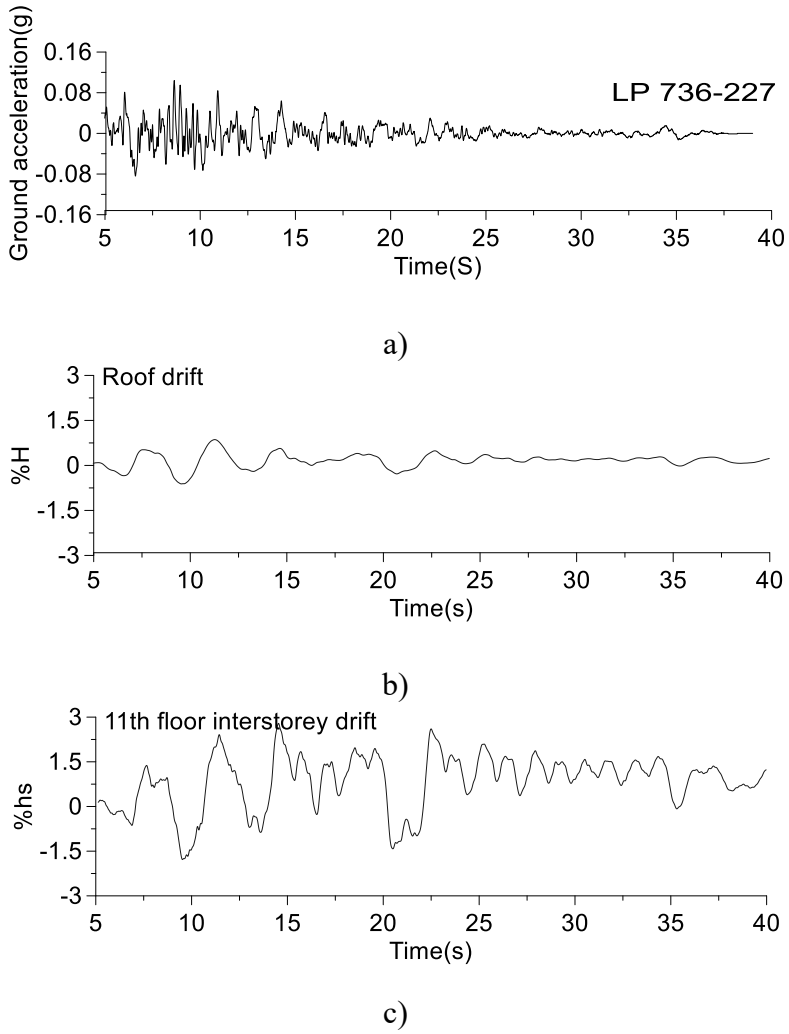

Figure 3-51 Response of 16-storey MD-CBF building under scaled #736 record: a) accelerogram, b) roof drift, c) interstorey drift time-history series recorded at 11th floor

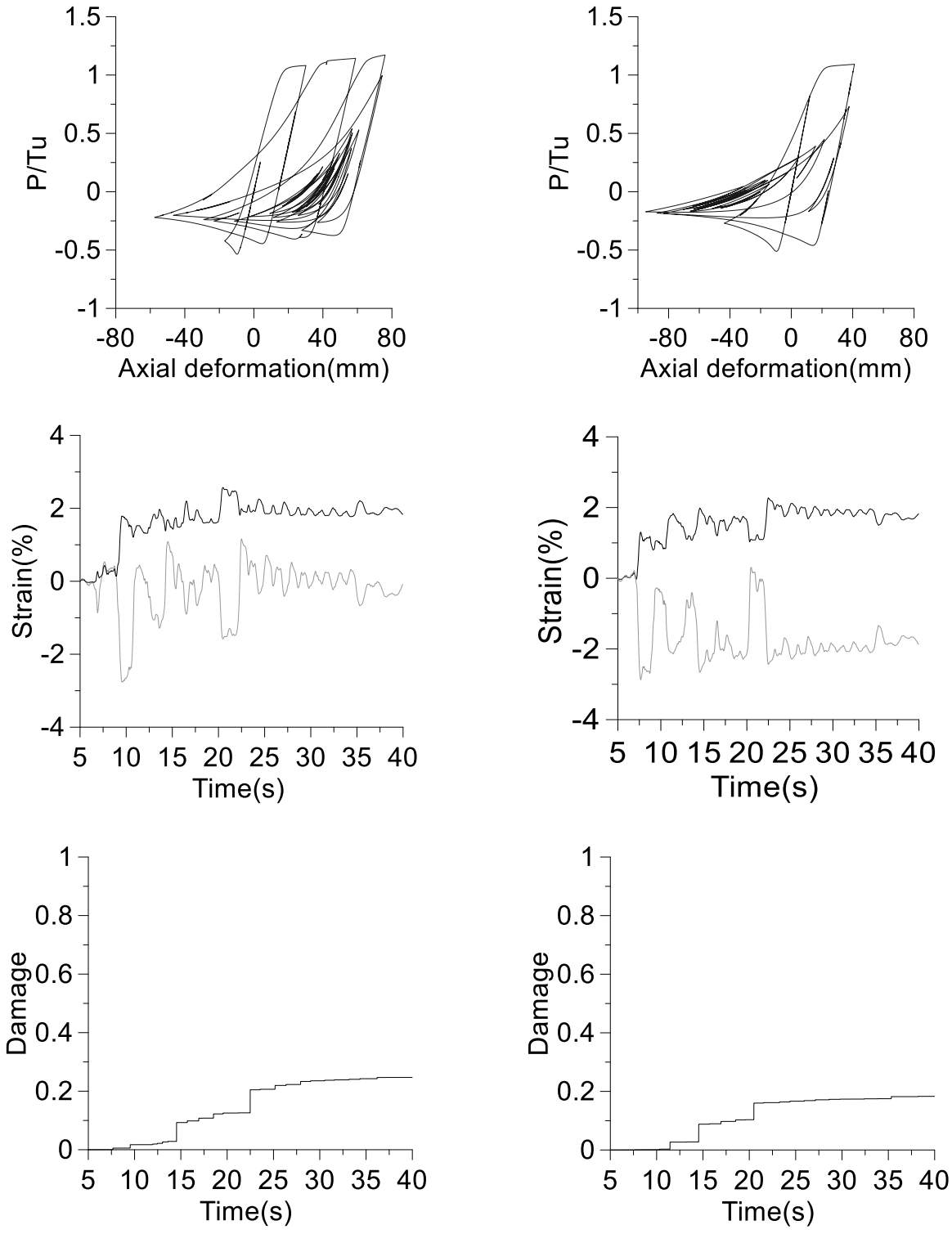

Figure 3-52 Hysteresis response of 11rd floor braces, their strain time-history series and DI of the outermost compressive fiber under the scaled #736 crustal record

compression fiber which indicates that 20% of brace capacity is consumed. It is worth noting that at the time sequence when a large cycle of strain occurs in the time-history series, a jump in the damage index file is observed which means that strain is incremented up in shorter time step. The behavior of 16-storey MD-CBF building under re-scaled Loma Preita record #736 is depicted in the Fig. 3-53 and Fig. 3-54. As shown, the interstorey drift increases to about 3% h_s, and the 11th floor of the building oscillates in one side without coming back to the initial equilibrium position. The left side brace experienced yielding in tension during at least three cycles and shows DI = 0.3.

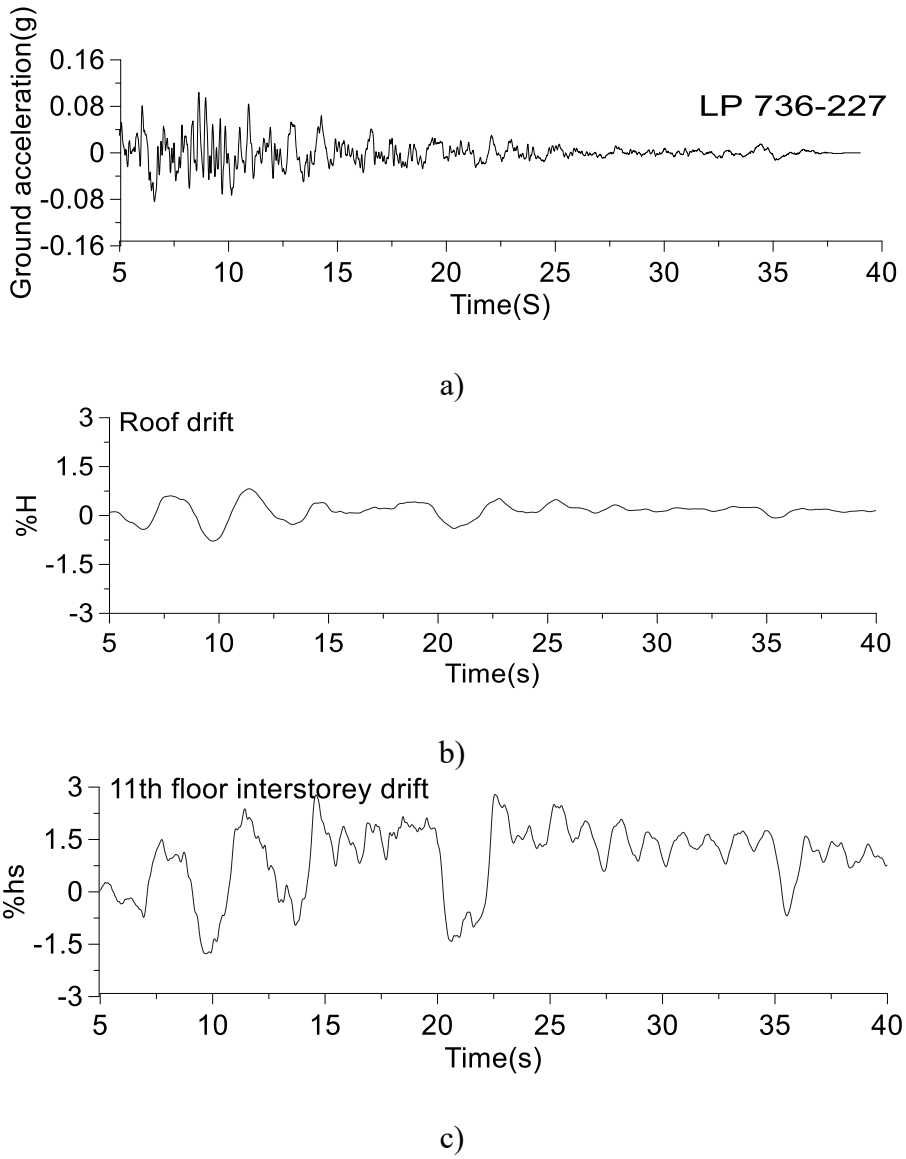

Figure 3-53 Response of 16-storey MD-CBF building under re-scaled #736 record: a) accelerogram, b) roof drift, c) interstorey drift time-history series recorded at 11th floor

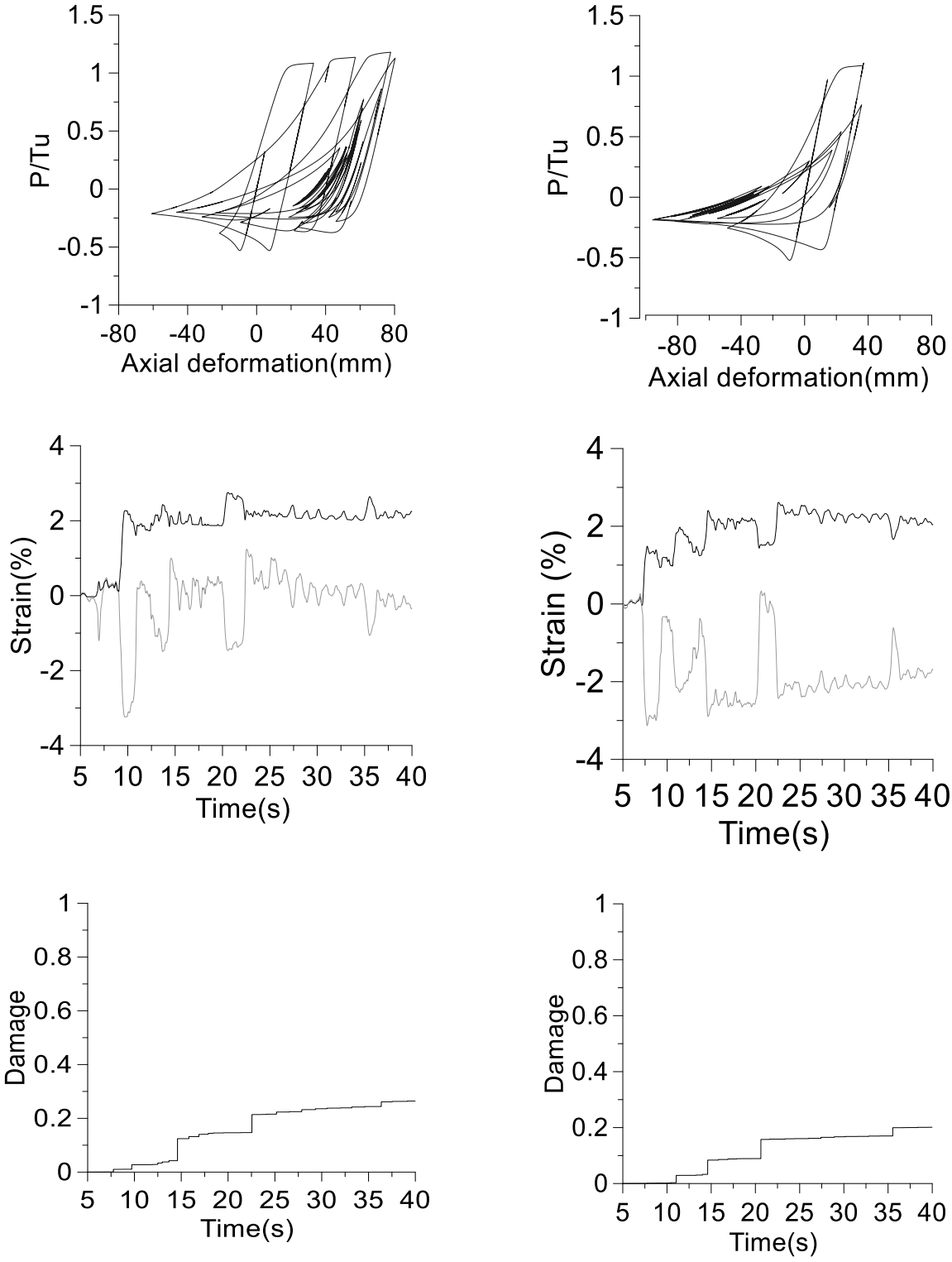

Figure 3-54 Hysteresis response of 11th floor braces, their strain time-history series and DI of the outermost compressive fiber under re-scaled #736 crustal record.

The response of the 16-storey MD-CBF building under the subduction record #MYG004 is presented in Figs. 3-55 and 3-56. For this record the scaling factor used is 1.0. The accelerogram, the time-history series of roof drift and interstorey drift recorded at the 12th floor where the peak occured is shown in Fig. 3-56.

To better emphasize the building response, it is presented between the time sequence 50 s and 150 s. Symmetrical oscillations were experienced by the floor which experiences the maximum interstorey drift of 2.76% h_s. The nonlinear hysteresis response of braces located at the 12th floor is illustrated in Fig. 3-56. It is observed that both braces buckled in compression and yielded in

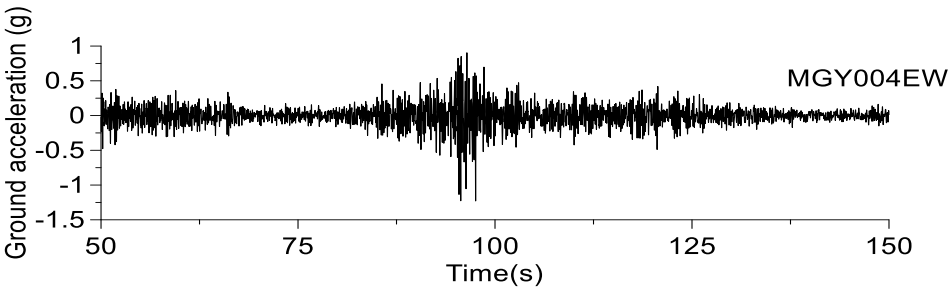

a)

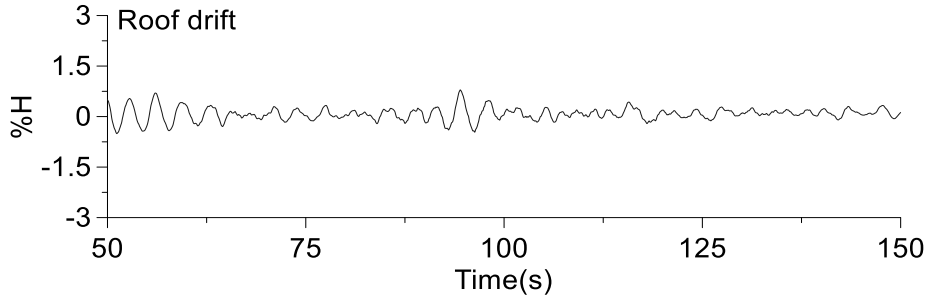

b)

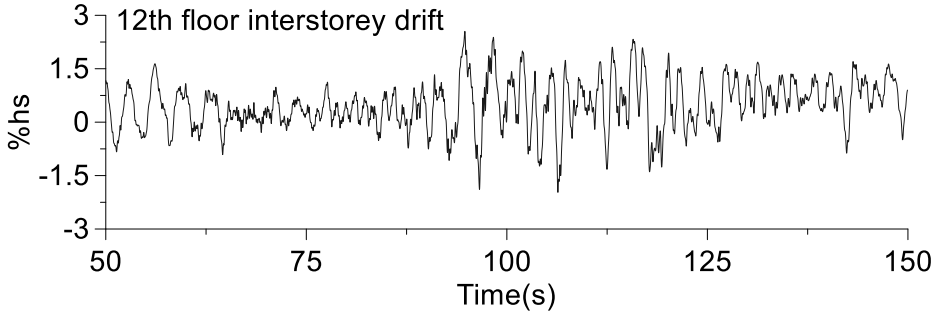

c)

Figure 3-55 Response of 16-storey MD-CBF building under #MYG004 subduction record: a) accelerogram, b) roof drift, c) interstorey drift time-history series recorded at the 12th floor

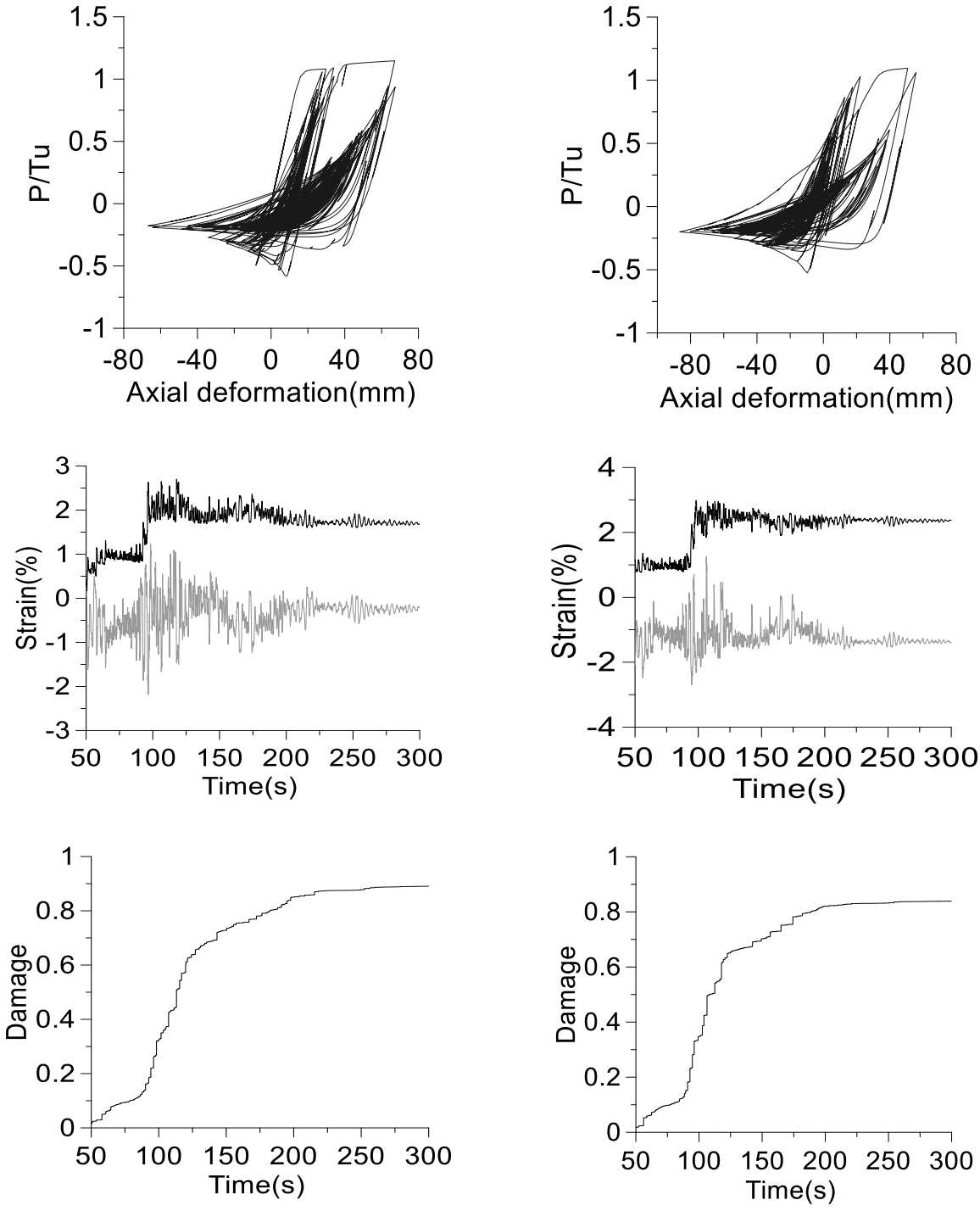

Figure 3-56 Hysteresis response of 12th floor braces, their strain time-history series and DI of the outermost compressive fiber under #MYG004 subduction record

tension. The cumulative strain of the outermost compression and tension fiber of critical brace cross-section, as well as the damage index are presented in the Fig. 3-56. The life strain of both

left and right braces reach 90% of their capacity.

To take into account the accidental torsion effect, the accelerogram was scaled with 1.2 factor. Thus, in Fig. 3-57 is shown the re-scaled accelogram, the time-history series of roof drift and interstorey drift recorded at the 12th floor where the peak was recorded. It is noted that at the time sequence t = 97 s, the building experienced a jump in interstorey drift reaching 5% h_s. After t = 97 s, the investigated 12th floor started to oscillate one side. The hysteresis response of braces located at the 12th floor is illustrated in Fig. 3-58. As depicted, both braces buckle in compression and

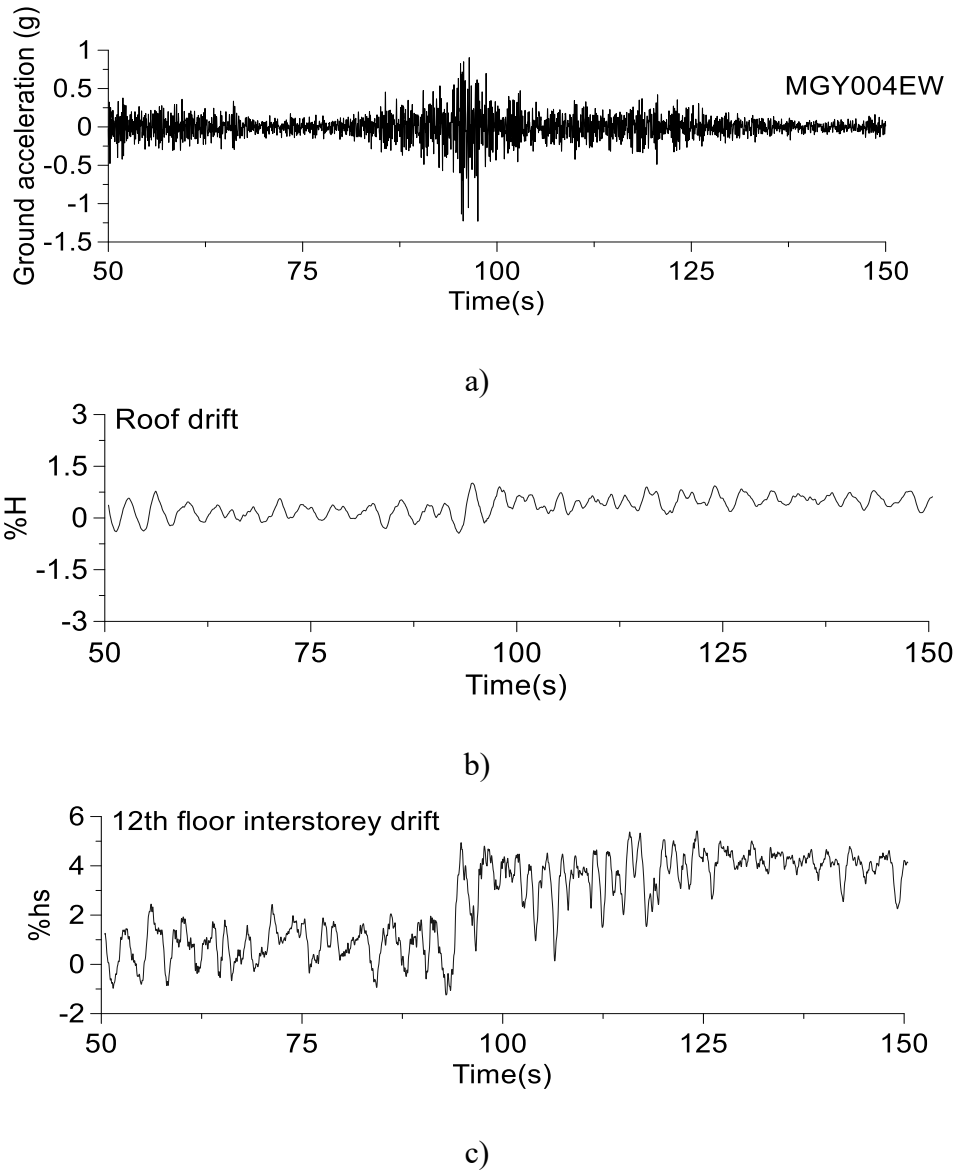

Figure 3-57 Response of 16-storey MD-CBF building under re-scaled #MYG004 subduction record: a) accelerogram, b) roof drift, c) interstorey drift time-history series at the 12th floor.

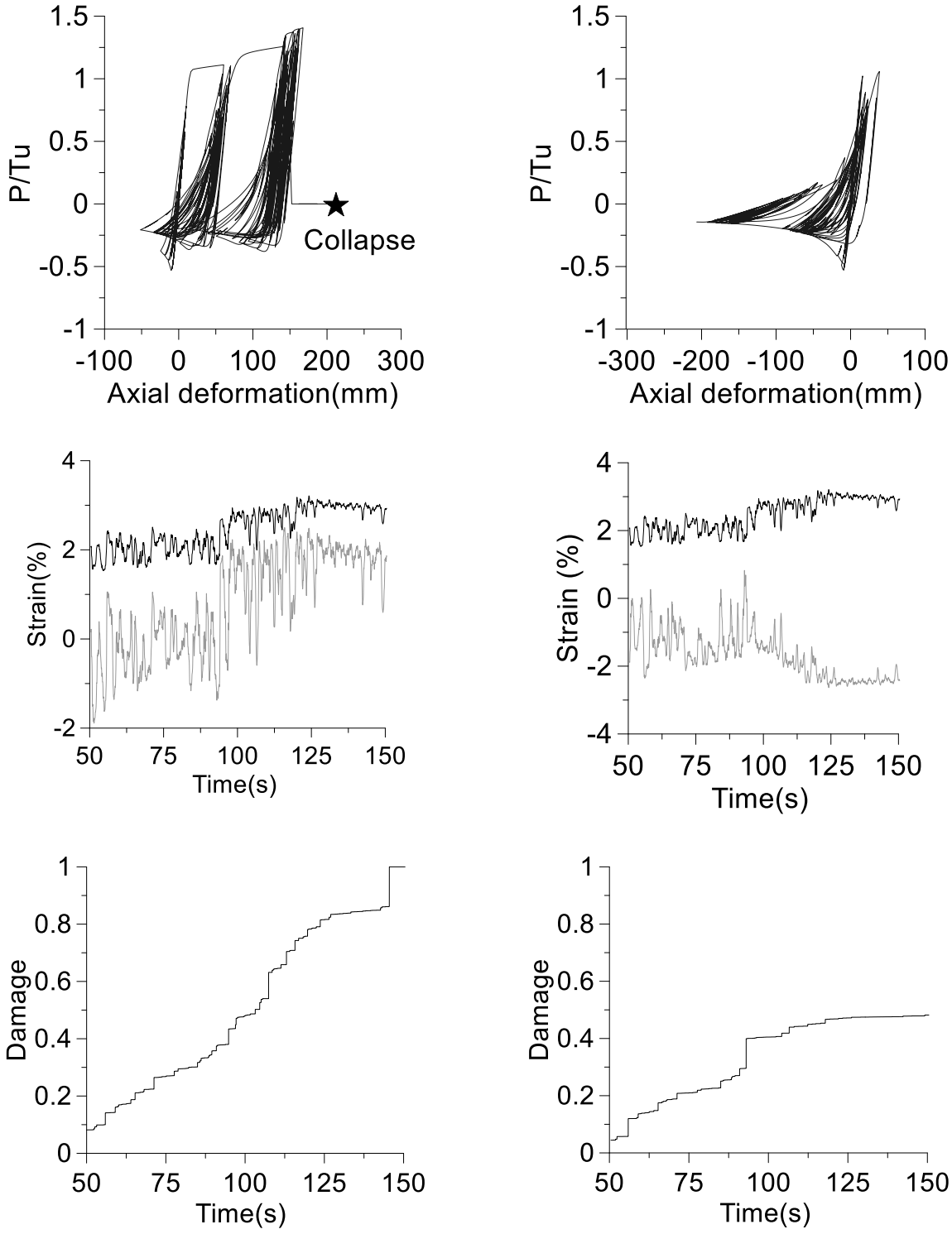

Figure 3-58 Hysteresis response of 12th floor braces, their strain time-history series and DI of the outermost compressive fiber under re-scaled #MYG004 subduction record.

yield in tension, while the left brace experienced initiation of failure caused by low-cycle fatigue time sequence of t = 146 s. There is an important difference in the time-history series of tensile

and compression strain recorded at the outermost tensile and compressive fiber of critical brace cross-section. At the time sequence corresponding to the main shock (t = 97 s) there is a jump in the time history series of compressive strain which means that a large amount of strain gets accumulated incrementally between t = 97 s and t = 146 s when the outermost compressive fiber reached failure. Meanwhile, at the same time sequence (t = 146 s), DI of left side brace is 1.0. Thus, during shaking, the left side brace of 16-storey building failed due to low-cycle fatigue, while the right side brace reached half of its capacity. It is noted that all crustal records were scaled to match or be above the code across the period of interest 0.2 T_1 – 1.5T_1. However, the subduction records selected from the megathrust Tohoku event were not scaled up. Thus, $S_a(T_1)$ corresponding to T_1 = 3.0 s of design spectrum corresponding to code demand is 0.135g and that resulted from MYG004 record is 0.225g.

3.6. Summary of Chapter three

This chapter presents the seismic response of low-rise, middle-rise, and high-rise MD-CBF buildings located in Victoria, B.C. on Site Class C. The main contributions to seismic hazard for Victoria are moderate-to-large crustal earthquakes of magnitudes M 7.0 – M 7.5 and the potential megathrust subduction earthquake of M 8.0 – M 9.0. Recent studies show that the distance from Victoria to the Cascadia subduction fault is about 50 km. The records from Tohoku earthquake recorded on stations located on similar geotechnical profile corresponding to firm soil are the proxy for the potential Cascadia subduction earthquake. It is also estimated that the return period for the subduction earthquakes is about 400 years and as the previous one was in January 1700, there is a high likelihood of such an earthquake in recent times. Using a scale factor of 1.0 for a set of seven selected subduction records of Tohoku earthquake it was determined that the demand is several times greater than the design spectrum (DS) for periods shorter than 0.4 s; between 0.4 s and 0.6 s is slightly above the DS; at 0.6 s, 1.0 s, and 1.8 s - 2.2 s equates the DS; between 0.6 s and 1.0 s, as well as, between 1.0 s and 1.8 s is slightly lower than DS with a lower value of about 0.8 DS at 0.8 s and 1.2 s, respectively. For longer periods than 2.2 s the mean of spectral acceleration is slightly below the DS. Comparing the subduction records with crustal records it was found that the former one shows the total duration and Trifunac duration about

seven time larger than the later and in consequence they subject the buildings to higher seismic demand.

The design of MD-CBF buildings followed the NBCC 2010 and CAN/CSA-S16-09 standard proceedings. The effect of accidental torsion and P-Δ was considered. The wind load was verified in order to assure elastic response of braced frames. Buildings with first-mode period > 1.0 s are considered dynamically sensitive to wind load and a dynamic procedure was employed. It is noted that all buildings but 16-storey were designed from earthquake loads that were greater than the wind loads. However, the size of bottom floors braces (1^{st} to 7^{th} floor) of 16-storey building were increased in the N-S direction in order to behave in the elastic range under wind loads.

To capture the nonlinear seismic response of studied MD-CBF buildings, a detailed numerical model able to simulate the nonlinear behaviour from yielding to failure was employed. In this study, the OpenSees software was selected. The desirable failure of MD-CBFs is the failure of braces caused by low-cycle fatigue. Although the OpenSees model is 2-D, it allows braces to buckle out-of-plane. Each gusset plate brace-to-frame connection resulted from design was simulated using two rotational springs and one torsional spring. The low-cycle fatigue model applied to HSS braces is that proposed by Tirca and Chen (2014). All HSS braces were simulated using the force-based nonlinear beam-column elements with distributed plasticity. It is worth to mention that the effect of accidental torsion cannot be simulated using the 2-D model and it was accounted for artificially by increasing the seismic demand with the ratio between the total base shear including that caused by accidental torsion and the base shear from earthquake loads. In this study, the length-to-width ratio of the prototype building is 2.25 and the shear amplification factor caused by accidental torsion computed with accidental eccentricity $0.1D_n$ is 1.2.

From analyses it was found that the buildings experienced the mean interstorey drift lower than 2.5% h_s and the mean residual interstorey drift lower than 0.5% h_s which is considered acceptable for buildings to be reparable after an earthquake event. The effect of subduction records characterized by several cycles increased the accumulation of compression strain in the outermost compression fiber of critical cross-section of HSS braces. At the floor where the peak interstorey drift was experienced, a slight increase in demand drives the critical floor to deflect one side until the braces of that floor reached failure. When an upper floor of a building higher

than 8-storey lost its strength, another floor at the bottom segment of the building became the critical floor. Thus, to increase the safety level, it is recommended to concentrate the energy dissipation at upper floors.

Chapter 4. Design and nonlinear analysis of high-rise Outrigger Braced Frame buildings

4.1. Overview of outrigger system

In general, the outrigger system is employed in slender high-rise buildings in order to reduce the overturning demand and to reduce the interstorey drift (TBI 2010). As is mentioned in the TBI 2010 guideline, the optimum location of outriggers and the capacity of an earthquake resistant system with inserted outrigger trusses is still unknown (e.g. Fig. 2-2). Although outriggers are used in several high-rise buildings there are not sufficient studies leading to a design methodology of earthquake resistant braced frames with outrigger trusses, labelled herein the Outrigger braced frame system.

Adding the outrigger system at the floor where damage is more likely to concentrate, it increases the floor stiffness and in consequence it mitigates the formation of storey mechanism. In this study, the main assumptions are as follows: i) the outrigger system is designed to respond in the elastic range while braces of CBFs perform in the nonlinear range, and ii) the CBF system is centrally located with the reference to both identical outriggers displaced to the right side and left side of the CBF.

Before coming out with a design method for the OBF system the following questions are raised:

1. What is the fitted geometry for outrigger trusses such that their diagonal members to be mainly loaded in tension than in compression?
2. How to identify the optimum location of outrigger(s) along the building height?
3. How to optimize the stiffness of outriggers in order to avoid the vertical stiffness irregularity of the OBF system?
4. How to design the gravity columns which support the far end of outriggers?

To answer these questions, the 12-storey and 16-storey MD-CBF buildings studied in the previous chapter are equipped with an outrigger truss system and are investigated hereafter.

4.2. Development of system concept

4.2.1 Case study: the 12-storey building

To answer the above questions, the case study selected is the 12-storey MD-CBF building located on Site Class C in Victoria B.C., investigated in Chapter 3. As mentioned earlier, the seismic force resisting system consists of two MD-CBFs located in the N-S direction and two identical MD-CBFs in the E-W direction E-W directions

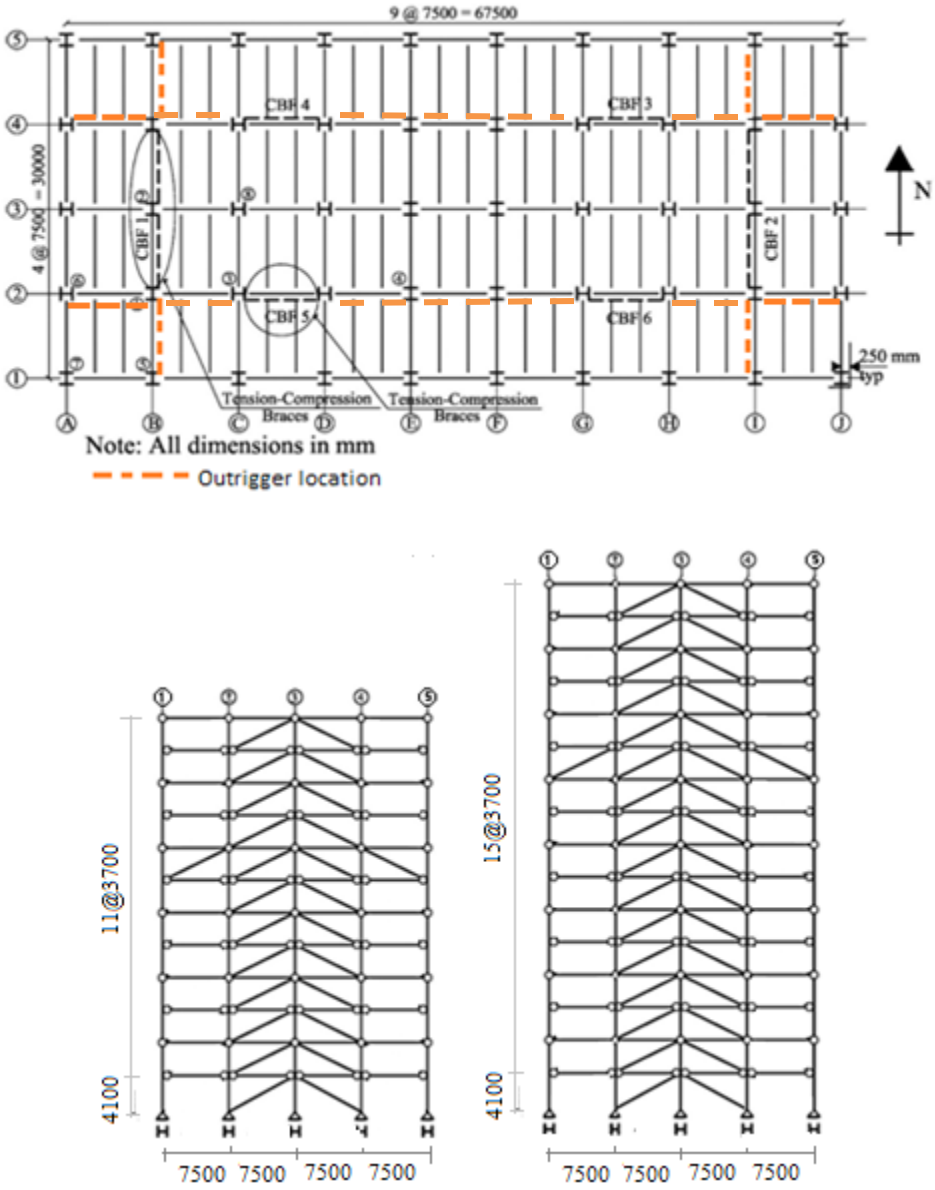

Figure 4-1 The 12-storey and 16-storey OBF bildings: a) plan and b) elevations

The building plan is symmetric and regular in both orthogonal directions. In the E-W direction, the outrigger trusses are located in grid lines "B" and "I" and in the N-S direction in grid lines "2" and "4". The MD-CBF system is characterized by $R_d = 3.0$ and $R_0 = 1.3$. The 12-storey building height and its seismic weight is 44.8 m and W= 124137 kN, respectively. The height of ground floor is 4.1 m and that of typical floor is 3.7 m. The code period corresponding to $2T_a$ is 2.24 s and the associated base shear is 5411 kN. Hence, the base shear for one 12-storey MD-CBF is 2706 kN. It is noted that torsion and P-Δ effect was included in design. The first-mode period resulted from linear dynamic analysis by means of modal response spectrum method using a 3-D model developed in ETABS software is also 2.24 s.

To investigate the effect of outrigger truss geometry on the response of 12-storey building, two geometrical models illustrated in in Fig. 4-2 are considered and labeled as follow:

- Model #1: The geometry of outrigger's diagonals is ascended as that of CBF braces.
- Model #2: The geometry of outrigger's diagonals is type chevron (2 braces per bay).

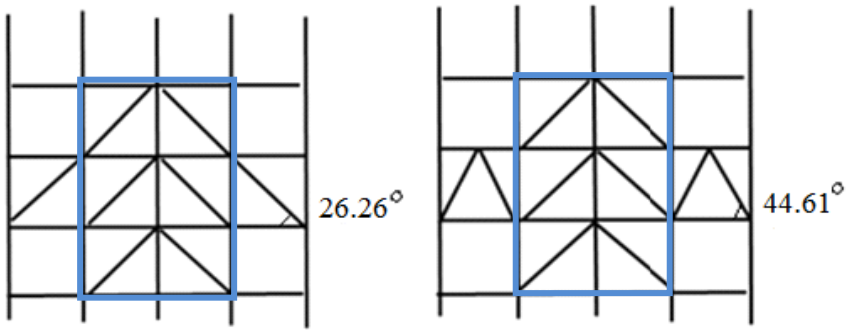

Figure 4-2 Various geometry for outrigger trusses: a) Model #1, b) Model #2

The distribution of storey drift along the height of the MD-CBF resulted from the ETABS model is given in Table 4-1 as well as, the ratio between the storey shear at a given floor and the base shear. As per Table 4-1, half of base shear is reached at the 9th floor while the maximum interstorey drift experienced by the MD-CBF occurred at the 8th floor (Fig. 4-3). Therefore, the 8th and 9th floors are potential locations for the outrigger trusses. It is noted that during the inelastic response of braces the lateral displacement shape is amplified. Hence, to reduce the

peak interstorey drift and to obtain a uniformly distributed damage along the building height, the first option is to install the outrigger system at the 8th floor.

The assumption made for the OBF system is to allow braces of the core system to yield in tension and buckle in compression (R_d = 3 and R_0 = 1.3) and to design the diagonal members of outrigger trusses by considering R_d = 1.5 and R_0 = 1.3.

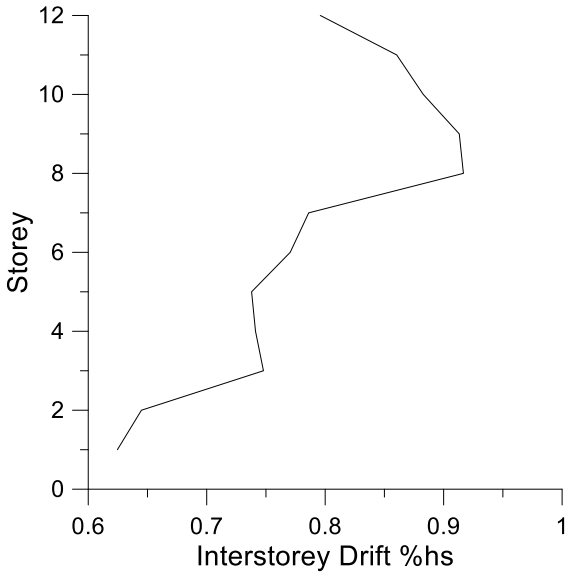

Figure 4-3 Vertical distribution of interstorey drift (N-S) resulted from modal analysis (ETABS)

Table 4-1 Storey shear per one bare MD-CBF of 12-storey building.(N-S) under seismic load

St.	St. height	Static equivalent method	Dynamic linear analysis (ETABS)		Ratio
		Storey shear, V	Storey shear, V	Storey shear including acc. torsion effect, V_d	V_d/V_{d_max}
	(m)	(kN)	(kN)	(kN)	
12	3.7	737	687	859	0.247
11	3.7	1059	1103	1379	0.396
10	3.7	1353	1338	1672	0.480
9	3.7	1619	1499	1874	0.539
8	3.7	1856	1591	1991	0.572
7	3.7	2064	1770	2213	0.636
6	3.7	2244	1873	2341	0.673
5	3.7	2395	2014	2518	0.722
4	3.7	2517	2201	2746	0.789
3	3.7	2610	2382	2976	0.855
2	3.7	2673	2581	3221	0.926
1	4.1	2707	2787	3478	1.000

To design the outrigger truss members located at the 8th floor, it is required to know the storey shear force carried by braces of the bare MD-CBF system. Then, this storey shear is redistributed between braces of MD-CBF and diagonal truss members as explained below. The size of brace members of bare MD-CBF was selected to provide compression resistance, C_r larger than the factored axial compression force, C_f, generated from earthquake, accidental torsion, and P-Δ effect. It is noted that the compression resistance of selected brace cross-sections may be bigger than the factored compression force because of the width-to-thickness ratio requirements and availability of cross-sections. The size of brace members is given in Table 4-2, as well as, the values of C_f, C_r, C_f/C_r ratio and the shear resistance provided by braces, V_r.

Table 4-2 Brace sizes of the 12-storey MD-CBF located in the N-S direction

St.	St. height (m)	Axial force in braces, C_f (kN)	Brace cross-section	C_r (kN)	C_f/C_r	V_r (kN)	V_r/V_{r_rmax}
12	3.7	479	HSS 152x152x8	524	0.91	941	0.21
11	3.7	769	HSS 178x178x9.5	902	0.85	1618	0.36
10	3.7	932	HSS 203x203x9.5	1130	0.82	2027	0.45
9	3.7	1045	HSS 203x203x9.5	1237	0.84	2219	0.5
8	3.7	1110	HSS 203x203x9.5	1237	0.90	2219	0.5
7	3.7	1234	HSS 203x203x13	1568	0.79	2813	0.62
6	3.7	1305	HSS 203x203x13	1568	0.83	2813	0.62
5	3.7	1404	HSS 228x228x13	1915	0.90	2813	0.62
4	3.7	1531	HSS 228x228x13	1915	0.80	3435	0.76
3	3.7	1659	HSS 228x228x13	1915	0.87	3435	0.76
2	3.7	1806	HSS 254x254x13	2518	0.71	4516	1.00
1	4.1	1982	HSS 254x254x13	2459	0.81	4316	0.96

Considering the outrigger system of Model #1 (Fig. 4-2) installed in the 8th floor, there are 4 braces to resist the storey shear force. Hence, the next step is to assume the amount of shear assigned to braces of MD-CBF and that assigned to trusses. As a first trial, it is assumed that half of the 8th storey shear is distributed to MD-CBF braces and the other half to outriggers designed with R_d = 1.5. From Table 4-1 it can be seen that the storey shear at the 8th floor is 1991 kN, while half of it is 996 kN. Thus, 996 kN is distributed to two braces of MD-CBF and 996 kN to two diagonals of outriggers. The angle between the MD-CBF brace and a horizontal line is $\alpha = 26.26^0$. Thus, the axial force transferred to the two MD-CBF braces is: $996/(2\cos\alpha) = 555$ kN which leads to HSS 152x152x9.5. The other half of shear force (996 kN) is distributed to the two

diagonals of outrigger designed with R_d =1.5. This leads to an axial force transferred to one diagonal of outrigger of (996x3/1.5)/(2 cosα) = 1110 kN and the chosen size is HSS178x178x13. When the outrigger Model #2 is selected, the 996 kN shear is distributed to four diagonals of outriggers. The angle between one diagonal of outrigger with a horizontal line is β = 44.61^0. Thus, the axial force transferred in one diagonal is (996x3/1.5)/(4 cosβ) = 700 kN and the selected member size is HSS152x152x9.5. All OBF member sizes are provided in Table 4-3.

Table 4-3 Size of braces and outrigger diagonals of OBF system

St	**Model # 1 outrigger system**		**Model #2 outrigger system**	
	Braces of core OBF	Diagonal brace of outrigger	Braces of core OBF	Diagonal brace of outrigger
12	HSS 152x152x8		HSS 152x152x8	
11	HSS 178x178x9.5		HSS 178x178x9.5	
10	HSS 203x203x9.5		HSS 203x203x9.5	
9	HSS 203x203x9.5		HSS 203x203x9.5	
8	HSS 152x152x9.5 HSS 127x127x9.5	2x1HSS 178x178x13 2x1HSS203x203x9.5	HSS 152x152x9.5 HSS 127x127x9.5	2x2HSS 152x152x9.5 2x2HSS 152x152x13
7	HSS 203x203x13		HSS 203x203x13	
6	HSS 203x203x13		HSS 203x203x13	
5	HSS 228x228x13		HSS 228x228x13	
4	HSS 228x228x13		HSS 228x228x13	
3	HSS 228x228x13		HSS 228x228x13	
2	HSS 254x254x13		HSS 254x254x13	
1	HSS 254x254x13		HSS 254x254x13	

When the computed brace sizes where added in the ETABS model and the analysis was completed by means of response spectrum method, the forces triggered in braces at the 8^{th} floor leads to lower size for the core OBF braces and larger size for outrigger diagonals as shown in red color in Table 4-3. The second step is to evaluate the vertical stiffness in order to keep the building regular. The normalized distribution of stiffness along the height of the building as resulted from ETABS is shown in Fig. 4-4 for the OBF system considering Model #1 outrigger inserted at the 8^{th} floor. The stiffness was normalized to the maximum stiffness obtained at the first floor. From Fig. 4-4 resulted that the stiffness at the 9^{th} floor is 68% of the stiffness of the 8^{th} floor and the stiffness of the 7^{th} floor is 62% of the stiffness of the 8^{th} floor where outriggers are located. In NBCC it is noted that vertical stiffness irregularity exists when the lateral stiffness in

a storey is less than 70% of the stiffness of any adjacent storey. Therefore, there is a need to slightly increase the stiffness of MD-CBF braces at the 7th floor. The stiffness of the 9th floor is accepted because the difference between 68% and 70% is less than 3%.

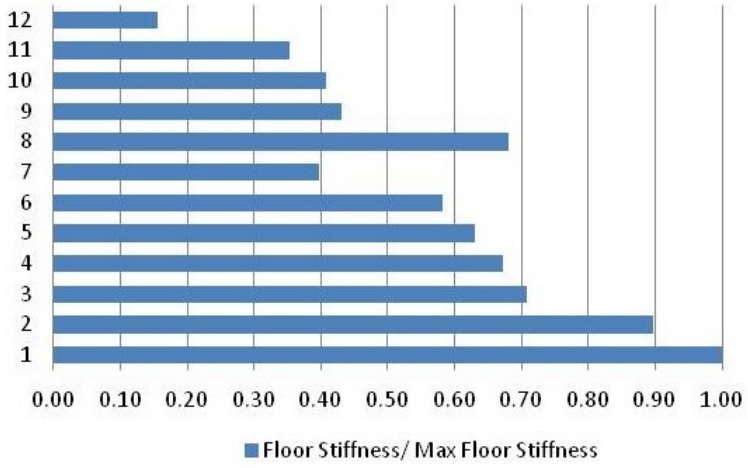

Figure 4-4 Vertical stiffness distribution of OBF system with Model #1 outrigger at 8th floor

For the OBF system with outrigger Model #2 located at the 8th floor, the distributed stiffness along the height of the building is shown in Fig.4-5 As a result, the stiffness at the 9th floor is 50% of that of the 8th floor and at the 7th floor it is 63% of that of 8th floor. Therefore, the Model #2 outriggers have a larger impact in the vertical stiffness distribution than Model #1 outriggers. To pass the vertical stiffness irregularity criterion, the 7th floor braces of the OBF system with Model # 1 outriggers were slightly increased and those with Model #2 outriggers were increased at the 7th and 9th floor as shown in red in Table 4-4.

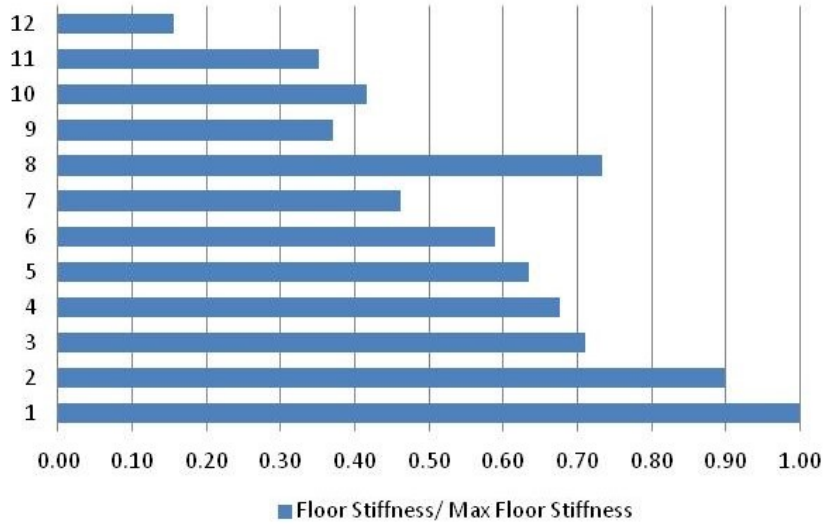

Figure 4-5 Vertical stiffness distribution of OBF system with Model #2 outrigger at 8th floor

Table 4-4 Final size of core braces of OBF and outrigger diagonals located at 8th floor

St	**Model # 1 outrigger system**		**Model #2 outrigger system**	
	Braces of core OBF	Diagonal brace of outrigger	Braces of core OBF	Diagonal brace of outrigger
12	HSS 152x152x8		HSS 152x152x8	
11	HSS 178x178x9.5		HSS 178x178x9.5	
10	HSS 203x203x9.5		HSS 203x203x9.5	
9	HSS 203x203x9.5		HSS 203x203x16	
8	HSS 127x127x9.5	2x1HSS 203x203x13	HSS 127x127x9.5	2x2HSS 152x152x13
7	HSS 203x203x16		HSS 203x203x16	
6	HSS 203x203x13		HSS 203x203x13	
5	HSS 228x228x13		HSS 228x228x13	
4	HSS 228x228x13		HSS 228x228x13	
3	HSS 228x228x13		HSS 228x228x13	
2	HSS 254x254x13		HSS 254x254x13	
1	HSS 254x254x13		HSS 254x254x13	

Using the size of braces and outriggers diagonals provided in Table 4-4 the resulting interstorey drift along the building height from the ETABS model is shown in Fig. 4-6. The figure shows that Model #1 outriggers provide better response than Model #2 outriggers. The effect of location of outriggers at the 8th floor implies reduction of interstorey drifts of the half upper floors.

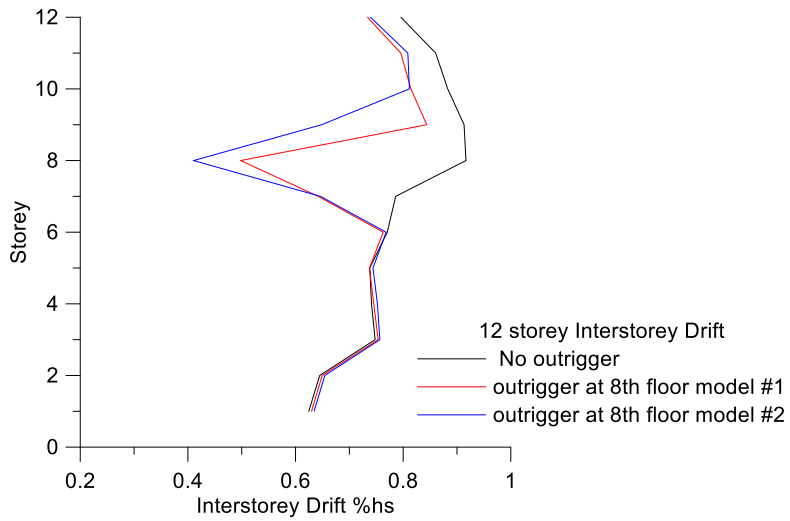

Figure 4-6 Interstorey drift of bare MD-CBF vs OBF system with outriggers at 8th floor from modal analysis

A similar procedure was applied to design the OBF system with outriggers Model #1 and Model #2 located at the 9th floor. The size of braces and outriggers diagonals is provided in Table 4-5 and the distribution of stiffness along the building height in given in Fig. 4-7 and Fig. 4-8, respectively.

Table 4-5 Size of core OBF braces and outriggers diagonals located at 9th floor

St.	**Model # 1 outrigger system**		**Model #2 outrigger system**	
	Braces of core OBF	Diagonal brace of outrigger	Braces of core OBF	Diagonal brace of outrigger
12	HSS 152x152x8		HSS 152x152x8	
11	HSS 178x178x9.5		HSS 178x178x9.5	
10	HSS 203x203x9.5		HSS 203x203x9.5	
9	HSS 152x152x9.5 HSS 127x127x9.5	2x1HSS 178x178x13 2x1HSS 203x203x13	HSS 152x152x9.5 HSS 127x127x9.5	2x2HSS 152x152x8.0 2x2HSS 152x152x13
8	HSS 203x203x9.5		HSS 203x203x9.5	
7	HSS 203x203x13		HSS 203x203x13	
6	HSS 203x203x13		HSS 203x203x13	
5	HSS 228x228x13		HSS 228x228x13	
4	HSS 228x228x13		HSS 228x228x13	
3	HSS 228x228x13		HSS 228x228x13	
2	HSS 254x254x13		HSS 254x254x13	
1	HSS 254x254x13		HSS 254x254x13	

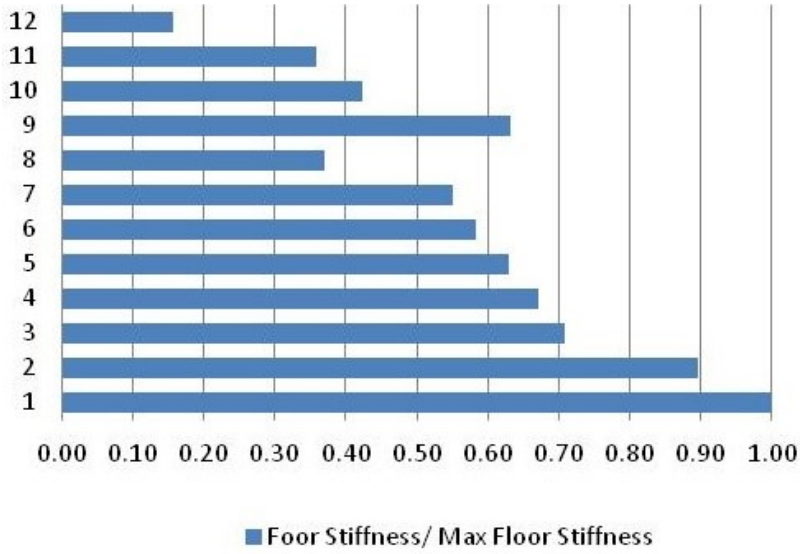

Figure 4-7 Vertical stiffness distribution of OBF system with Model #1 outrigger at 9th floor

From Fig. 4-7 it is observed that the stiffness at the 10th floor is 68% of the stiffness at the 9th floor and that of the 8th floor is 59%. When outriggers in Model #2 are located at the 9th floor, the vertical stiffness distribution resulted from the ETABS model is plotted in Fig. 4-8. As a result, the stiffness of the 10th floor is 53% of that of the 9th floor and that of the 8th floor is 57% of the stiffness of the 8th floor which leads to structural irregularity of Type 1. To overcome the induced irregularity type, an optimization of member sizes was conducted and the cross-sections are given in Table 4-6.

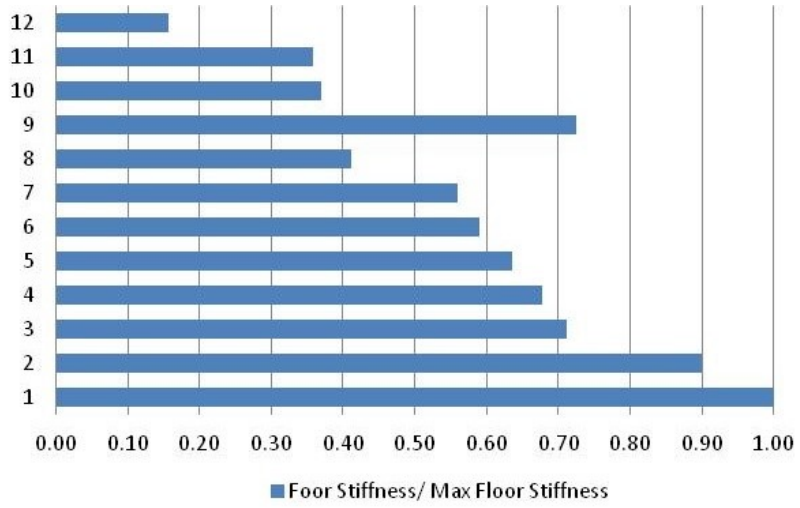

Figure 4-8 Vertical stiffness distribution of OBF system with Model #2 outrigger at 9th floor

The interstorey drift of the 12-storey bare MD-CBF building and that resulted for the 12-storey OBF with outriggers of Model #1 and Model #2 is plotted in Fig. 4-9. As resulted from the shape of interstorey drift distribution, a more uniform pattern was obtained for the OBF system with outrigger of Model #1 which was selected for further investigations.

Table 4-6 Final size of core braces of OBF and outrigger diagonals located at 9th floor

St.	**Model # 1 outrigger system**		**Model #2 outrigger system**	
	Braces of core OBF	Diagonal brace of outrigger	Braces of core OBF	Diagonal brace of outrigger
12	HSS 152x152x8		HSS 152x152x8	
11	HSS 178x178x9.5		HSS 178x178x9.5	
10	HSS 203x203x9.5		HSS 203x203x13	
9	HSS 127x127x9.5	2x1HSS 203x203x13	HSS 127x127x8	2x2HSS 152x152x13
8	HSS 203x203x13		HSS 203x203x13	
7	HSS 203x203x13		HSS 203x203x13	
6	HSS 203x203x13		HSS 203x203x13	
5	HSS 228x228x13		HSS 228x228x13	
4	HSS 228x228x13		HSS 228x228x13	
3	HSS 228x228x13		HSS 228x228x13	
2	HSS 254x254x13		HSS 254x254x13	
1	HSS 254x254x13		HSS 254x254x13	

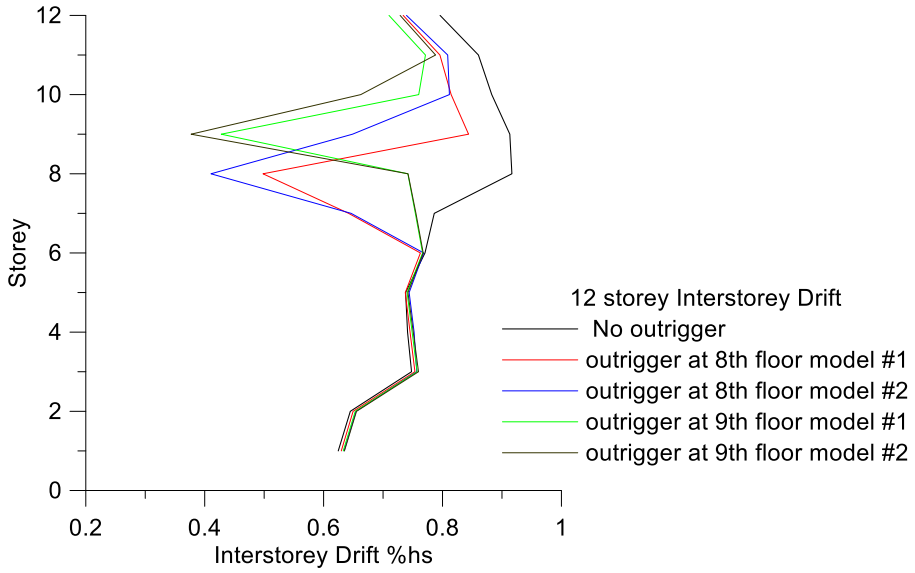

Figure 4-9 Comparison between interstorey drift of 12-storey MD-CBF building and OBF building with outriggers of Model #1 and Model #2 located at 8th or 9th floors resulted from modal analysis

The proposed location for the outrigger in this study is compared with the location recommended in the chart provided by Smith and Coull (1991). Computing the parameters presented in Section 2.1.2 of this study, it results $\alpha = 3.19 \times 10^{-5}$ and $\beta = 4.34$. Then, using the Smith and Coull chart it results $\omega = 0.36$ which leads to $x_1/H \sim 0.3$. Considering the building height 44.8 m, the proposed optimum location for outrigger measured from the top is 0.3 x 44.8 = 13.44 m which is close to 14.8 m concluded in this study.

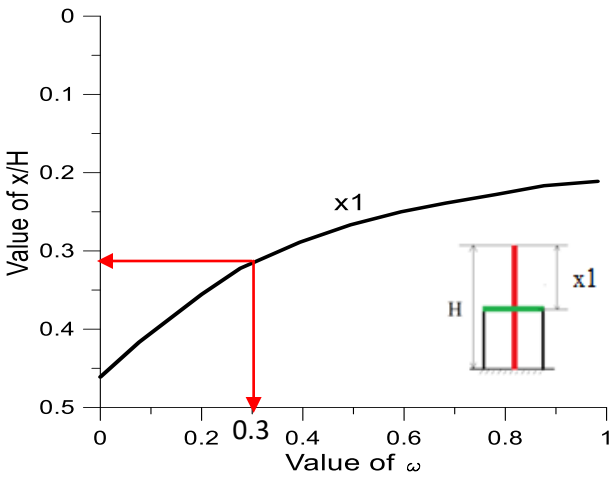

Figure 4-10 The optimum outrigger location for the 12-storey OBF building using the chart adapted from Smith and Coull (1991)

4.2.2 Case study: the 16-storey building

To verify the design approach considered for the 12-storey OBF building, the same design method was applied to the 16-storey OBF building. As noted in Chapter 3, the height of ground floor is 4.1 m, that of typical floor is 3.7 m, the building height is 59.6 m and its seismic weight is W= 167388 kN. The code period corresponding to $2T_a$ is 2.98 s and the associated base shear resulted from the equivalent static force procedure is 6180 kN. As mentioned in Chapter 3, the building is braced by two adjacent MD-CBF systems in the N-S direction which leads to 3090 kN per one bare MD-CBF. However, when torsion and P-Δ effect were included in design the base shear increased from 3090 kN to 3865 kN as shown in Table 4-7. The fundamental period resulted from the linear dynamic analysis by means of the modal response spectrum method applied on 3-D model developed in Etabs software was found to be 3.04 s.

The distribution of storey shear along the height of the MD-CBF located in the N-S direction resulted from the ETABS model is given in Table 4-7, as well as, the ratio between the storey shear at a given floor and the base shear. As per Table 4-7, half of base shear is reached at the 11^{th} floor while the maximum interstorey drift experienced by the bare MD-CBF occurred at the

11^{th} and 12^{th} floors (Fig. 4-11). Therefore, the 11^{th} and 12^{th} floors are potential locations for outrigger trusses.

The same design method explained for the 12-storey OBF building was applied for the 16-storey building. The size of brace members of bare MD-CBF is given in Table 4-8. These brace sizes were selected to provide compression resistance, C_r larger than the factored axial compression force, C_f, generated from earthquake loads including the effect of accidental torsion and the P-Δ effect. The brace compression resistance may be greater than the factored compression force because of the with-to-thickness ratio requirements and availability of cross-sections. The shear resistance provided by braces is noted V_r and is also provided in Table 4-8.

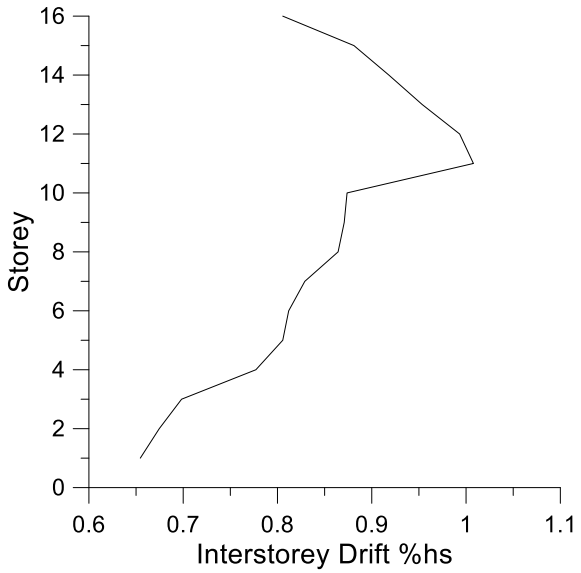

Figure 4-11 Vertical distribution of interstorey drift resulted from modal analysis (ETABS)

Table 4-7 Storey shear per one bare MD-CBF of 16-storey building (N-S direction).

St.	St. height	Static equivalent method	Dynamic linear analysis (ETABS)		Ratio
		Storey shear, Vs	Storey shear	Storey shear including acc. torsion effect	V_d/V_{d_Mmax}
	(m)	(kN)	(kN)	(kN)	
16	3.7	899	552	693	0.179
15	3.7	1167	942	1180	0.305
14	3.7	1418	1192	1488	0.385
13	3.7	1652	1354	1693	0.438
12	3.7	1868	1483	1860	0.481
11	3.7	2067	1625	2039	0.528
10	3.7	2249	1747	2187	0.566
9	3.7	2414	1896	2376	0.615
8	3.7	2561	2011	2518	0.651
7	3.7	2691	2135	2674	0.692
6	3.7	2803	2166	2714	0.702
5	3.7	2896	2417	3029	0.784
4	3.7	2972	2489	3118	0.807
3	3.7	3030	2633	3299	0.853
2	3.7	3069	2767	3461	0.895
1	4.1	3090	3090	3865	1.0

Table 4-8 Brace sizes of a 16-storey MD-CBF in the N-S direction and the characteristic forces

St.	St. height (m)	Total forces in braces, C_f (kN)	Brace sizes	C_r (kN)	C_f/C_r	V_r (kN)	V_r/V_{rmax}
16	3.7	395	HSS 152x152x8	524	0.75	940	0.21
15	3.7	672	HSS 178x178x9.5	902	0.75	1618	0.36
14	3.7	848	HSS 203x203x9.5	1237	0.69	2219	0.49
13	3.7	965	HSS 203x203x9.5	1237	0.78	2219	0.49
12	3.7	1060	HSS 203x203x9.5	1237	0.86	2219	0.49
11	3.7	1162	HSS 203x203x9.5	1237	0.94	2219	0.49
10	3.7	1246	HSS 203x203x13	1568	0.79	2812	0.62
9	3.7	1354	HSS 203x203x13	1568	0.86	2812	0.62
8	3.7	1435	HSS 203x203x13	1568	0.92	2812	0.62
7	3.7	1524	HSS 228x228x13	1915	0.80	3435	0.76
6	3.7	1650	HSS 228x228x13	1915	0.86	3435	0.76
5	3.7	1776	HSS 228x228x13	1915	0.93	3435	0.76
4	3.7	1895	HSS 228x228x13	1915	0.99	3435	0.76
3	3.7	2008	HSS 254x254x13	2518	0.80	4516	1.00
2	3.7	2121	HSS 254x254x13	2518	0.84	4516	1.00
1	4.1	2240	HSS 254x254x13	2459	0.91	4315	0.96

Considering the outrigger Model #1 (Fig. 4-2) installed at the 11th floor of the 16-storey OBF system, at this particular floor, there are four braces to resist the storey shear. As per the proposed design method, half of the storey shear developed at the 11th floor is distributed to braces of the core system and half to the two diagonals of outriggers proportioned for R_d =1.5 and R_0 = 1.3. As indicated in Table 4-7, the storey shear at the 11th floor is 2039 kN. Thus, half of it equal to 1020 kN is distributed to two braces of the core system and 1020 kN to the two diagonals of outriggers. It is noted that the angle between the brace and a horizontal line is $\alpha = 26.26^0$. The axial force transferred in each of the two core braces located at the11th floor is: $1020/(2\cos\alpha)$ = 568 kN which leads to HSS 152x152x13 and the axial force triggered in each of the two diagonals of outriggers designed with R_d = 1.5 is $(1020x3/1.5)/(2\cos\alpha)$ = 1137 kN which leads to HSS203x203x13.

When the outrigger Model #3 is selected and inserted at the 11th floor of the OBF system, half of storey shear assigned to outriggers is assigned to four diagonal members instead of two. This leads to an axial force per diagonal of $(1020x3/1.5)/(4\cos\beta)$ = 716 kN, where $\beta = 44.61^0$. The selected diagonal is HSS152x152x13. The size of OBF core braces and diagonals of outriggers are provided in Table 4-9.

When the computed brace sizes were added in the ETABS model and the analysis was completed by means of response spectrum method, the forces triggered in braces at the 11th floor leads to lower sizes for braces of the OBF core and larger sizes for outrigger diagonals as shown in red color in Table 4-9. Hence, the second step is to evaluate the vertical stiffness in order to keep the building regular. The normalized distribution of stiffness along the height of the building as resulted from ETABS is shown in Fig. 4-12 for the 16-storey OBF system considering Model #1 outrigger inserted at the 11th floor. The stiffness was normalized to maximum stiffness obtained at the first floor. From Fig. 4-12 resulted that the stiffness at the 12th floor is 70% of the stiffness of the 11th floor and the stiffness of the 10th floor is 59% of the stiffness of the 11th floor. In NBCC it is noted that vertical stiffness irregularity exists when the lateral stiffness in a storey is less than 70% of the stiffness of any adjacent storey. Therefore, there is a need for a slight increase of core braces stiffness at the 10th floor. The storey stiffness of the 12th floor is accepted.

Table 4-9 Size of braces and outrigger diagonals located at 11th floor

St	**Model # 1 outrigger system**		**Model #2 outrigger system**	
	Braces of OBF core	Diagonal brace of outrigger	Braces of OBF core	Diagonal brace of outrigger
16	HSS 152x152x8		HSS 152x152x8	
15	HSS 178x178x9.5		HSS 178x178x9.5	
14	HSS 203x203x9.5		HSS 203x203x9.5	
13	HSS 203x203x9.5		HSS 203x203x9.5	
12	HSS 203x203x9.5		HSS 203x203x9.5	
11	HSS 152x152x13 HSS 127x127x9.5	2x1HSS 203x203x13 2x1HSS 228x228x13	HSS 152x152x13 HSS 127x127x9.5	2x2HSS 152x152x13 2x2HSS 178x178x9.5
10	HSS 203x203x13		HSS 203x203x13	
9	HSS 203x203x13		HSS 203x203x13	
8	HSS 203x203x13		HSS 203x203x13	
7	HSS 228x228x13		HSS 228x228x13	
6	HSS 228x228x13		HSS 228x228x13	
5	HSS 228x228x13		HSS 228x228x13	
4	HSS 228x228x13		HSS 228x228x13	
3	HSS 254x254x13		HSS 254x254x13	
2	HSS 254x254x13		HSS 254x254x13	
1	HSS 254x254x13		HSS 254x254x13	

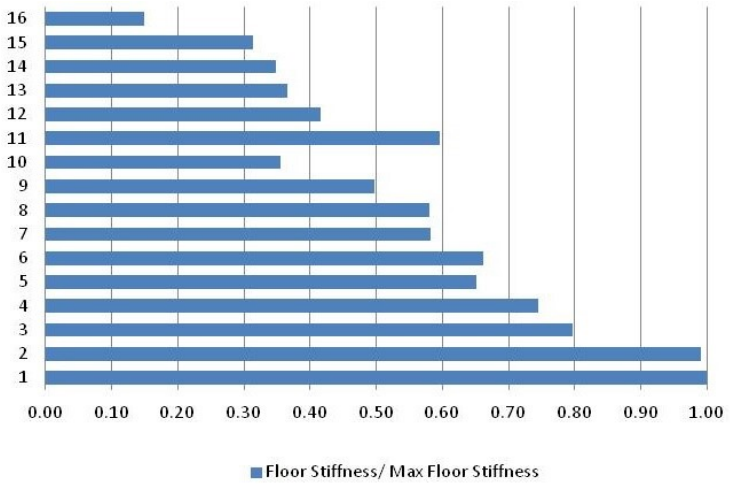

Figure 4-12 Vertical stiffness distribution of OBF system with Model #1 outrigger at 11th floor

For the OBF system with outrigger Model #2 located at the 11th floor, the distributed stiffness along the height of the building is shown in Fig. 4-13. It is found that the storey stiffness of the 12th floor is 51% of that of the 11th floor and the storey stiffness of the 10th floor is 61% of that of 11th floor. Therefore, Model #2 outriggers have a large impact in the vertical distribution of stiffness among floors than Model #1 outriggers. To pass the vertical stiffness irregularity criterion, the 10th floor braces of the OBF system with Model # 1 outriggers where slightly increase and those with Model #3 outriggers where increase at the 10th and 12th floor as shown in red in Table 4-10.

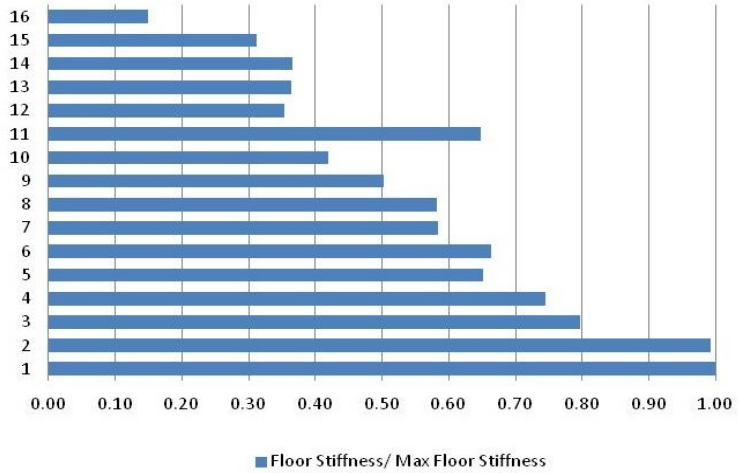

Figure 4-13 Vertical stiffness distribution of OBF system with Model #2 outrigger at 11th floor

Using the size of braces and outriggers diagonals provided in Table 4-10, the vertical distribution of interstorey drift along the building height resulted from the ETABS model is shown in Fig. 4-14. Thus, it is shown from Figure 4-14 that Model #1 outriggers provide better response than Model #2 outriggers. The effect of location of outriggers at the 11th floor implies reduction of interstorey drifts at the upper half floors.

Table 4-10 Final size of core braces of OBF and outrigger diagonals located at 11th floor

St	**Model # 1 outrigger system**		**Model #2 outrigger system**	
	Braces of OBF core	Diagonal brace of outrigger	Braces of OBF core	Diagonal brace of outrigger
16	HSS 152x152x8		HSS 152x152x8	
15	HSS 178x178x9.5		HSS 178x178x9.5	
14	HSS 203x203x9.5		HSS 178x178x9.5	
13	HSS 203x203x9.5		HSS 203x203x9.5	
12	HSS 203x203x9.5		HSS 203x203x13	
11	HSS 127x127x9.5	2x1HSS 228x228x13	HSS 127x127x9.5	2x2HSS 178x178x9.5
10	HSS 203x203x16		HSS 203x203x16	
9	HSS 203x203x13		HSS 203x203x13	
8	HSS 203x203x13		HSS 203x203x13	
7	HSS 228x228x13		HSS 228x228x13	
6	HSS 228x228x13		HSS 228x228x13	
5	HSS 228x228x13		HSS 228x228x13	
4	HSS 228x228x13		HSS 228x228x13	
3	HSS 254x254x13		HSS 254x254x13	
2	HSS 254x254x13		HSS 254x254x13	
1	HSS 254x254x13		HSS 254x254x13	

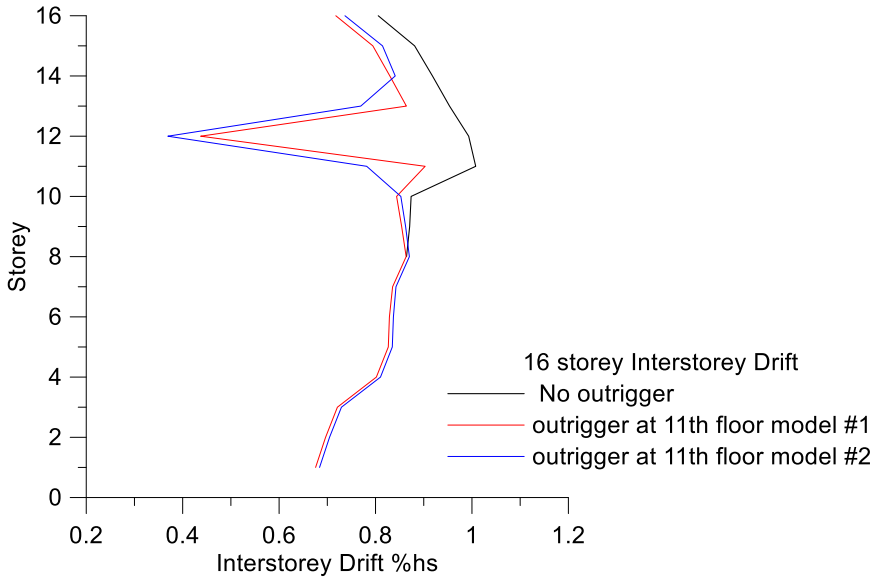

Figure 4-14 Interstorey drift for the MD-CBF vs. the OBF system with outriggers at 11th floor from modal analysis

A similar procedure was applied to design the OBF system with outriggers Model #1 and Model #2 located at the 12th floor. The size of braces and outriggers diagonals is provided in Table 4-11 and the vertical distribution of stiffness along the building height is shown in Fig. 4-15 and Fig. 4-16, respectively. From Fig. 4-15 it is observed that the stiffness of the 13th floor is 66% of the storey stiffness of the 12th floor where outriggers are inserted, while the stiffness of the 11th floor is 52% of the storey stiffness of 12th floor. When outriggers of Model #2 are located at the 12th floor the stiffness distribution resulted from the ETABS model is plotted in Fig. 4-16. As observed, the stiffness of the 13th floor is 50% of the storey stiffness of the 12th floor where outriggers are inserted and the stiffness in the 11th floor is 54% of the stiffness of 12th floor. This leads to structural irregularity of Type 1. To overpass this drawback, the size of braces at floors with outriggers were reevaluated and are provided in Table 4-12.

Table 4-11 Size of braces and outriggers diagonals located at 12th floor

St	**Model # 1 outrigger system**		**Model # 2 outrigger system**	
	Braces of OBF core	Diagonal brace of outrigger	Braces of OBF core	Diagonal brace of outrigger
16	HSS 152x152x8		HSS 152x152x8	
15	HSS 178x178x9.5		HSS 178x178x9.5	
14	HSS 203x203x9.5		HSS 203x203x9.5	
13	HSS 203x203x9.5		HSS 203x203x9.5	
12	HSS152x152x13 HSS127x127x9.5	2x1HSS 178x178x13 2x1HSS 228x228x13	HSS152x152x13 HSS127x127x9.5	2x2HSS152x152x13 2x2HSS 178x178x13
11	HSS 203x203x9.5		HSS 203x203x9.5	
10	HSS 203x203x13		HSS 203x203x13	
9	HSS 203x203x13		HSS 203x203x13	
8	HSS 203x203x13		HSS 203x203x13	
7	HSS 228x228x13		HSS 228x228x13	
6	HSS 228x228x13		HSS 228x228x13	
5	HSS 228x228x13		HSS 228x228x13	
4	HSS 228x228x13		HSS 228x228x13	
3	HSS 254x254x13		HSS 254x254x13	
2	HSS 254x254x13		HSS 254x254x13	
1	HSS 254x254x13		HSS 254x254x13	

The vertical distribution of interstorey drift of the 16-storey bare MD-CBF building and that resulted for the 16-storey OBF with outriggers Model #1 and Model #3 is plotted in Fig. 4-17. As observed, the OBF system with outrigger Model #1 provides a more uniform distribution and shows reduction of peak interstorey drift encountered at upper levels. Thus, this later model was selected for further investigations.

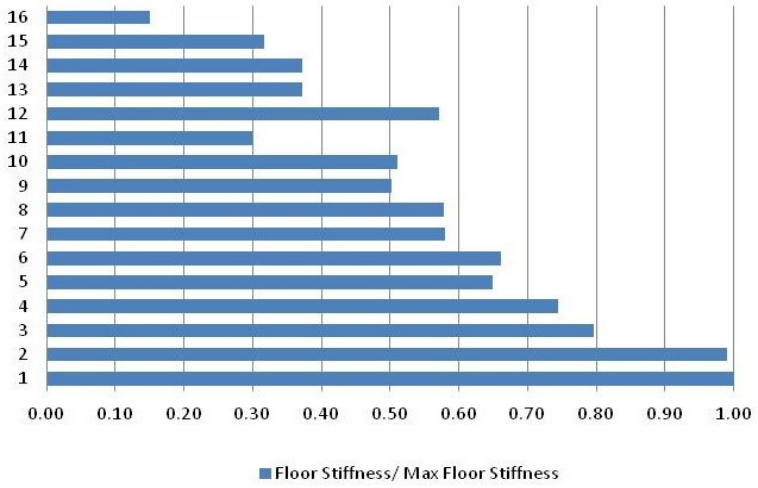

Figure 4-15 Vertical stiffness distribution of OBF system with Model #1 outrigger at 12th floor

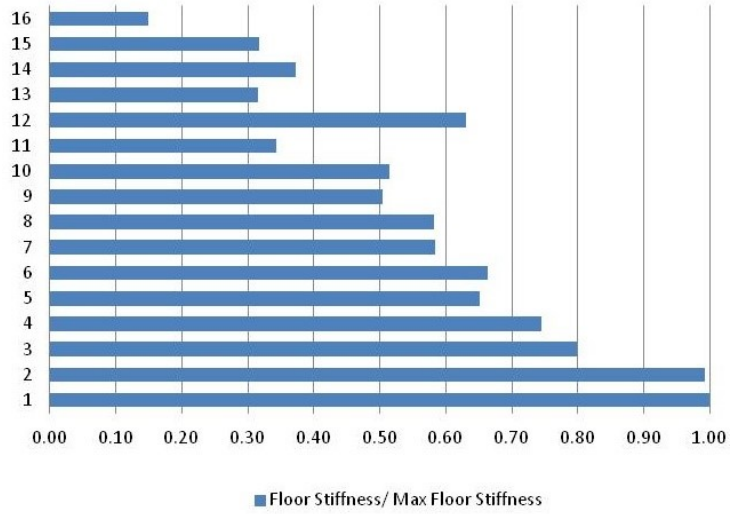

Figure 4-16 Vertical stiffness distribution of OBF system with Model #2 outrigger at 12th floor

Table 4-12 Final size of core braces of OBF and outrigger diagonals located at 12th floor

St	Model # 1 outrigger system		Model # 2 outrigger system	
	Braces of OBF core	Diagonal brace of outrigger	Braces of OBF core	Diagonal brace of outrigger
16	HSS 152x152x8		HSS 152x152x8	
15	HSS 178x178x9.5		HSS 178x178x9.5	
14	HSS 203x203x9.5		HSS 203x203x9.5	
13	HSS 203x203x9.5		HSS 203x203x13	
12	HSS127x127x9.5	2x1HSS 228x228x13	HSS127x127x9.5	2x1HSS 203x203x9.5
11	HSS 203x203x13		HSS 203x203x13	
10	HSS 203x203x13		HSS 203x203x13	
9	HSS 203x203x13		HSS 203x203x13	
8	HSS 203x203x13		HSS 203x203x13	
7	HSS 228x228x13		HSS 228x228x13	
6	HSS 228x228x13		HSS 228x228x13	
5	HSS 228x228x13		HSS 228x228x13	
4	HSS 228x228x13		HSS 228x228x13	
3	HSS 254x254x13		HSS 254x254x13	
2	HSS 254x254x13		HSS 254x254x13	
1	HSS 254x254x13		HSS 254x254x13	

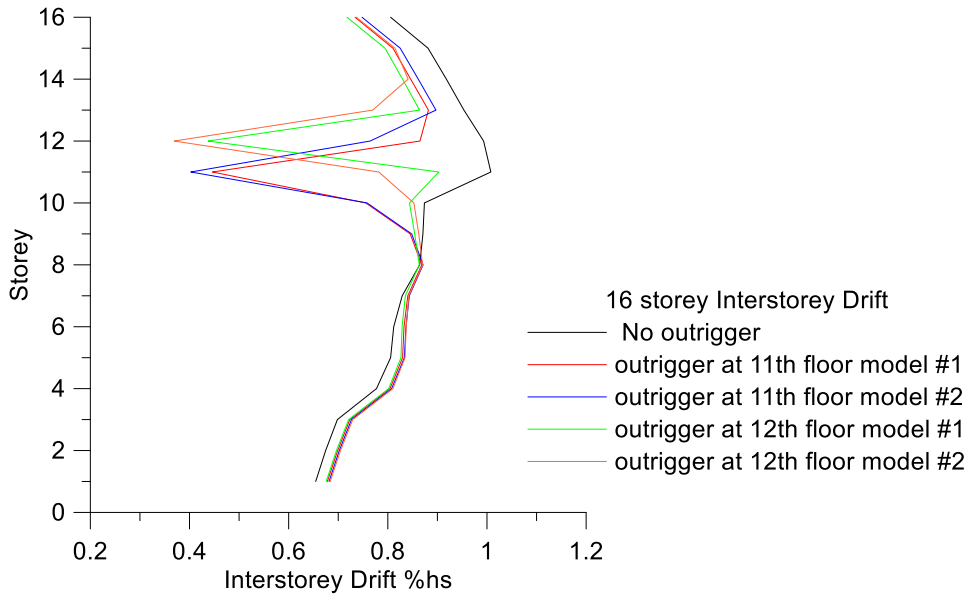

Figure 4-17 Comparison between interstorey drift resulted for 16-storey MD-CBF building and OBF building with outriggers Model #1 and Model #2 located at 11th or 12th floor resulted from modal analysis

The proposed floor location for the outrigger system resulted from this study is compared with the predicted location x1 that was given in the chart of Smith and Coull (1991) and replicated in Fig. 4-18. Computing the parameters according to the equations provided in Section 2.1.2 of this study, it results $\alpha = 2.34 \times 10^{-5}$, $\beta = 3.29$ and $\omega = 0.27$. Considering the value of ω, from the chart proposed by Smith and Coull (1991) it results $x1/H \sim 0.33$ which leads to $x1 = 0.3 \times 59.6 = 19.67$ m which is not far from the proposed distance x1 = 18.5 m.

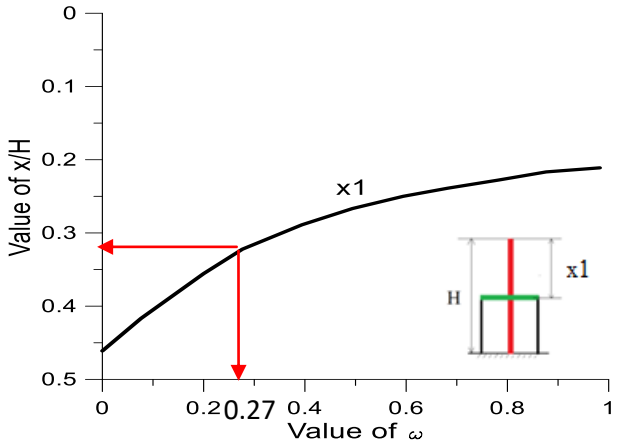

Figure 4-18 The optimum outrigger location for the 16-storey OBF building using the chart adapted from Smith and Coull (1991)

4.2.3 General recommendations for outriggers geometry and location

From the numerical study presented above, it can be concluded that:

1- In the case of outriggers located within a floor along the building height, the recommended optimum location is: i) at the floor where storey shear reaches half of the base shear which in general corresponds to $0.75h_n$ measured from the bottom floor and ii) at the floor experiencing maximum interstorey drift. Herein, h_n is the building height. Both scenarios should be studied to identify the optimum location for outriggers.

2- The floor where outriggers are inserted, as well as the adjacent floors, experienced substantially reduced interstorey drift. When outriggers are located at a floor within the upper half, they do not influence the vertical distribution of interstorey drift for the lower half floors.

3- Model #1 outrigger is recommended in comparison with Model #2 because it brings smaller stiffness to the system. Adding large amount of stiffness at a floor could introduce irregularity of Type 1 known as vertical stiffness irregularity.
4- Adding outriggers within a floor will not lead to substantial increase of axial force in gravity column located at the far end of outrigger.
5- For the design of an OBF system, the capacity design is applied which is similar with that for the MD-CBF system. The main assumption is that braces of concentrically braced frame are designed to yield in tension and buckle in compression while the diagonals of outriggers behave mostly in the elastic range. In this study, the concentrically braced frame core is designed with $R_d = 3$ and $R_o = 1.3$ and diagonals of outriggers for $R_d = 1.5$ and $R_o = 1.3$. The design was first done by using $R_d = 3$ and $R_o = 1.3$ by using ETABS software, and the axial forces in all braces were determined with the above values of R_d, R_0. The axial forces in the outrigger braces was then modified to be in elastic range by multiplying the axial forces in the outrigger braces which were obtained from ETABS model by $R_d = 3$ (elastic value), then dividing it by $R_d = 1.5$ for outrigger diagonal members to get an equivalent elastic force.
6- The optimum location proposed for one floor outrigger trusses matches with that recommended by Smith and Coull (1991).

All these observations will be hereafter verified through nonlinear dynamic analysis using the OpenSees software.

4.3. Nonlinear Seismic Response of High-rise Outrigger Braced Frame Buildings

In this section, the seismic response of the 12-storey and 16-storey OBF buildings that employ Model #1 outriggers is presented. In the case of 12-storey OBF building the outrigger trusses are located at the 8^{th} floor and the system member sizes are showed in Table 4-4. In the case of 16-storey OBF building the outriggers are located at the 11^{th} floor and the system member sizes are given in Table 4-10. The seismic response is associated to the design level. The

nonlinear dynamic analysis is carried out using the OpenSees software. The same modelling approach as explained in Chapter 3 is used. Diagonals of outrrigers are modeled as brace members using Steel 02 material. A summary of the 12-storey and 16-storey OBF building response in terms of first-mode and second-mode period resulted from OpenSees and the associated base shear is given in Table 4-13. As shown in Table 4-13, the first-mode period of the OBF system is slightly lower than that resulted for the MD-CBF system. The difference is about 5% but the maximum interstorey drift is substantially reduced. The base shear V_d without the consideration of accidental torsion effect is provided in Table 4-13 as well.

Table 4-13 Dynamic characteristics of the 12-storey and 16-storey OBF buildings from OpenSees

Building ID	**Height** (m)	$\mathbf{T_1}$ (s)	$\mathbf{T_2}$ (s)	$\mathbf{V_d}$ (kN)
12-storey	44.8	2.15	0.76	5574
16-storey	59.6	2.87	0.99	7496

The same set of crustal and the set of subduction ground motions as given in Chapter 3 are considered. The seismic response recorded in terms of interstorey drift and residual interstorey drift is presented below.

4.3.1. Nonlinear seismic response of 12-storey and 16-storey OBF buildings expressed in terms of lateral deflection

The interstorey drift of the 12-storey and 16-storey OBF buildings subjected to both sets of crustal and subduction ground motions is discussed below. It is noted that the shear generated from torsion caused by accidental eccentricity was considered in the preliminary design in addition to the P-Δ effect and the ratio between the total base shear including the shear from torsion caused by accidental eccentricity and the base shear without the consideration of accidental eccentricity is about 1.2 for both buildings. The OpenSees model is based on 2-D structure geometry and it cannot capture the effect caused by accidental torsion. In order to obtain consistent results, the accelerograms of both crustal and subduction sets used as seismic load input were re-amplified by the above 1.2 factor. Initially, all accelerograms were scaled such that their response spectrum to match or be above the design spectrum for Victoria (Site Class C) across the interval $0.2T_1$-$1.5T_1$. The interstorey drift resulted from OpenSees before the

application of correction factor 1.2 is depicted for both buildings subjected to both sets of ground motions in Fig. 4-19. As illustrated, there is a substantial reduction of interstorey drift at the floor where the outriggers are located and the interstorey drift at any floor is lower that the code limit of 2.5%h_s. The 50 percentile and 84 percentiles of interstorey drift are also provided.

When accelerograms are amplified by the correction factor, the demand increases and the interstorey drift for both 12-storey and 16-storey OBF buildings subjected to both sets of crustal and subduction ground motions is plotted in Fig. 4-20

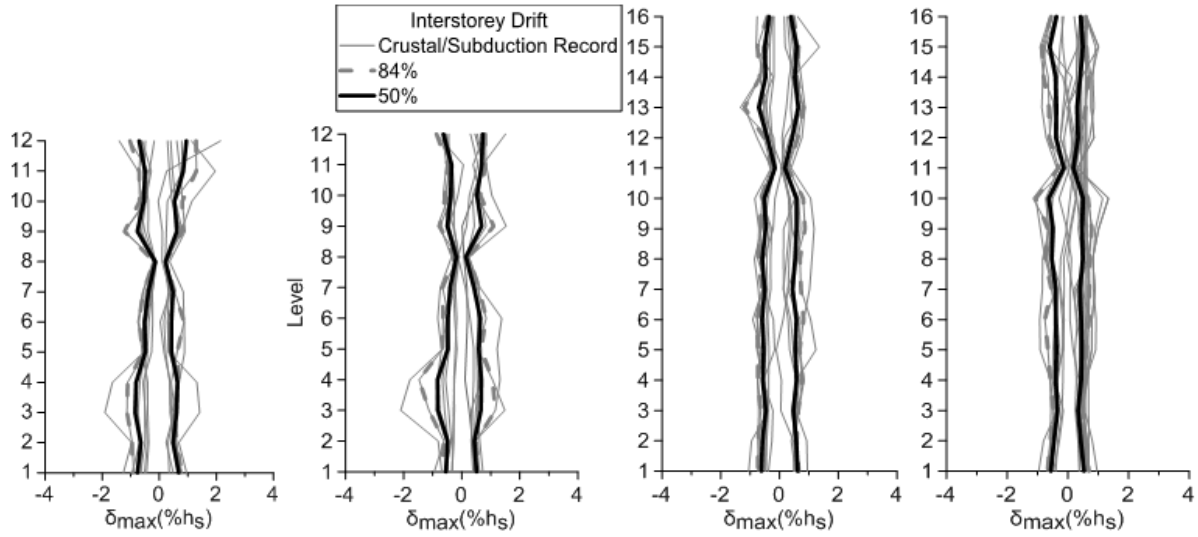

(C) (S) (C) (S)

Figure 4-19 Interstorey drift of 12-st. and 16-st. OBF buildings plotted without the consideration of correction factor and computed under the set of crustal records (C) and subduction records (S)

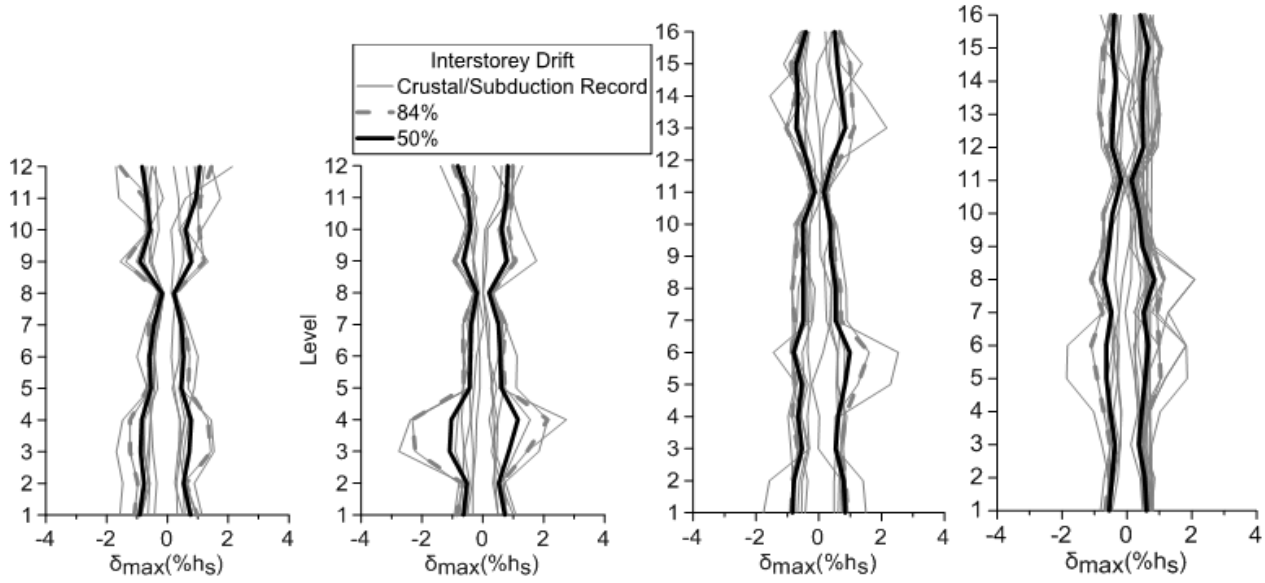

(C) (S) (C) (S)

Figure 4-20 Interstorey drift of 12-st. and 16-st. OBF buildings plotted with the consideration of correction factor 1.2, computed under the set of crustal records (C) and subduction records (S)

It is observed from the results that the interstorey drift at the location of outriggers is unchanged. However, when the buildings were subjected to crustal records the interstorey drift was slightly amplified at the upper floors above the outriggers, whereas for the subduction ground motions, the amplification of the interstorey drift was observed at the floors below the outriggers. The peak values of the interstorey at 84 percentile was found to be 1.56% h_s, which was recorded at the top floor of the 12-storey OBF building under the Loma Prieta record #767; and under the subduction records, it occurred for MYG004 record at the 4th floor (2.32% h_s). Although the demand increased, the peak of 84 percentile interstorey drift was still within the code limit of 2.5% h_s. Similarly, for the 16-storey OBF building, the peak of 84 percentile interstorey drift is below the code limit.

The residual interstorey drift was also recorded for both 12-storey and 16-storey OBF buildings subjected to both sets of ground motions. The residual interstorey drift is plotted for both buildings under both sets of records without the consideration of correction factor in Fig. 4-21and with the consideration of correction factor 1.2 in Fig. 4-22.

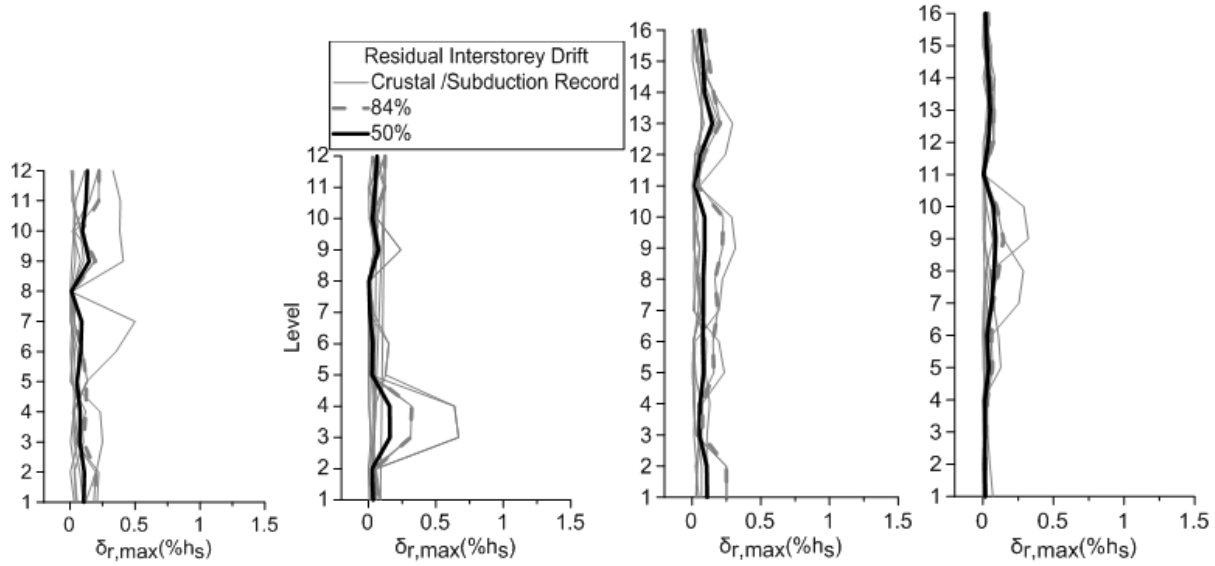

(C) (S) (C) (S)

Figure 4-21 Residual interstorey drift of 12-st. and 16-st. OBF buildings plotted without the consideration of correction factor under the set of crustal (C) and subduction records (S)

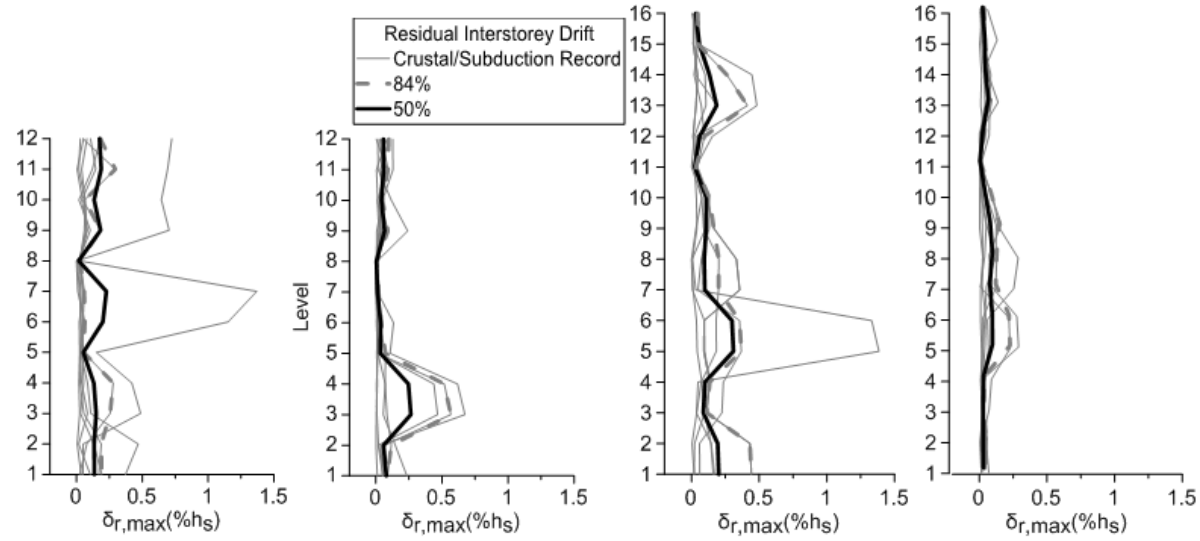

(C) (S) (C) (S)

Figure 4-22 Residual interstorey drift of 12-st. and 16-st. OBF buildings plotted with the consideration of correction factor 1.2 under the set of crustal (C) and subduction records (S)

As observed from Fig. 4-22, there is an amplification of residual interstorey drift at the 3rd and 4th floor of the 12-storey OBF under the subduction records. Herein, the peak of 84 percentile residual interstorey drift is 0.58% h_s. It is noted that this value is slightly higher than the recommended value of 0.5% h_s as reported in the literature in order to consider the building reparable in the aftermath of an earthquake event.

4.3.2. Nonlinear seismic response of 12-storey and 16-storey OBF buildings in terms of damage index of braces

For both studied high-rise buildings the damage index (DI) at the level of core braces was calculated. The procedure was explained in Chapter 3. The damage index computed for braces of the 12-storey and 16-storey OBF is plotted in Fig. 4-23 under both sets of ground motions without the application of correction factor and in Fig. 4-24 with the consideration of correction factor of 1.2. As depicted, in case of the 12-storery building the damage index, DI, was concentrated at the 3rd and 4th floor, as well as at the 9th and 12 floors under the subduction ground motion set. Slight demand is observed at upper floors under the crustal ground motions. This trend is similar for the 16-storey OBF building.

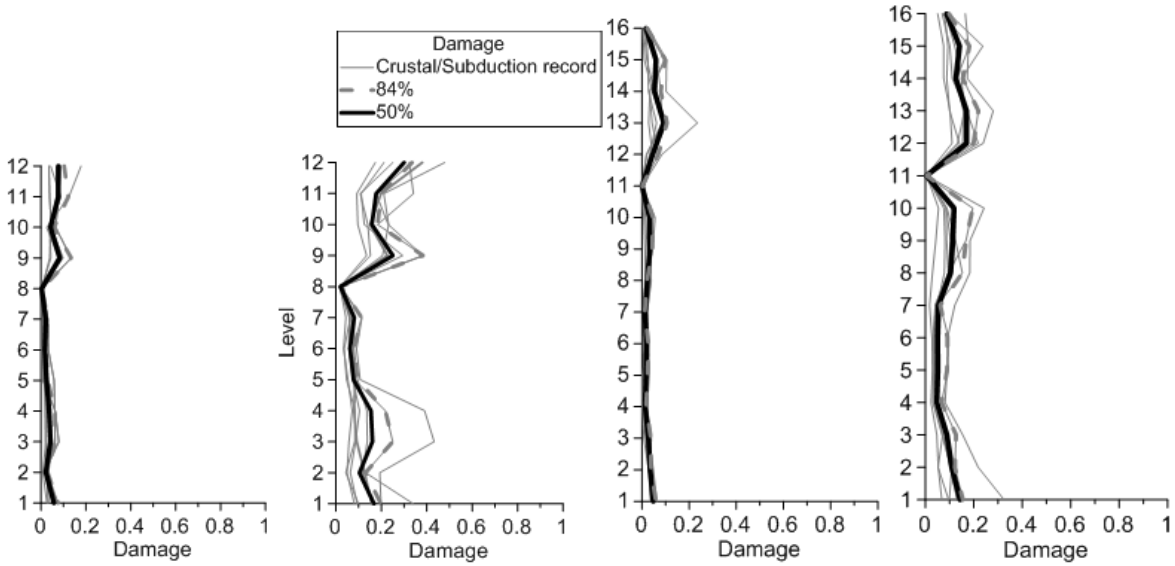

C) (S) (C) (S)

Figure 4-23 Damage index computed for braces of 12-st. and 16-st. OBF buildings plotted under the set of crustal (C) and subduction records (S) without the consideration of correction factor

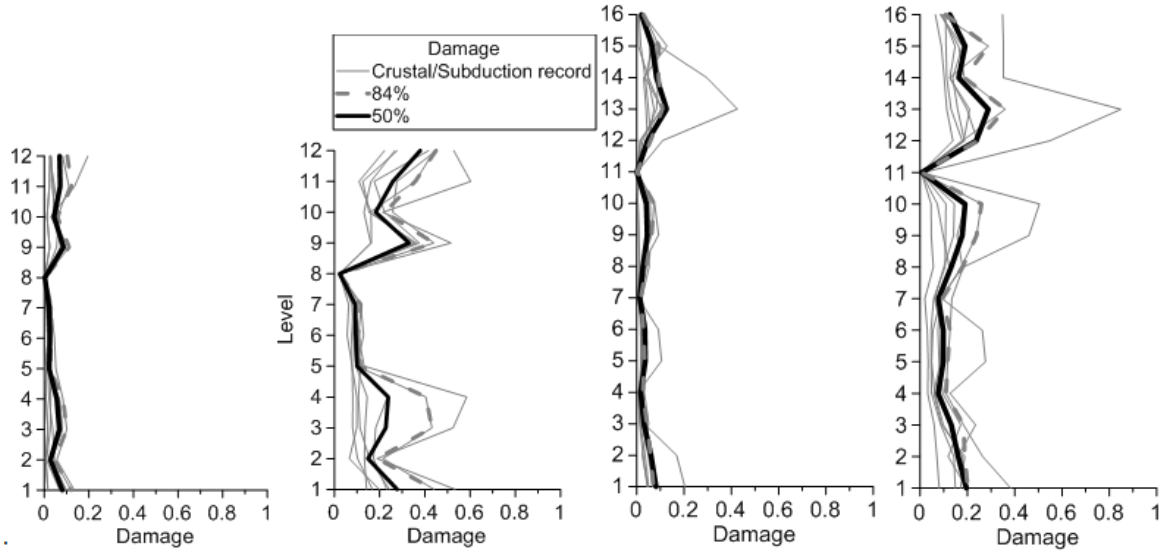

(C) (S) (C) (S)

Figure 4-24 Damage index computed for braces of 12-st. and 16-st. OBF buildings plotted under the set of crustal (C) and subduction records (S) with the consideration of correction factor

As shown in Fig. 4-24, the damage of braces increases at higher rate under the subduction records than under the crustal records. It is noted that a DI = 1.0 means failure of the outermost fiber of the brace cross-section at that floor. Thus, in the case of 12-storey OBF building, the peck of 84 percentile DI occurred at the 3rd floor, 9th floor, and 12th floor were damage accumulated in floor braces is about 42%. A similar value of DI occurred at the 13th floor of the 16-storey OBF building.

4.3.3. Seismic response of 12-st OBF building under crustal record #767 and subduction record MYG004

To analyze the response of the 12-story OBF building under the crustal #767 record Loma Prieta, a time-history series of roof drift and roof interstorey drift is plotted in Fig. 4-25 together with the scaled accelerogram. As shown, the peak interstorey drift is 2.24% h_s which is within the code limit. As depicted, the behavior of building deflection is approximately symmetric. The nonlinear hysteresis response of the left and right braces located at the top floor is given in Fig. 4-26. As observed, both braces buckle in compression and yield in tension.

In Fig. 4-26a, the axial force in the brace is normalized to the probable tensile force. In Fig. 4-26b is plotted the time-history series of strain recorded in the outermost compression fiber

and tensile fiber of middle brace's length cross-section. From time-history series of compression strain it is observed that the braces still possess life strain before failure because the amplitude of compressive strain diminishes toward the end of ground motion and is still preserved in the negative side. From the study reported in Tirca and Chen (2014) and Hasiao et al. (2012) it is found that a brace reaches failure when the compressive strain recorded for a cross-sectional fiber acting in compression changes to tension. Figure 4-26c illustrates the damage index of the same outermost cross-sectional fiber of HSS brace. As shown, the ratio is less than 1.0 which means that both braces still possess inelastic strength capacity.

Figure 4-27 shows the response of the structure subjected to the acceleration amplitude of ground motions modified by the correction factor 1.2 to account for accidental torsion. The figure shows the scaled accelerogram, roof drift and maximum interstorey drift recorded at the roof level among floors. Similarly, the response of the 12-storey OBF building in term of lateral deflection has the same tendency as shown in Fig. 4-25. Then, the inelastic behavior of top floor braces, the time-history series of tensile and compressive strain as well as the brace damage index is illustrated in Fig. 4-28. Comparison of the results in Fig. 4-26 and Fig. 4-28 reveals no large difference in the behavior.

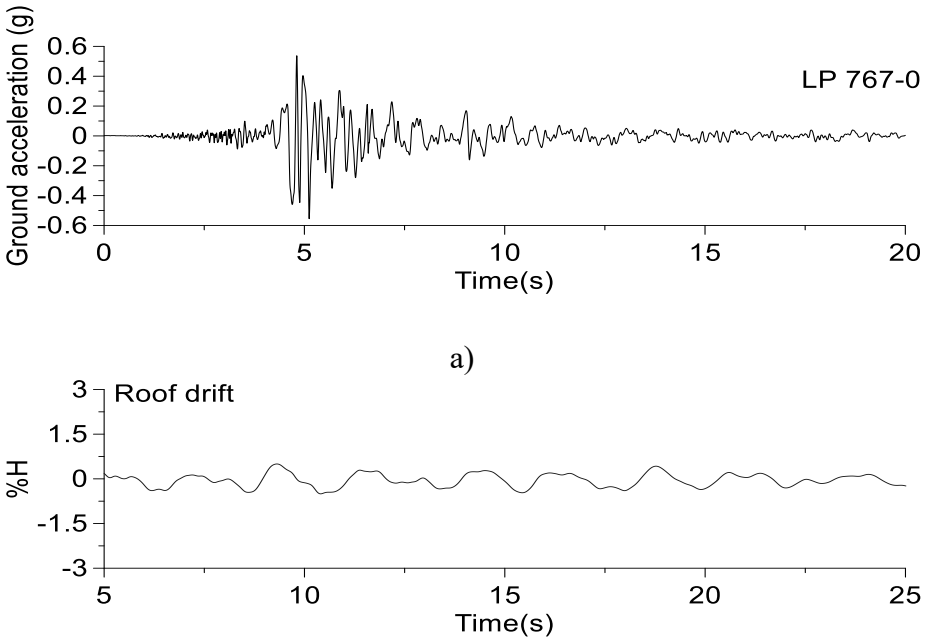

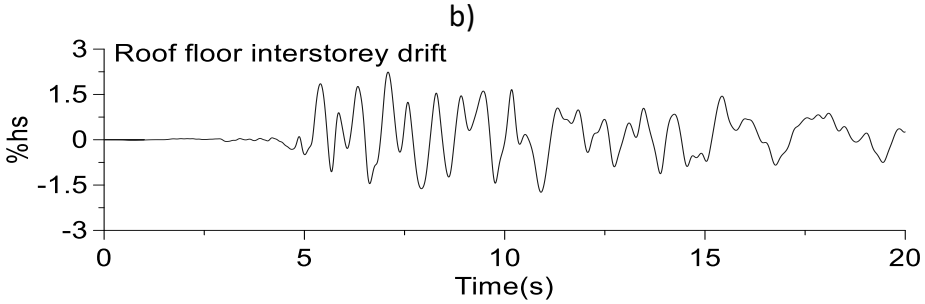

c)

Figure 4-25 Response of 12-storey OBF building under #767 record: a) accelerogram, b) roof drift, c) interstorey drift time-history series recorded at roof

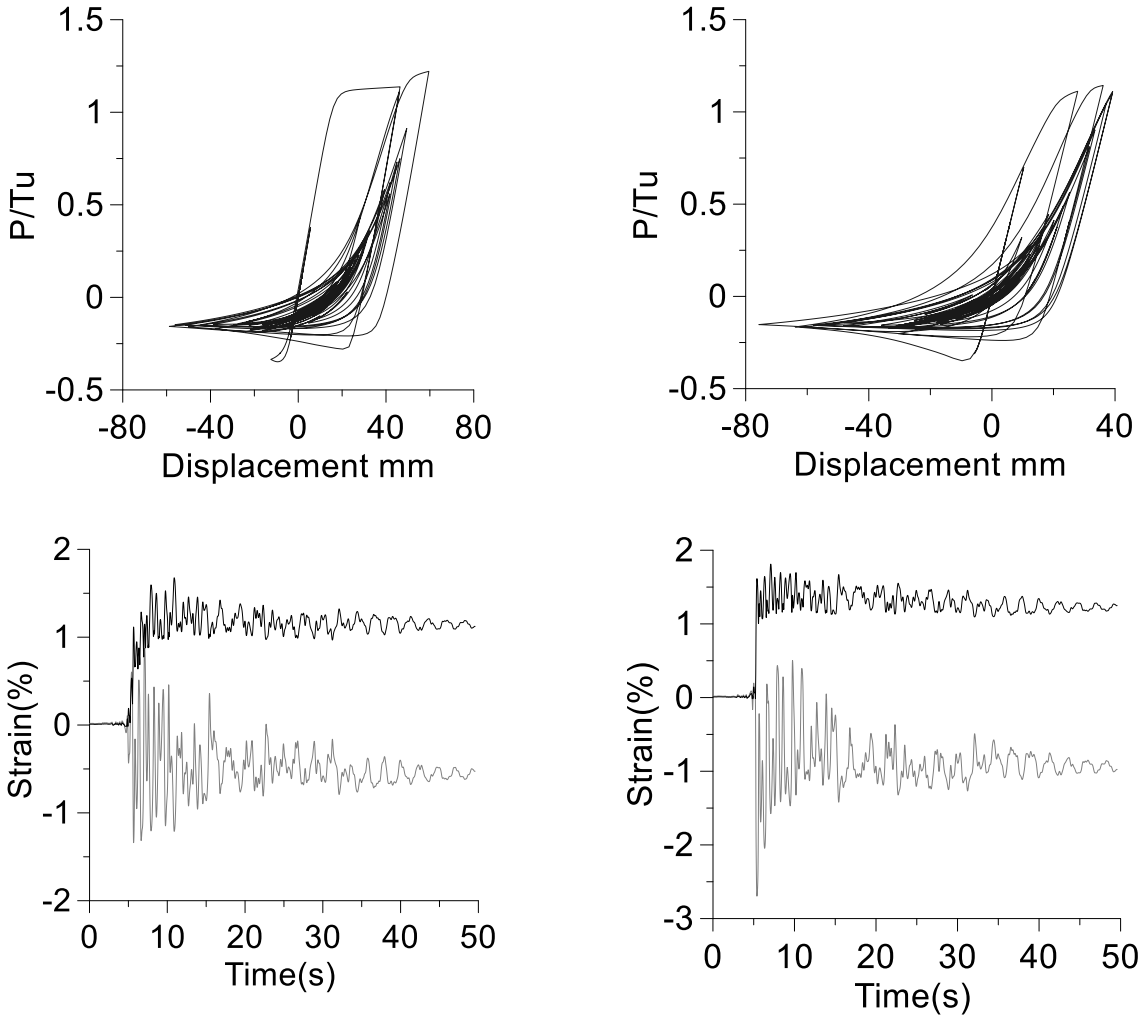

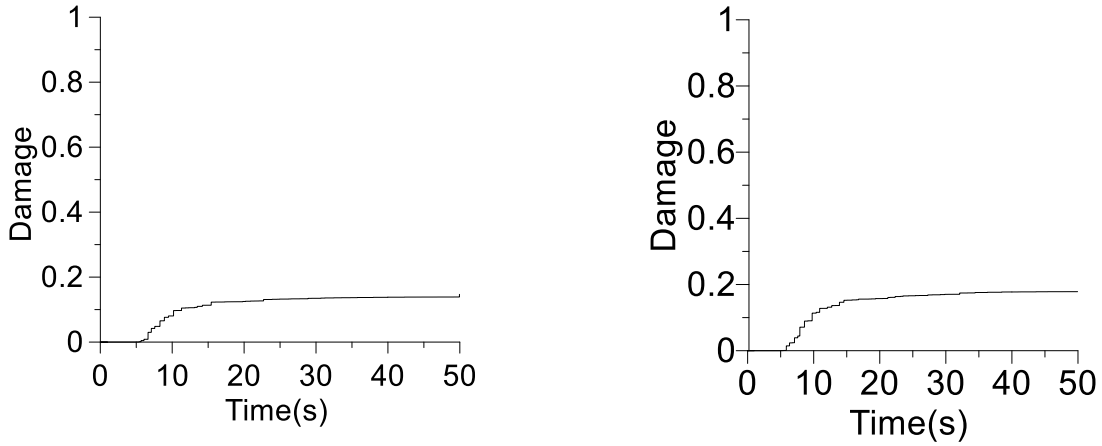

Figure 4-26 Hysteresis response, strain time-history series, and damage index of left and right brace located at the top floor under the scaled #767 crustal record

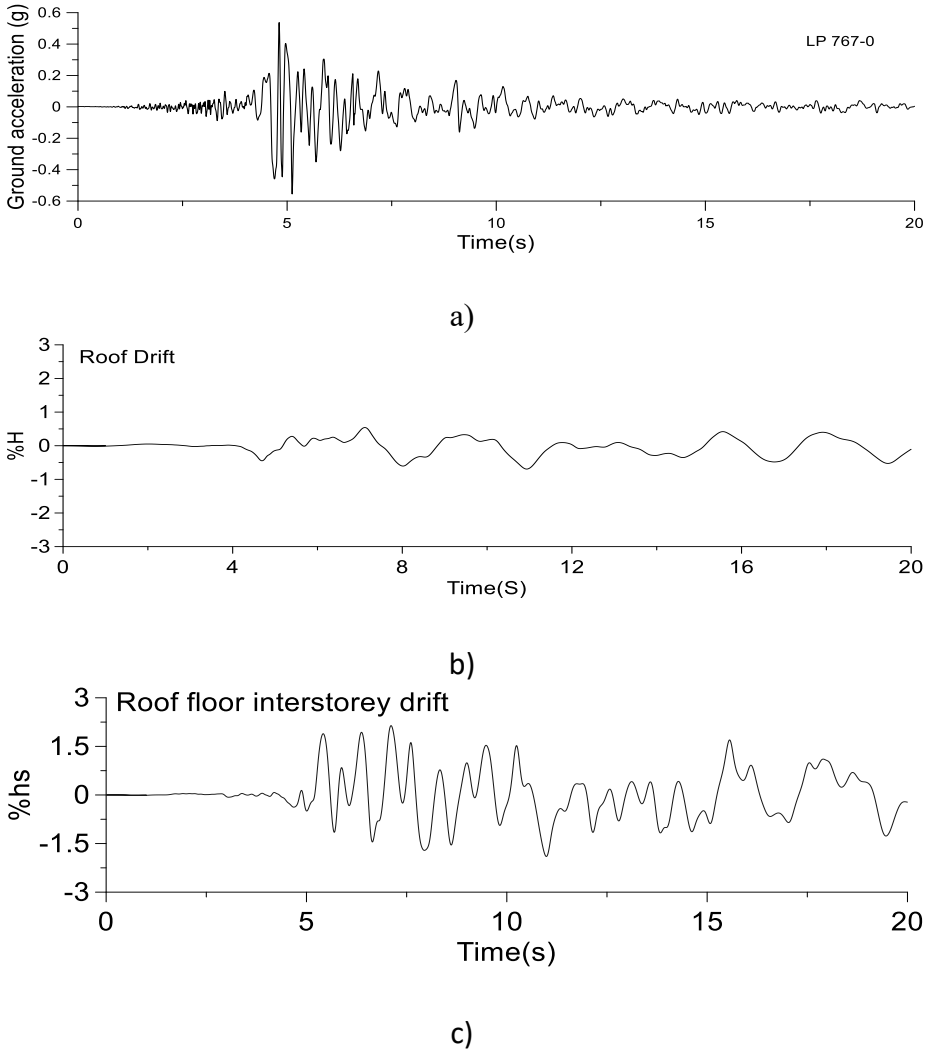

Figure 4-27 Response of 12-storey OBF building under #767 record amplified by correction factor 1.2: a) accelerogram, b) roof drift, c) time-history series of interstorey drift at roof

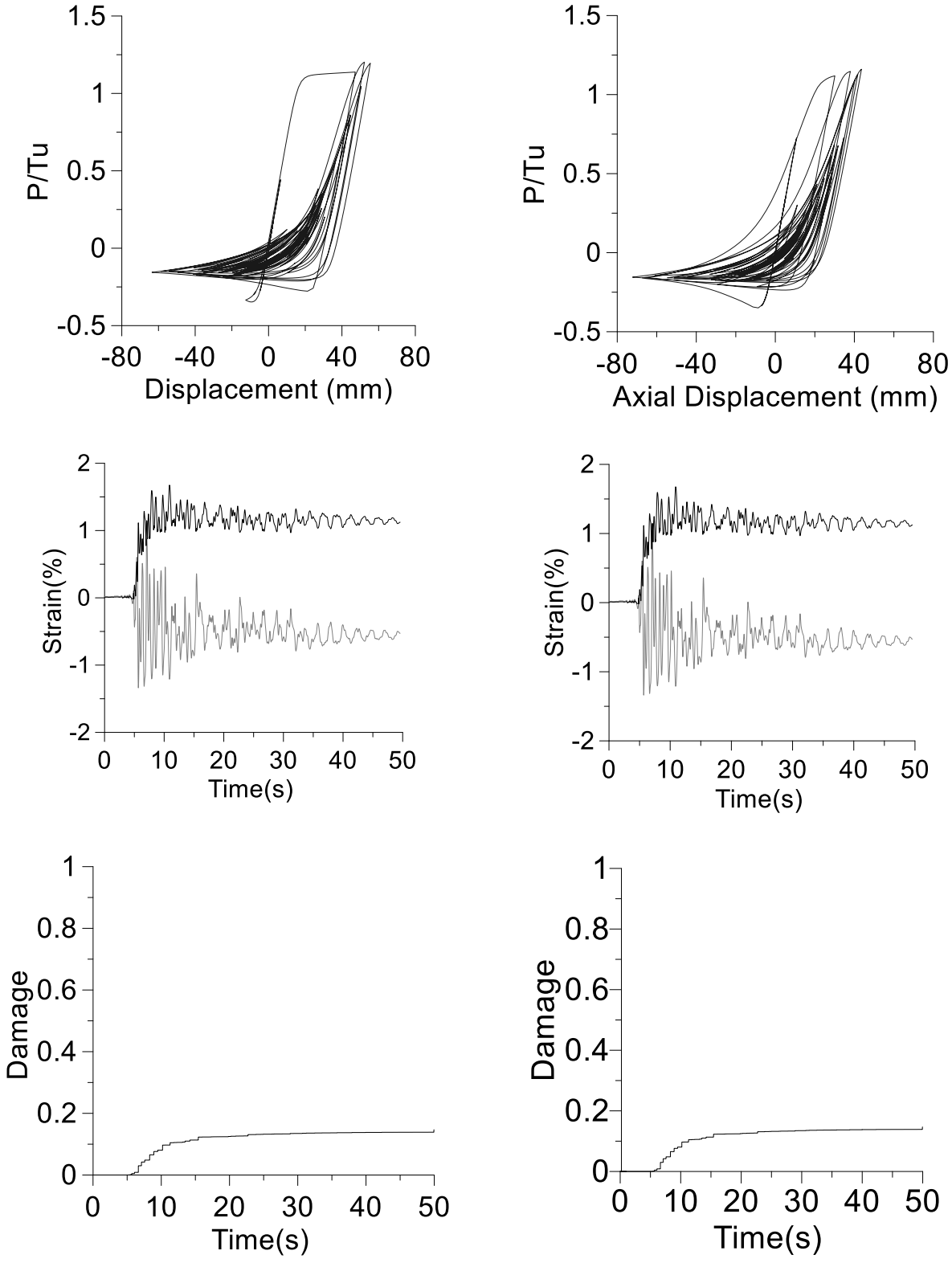

Figure 4-28 Hysteresis response, strain time-history series, and damage index of left and right braces of top floor under the scaled #767 crustal record amplified by correction factor 1.2

The response of the 12-storey OBF under the subduction record MYG004 is presented below. Figure 4-29 presents the accelerogram with an applied scaling factor equal 1.0, as well as the time-history series of roof drift and interstorey drift recorded at the 3rd floor where the peak interstorey drift among floors was experienced.

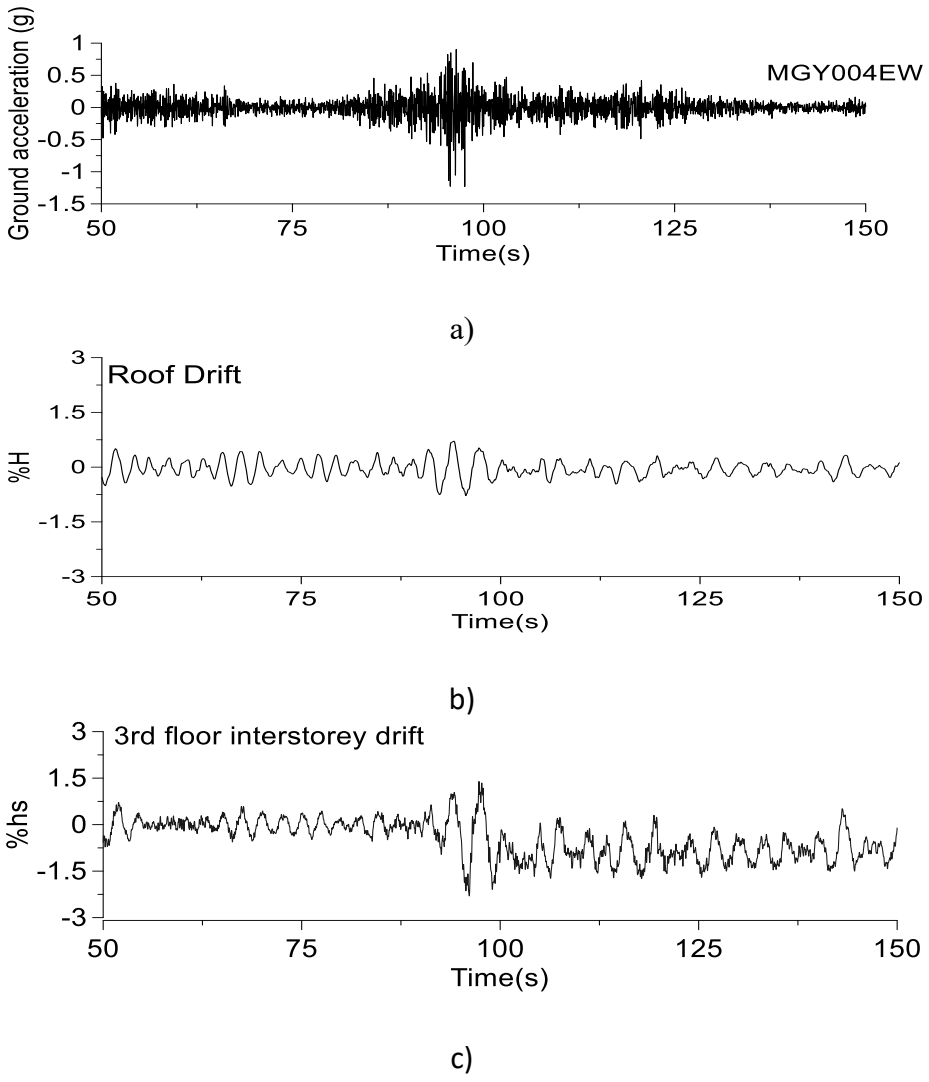

Figure 4-29 Response of 12-storey OBF building under #MYG004 subduction record: a) accelerogram, b) roof drift, c) time-history series interstorey drift recorded at 3rd floor

To better emphasize the building behaviour only the response between the time sequence 50 s and 150 s is presented. After the occurrence of main shock at time sequence 96 s, the building deflected laterally on one side. The maximum interstorey drift is 2.34% h_s. The nonlinear hysteresis response of braces located at the 3rd floor is illustrated in Fig. 4-30.

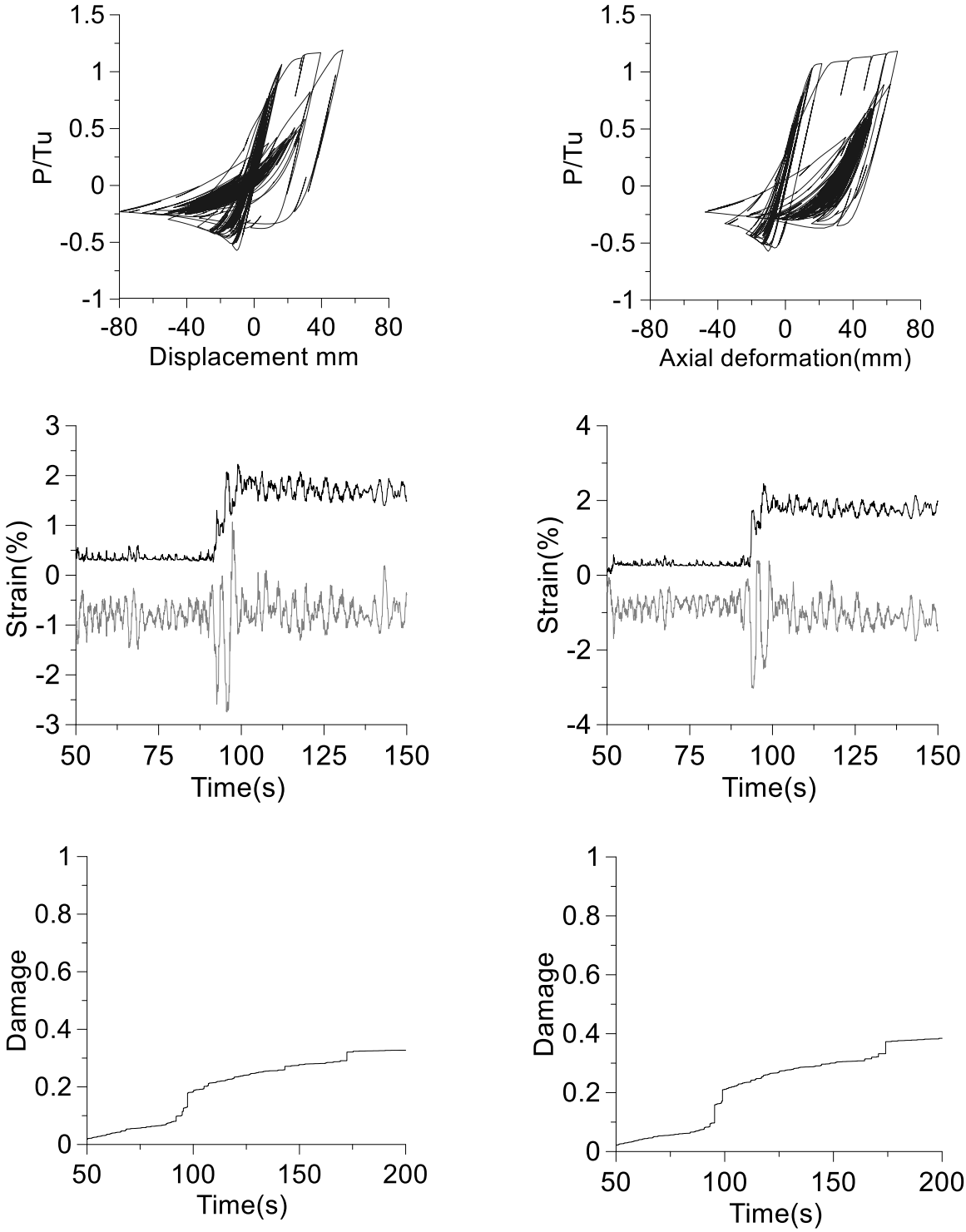

Figure 4-30 Hysteresis response, strain time-history series, and damage index of both left and right braces of 3rd floor under #MYG004 subduction record

As observed from Fig. 4-30 both braces buckle in compression and yield in tension. There is an important difference in the time-history series of tensile and compression strain recorded at the outermost fiber of mid-length brace cross-section. At the time sequence corresponding to the main shock (t = 96 s) there is a jump in the time history series of tensile strain which means that large amount of strain was suddenly accumulated. Meanwhile, at the same time sequence, the compressive strain increase in the tensile side. At the time that the jump in strain is recorded, a jump in the damage index of brace is also recorded. To summarize, under both selected crustal (#767) and subduction (MYG004) record, the peak interstorey drift has similar amplitude but larger strain is accumulated under the subduction record leading to shorter life strain.

In Fig. 4-31 is shown the response in term of roof drift and interstorey drift obtained under the

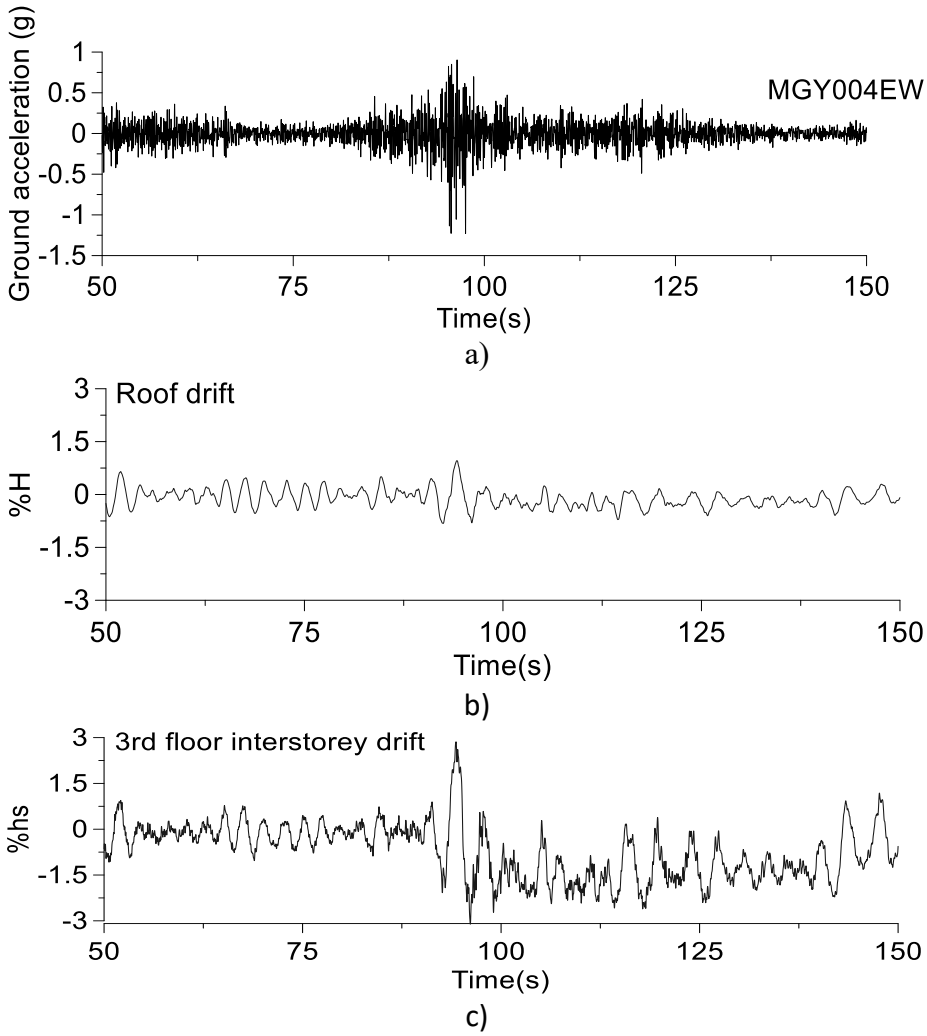

Figure 4-31 Response of 12-storey OBF building under #MYG004 subduction record amplified by 1.2: a) accelerogram, b) roof drift, c) time-history series of interstorey drift at the 3rd floor.

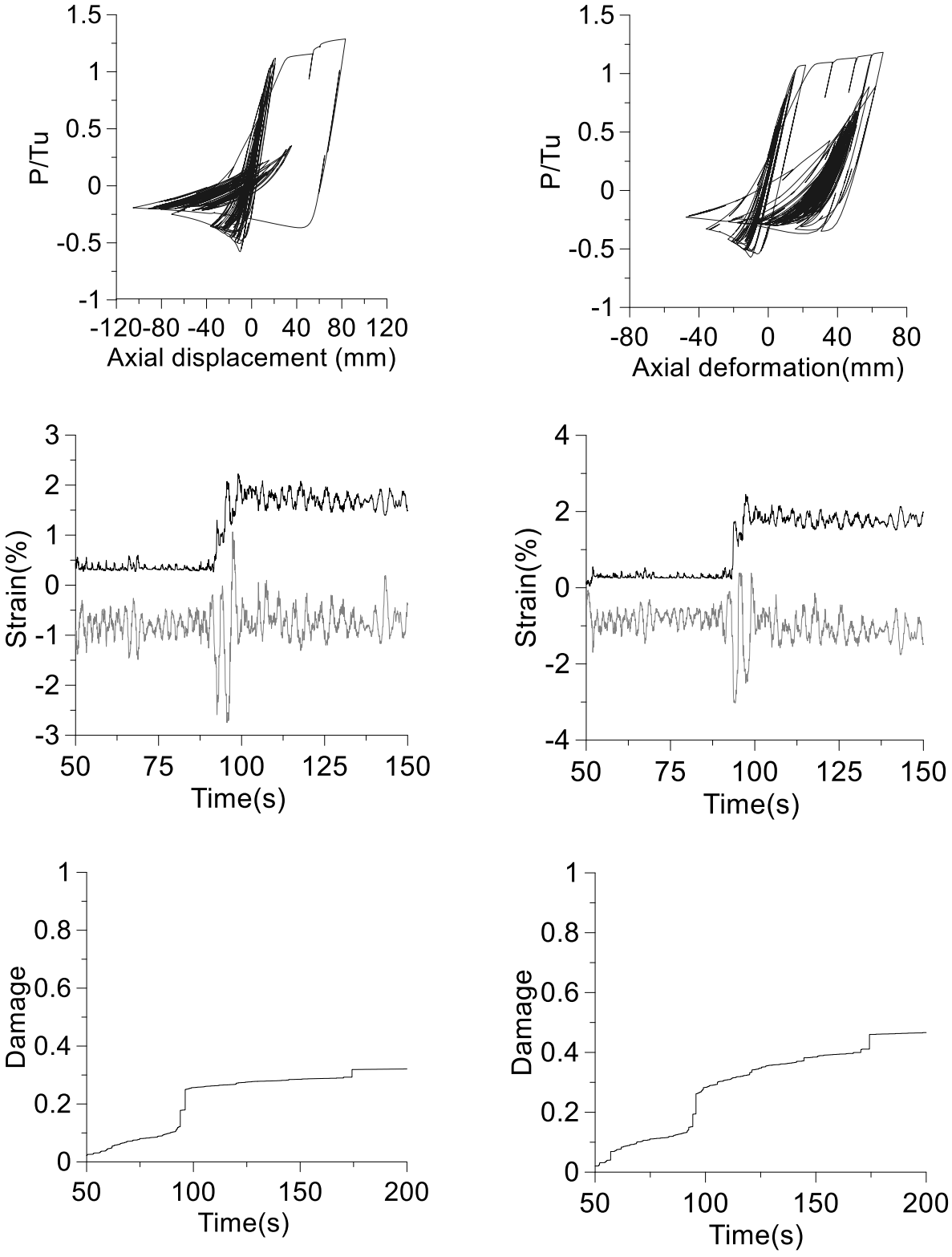

Figure 4-32 Hysteresis response, strain time-history series, and damage index of both left and right braces of 3rd floor under #MYG004 subduction record amplified by correction factor 1.2

same MYG004 record amplified by the correction factor 1.2. In Fig. 4-32 is plotted the hysteresis loops of both braces located at the 3rd floor resulted under the same subduction record MYG004 amplified by the correction factor 1.2. As shown in the figure, both braces buckle in compression and yield in tension. An amplified jump in the tensile strain is recorded at the same time sequence 96 s, while the damage index recorded for the HSS brace increases to 52%.

4.3.4. Seismic response of 16-st OBF building under crustal record #736 and subduction record MYG004

The response of the 16-story OBF building under the crustal record #736 (Loma Prieta), and a time-history series of roof drift and roof interstorey drift are plotted in Fig. 4-33 together with the scaled accelerogram. As shown, the peak interstorey drift of 1.5% h_s occurred at the 9th floor which is within the code limit.

Nonlinear time-history response of left and right braces of the 9th floor of 16-storey OBF building subjected to #736 crustal record is shown in Fig. 4-34. The HSS brace on the left side exhibits buckling in compression and yielding in tension, while the brace on the right side shows large deformations while acting in compression. The strain time-history series of the left and right HSS core braces of the 9th floor level is also plotted in Fig. 4-34. It is observed that a larger compression strain of 2.1% is developed in the right brace. In both cases, the damage index is less than 10% of brace capacity.

Increasing the acceleration amplitude of crustal ground motion #736 by the correction factor 1.2 results in an increase in the interstorey drift and damage accumulated in the core HSS braces. Fig. 4-35 shows the scaled accelerogram, time-history series of roof drift and interstorey drift recorded at the 5th floor. It is noted that the 5th floor was selected because it shows the larger peak deflection (2.54% h_s) and the structure started to deform on one side. The inelastic hysteresis loops of 5th floor left and right core braces, the time-history series of tensile and compressive strain, as well as, the brace damage index is illustrated in Fig. 4-36. As depicted, the left HSS brace shows large hysteresis loops after undergoing buckling and yielding in tension. Comparatively, the right brace was loaded first in compression and shows large deformations after buckling was experienced. In terms of compressive strain, the maximum value of 3.17%

was exhibited by the right side brace. A damage index of around 15% of brace capacity was recorded. Comparing the response of braces as shown in Fig. 4-34 and Fig. 4-36, an important change in behavior especially in term of interstorey drift and strain time-history series has been observed.

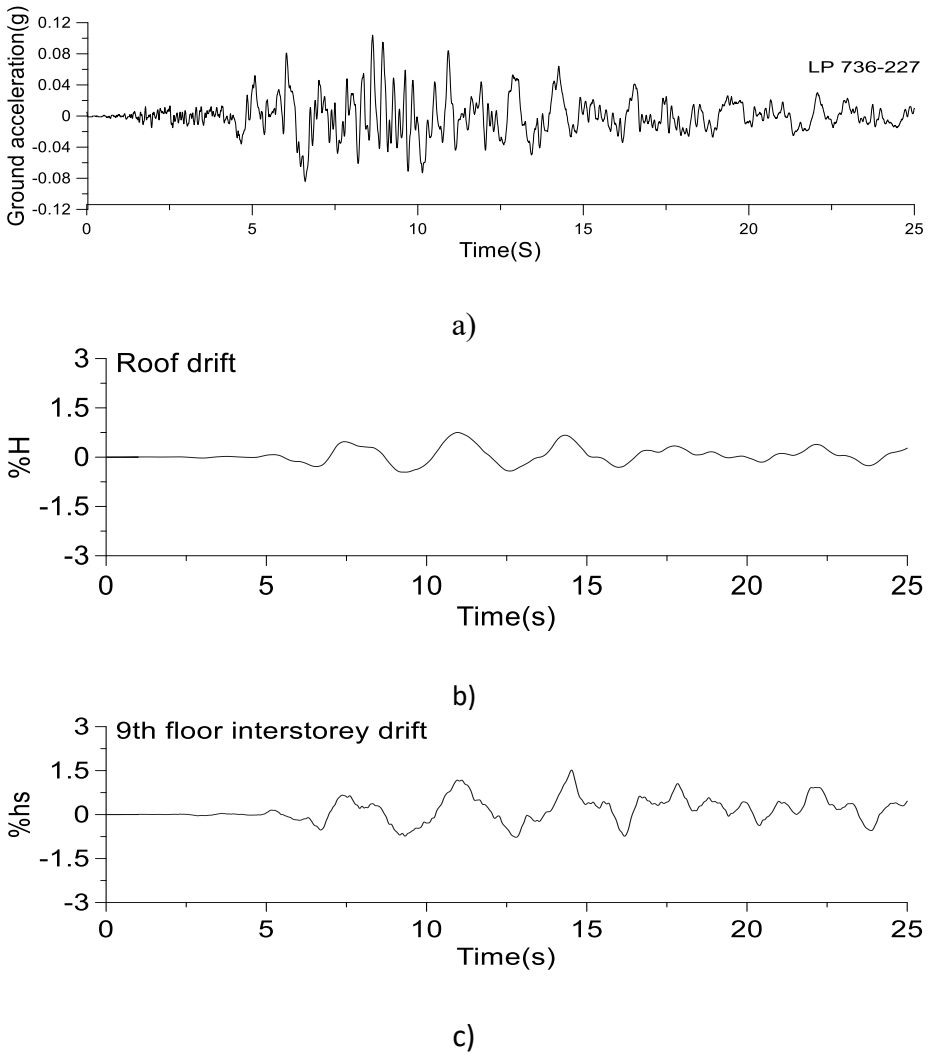

Figure 4-33 Response of 16-storey OBF building under #736 record: a) accelerogram, b) roof drift, c) time-history series of interstorey drift recorded at 9th floor

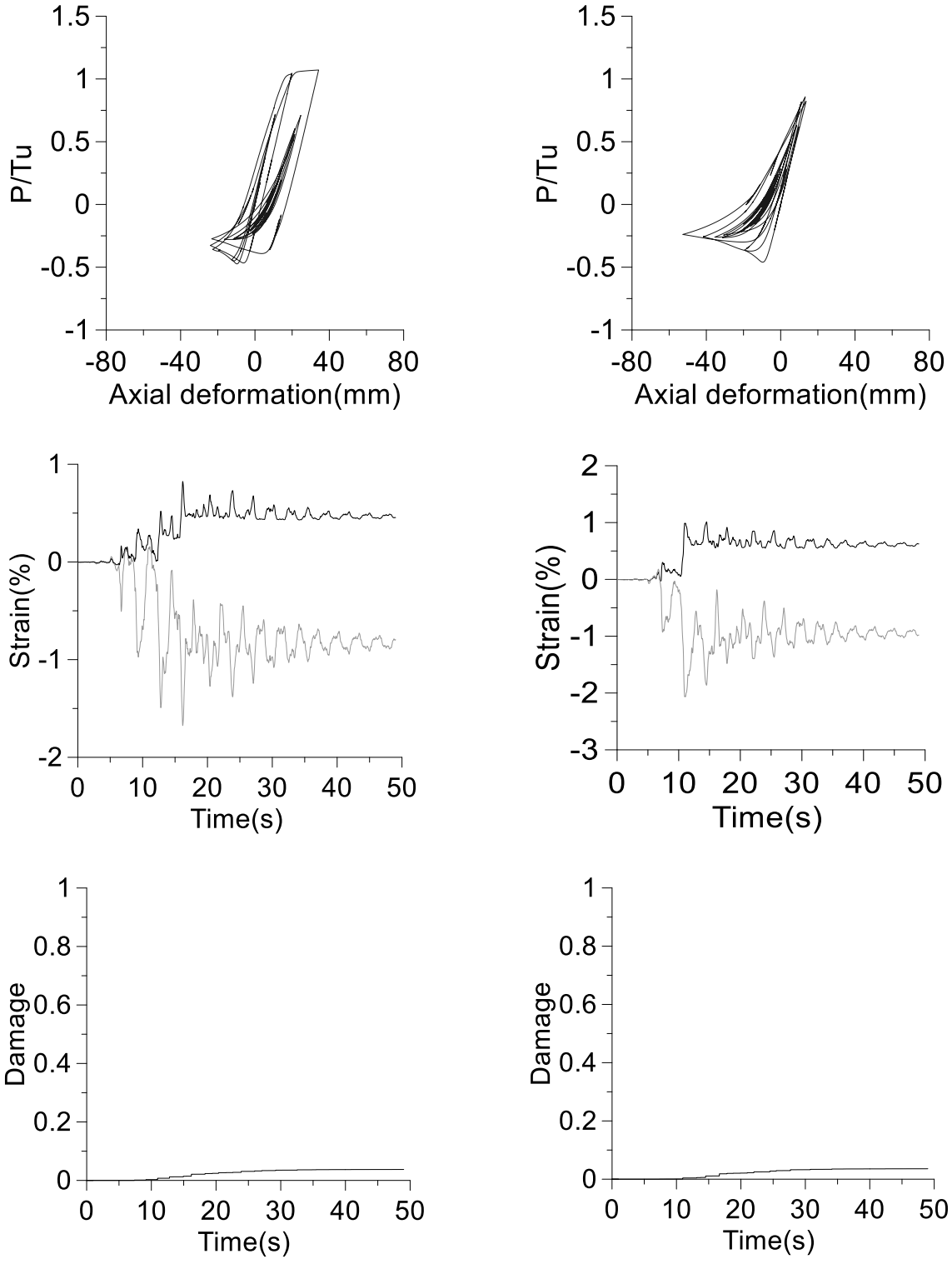

Figure 4-34 Hysteresis response, strain time-history series, and damage index of both left and right HSS braces located at the 9th floor under scaled #736 crustal record

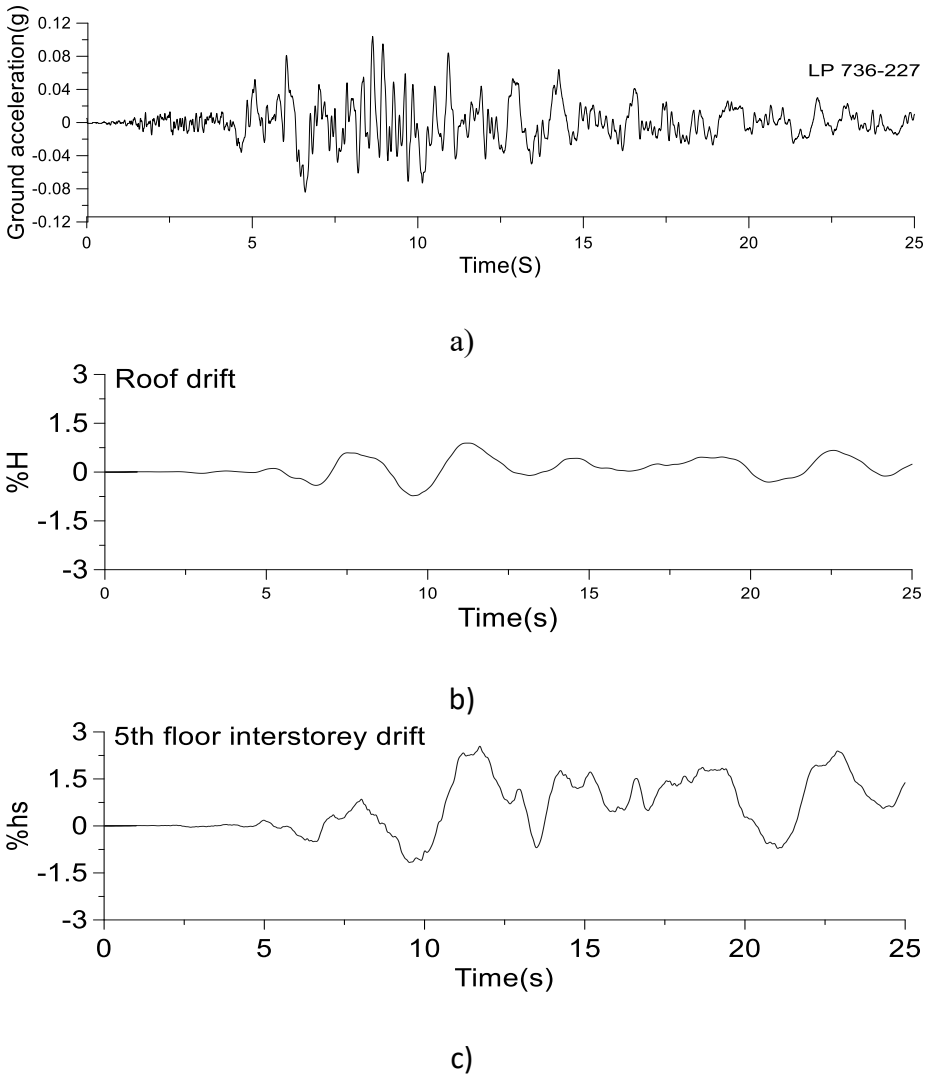

Figure 4-35 Response of 16-storey OBF building under #736 record amplified by correction factor 1.2: a) accelerogram, b) roof drift, c) interstorey drift time-history series of 5th floor.

The response of the 16-storey OBF building under the subduction record MYG004 is presented below. Hence, Figure 4-37 presents the accelerogram with an applied scaling factor equal to 1.0, as well as, the time-history series of roof drift and interstorey drift recorded at the 9th floor where the peak interstorey drift was recorded. To better emphasize the building behavior only the response between the time sequence 50 s and 150 s is presented. As resulted, the maximum interstorey drift is 1.6% h_s and is within the code limits. In Fig. 4-38 is shown the nonlinear hysteresis response of left and right HSS braces located at the 9th floor, the strain time-history series, and brace damage index.

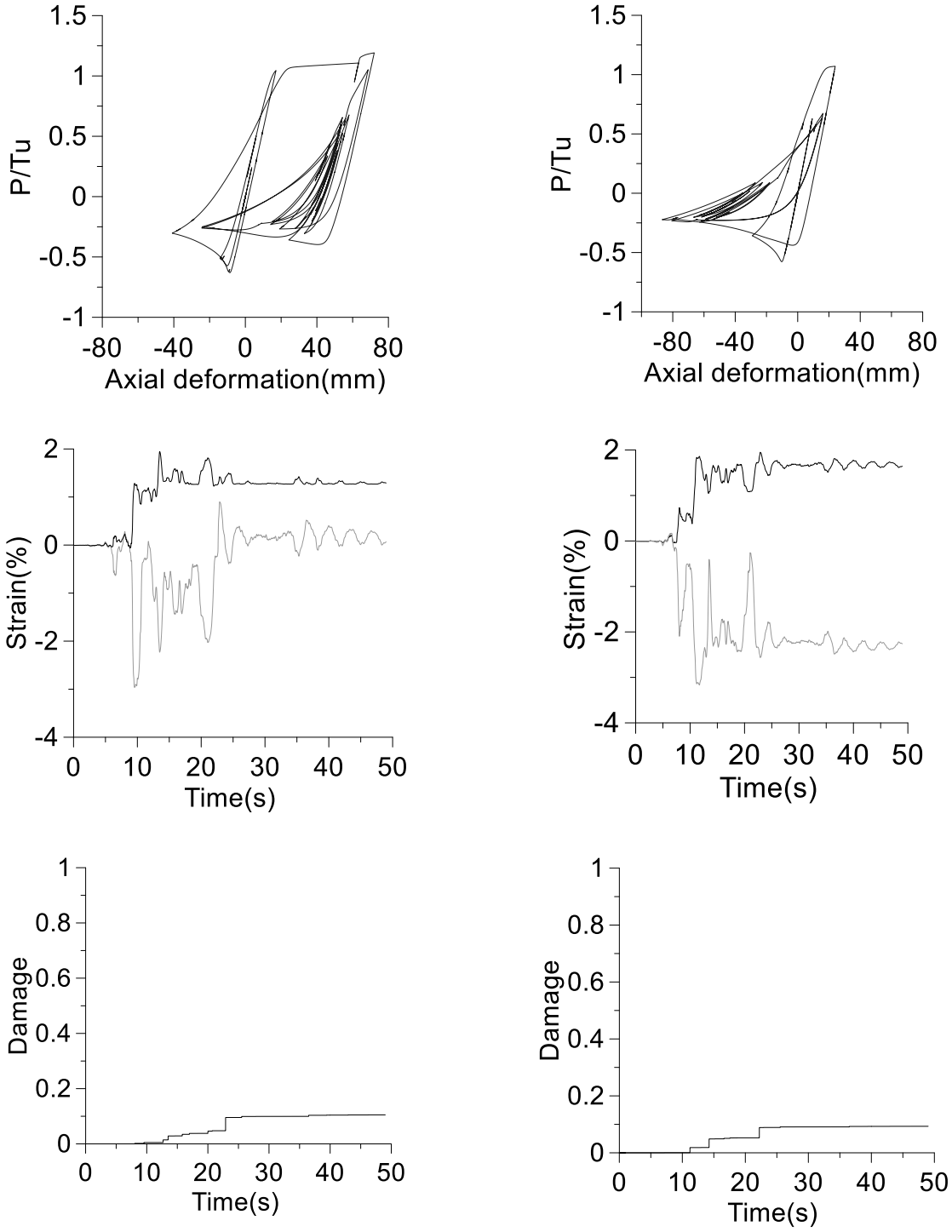

Figure 4-36 Hysteresis response, strain time-history series, and damage index of left and right braces of 5th floor under the scaled #736 crustal record amplified by correction factor 1.2.

It is observed that the left HSS brace buckles in compression and yields in tension while the right HSS brace experienced larger deformation in compression after buckling. Regarding the time-

history series of compression strain, both braces experienced similar peak strain of 2%. The maximum damage index reach by braces is 22% of their capacity.

The seismic response recorded in terms of time-history series of roof drift and interstorey drift of the 8th floor obtained under the same MYG004 record amplified by the correction factor 1.2 is showed in Fig. 4-39 As depicted, the peak interstorey drift recorded at the 8th floor increases to 2.8% h_s, which is above the code limit of 2.5% h_s. As shown in Fig. 4-39 at time sequence 94.59 s, there is a jump in the time-history series of interstorey drift. After that the building oscillates on one side.

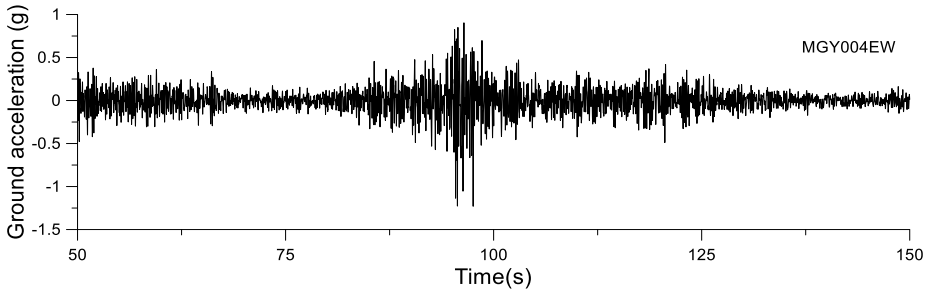

a)

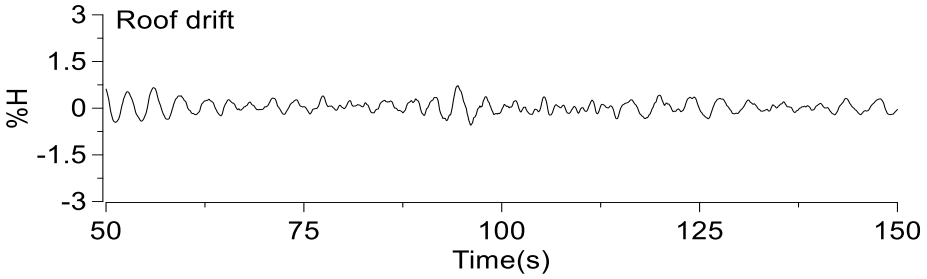

b)

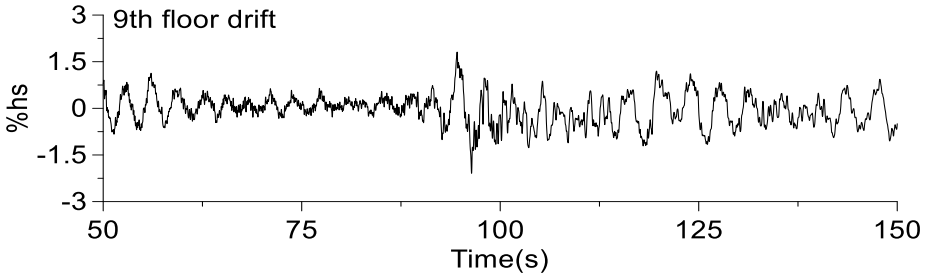

c)

Figure 4-37 Response of 16-storey OBF building under #MYG004 subduction record: a) accelerogram, b) roof drift, c) interstorey drift time series recorded at the 9th floor.

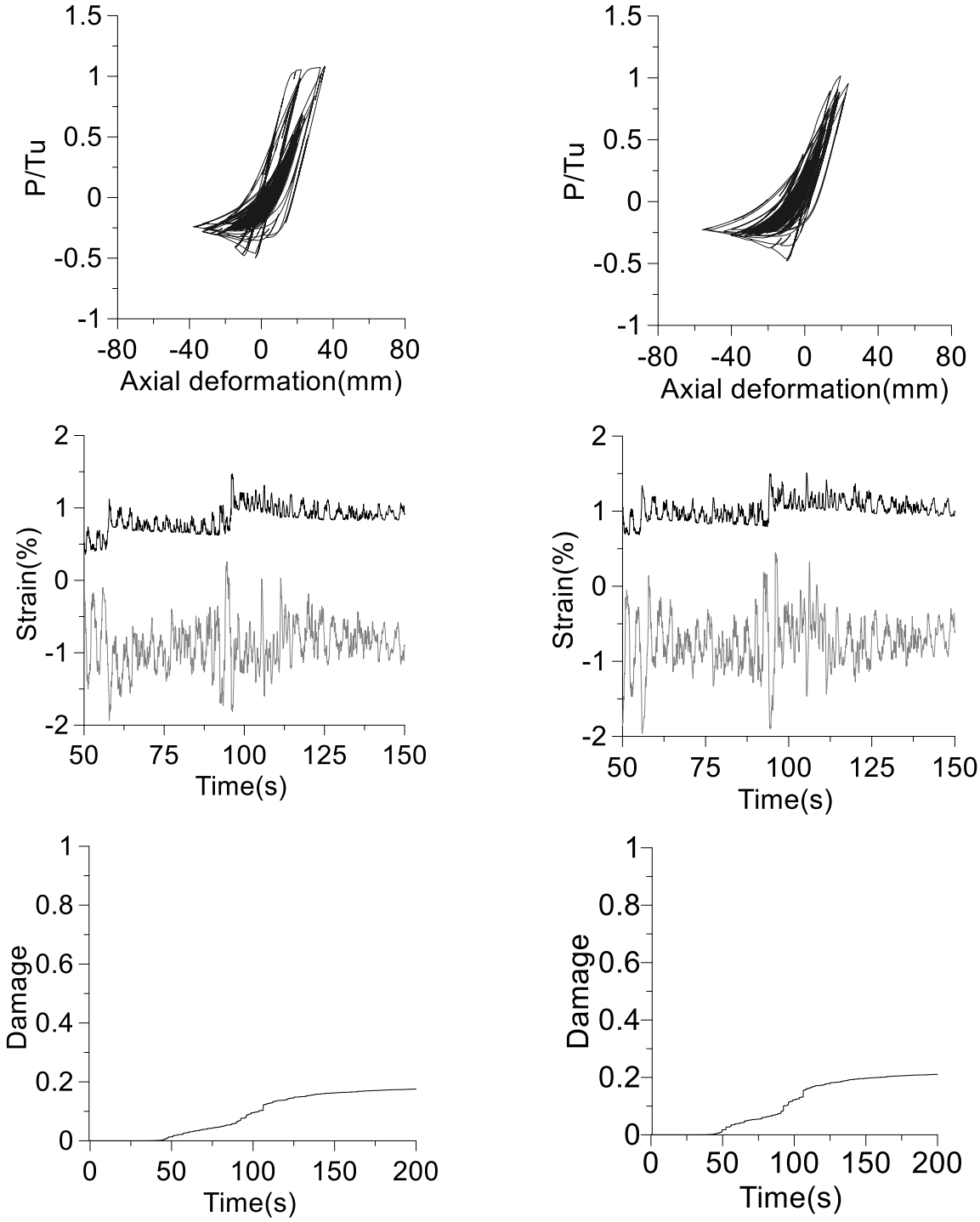

Figure 4-38 Hysteresis response, strain time-history series, and damage index of left and right braces located at the 9th floor under #MYG004 subduction record

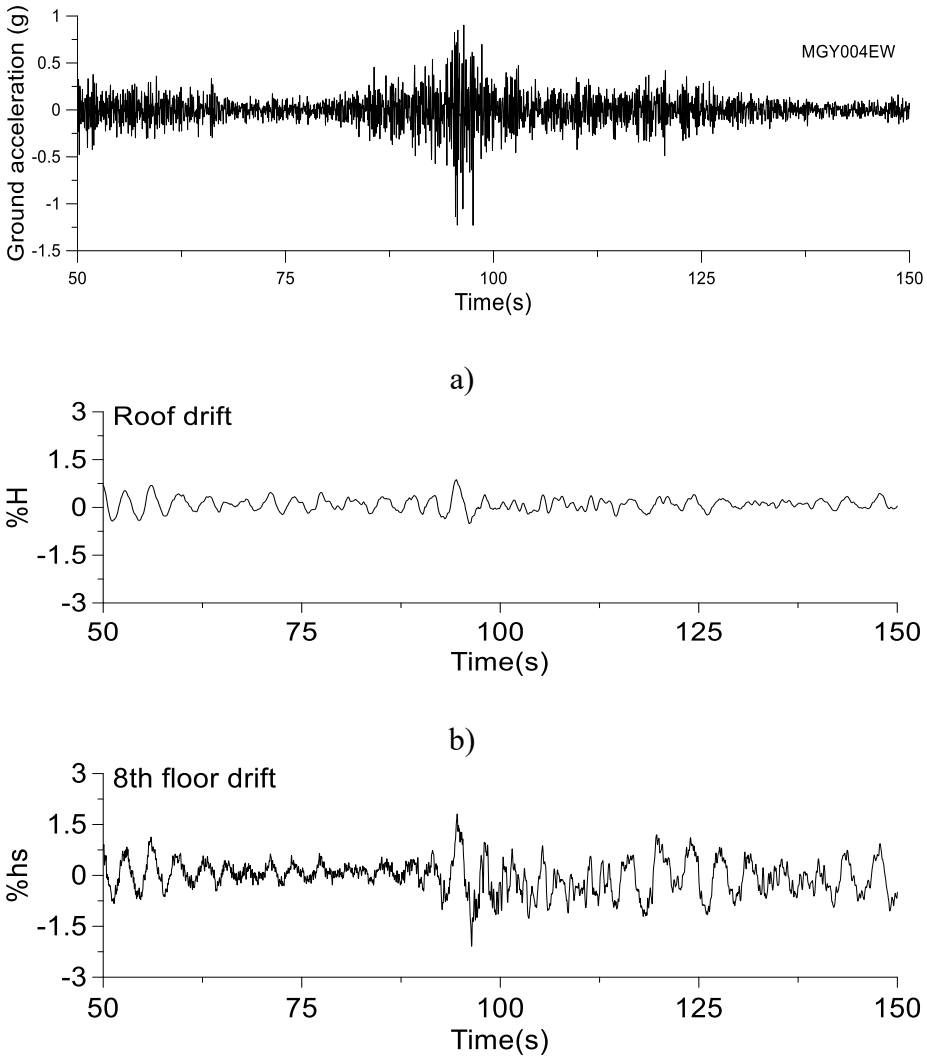

Figure 4-39 Response of 16-storey OBF building under #MYG004 subduction record amplified by 1.2: a) accelerogram, b) roof drift, c) interstorey drift time-history series of 8th floor

Figure 4-40 shows the hysteresis loops of the left and right braces located at the 8th floor, as well as, the strain time-history series and braces damage index. As depicted, both braces show buckling in compression and yielding in tension with large hysteresis loops. However, the left brace shows a pronounced jump in the time-history series of compression strain than the left brace. The jump occurred at the same time sequence 94.59 s as noted above. The peak compression strain recorded is 2.5% and the damage index of braces is 25% of their capacity.

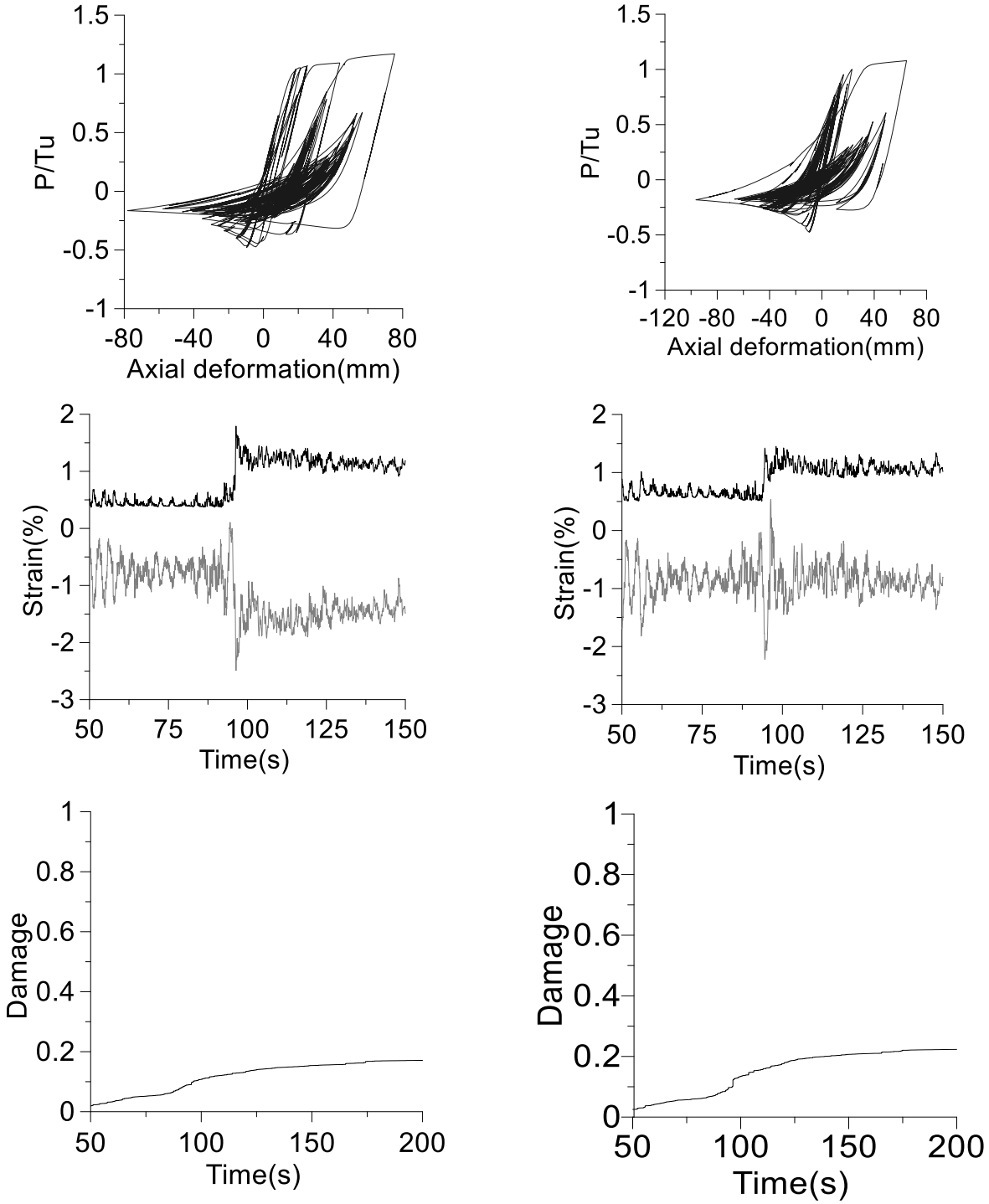

Figure 4-40 Hysteresis response, strain time-history series, and damage index of left and right braces of 8th floor under the #MYG004 subduction record amplified by correction factor 1.2

4.4. Summary of Chapter four

A design method for the OBF system is proposed and validated through nonlinear time-history analysis using detailed numerical models developed in the OpenSees software. To develop the method, three items referring to: i) outrigger truss's geometry, ii) dissipative capacity of diagonal members of outriggers and iii) optimum location of outrigger trusses among the building floors were investigated.

To solve the above items, two models proposed for the outrigger truss geometry were discussed, a method to find the optimum location for outriggers along the building height is proposed, and assumptions concerning the dissipative capacity of outriggers diagonals are presented. The models proposed for the outrigger truss geometry depends on the number of bays formed by gravity columns displaced on each side of the OBF core system. In this study, the difference between the two models consists on the number of diagonal members inserted in each gravity column bay. It was concluded that using two diagonal members per bay it leads to larger storey stiffness that in the case of a single diagonal member. It is worth to note that storey stiffness was controlled at the location of outrigger trusses in order to avoid the vertical stiffness irregularity, known as Type 1 in NBCC.

Referring to the dissipative capacity of outrigger diagonal members there may be three variants: a) $R_d = 1.5$ and $R_0 = 1.3$ as per conventional construction braced frame; b) $R_d = 3$, $R_0 = 1.3$ as per braces of MD-CBF core system and c) $R_d = 4$ and $R_0 = 1.2$ as per ductile buckling-restrained braced frame provided in NBCC or other type of fuses. However, in this study only the first case was considered while the others are recommended for future studies. The recommended optimum location for one floor outrigger along the building height may be selected as: i) the floor level where storey shear reaches half of the base shear and ii) the floor experiencing maximum interstorey drift. It is noted that both scenarios should be considered. Herein, the former scenario leads to a floor level located at 2/3 h_n measured from the ground, where h_n is the building height.

Therefore, the design of OBF system is a two-step process: i) firstly, design the core system made of MD-CBFs; and ii) secondly, design the composed system consisted of a core plus

outriggers. In this thesis, only the MD-CBF designed with $R_d = 3.0$ and $R_0 = 1.3$ was considered for the OBF's core system. However, other types of braced frames as eccentrically braced frames can also be employed for the OBF's core. The same principles as those required in the NBCC and CSA/S16 standard were used to design the MD-CBFs. Concerning the design of outrigger system, the far end columns were proportioned to carry the tributary gravity loads in addition to axial forces triggered from outriggers by applying the capacity design principle. However, it was observed that axial forces in these exterior columns did not increase much.

Applications for high-rise OBF buildings were conducted for a 12-storey and 16-storey office building located in Victoria, BC on Site Class C. Both buildings were subjected to crustal and subduction ground motion sets typical for the region. The results show a substantial reduction of interstorey drift at the floor where the outriggers are located, reduction of interstorey drift at all floors above the location of outriggers, the interstorey drift at any floor is lower that the code limit of 2.5% h_s, while the residual interstorey drift is lower than 0.5% h_s recommended for reparable buildings in the aftermath of an earthquake event.

It is concluded that high-rise OBF buildings show better seismic performance than traditional concentrically braced frame buildings when subjected to crustal and subduction records.

Chapter 5. Performance evaluation

5.1. Methodology for performance evaluation

To evaluate the performance of low-rise, middle-rise and high-rise MD-CBF buildings and that of high-rise OBF buildings subjected to crustal and subduction ground motion sets the assessment of collapse safety is conducted according to FEMA P695 procedure. In this study, the low-rise buildings are the 2-storey and 4-storey MD-CBFs, the middle-rise is the 8-storey MD-CBF and the high-rise are the 12-storey and 16-storey MD-CBF buildings, as well as the 12-storey and 16-storey OBF buildings. It is noted that NBCC limits the height of MD-CBF buildings in high risk seismic zones to 60 m. To overcome this height limit, it was proposed to add outrigger trusses to MD-CBFs forming the OBF system.

For assessing the collapse safety, the FEMA P695 procedure presented in Chapter 2 is applied. According to this procedure, the building passes the acceptance criteria if ACMR $\geq$ $ACMR_{10\%}$; where, ACMR is the adjusted collapse margin ratio and $ACMR_{10\%}$ is the the minimum permissible ACMR value corresponding to the 10% probability of collapse under a set of scaled ground motions. This procedure incorporates factors accounting for aleatoric and epistemic uncertainties. If the structure did not meet the performance acceptance criteria, the computed collapse margin ratio should increase which means that the strength of members of the earthquake resisting system should also increase.

The first step in the assessment of collapse safety is to employ incremental dynamic analysis and to compute the IDA curve from yielding to failure for each studied building under each individual ground motion of the crustal and subduction set. Each point of the IDA curve is mapped by knowing the coordinate of the Intensity Measure (IM) and the associated Damage Measure (DM). Herein, IM is the 5% damped spectral acceleration corresponding to the first-mode period $S_a(T_1;5\%)$ and DM is the associated peak interstorey drift among floors $\delta_{max}(\%h_s)$.

The second step is to calculate the collapse margin ratio (CMR) for each building and each ground motion set. The CMR = $S_a(\overline{T_1})/S_a(T_1)$, where S_a (T_1) is the 2%/50 years design spectral acceleration ordinate at the first-mode period of building structure (T_1) ,and $S_a(\overline{T_1})$ is defined as

the value at which 50% of ground motions produced building collapse. In the numerical model, the collapse is capture when the first brace reached failure and the model experiences numerical instability. This limit state is labeled *collapse prevention*.

The third step is to calculate the adjusted collapse margin ratio (ACMR) computed from the following equation: $ACMR = CMR\ x\ SSF$, where SSF is the spectral shape factor calculated from Table 7-1 of FEMA P695. The SSF factor incorporates the effect of frequency content of ground motion set and it depends on the first-mode period of the studied structure (T_1), and the period-based ductility factor $\mu_t = \delta_u / \delta_{y,eff}$. To define the period based ductility μ_t, a non-linear static pushover analysis should be performed. The pushover curve computed for the 2-storey MD-CBF building is shown in Fig. 5-1, whereas δ_u is the ultimate displacement and $\delta_{y,eff}$ is the elastic displacement that corresponds to the maximum base shear V_{max}. Knowing μ_t and T_1 the SSF factor is selected from the Table (7-1) of FEMA P695.

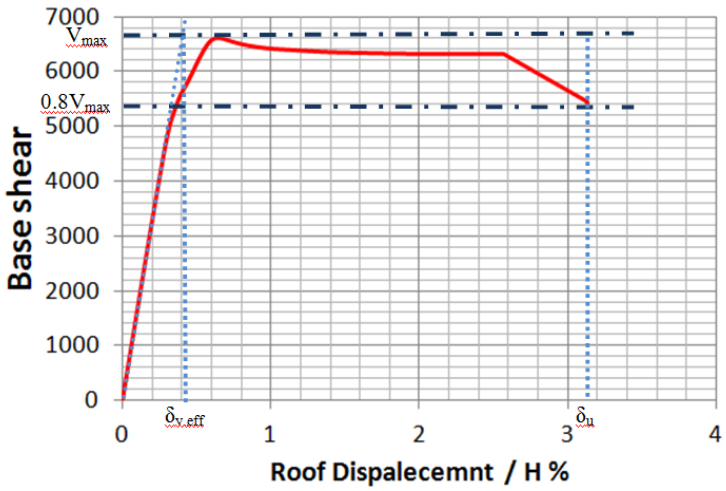

Figure 5-1 Nonlinear static curve computed for 2-storey MD-CBF building

The fourth step is to define the total system collapse uncertainty, β_{TOT}, considered for the assessment of collapse safety. Two sources of uncertainties were considered in this study, the aleatoric uncertainty and epistemic uncertainty (Ellingwood et al., 2007). Aleatoric uncertainty measures the randomness in the seismic capacity of the structure, while epistemic uncertainty depends on the quality of the analysis. The value of aleatoric uncertainty (β_R) was taken from Equation (2-9**)** which is equal to the square root of the sum of the squares of β_{RR} and β_{RU}, where

β_{RR} is the aleatoric component of uncertainty given in Equation (2-10) and β_{RU} is the epistemic uncertainty taken equal to 0.20 as recommended by Ellingwood et al. (2007). The β_{RR} is dependent on $\beta_{D|Sa}$ and β_C, the β_C is considered as 0.25, while the $\beta_{D|Sa}$ is calculated from Equation (2-11) through nonlinear regression analysis, which could be transformed to simple linear regression analysis as shown in Equation (2-13).

The fifth step is to calculate the $ACMR_{10\%}$ using Table 7-3 of FEMA P695. It is noted that Table 7-3 provides acceptable values of $ACMR_{10\%}$ based on total system collapse uncertainty, β_{TOT}. The acceptance criteria occurs if $ACMR \geq ACMR_{10\%}$.

The six step is to compute fragility curves corresponding to different limit states such that: immediate occupancy (I.O.) defined when the first brace in the system reached buckling, the code design limit state (CD) and the collapse prevention limit state (CP) defined when the first brace reached failure. Thus, fragility analysis is used to determine the probabilistic safety margins against a specific identified event at a defined limit state (Wen et al., 2004). Fragility functions are derived from parameters estimated using IDA curves.

5.2. Assessment of collapse safety of low-rise MD-CBF buildings

The low-rise buildings studied here are the 2-storey and 4-storey MD-CBF buildings located in Victoria B.C. on site Class C.

5.2.1. Assessment of collapse safety of 2-storey MD-CBF building

The incremental dynamic analysis curves (IDA) are constructed for two sets of crustal and subduction ground motions. Each set consists of seven ground motions. The IDA curves associated to both ground motion sets are illustrated in Fig. 5-2. In the figure, the IDA curve obtained for a ground motion is plotted with a grey line and the 50th percentile of all seven IDA curves is plotted with black line. Each IDA curve is composed of softening and hardening segments. As shown, the 50th percentile IDA curve of subduction records consists of more softening segments than that obtained under the crustal record set. Softening segments indicate that the damage is accumulated at higher rates.

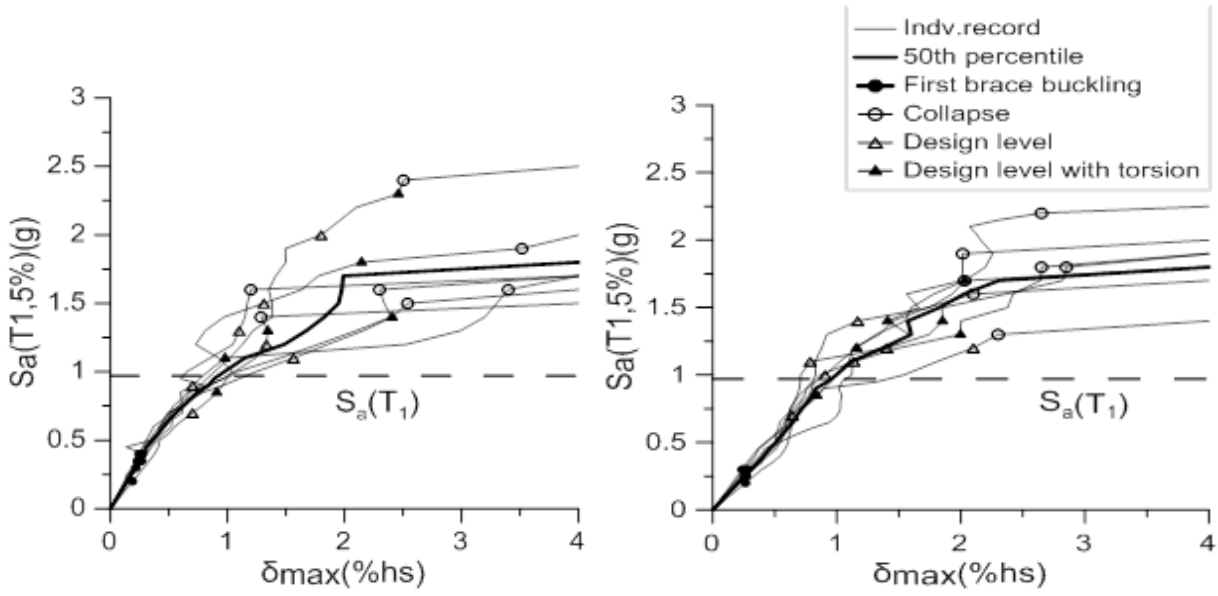

a) b)

Figure 5-2 IDA curves of 2-storey MD-CBF building subjected to: a) crustal ground motions, b) subduction ground motions

In Fig. 5-2, the black filled circle indicates the first buckling of a brace member, the triangle indicates the spectral acceleration ordinate at T_1 of each ground motion scaled to match the design spectrum, and the white (unfilled) circle indicates the failure of a brace member which leads to dynamic instability and convergence problem. The difference between the white and black triangles is explained below.

It is noted that the model in OpenSees is 2-D but is generated using six degree of freedom to allow braces to behave in a three dimensional system including the out-of-plan buckling. Thus, the model cannot capture the effect of torsion caused by accidental eccentricity, but it accounts for the P-Δ effect. In the preliminary design, shear caused by torsion and P-Δ was considered. To match the simulation with design, the increase in shear demand caused by accidental eccentricity was artificially accounted for by amplifying the seismic demand expressed by $S_a(T_1)$ ordinate with the ratio between the shear including shear caused by torsion due to accidental eccentricity and the shear from seismic loading. Here, the amplification of forces due to accidental torsion is calculated as 1.18. The first-mode period of the 2-storey building resulted from the OpenSees model is T_1 = 0.38 s which implies $S_a(T_1)$ = 0.97g. When torsion caused by accidental eccentricity is considered the corresponded $S_a(T_1)$ is amplified with the same 1.18 factor. Hence,

the selected seven crustal ground motions are amplified in order to match the design spectrum between $0.2T_1$ to $1.5T_1$ which means from 0.076 s to 0.57 s. It is noted that all records were scaled more above the design spectrum in the interval 0.18 s to 0.76 s in order to match the design spectrum at shorter periods than 0.18 s. Moreover, it was verified that the mean of the response spectra of seven crustal ground motions matches the amplified design spectrum with the correction factor (1.18) in the interval 0.18 s to 0.57 s. In Fig. 5-2, the increment in shear demand caused by accidental torsion is illustrated with the black filled triangle. The collected data from the IDA curves are summarized in Table 5-1 for the crustal record set and in Table 5-2 for the subduction record set. As given, the pair of interstorey drift and $S_a(T_1)g$ associated to the code design level and amplified code design level to account for the accidental torsion effect are provided for comparison purpose.

Table 5-1 Centralized data from IDA curves of the 2-storey MD-CBF building subjected to crustal record set

Record	First brace buckling		Design level		Amplified design level		Collapse prevention	
	$S_a(T_1)g$	$\delta_{max}(\%h_s)$	$S_a(T_1)g$	$\delta_{max}(\%h_s)$	$S_a(T_1)g$	$\delta_{max}(\%h_s)$	$S_a(T_1)g$	$\delta_{max}(\%h_s)$
C1	0.35	0.244	1.55	1.311	1.83	2.146	1.90	3.517
C2	0.35	0.269	0.92	0.762	1.07	0.980	1.60	3.400
C3	0.35	0.231	1.70	1.410	2.00	1.800	2.40	2.504
C4	0.30	0.221	1.26	1.332	1.42	1.345	1.40	1.286
C5	0.40	0.242	1.00	0.650	1.33	1.170	1.60	1.200
C6	0.20	0.191	0.73	0.780	0.85	0.909	1.60	2.300
C7	0.40	0.274	1.18	1.565	1.39	2.408	1.50	2.540
Median	0.35	0.244	1.18	1.311	1.39	1.345	1.60	2.540

Table 5-2 Centralized data from IDA curves of the 2-storey MD-CBF building subjected to subduction record set

Record	First brace buckling		Design level		Amplified design level		Collapse prevention	
	$S_a(T_1)g$	$\delta_{max}(\%h_s)$	$S_a(T_1)g$	$\delta_{max}(\%h_s)$	$S_a(T_1)g$	$\delta_{max}(\%h_s)$	$S_a(T_1)g$	$\delta_{max}(\%h_s)$
S1	0.30	0.236	1.00	0.905	1.20	1.160	1.70	2.030
S2	0.30	0.277	1.20	2.100	1.3	2.300	1.30	2.300
S3	0.25	0.269	0.70	0.641	0.85	0.836	1.60	2.100
S4	0.25	0.260	1.10	1.127	1.40	1.851	1.80	2.850
S5	0.30	0.256	1.10	1.137	1.30	1.996	1.80	2.650
S6	0.20	0.264	1.40	1.168	1.70	2.031	2.20	2.650
S7	0.25	0.260	1.10	0.784	1.40	1.410	1.90	2.015
Median	0.25	0.260	1.10	1.127	1.30	1.851	1.80	2.300

From Tables 5-1 and 5-2 it is observed that the interstorey drift associated to the first brace buckling is almost the same for the two sets of records. At the collapse prevention limit state the 2-storey MD-CBF building fails at almost similar median seismic demand $S_a(T_1)$ while experiencing similar median interstorey drift under both crustal and subduction ground motion sets showing 2.54%h_s and 2.30%h_s, respectively. In case of subduction records, the maximum inter-storey drift of 2.1%h_s resulted for the design level $S_a(T_1)$ = 1.2g under S2 record and the C.P. limit state corresponded to $S_a(T_1)$ = 1.3g. For the collapse prevention points under crustal records, the maximum displacement was under crustal record C1 with value equal to 3.517%h_s and $S_a(T_1)$ = 1.9g. In the case of subduction records, the maximum interstorey drift of 2.85%h_s corresponding to $S_a(T_1)$ = 1.8g was recorded for S4 ground motion. Table 5-3 shows the calculation of total system uncertainty for the 2-storey MD-CBF building under crustal and subduction records.

Table 5-3 Total system uncertainty calculation for 2-storey MD-CBF building

Building	2 -story MD-CBF	
Ground motions	Crustal ground motions	Subduction ground motions
Seismic demand	$\delta_{max} = 1.01S_a^{1.27}$	$\delta_{max} = 1.13S_a^{1.11}$
Aleatoric uncertainty	$\beta_{RR} = 0.39$	$\beta_{RR} = 0.37$
Record to record uncertainty	$\beta_{D\|Sa} = 0.297$	$\beta_{D\|Sa} = 0.244$
Total system uncertainty	$\beta_{TOT} = 0.44$	$\beta_{TOT} = 0.40$

Fragility curves for the 2-storey MD-CBF building under crustal and subduction records are shown in Figure 5-3. For example, the fragility function computed at C.P. follows a lognormal distribution and has a median value of the collapse ground motion intensity $S_a(T_1)$ and a lognormal standard deviation β_{TOT} given in Table 5-3. Similarly, fragility curves corresponding to immediate occupancy, I.O. and code design, C.D. are presented.

The verification for collapse safety criteria is presented for the 2-storey MD-CBF building subjected to both crustal and subduction record sets in Table 5-4.

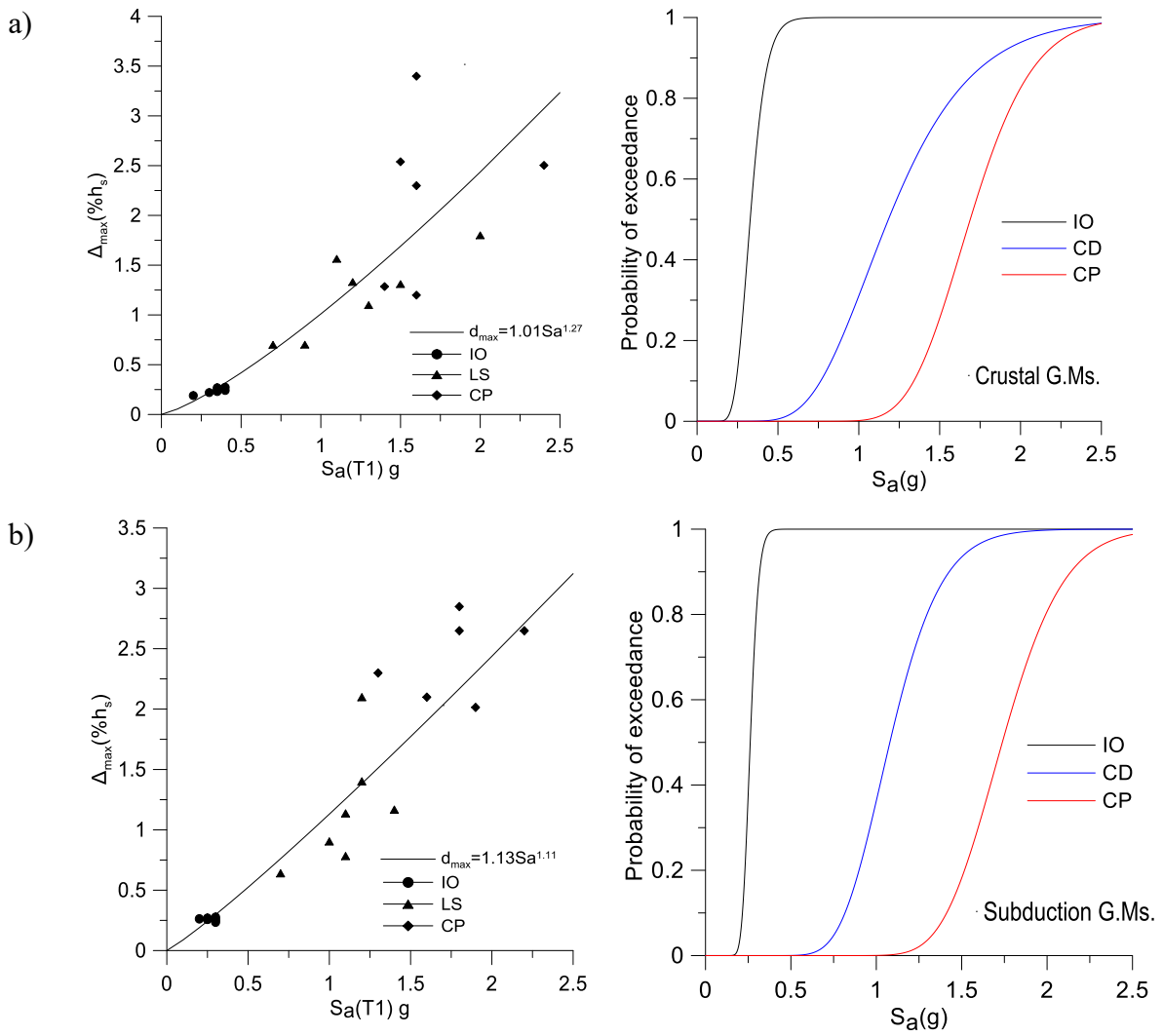

Figure 5-3 Regression analysis and fragility curves for 2-storey MD-CBF building subjected to: a) crustal ground motions, b) subduction ground motions

The collapse assessment for the 2-storey MD-CBF building shows that the building is safe under crustal and subduction records since the ACMR > $ACMR_{10\%}$. It is also noted that CMR is similar under the both ground motion sets. However, when the demand was increase to account for the effect of accidental torsion the building also passes the collapse safety criteria when subjected to both ground motion sets. It is noted that the second-mode period is $T_2 = 0.16$ s.

Table 5-4 Verification of collapse safety criteria for the 2-storey MD-CBF building (T1 = 0.38s)

2-Storey MD-CBF-Building (T_1=0.38 s)		
Parameters	Crustal Records	Subduction records
$S_a(T_1)$	0.97g	0.97
$S_a(T_1)$ [torsion consideration]	1.17g	1.17
$S_a(\overline{T_1})$	1.60g	1.80
CMR= $S_a(\overline{T_1})/S_a(T_1)$	1.65	1.85
CMR [torsion consideration]	1.37	1.53
β_{TOT}	0.44	0.40
ACMR	2.11	2.30
ACMR [torsion consideration]	1.75	1.92
$ACMR_{10\%}$	1.73	1.67
Pass/Fail	**Pass**	**Pass**
Pass/Fail [torsion consideration]	**Pass**	**Pass**

5.2.2. Assessment of collapse safety of 4-storey MD-CBF building

The IDA curves for the 4-storey MD-CBF subjected to both sets of ground motions are presented in Fig. 5-4.

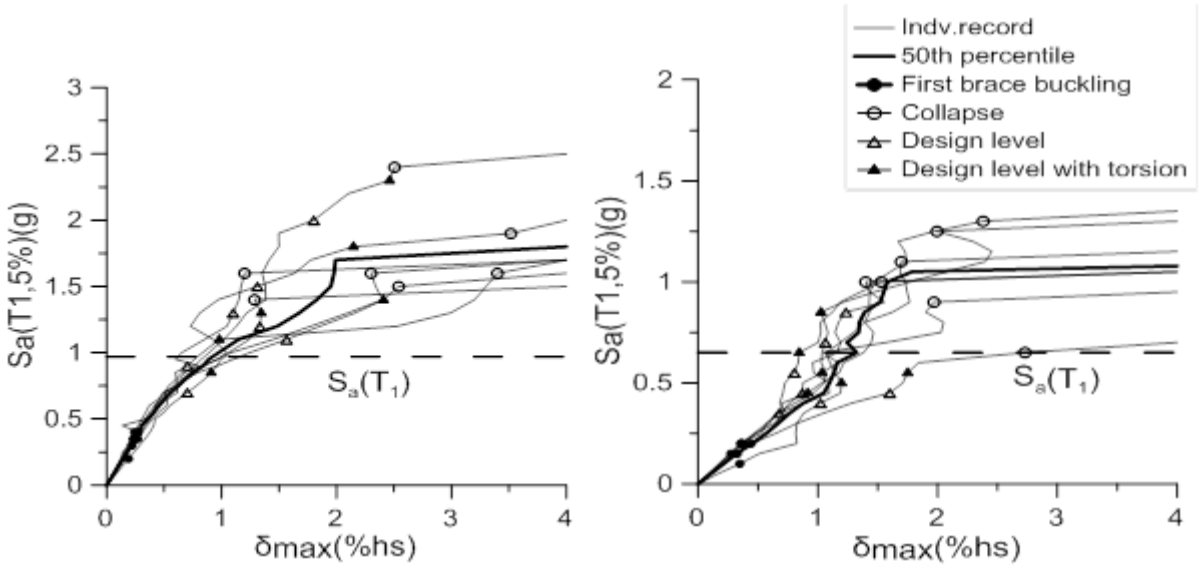

a) b)

Figure 5-4 IDA curves of 4-storey MD-CBF building subjected to: a) crustal ground motions, b) subduction ground motions

The same symbols used to emphasize the seismic response of the 2-storey MD-CBF building are maintained. It is noted that the first-mode period of the 4-storey MD-CBF building is 0.69 s and

the interval of interest is from 0.14 s to 1.04 s. The ordinate of design spectrum corresponding to T_1 = 0.69 s is $S_a(T_1)$ = 0.64 g. The median of response spectrum of scaled ground motions is almost overlapping the design spectrum. Again, to take into account the shear caused by accidental torsion effect the ratio used to amply the demand is 1.18. The centralized response of building summarized from the IDA curves resulted under the crustal ground motions set and subduction ground motions set is given in Table 5-5 and Table 5-6, respectively.

Table 5-5 Centralized data from IDA curves of the 4-storey MD-CBF building subjected to crustal record set

Record	First brace buckling		Design level		Amplified design level		Collapse prevention	
	$S_a(T_1)g$	$\delta_{max}(\%h_s)$	$S_a(T_1)g$	$\delta_{max}(\%h_s)$	$S_a(T_1)g$	$\delta_{max}(\%h_s)$	$S_a(T_1)g$	$\delta_{max}(\%h_s)$
C 1	0.20	0.316	0.65	1.149	0.80	1.456	1.05	2.500
C 2	0.20	0.322	1.00	1.060	1.20	1.250	1.50	2.300
C 3	0.15	0.358	0.55	0.806	0.70	0.910	1.05	2.700
C 4	0.20	0.378	0.55	1.100	0.70	1.545	1.35	2.400
C 5	0.20	0.316	0.85	1.006	1.00	1.252	1.25	2.700
C 6	0.20	0.303	0.50	1.090	0.60	2.050	0.70	2.400
C 7	0.25	0.343	0.75	0.920	0.90	0.950	1.20	1.650
Median	0.20	0.322	0.65	1.060	0.80	1.252	1.20	2.400

Table 5-6 Centralized data from IDA curves of the 4-storey MD-CBF building subjected to sbduction record set

Record	First brace buckling		Design level		Amplified design level		Collapse prevention	
	$S_a(T_1)g$	$\delta_{max}(\%h_s)$	$S_a(T_1)g$	$\delta_{max}(\%h_s)$	$S_a(T_1)g$	$\delta_{max}(\%h_s)$	$S_a(T_1)g$	$\delta_{max}(\%h_s)$
S1	0.20	0.443	0.40	1.022	0.50	1.197	1.30	2.380
S2	0.20	0.362	0.85	1.234	1.00	1.400	1.00	1.400
S3	0.20	0.358	0.55	0.803	0.65	0.845	1.00	1.531
S4	0.10	0.349	0.45	1.600	0.55	1.750	0.65	2.730
S5	0.15	0.276	0.35	0.678	0.45	0.916	1.10	1.697
S6	0.20	0.374	0.70	1.063	0.85	1.026	1.25	1.995
S7	0.15	0.328	0.45	0.871	0.55	1.034	0.90	1.970
Median	0.20	0.362	0.45	1.022	0.55	1.034	1.00	1.970

From Tables 5-5 and 5-6 it is observed that the median interstorey drift at the first brace buckling is the same for the two sets of records. At the collapse prevention limit state, the 4-storey building fails at lower median seismic demand under the subduction ground motion set than the crustal ground motion set (e.g. $S_a(T_1)$ = 1.20g for crustal records and $S_a(T_1)$ = 1.00 g for subduction ground motions). Furthermore, at the design level, the maximum inter-storey drift of

1.149 $\%h_s$ occurred under the crustal record C1 and corresponds to $S_a(T_1)$ equal to 0.65g. When the amplification required to simulate the accidental torsion effect is considered, the maximum interstorey drift of $2.05h_s$ is obtained under under the C6 record. From the scaled response spectrum of subduction records using a scaling factor of 1.0, it is found that the value of the mean response spectrum at the first mode period is slightly lower, which is 0.45g instead of 0.64 g. It means that the demand is slightly lower than the design spectrum leading to slightly larger interstorey drift values than those shown in Table 5-5. When the correction factor accounting for the effect of accidental torsion was considered, the median value of $S_a(T_1)$ = 0.55 g is close to design spectrum. However, the demand in interstorey drift increase by only 1.2% when the median of response spectrum at the first mode period increase from $S_a(T_1)$ = 0.45g to 0.55g.

Among the interstorey drift values obtained under crustal ground motions that correspond to collapse preventions, the maximum interstorey drift of $2.7\%h_s$ is associated to $S_a(T_1)$ = 1.25g and was obtained under the C5 record. In the case of subduction records, the maximum interstorey drift recorded under S4 ground motion is similar, but it occurred at half value of acceleration response spectrum (S_a (T_1) =0.65g). Therefore, under both sets of ground motions the median interstorey drift at the collapse prevention limit state is below $2.5\%h_s$. Table 5-7 shows the calculation of total system uncertainty, β_{TOT} for the 4-storey MD-CBF building under crustal and subduction records.

Table 5-7 Total system uncertainty calculation for 4-storey MD-CBF building

Building	4-story MD-CBF	
Ground motions	Crustal ground motions	Subduction ground motions
Aleatoric uncertainty	β_{RR}=0.38	β_{RR} =0.39
Record to record uncertainty	$\beta_{D\|Sa}$ = 0.286	$\beta_{D\|Sa}$=0.295
Seismic demand	$\delta_{max}=1.7S_a^{0.98}$	$\delta_{max}=1.77S_a^{0.85}$
Total system uncertainty	β_{TOT}=0.44	β_{TOT}=0.43

Fragility curves for the 4-storey MD-CBF building under crustal and subduction records are shown in Figure 5-5.

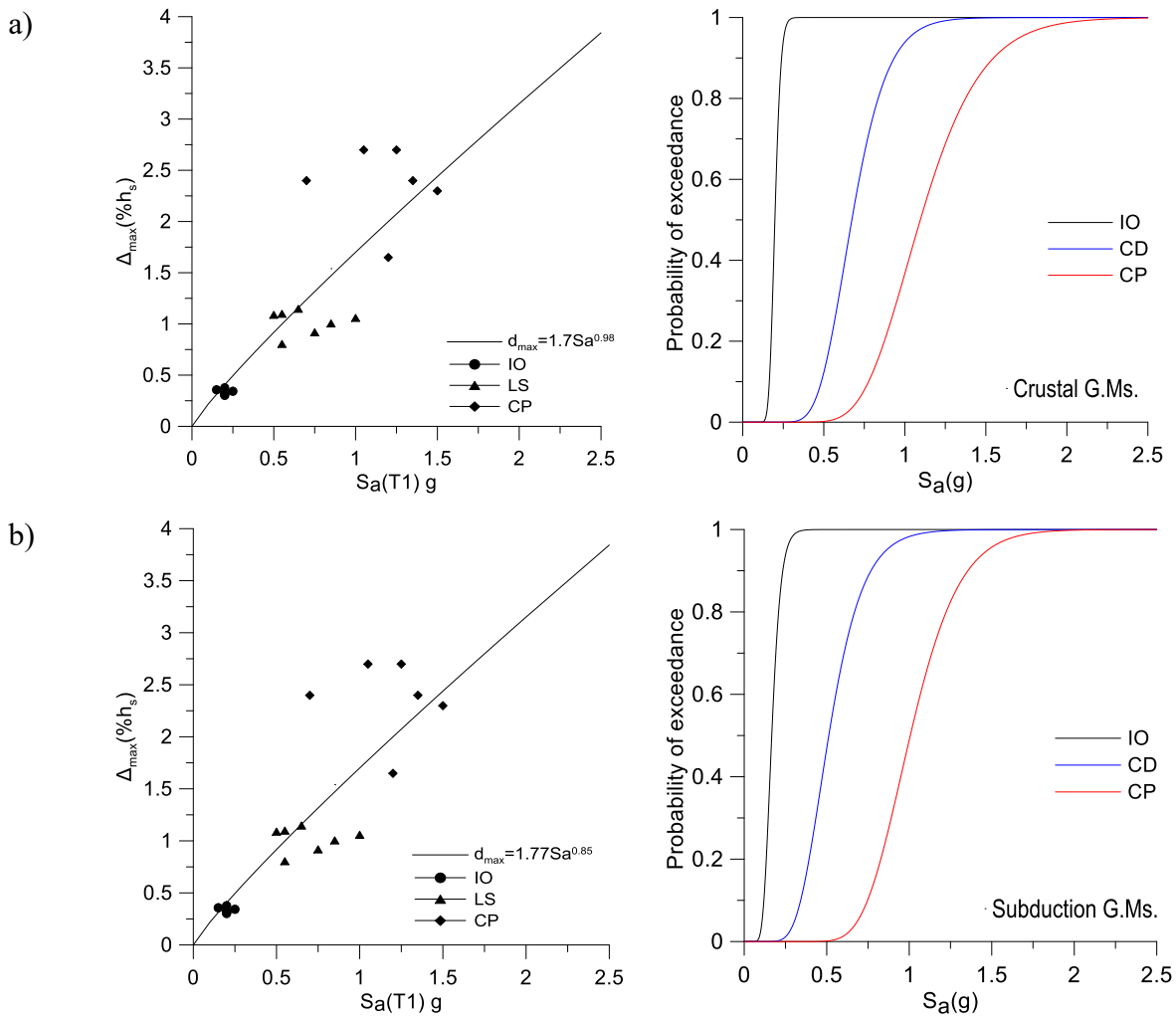

Figure 5-5 Regression analysis and fragility curves for 4-storey MD-CBF building subjected to: a) crustal ground motions, b) subduction ground motions

The verification for collapse safety criteria is presented for the 4-storey MD-CBF building subjected to both crustal and subduction record sets in Table 5-8. The collapse margin ratio computed for the 4-storey MD-CBF building is also presented in Table 5-8.

Table 5-8 Verification of collapse safety criteria for the 4-storey MD-CBF building (T_1 = 0.76 s)

4-Storey MD-CBF Building (T_1= 0.76 s)		
Parameters	Crustal records	Subduction records
$S_a(T_1)$	0.64	0.64
$S_a(T_1)$ [torsion consideration]	0.77	0.77
$S_a(\overline{T_1})$	1.20	1.00
CMR= $S_a(\overline{T_1})$/ $S_a(T_1)$	1.87	1.56
CMR [torsion consideration]	1.56	1.30
β_{TOT}	0.44	0.43
ACMR	2.35	1.96
ACMR [torsion consideration]	1.97	1.64
$ACMR_{10\%}$	1.73	1.72
Pass/Fail	**Pass**	**Pass**
Pass/Fail [torsion consideration]	**Pass**	**Fail**

From Table 5-8 it is observed that the collapse safety verification ACMR>$ACMR_{10\%}$ occurs for both ground motion sets when the accidental torsion effect was not accounted for. When the demand was increased to account for the accidental torsion effect, the CMR was substantially reduced resulting in the failure of the collapse safety criteria under subduction ground motions. In general, the CMR value is lower under subduction records than crustal records which means that damage accumulates at higher rates under subduction records.

5.3. Assessment of collapse safety for the middle-rise MD-CBF building

The middle-rise building under investigation is the 8-storey MD-CBF building located in Victoria B.C. on site Class C.

5.3.1. Assessment of collapse safety of 8-storey MD-CBF building

The IDA curves of the 8-storey MD-CBF building resulted under both ground motions sets are illustrated in Fig. 5-6. The same symbols used above in the IDA curves were retained.

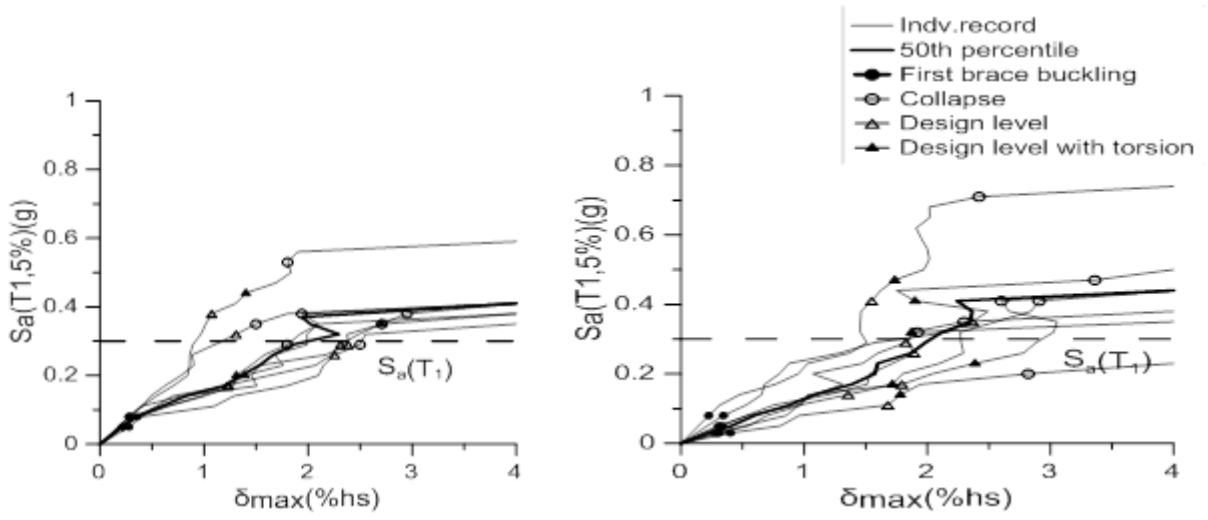

Figure 5-6 IDA curves for the 8-storey MD-CBF building subjected to: a) crustal ground motions, b) subduction ground motions

The data collected from the IDA curves is presented in Table 5-9 and is associated to crustal ground motions. Data presented in Table 5-10 is associated to subduction records. It is noted that the first-mode period of the 8-storey MD-CBF building resulted from OpenSees is 1.4 s and the acceleration design spectrum ordinate for T_1 = 1.4 s is 0.29 g. When the effect of accidental eccentricity is considered and the demand is amplified by 1.18 the value of $S_a(T_1)$ becomes 0.34g.

Table 5-9 Centralized data from IDA curves of the 8-storey MD-CBF building subjected to crustal record set

Record	First brace buckling		Design level		Amplified design level		Collapse prevention	
	$S_a(T_1)$g	$\delta_{max}(\%h_s)$	$S_a(T_1)$g	$\delta_{max}(\%h_s)$	$S_a(T_1)$g	$\delta_{max}(\%h_s)$	$S_a(T_1)$g	$\delta_{max}(\%h_s)$
C 1	0.08	0.293	0.34	1.308	0.40	1.460	0.44	1.520
C 2	0.05	0.221	0.20	1.310	0.23	1.440	0.38	1.800
C 3	0.05	0.214	0.21	1.389	0.25	1.530	0.44	1.940
C 4	0.05	0.280	0.26	2.255	0.30	2.370	0.35	2.500
C 5	0.08	0.359	0.30	2.310	0.36	2.703	0.44	2.950
C 6	0.08	0.279	0.38	1.074	0.44	1.402	0.59	1.803
C 7	0.08	0.277	0.30	2.373	0.34	2.380	0.38	2.710
Median	0.08	0.279	0.30	1.389	0.34	1.530	0.42	1.940

Table 5-10 Centralized data from IDA curves of the 8-storey MD-CBF building subjected to subduction record set

Record	First brace buckling		Design level		Amplified design level		Collapse prevention	
	$S_a(T_1)g$	$\delta_{max}(\%h_s)$	$S_a(T_1)g$	$\delta_{max}(\%h_s)$	$S_a(T_1)g$	$\delta_{max}(\%h_s)$	$S_a(T_1)g$	$\delta_{max}(\%h_s)$
S1	0.03	0.283	0.14	1.357	0.17	1.717	0.41	2.908
S2	0.05	0.304	0.29	1.826	0.32	1.920	0.32	1.920
S3	0.08	0.344	0.35	2.366	0.41	1.900	0.47	3.360
S4	0.03	0.400	0.11	1.679	0.14	1.781	0.20	2.820
S5	0.08	0.225	0.41	1.547	0.47	1.736	0.71	2.420
S6	0.03	0.311	0.17	1.793	0.23	2.387	0.41	2.602
S7	0.05	0.332	0.26	1.892	0.32	1.871	0.35	2.300
Median	0.05	0.311	0.26	1.793	0.32	1.871	0.41	2.602

From Tables 5-9 and 5-10 it is observed a small increase of median interstorey drift recorded at the amplified design level versus the design level. However, at design level the $S_a(T_1)$ is slightly lower under the subduction records than under the crustal records (e.g. 0.26g versus 0.30g). This occurred because the scaling factor used for the mega-thrust magnitude 9 Tohoku records were considered equal to 1.0. In terms the interstorey drift value at design levels, the values are within the code limit of $2.5\%h_s$.

For the collapse prevention limit state under crustal records, the maximum interstorey drift of $2.95\%h_s$ occurred under crustal record C5 for $S_a(T_1) = 0.41g$. In the case of subduction records the maximum interstorey drift of $3.36\%h_s$ corresponding to $S_a(T_1) = 0.47g$ was recorded for S3 record.

Table 5-11 shows the calculation of total system uncertainty, β_{TOT}, for the 8-storey MD-CBF building under crustal and subduction records.

Table 5-11 Total system uncertainty calculation for 8-storey MD-CBF building

Building	8-story MD-CBF	
Ground motions	Crustal ground motions	Subduction ground motions
Aleatoric uncertainty	$\beta_{RR} = 0.44$	$\beta_{RR} = 0.5$
Record to record uncertainty	$\beta_{D\|Sa} = 0.360$	$\beta_{D\|Sa} = 0.435$
Seismic demand	$\delta_{max} = 6.67S_a^{1.13}$	$\delta_{max} = 5.35S_a^{0.84}$
Total system uncertainty	$\beta_{TOT} = 0.47$	$\beta_{TOT} = 0.50$

Fragility curves for the 8-storey MD-CBF building under crustal and subduction records are shown in Figure 5-7.

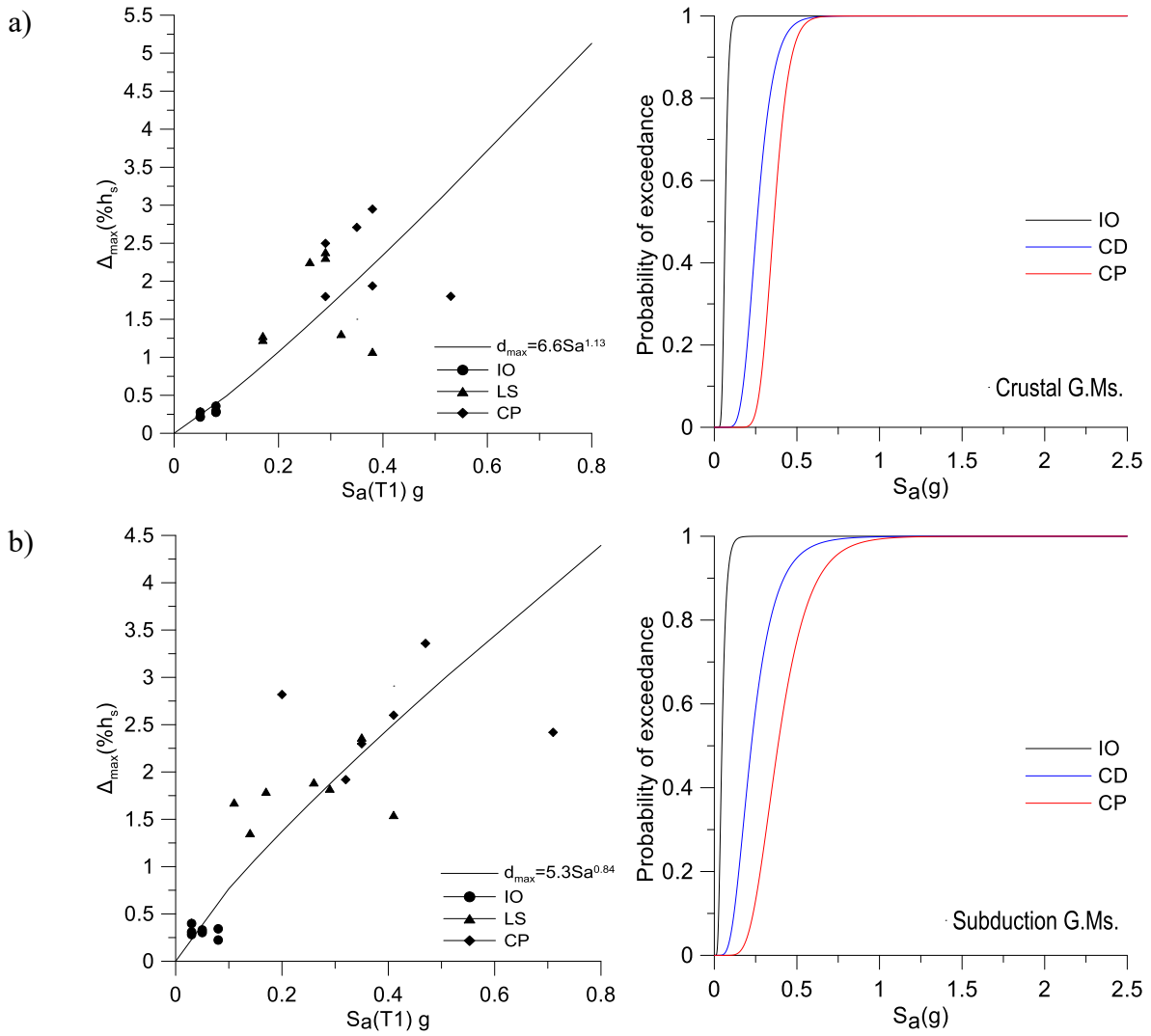

Figure 5-7 Regression analysis and fragility curves for 8-storey MD-CBF building subjected to: a) crustal ground motions, b) subduction ground motions

The verification for collapse safety criteria is presented for the 8-storey MD-CBF building subjected to both crustal and subduction record sets in Table 5-12.

Table 5-12 Verification of collapse safety criteria for the 8-storey MD-CBF building (T_1 =1.4 s)

8-Storey MD-CBF Building (T_1=1.4 s)		
Parameters	Crustal records	Subduction records
$S_a(T_1)$	0.29	0.29
$S_a(T_1)$ [torsion consideration]	0.34	0.34
$S_a(\overline{T_1})$	0.44	0.41
CMR= $S_a(\overline{T_1})$/ Sa(T1)	1.51	1.41
CMR [torsion consideration]	1.30	1.21
β_{TOT}	0.47	0.50
ACMR	2.08	1.95
ACMR [torsion consideration]	1.80	1.67
$ACMR_{10\%}$	1.80	1.90
Pass/Fail	**Pass**	**Pass**
Pass/Fail [torsion consideration]	**Pass**	**Fail**

The collapse assessment conducted for the 8-storey MD-CBF building under both sets of ground motions shows that the building passes the safety criteria under the crustal and subduction records when considering design level, while it fails to pass when the demand was increase to account on the accidental torsion effect. In this latter case, ACMR <$ACMR_{10\%}$.

5.4. Assessment of collapse safety for high-rise MD-CBF buildings

The high-rise buildings under investigation are the 12-storey and 16-storey MD-CBF buildings located in Victoria B.C. on site Class C.

5.4.1. Assessment of collapse safety of 12-storey MD-CBF building

The first-mode period of 12-storey MD-CBF building is 2.27 s and the $S_a(T_1)$ is 0.16g. The IDA curves computed for the 12-storey MD-CBF building subjected to both sets of ground motions are presented in Fig. 5-8. The same symbols used in the previous IDA curves were retained. Centralized data from the IDA curves for the crustal records is provided in Table 5-13 and that for the subduction records is given in Table 5-14.

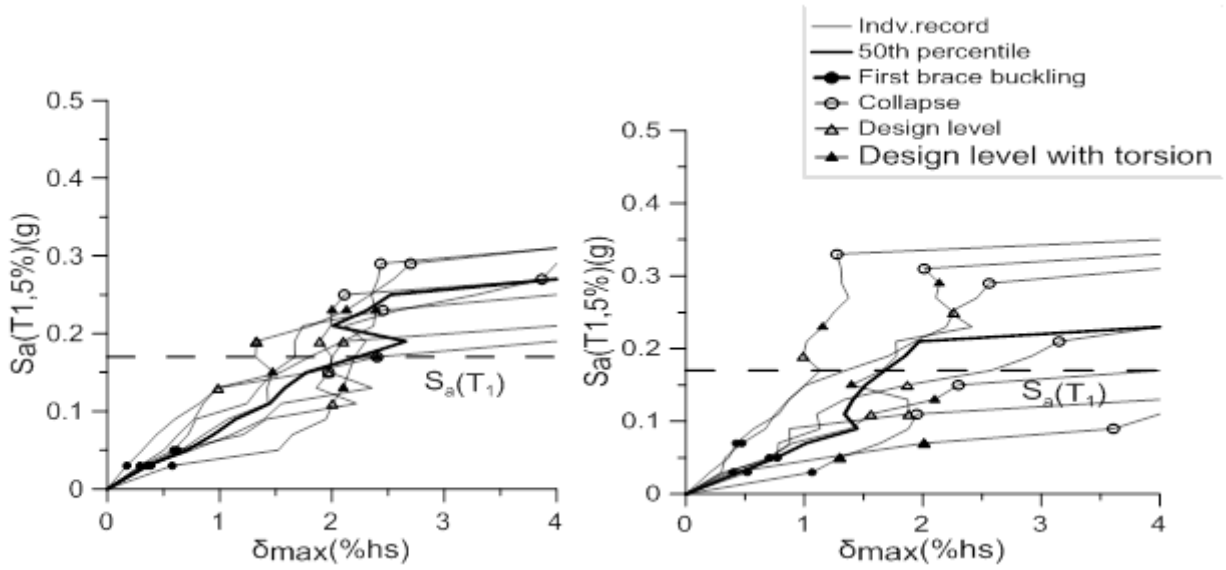

a) b)

Figure 5-8 IDA curves of the 12-storey MD-CBF building subjected to: a) crustal ground motions, b) subduction ground motions

From Tables 5-13 and 5-14 it is observed that median interstorey drift at the design level and amplified design level is very close. It is noted that using scaling factor 1.0 for subduction records, the mean of 7 subduction ground motions is 23% lower than design spectrum associated to the first-mode period (e.g. $S_a(T_1)$ = 0.13 g instead of 0.16 g). However, at the collapse prevention limit state, the median $S_a(T_1)$ is slightly lower in the case of subduction ground motions then in the case of crustal ground motions (e.g. 0.21g versus 0.25g), while the associated median interstorey drift is close to 2.5%h_s.

Table 5-13 Centralized data from IDA curves of the 12-storey MD-CBF building subjected to crustal record set

Record	First brace buckling		Design level		Amplified design level		Collapse prevention	
	$S_a(T_1)$g	$\delta_{max}(\%h_s)$	$S_a(T_1)$g	$\delta_{max}(\%h_s)$	$S_a(T_1)$g	$\delta_{max}(\%h_s)$	$S_a(T_1)$g	$\delta_{max}(\%h_s)$
C 1	0.03	0.355	0.19	1.890	0.23	2.000	0.25	2.110
C 2	0.03	0.387	0.11	1.429	0.15	1.470	0.23	2.453
C 3	0.05	0.589	0.19	1.328	0.23	2.128	0.29	2.700
C 4	0.03	0.577	0.10	2.004	0.13	2.100	0.27	3.869
C 5	0.03	0.292	0.19	2.100	0.23	2.390	0.29	2.434
C 6	0.03	0.173	0.14	0.985	0.15	1.810	0.17	2.402
C 7	0.05	0.625	0.15	1.970	0.19	2.100	0.15	1.970
Median	0.03	0.387	0.15	1.890	0.19	2.100	0.25	2.434

Table 5-14 Centralized data from IDA curves of the 12-storey MD-CBF building subjected to subduction record set

Record	First brace buckling		Design level		Amplified design level		Collapse prevention	
	$S_a(T_1)g$	$\delta_{max}(\%h_s)$	$S_a(T_1)g$	$\delta_{max}(\%h_s)$	$S_a(T_1)g$	$\delta_{max}(\%h_s)$	$S_a(T_1)g$	$\delta_{max}(\%h_s)$
S1	0.03	1.066	0.05	1.300	0.06	1.330	0.11	1.950
S2	0.05	0.771	0.15	1.869	0.21	3.150	0.21	3.150
S3	0.07	0.474	0.25	2.260	0.29	2.139	0.31	2.012
S4	0.03	0.400	0.07	2.010	0.08	2.018	0.09	3.609
S5	0.07	0.426	0.19	0.990	0.23	1.154	0.33	1.276
S6	0.05	0.705	0.11	1.881	0.15	1.397	0.29	2.561
S7	0.03	0.519	0.11	1.562	0.13	2.100	0.15	2.300
Median	0.05	0.519	0.11	1.869	0.15	2.100	0.21	2.300

At collapse prevention limit state, the maximum interstorey drift of 3.869%h_s occurred under the C4 crustal record at $S_a(T_1)$ = 0.27g. In the case of subduction records the maximum interstorey drift of 3.609%h_s corresponding to $S_a(T_1)$ = 0.09g was recorded for S4 ground motion.

Table 5-15 shows the calculation of total system uncertainty for the 12-storey MD-CBf building under crustal and subduction records.

Table 5-15 Total system uncertainty calculation for 12-storey MD-CBF building

Building	12-story MD-CBF	
Ground motions	Crustal ground motions	Subduction ground motions
Aleatoric uncertainty	β_{RR}= 0.39	$\beta_{RR} = 0.47$
Record to record uncertainty	$\beta_{D\|Sa} = 0.304$	$\beta_{D\|Sa}$=0.4
Seismic demand	$\delta_{max} = 9.86S_a^{0.94}$	$\delta_{max} = 4.63S_a^{0.55}$
Total system uncertainty	β_{TOT} = 0.44	β_{TOT} = 0.50

Fragility curves for the 12-storey MD-CBF building under crustal and subduction records are shown in Figure 5-9.

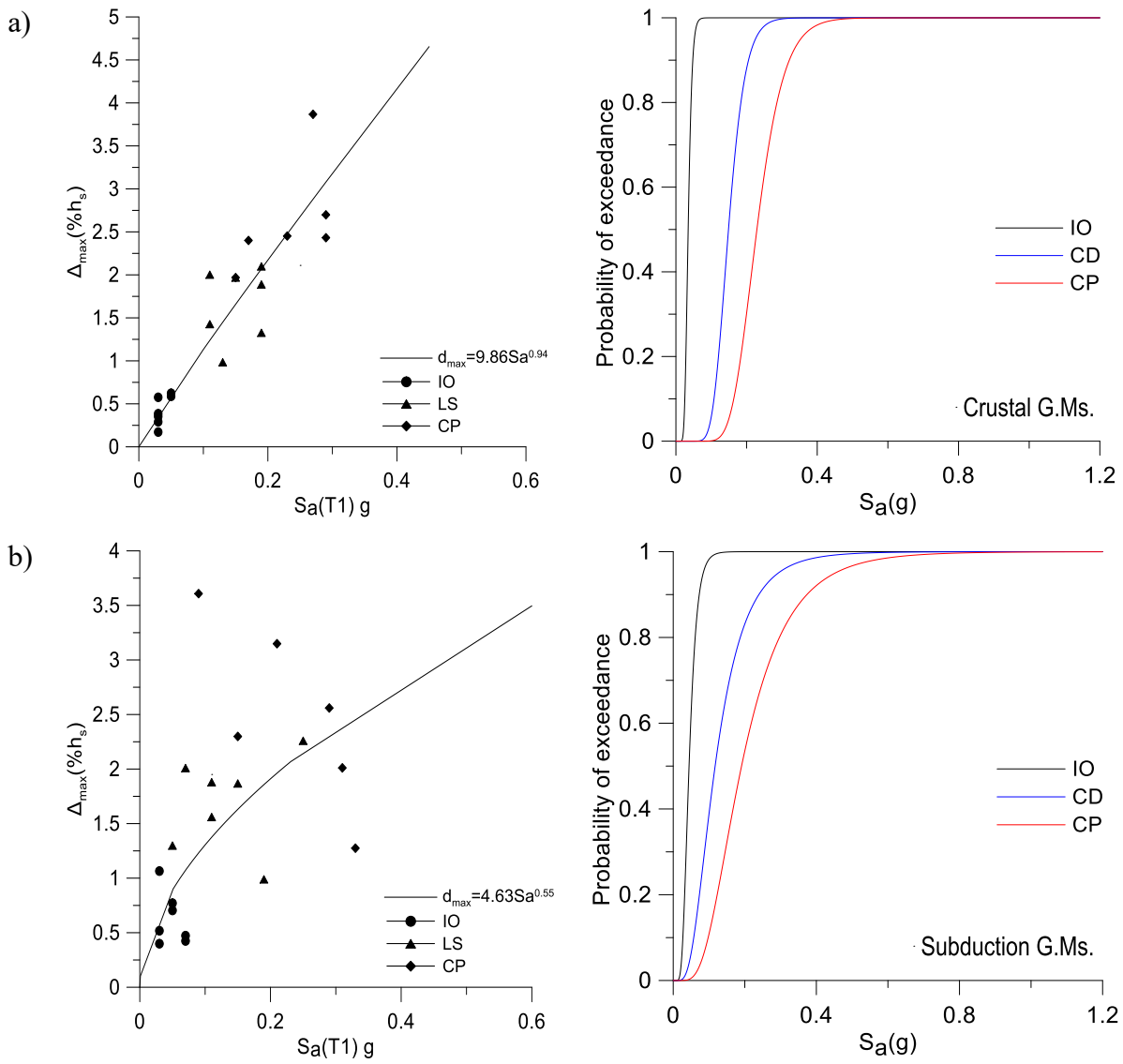

Figure 5-9 Regression analysis and fragility curves for 12-storey MD-CBF building subjected to: a) crustal ground motions, b) subduction ground motions

The verification for collapse safety criteria is presented for the 12-storey MD-CBF building subjected to both crustal and subduction record sets in Table 5-16.

Table 5-16 Verification of collapse safety criteria for 12-storey MD-CBF building (T_1 = 2.27s)

12-Storey MD-CBF Building(T_1 = 2.27 s)		
Parameters	Crustal records	Subduction records
$S_a(T_1)$	0.16	0.16
$S_a(T_1)$ [torsion consideration]	0.19	0.19
$S_a(\overline{T_1})$	0.25	0.21
CMR= $S_a(\overline{T_1})$/ Sa(T1)	1.56	1.31
CMR [torsion consideration]	1.32	1.11
β_{TOT}	0.44	0.50
ACMR	2.18	1.83
ACMR [torsion consideration]	1.85	1.56
$ACMR_{10\%}$	1.78	1.90
Pass/Fail	**Pass**	**Fail**
Pass/Fail [torsion consideration]	**Pass**	**Fail**

Table 5-16 shows greater CMR value resulted under the crustal records set than under the subduction records set. Although the 12-storey MD-CBF building passes the collapse safety criteria when subjected to the crustal records set and the results are reported to the design spectrum ordinate associated to the first mode period of 2.27 s, it does not pass the collapse safety criteria when subjected to subduction ground motions set. In the latter case $ACMR<ACMR_{10\%}$. Thus, in order to pass the collapse safety criteria when subjected to subduction ground motions the strength of 12-storey MD-CBF building should increase.

5.4.2. Assessment of collapse safety of 16-storey MD-CBF building

The IDA curves computed for the 16-storey MD-CBF building subjected to both sets of ground motions are presented in Fig. 5-10. The same symbols used in the previous IDA curves were retained. The first-mode period of 16-storey MD-CBF building is 3.01 s and the $S_a(T_1)$ is 0.135g. Centralized data from the IDA curves resulted under the signature of crustal records set is provided in Table 5-17 and that under the subduction records is Table 5-18.

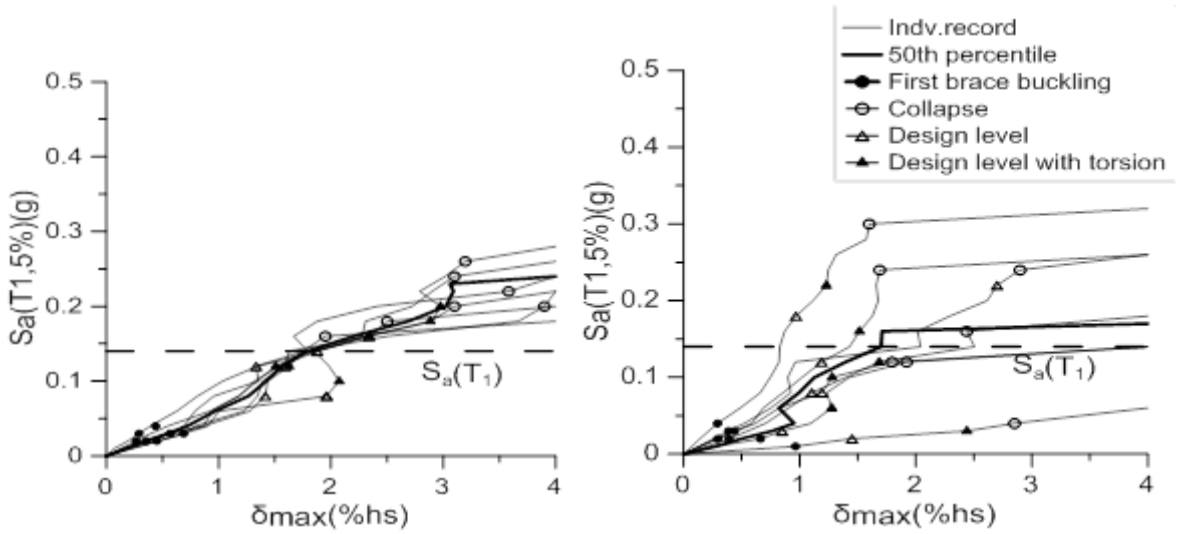

Figure 5-10 IDA curves of 16-storey MD-CBF building subjected to: a) crustal ground motions, b) subduction ground motions

Table 5-17 Centralized data from IDA curves of the 16-storey MD-CBF building subjected to crustal record

Record	First brace buckling		Design level		Amplified design level		Collapse prevention	
	$S_a(T_1)g$	$\delta_{max}(\%h_s)$	$S_a(T_1)g$	$\delta_{max}(\%h_s)$	$S_a(T_1)g$	$\delta_{max}(\%h_s)$	$S_a(T_1)g$	$\delta_{max}(\%h_s)$
C 1	0.02	0.356	0.09	1.416	0.12	1.626	0.16	1.950
C 2	0.02	0.264	0.10	1.345	0.12	1.509	0.22	3.581
C 3	0.03	0.689	0.09	1.960	0.10	2.073	0.24	3.100
C 4	0.02	0.450	0.13	1.594	0.16	2.340	0.18	2.500
C 5	0.03	0.567	0.15	1.877	0.18	2.884	0.20	3.100
C 6	0.03	0.291	0.17	2.338	0.20	2.975	0.26	3.195
C 7	0.04	0.439	0.13	1.333	0.16	2.501	0.20	3.900
Median	0.03	0.439	0.13	1.594	0.16	2.340	0.20	3.100

Table 5-18 Centralized data from IDA curves of the 16-storey MD-CBF building subjected to subduction record

Record	First brace buckling		Design level		Amplified design level		Collapse prevention	
	$S_a(T_1)g$	$\delta_{max}(\%h_s)$	$S_a(T_1)g$	$\delta_{max}(\%h_s)$	$S_a(T_1)g$	$\delta_{max}(\%h_s)$	$S_a(T_1)g$	$\delta_{max}(\%h_s)$
S1	0.02	0.662	0.03	0.847	0.06	1.276	0.12	1.921
S2	0.03	0.387	0.22	2.700	0.24	2.900	0.24	2.900
S3	0.02	0.294	0.08	1.192	0.10	1.279	0.12	1.796
S4	0.01	0.964	0.02	1.451	0.03	2.440	0.04	2.852
S5	0.04	0.292	0.18	0.968	0.22	1.230	0.30	1.600
S6	0.03	0.438	0.12	1.188	0.16	1.515	0.24	1.690
S7	0.02	0.391	0.08	1.104	0.12	1.685	0.16	2.439
Median	0.02	0.391	0.08	1.192	0.12	1.515	0.16	1.921

From Tables 5-17 and 5-18 it is observed that interstorey drift at the first brace buckling is similar for the two sets of records. The interstorey drift at all other limit states shown in the above tables is larger under the crustal ground motion set than under the subduction record set. It is noted that at design level the mean of $S_a(T_1)$ computed from 7 records is about 15% lower in the case of subduction record set scaled with 1.0 than under the crustal record set. However, at the collapse prevention limit state the 16-storey MD-CBF building fails at lower seismic demand under the subduction ground motion set than the crustal ground motion set. At the design level, the maximum interstorey drift of $2.338\%h_s$ occurred under the crustal record C6 and corresponds to $S_a(T_1)$ equal to 0.17g, and $2.97\%h_s$ at the design level with torsion consideration and corresponds to $S_a(T_1)$ equal to 0.2 g. In case of subduction records, the interstorey drift of $2.7\%h_s$ resulted for the design level under S2 record and the associated $S_a(T_1)$ is 0.22 g. It seems that S2 record shows an increase of spectral acceleration ordinates at longer periods. At the collapse prevention limit state under crustal records, the maximum interstorey drift of $3.9\%h_s$ occurred under crustal record C7 at $S_a(T_1) = 0.2g$. In the case of subduction records the maximum inter-storey drift of $2.9\%h_s$ corresponding to $S_a(T_1) = 0.24g$ was recorded for S2 ground motion.

Table 5-19 shows the calculation of total system uncertainty for the 16-storey MD-CBF buildings under crustal and subduction records.

Fragility curves for the 16-storey MD-CBF building under crustal and subduction records are shown in Figure 5-11.

Table 5-19 Total system uncertainty calculation for 16-storey MD-CBF building

Building	16 story MD-CBF	
Ground motions	Crustal ground motions	Subduction ground motions
Aleatoric uncertainty	β_{RR}=0.36	$\beta_{RR} = 0.47$
Record to record uncertainty	$\beta_{D\|Sa} = 0.255$	$\beta_{D\|Sa}$=0.4
Seismic demand	$\delta_{max}=12.69S_a^{0.93}$	$\delta_{max}=3.76S_a^{0.46}$
Total system uncertainty	β_{TOT}=0.41	β_{TOT}=0.50

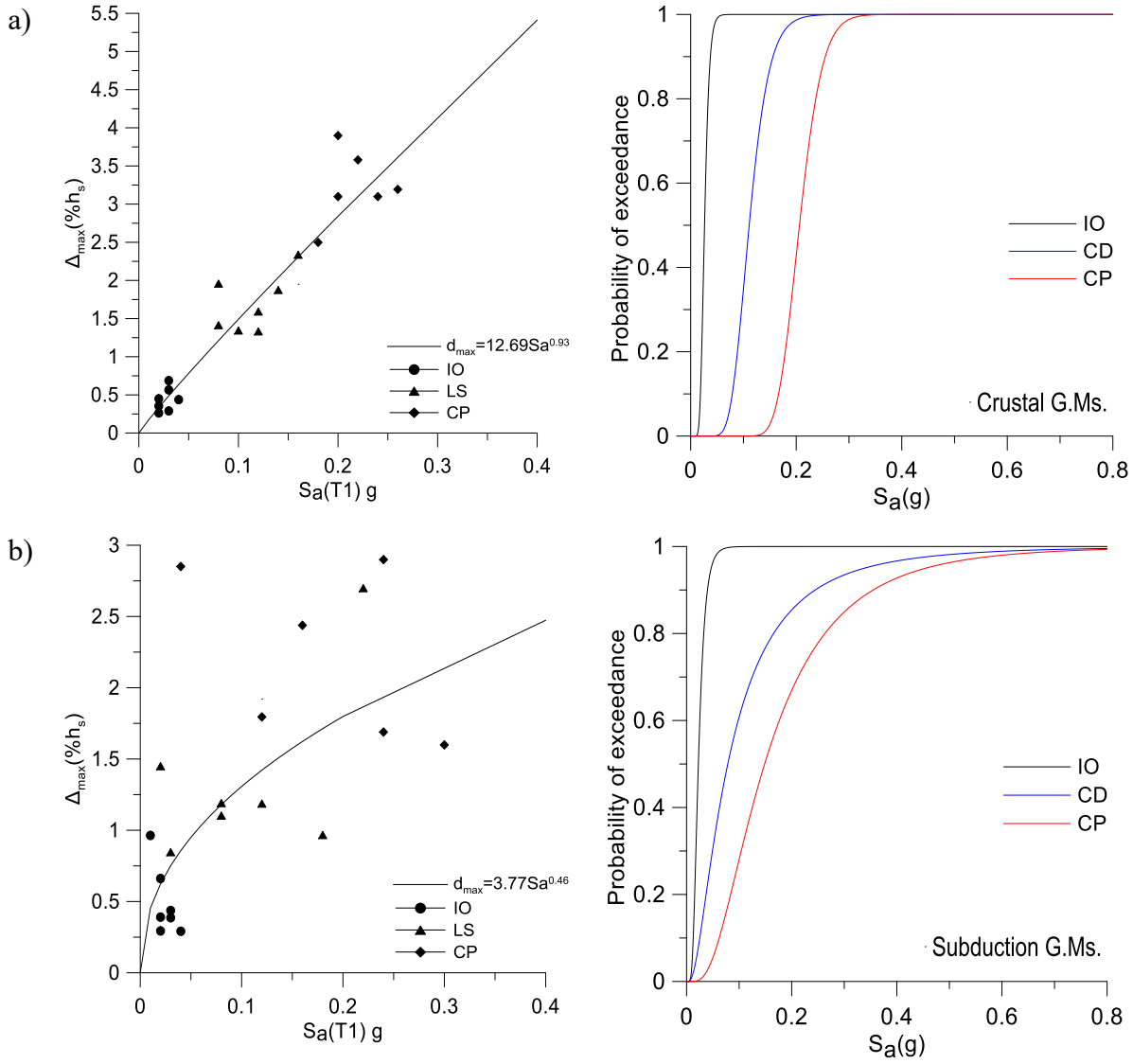

Figure 5-11 Regression analysis and fragility curves for 16-storey MD-CBF building subjected to: a) crustal ground motions, b) subduction ground motions

The verification for collapse safety criteria is presented for the 16-storey MD-CBF building subjected to both record sets is shown in Table 5-20.

Table 5-20 Verification of collapse safety criteria for 16-storey MD-CBF building (T_1 = 3.0 s)

16-Storey MD-CBF Building (T_1= 3.0 s)		
Parameters	Crustal records	Subduction records
$S_a(T_1)$	0.135	0.135
$S_a(T_1)$ [torsion consideration]	0.155	0.155
$S_a(\overline{T_1})$	0.20	0.16
CMR= $S_a(\overline{T_1})$/ Sa(T1)	1.48	1.19
CMR [torsion consideration]	1.29	1.03
β_{TOT}	0.41	0.50
ACMR	2.07	1.66
ACMR [torsion consideration]	1.81	1.45
$ACMR_{10\%}$	1.69	1.90
Pass/Fail	**Pass**	**Fail**
Pass/Fail [torsion consideration]	**Pass**	**Fail**

From Table 5-20 is shown that the 16-storey MD-CBF building passes the collapse safety criteria under the crustal record set and fails under the subduction record set. Therefore, when the building is subjected to subduction ground motions, it is prone to dynamic instability and the strength and stiffness should increase.

5.5. Assessment of collapse safety of high-rise Outrigger Braced Frame Buildings

In this section the collapse assessment of the 12-storey and 16-storey OBF buildings located in Victoria, B.C. on Site Class C is conducted. The collapse assessment is carried out according with FEMA P695 requirements as mentioned above.

5.5.1. Assessment of collapse safety of 12-storey OBF building

The IDA curves computed for the 12-storey OBF building under both sets of ground motions are illustrated in Fig. 5-12. It is noted that outrigger trusses are installed at the 8th floor as explained in Chapter 4. The first mode period is T_1= 2.15 s which is lower than the first mode period of the 12-storey MD-CBF building. The $S_a(T_1)$ value corresponding to T_1 = 2.15 s is 0.17 g. The same symbols used above in the IDA curves figures were retained.

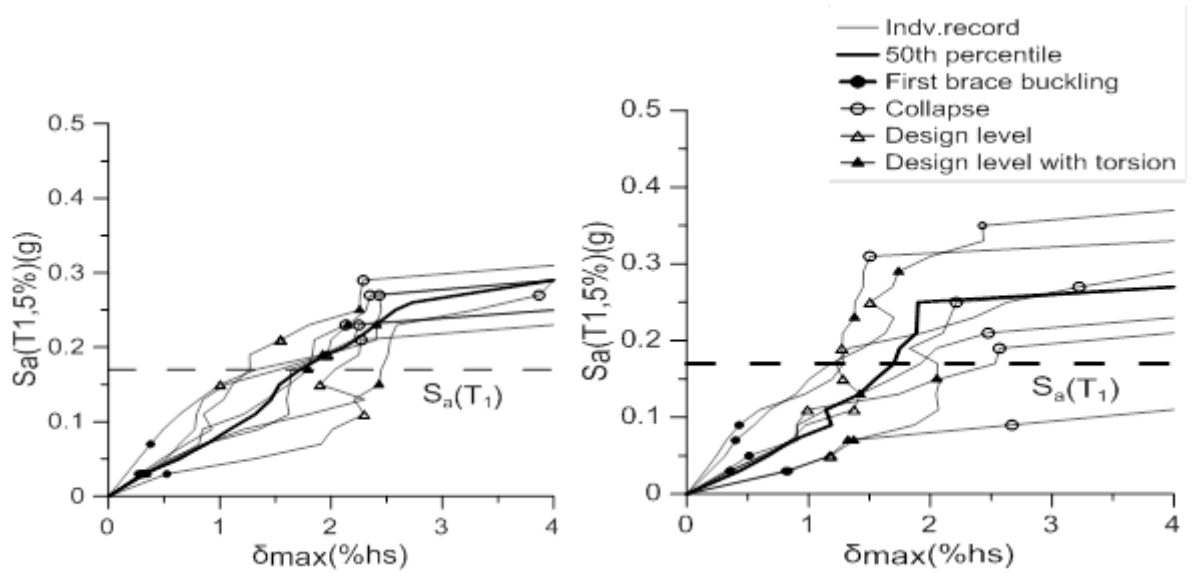

a) b)

Figure 5-12 IDA curves of 12-storey OBF building subjected to: a) crustal ground motions, b) subduction ground motions

All data collected from the IDA curves of 12-storey OBF building subjected to the crustal record set is centralized in Table 5-21 and data collected from the IDA curves obtained for the subduction record set is centralized in Table 5-22.

Tables 5-21 and 5-22 show about similar median interstorey drift values at the collapse prevention limit state under both sets of ground motions, as well as about similar median $S_a(T_1)$ value in the range 0.27g - 0.25g. At the design limit state, the 12-storey OBF building subjected to crustal records experienced maximum interstorey drift of 2.298%h_s under the C4 record. Analyzing the peak interstorey drift response at the design level under both sets of ground motions it results lower

Table 5-21 Centralized data from IDA curves of the 12-storey OBF building under crustal records

Record	First brace buckling		Design level		Amplified design level		Collapse prevention	
	$S_a(T_1)g$	$\delta_{max}(\%h_s)$	$S_a(T_1)g$	$\delta_{max}(\%h_s)$	$S_a(T_1)g$	$\delta_{max}(\%h_s)$	$S_a(T_1)g$	$\delta_{max}(\%h_s)$
C 1	0.03	0.317	0.22	2.070	0.23	2.150	0.27	2.350
C 2	0.03	0.300	0.13	1.416	0.17	1.792	0.23	2.130
C 3	0.03	0.269	0.21	1.547	0.25	2.256	0.29	2.289
C 4	0.03	0.524	0.12	2.298	0.15	2.430	0.27	3.869
C 5	0.03	0.307	0.19	1.954	0.23	2.410	0.27	2.434
C 6	0.07	0.378	0.15	1.004	0.19	1.924	0.23	2.250
C 7	0.03	0.349	0.16	1.900	0.19	2.250	0.21	2.270
Median	0.03	0.317	0.16	1.900	0.19	2.250	0.27	2.350

Table 5-22 Centralized data from IDA curves of the 12-st. OBF building under subduction records

Record	First brace buckling		Design level		Amplified design level		Collapse prevention	
	$S_a(T_1)g$	$\delta_{max}(\%h_s)$	$S_a(T_1)g$	$\delta_{max}(\%h_s)$	$S_a(T_1)g$	$\delta_{max}(\%h_s)$	$S_a(T_1)g$	$\delta_{max}(\%h_s)$
S1	0.03	0.812	0.05	1.185	0.07	1.370	0.19	2.568
S2	0.05	0.512	0.15	1.283	0.21	1.938	0.27	3.222
S3	0.07	0.400	0.25	1.504	0.29	1.739	0.35	2.428
S4	0.03	0.835	0.05	1.173	0.07	1.324	0.09	2.671
S5	0.09	0.430	0.19	1.272	0.23	1.377	0.31	1.504
S6	0.03	0.353	0.11	0.990	0.15	2.054	0.25	2.213
S7	0.03	0.358	0.11	1.374	0.13	1.423	0.21	2.475
Median	0.03	0.430	0.11	1.272	0.15	1.423	0.25	2.475

values than the code limit. However, in the case of subduction records, using a scaling factor of 1.0 for the design level, the mean of 7 subduction records (demand) is 30% lower than in the case of crustal ground motions. Comparing the interstorey drift resulted at collapse prevention limit state under C4 and S2 records it is found that that failure occurs at the same value of $S_a(T_1)$ = 0.27g, while the 12-storey OBF building undergoes larger interstorey drift under crustal record than subduction record. Table 5-23 shows the calculation of total system uncertainty, β_{TOT}, for the 12-storey OBF buildings under crustal and subduction records.

Table 5-23 Total system uncertainty calculation for 12-storey OBF building

Building	12-story OBF	
Ground motions	Crustal ground motions	Subduction ground motions
Aleatoric uncertainty	β_{RR}= 0.39	β_{RR} = 0.47
Record to record uncertainty	$\beta_{D\|Sa}$ = 0.304	$\beta_{D\|Sa}$= 0.4

Seismic demand	$\delta_{max} = 8.94S_a^{0.94}$	$\delta_{max} = 4.62S_a^{0.61}$
Total system uncertainty	$\beta_{TOT} = 0.44$	$\beta_{TOT} = 0.50$

Fragility curves for the 12-storey OBF building under crustal and subduction records are shown in Figure 5-13. The verification for collapse safety criteria is presented for the 12-storey OBF building subjected to both crustal and subduction record sets is given in Table 5-24. The collapse margin ratio is also given in Table 5-24.

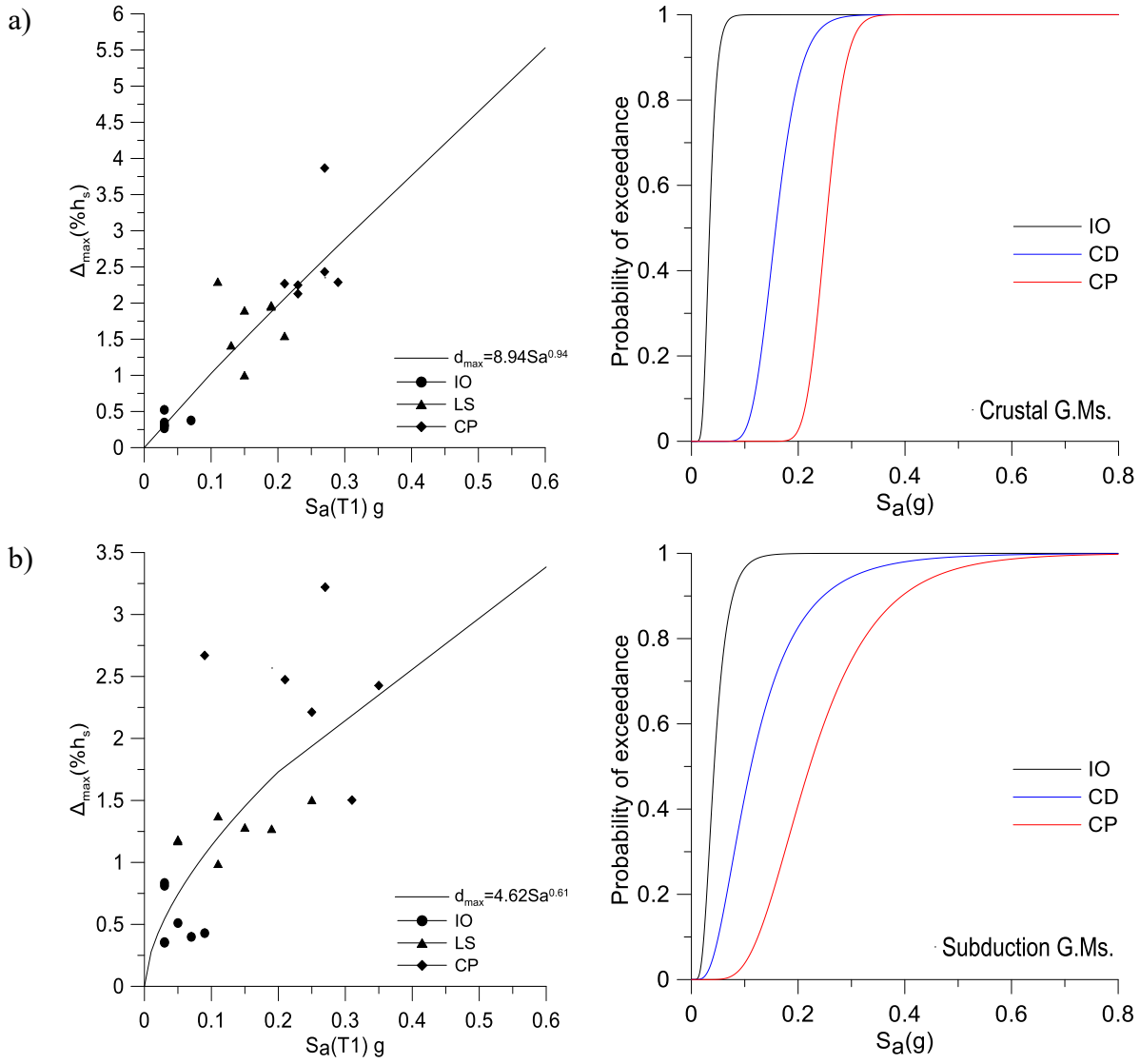

Figure 5-13 Regression analysis and fragility curves for 12-storey OBF building subjected to: a) crustal ground motions, b) subduction ground motions

Table 5-24 Verification of collapse safety criteria for 12-storey OBF building

12-Storey OBF Building (T_1 = 2.15 s)		
Parameters	Crustal records	Subduction records
$S_a(T_1)$	0.17	0.17
$S_a(T_1)$ [torsion consideration]	0.20	0.20
$S_a(\overline{T_1})$	0.27	0.25
CMR= $S_a(\overline{T_1})$/Sa(T1)	1.59	1.47
CMR [torsion consideration]	1.35	1.25
β_{TOT}	0.44	0.50
ACMR	2.23	2.06
ACMR [torsion consideration]	1.89	1.75
$ACMR_{10\%}$	1.68	1.90
Pass/Fail	**Pass**	**Pass**
Pass/Fail [torsion consideration]	**Pass**	**Fail**

From Table 5-24 is shown that the CMR of 12-storey OBF building is larger under the crustal ground motion set than the subduction record set and is able to pass the collapse safety criteria of ACMR ≥ $ACMR_{10\%}$ when subjected to crustal ground motions. However, when the effect of accidental torsion is considered, the 12-storey OBF building fails to pass the collapse safety criteria when subjected to the subduction record set.

5.5.2. Assessment of collapse safety of 16-storey OBF building

The IDA curves computed for the 16-storey OBF building under both sets of ground motions are illustrated in Fig. 5-14. It is noted that outrigger trusses are installed at the 11th floor as explained in Chapter 4. The first mode period is T_1 = 2.87 s which is lower than the first mode period of the 16-storey MD-CBF building. The $S_a(T_1)$ value corresponding to T_1 = 2.87 s is 0.14 g. The same symbols used above for the IDA curves figures were retained.

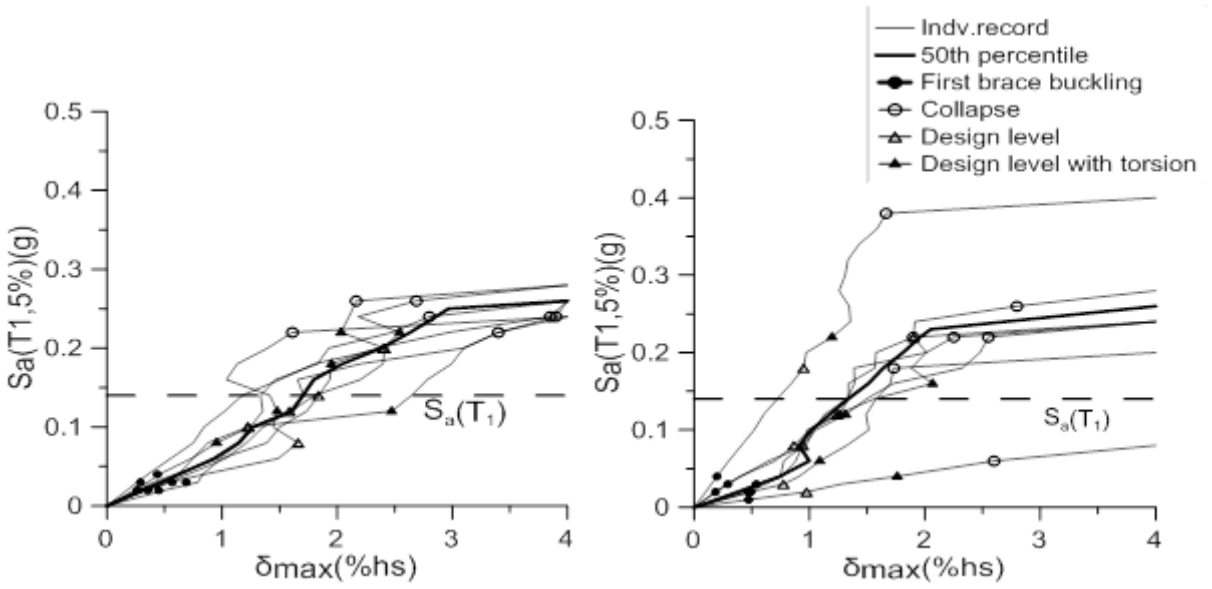

a) b)

Figure 5-14 IDA curves for 16-storey OBF building subjected to: a) crustal ground motions, b) subduction ground motions

All data collected from the IDA curves obtained for the crustal record set is centralized in Table 5-25 and data collected from the IDA curves obtained for the subduction record set is centralized in Table 5-26.

Table 5-25 Centralized data from IDA curves of the 16-storey OBF building under crustal record

Record	First brace buckling		Design level		Amplified design level		Collapse prevention	
	$S_a(T_1)g$	$\delta_{max}(\%h_s)$	$S_a(T_1)g$	$\delta_{max}(\%h_s)$	$S_a(T_1)g$	$\delta_{max}(\%h_s)$	$S_a(T_1)g$	$\delta_{max}(\%h_s)$
C 1	0.02	0.356	0.11	1.460	0.12	1.478	0.22	1.611
C 2	0.02	0.264	0.11	1.253	0.12	1.350	0.24	2.800
C 3	0.03	0.689	0.11	1.625	0.12	2.472	0.24	3.900
C 4	0.02	0.450	0.15	1.836	0.18	1.950	0.24	3.852
C 5	0.03	0.567	0.18	2.011	0.22	2.033	0.26	2.165
C 6	0.03	0.291	0.14	2.300	0.18	2.443	0.26	2.688
C 7	0.04	0.439	0.14	1.585	0.16	1.656	0.22	3.400
Median	0.03	0.439	0.14	1.625	0.16	1.950	0.24	2.800

Table 5-26 Centralized data from IDA curves of the 16-st. OBF building under subduction record

Record	First brace buckling		Design level		Amplified design level		Collapse prevention	
	$S_a(T_1)g$	$\delta_{max}(\%h_s)$	$S_a(T_1)g$	$\delta_{max}(\%h_s)$	$S_a(T_1)g$	$\delta_{max}(\%h_s)$	$S_a(T_1)g$	$\delta_{max}(\%h_s)$
S1	0.02	0.492	0.03	0.773	0.06	1.088	0.18	1.730
S2	0.03	0.292	0.22	1.901	0.24	1.913	0.26	2.798
S3	0.02	0.186	0.08	0.863	0.12	1.263	0.22	1.900
S4	0.01	0.472	0.02	0.974	0.04	1.760	0.06	2.599
S5	0.04	0.198	0.18	0.948	0.22	1.195	0.38	1.664
S6	0.03	0.540	0.12	1.238	0.16	2.066	0.22	2.250
S7	0.02	0.470	0.08	0.941	0.12	1.313	0.22	2.550
Median	0.02	0.470	0.08	0.948	0.12	1.313	0.22	2.250

Tables 5-25 and 5-26 show larger median interstorey drift values under the crustal ground motion set than under the subduction ground motion set. At the collapse prevention limit state, the failure occurred at the median $S_a(T_1)$ = 0.24 g under crustal records and 0.22 g under the subduction records. At the design limit state, the 16-storey OBF building subjected to crustal records experienced maximum interstorey drift of 2.472%h_s under the C3 record. Analyzing the interstorey drift response at the design level under both sets of ground motions it results lower values than the code limit of 2.5%h_s. However, in the case of subduction records, using a scaling factor of 1.0 for the design level, the demand (the mean of 7 ground motions) is found to be 14% lower than in the case of crustal ground motions.

Table 5-27 shows the calculation of total system uncertainty, β_{TOT} for the 16-storey OBF buildings under crustal and subduction records.

Table 5-27 Total system uncertainty calculation for 16-storey OBF building

Building	16-story OBF	
Ground motions	Crustal ground motions	Subduction ground motions
Aleatoric uncertainty	β_{RR}= 0.47	β_{RR} = 0.47
Record to record uncertainty	$\beta_{D\|Sa}$ = 0.4	$\beta_{D\|Sa}$= 0.4
Seismic demand	$\delta_{max} = 8.61S_a^{0.82}$	$\delta_{max} = 4.32S_a^{0.58}$
Total system uncertainty	β_{TOT} = 0.50	β_{TOT} = 0.50

Fragility curves for the 12-storey OBF building under crustal and subduction records are shown in Figure 5-15.

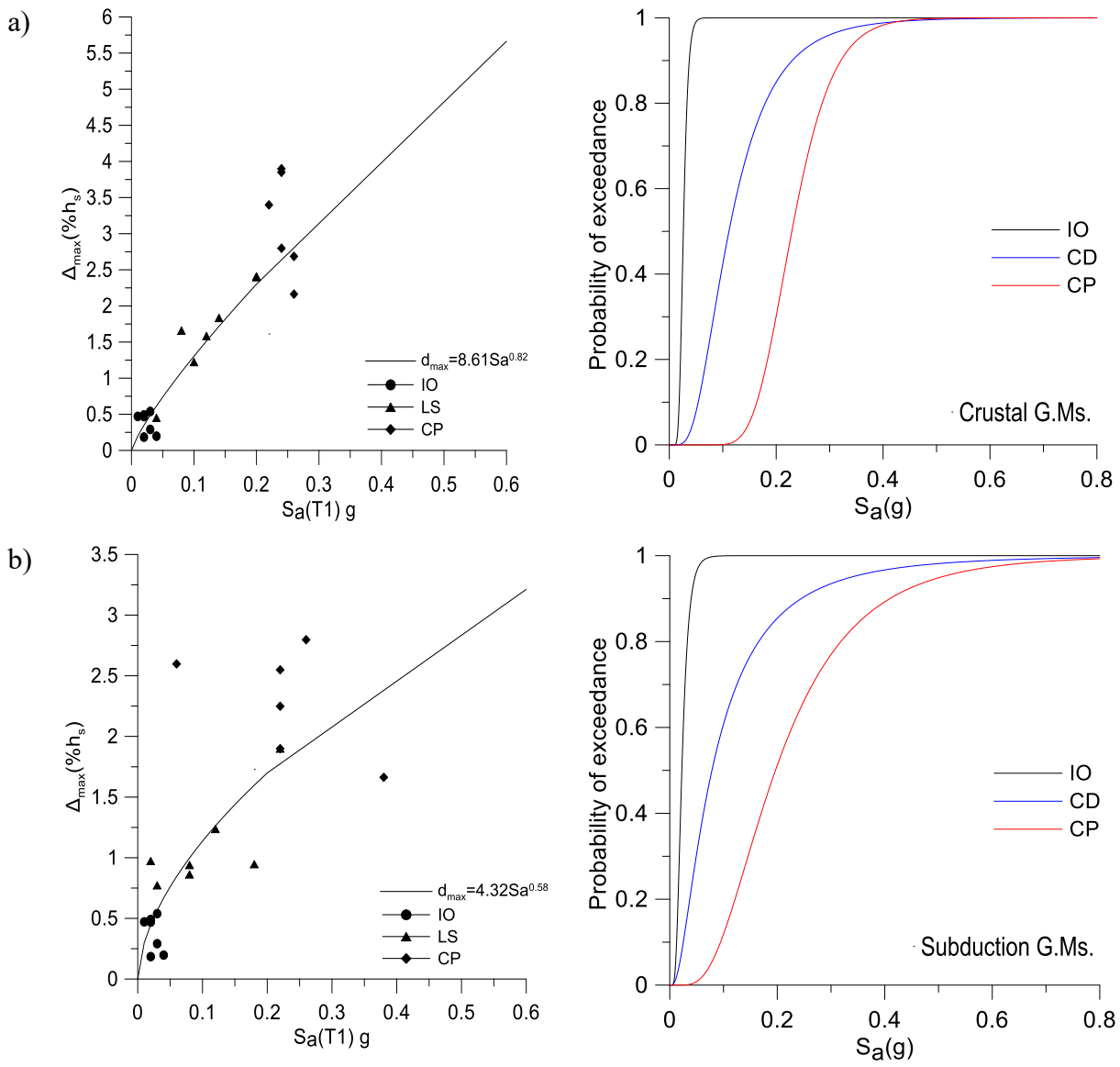

Figure 5-15 Regression analysis and fragility curves for 16-storey OBF building subjected to: a) crustal ground motions, b) subduction ground motions

The verification for collapse safety criteria is presented for the 16-storey OBF building subjected to both crustal and subduction record sets is given in Table 5-28.

Table 5-28 Verification of collapse safety criteria for 16-storey OBF building

16-Storey OBF Building (T_1 = 2.87 s)		
Parameters	Crustal records	Subduction records
$S_a(T_1)$	0.14	0.14
$S_a(T_1)$ [torsion consideration]	0.17	0.17
$S_\alpha(\overline{T_1})$	0.24	0.22
CMR= $S_\alpha(\overline{T_1})/S_a(T_1)$	1.71	1.57
CMR [torsion consideration]	1.41	1.29
β_{TOT}	0.50	0.50
ACMR	2.39	2.20
ACMR [torsion consideration]	1.97	1.81
$ACMR_{10\%}$	1.90	1.90
Pass/Fail	**Pass**	**Pass**
Pass/Fail with torsion	**Pass**	**Fail**

From Table 5-28 is shown that the CMR of 16-storey OBF building is larger under the crustal ground motion set than the subduction record set and is able to pass the collapse safety criteria of ACMR ≥ $ACMR_{10\%}$ when subjected to crustal ground motions. However, when the effect of accidental torsion is considered, the 16-storey OBF building fails to pass the collapse safety criteria when subjected to the subduction record set.

5.6. Summary of Chapter 5

Chapter 5 shows the collapse assessment for the low-rise, middle-rise, and high-rise MD-CBF buildings, as well as high-rise OBF buildings under two sets of records: crustal and subduction. The assessment for collapse safety was conducted according to FEMA P695 procedure. The findings are as follows:

1. The study shows that the low-rise (2-storey and 4-storey) MD-CBF buildings and middle-rise (8-storey) MD-CBF buildings are able to pass the collapse safety criteria ACMR ≥ $ACMR_{10\%}$ when subjected to both crustal and subduction ground motion sets. The $S_a(T_1)$ value involved in the assessment corresponds to the first mode period of design spectrum. When $S_a(T_1)$ value was artificially increased to account for additional shear caused by torsion due to accidental eccentricity, the collapse safety criteria passes under subduction and crustal records for the 2-storey building and also verified for the 4-storey and 8-

storey MD-CBF buildings subjected to crustal ground motions, while for the 4-storey and 8-storey MD-CBF buildings, the collapse safety criteria fails under the subduction records.

2. The 12-storey and 16-storey MD-CBF buildings are able to pass the collapse safety criteria ACMR $\geq$ $ACMR_{10\%}$ when subjected to crustal ground motions and fails under the subduction ground motion set. Similarly, when $S_a(T_1)$ value was artificially increased to account for additional shear caused by torsion due to accidental eccentricity, the collapse safety criteria passes under the crustal ground motion set but fails to pass under the subduction ground motion set.
3. In all cases, the collapse margin ration (CMR) computed for MD-CBF buildings is greater when buildings are subjected to crustal ground motion set versus the subduction ground motion set.
4. Evaluation of seismic performance of 12-storey and 16-storey OBF buildings shows that these buildings are able to pass the collapse safety criteria ACMR $\geq$ $ACMR_{10\%}$ when subjected to both crustal and subduction ground motion sets. In addition, both buildings subjected to crustal ground motion set are able to sustain increase $S_a(T_1)$ value incorporating the effect of additional shear caused by torsion due to accidental eccentricity. However, this is not the case when the studied OBF buildings are subjected to subduction ground motions. It is observed that the OBF buildings provide increased margin safety as compared to the corresponding MD-CBF buildings located in high risk seismic areas. When buildings are subjected to mega-thrust magnitude 9 Tohoku records, for similar demand, damage accumulates at higher rates than under crustal ground motions. Hence, special attention should be given when designing buildings in B.C. where both types of ground motions are expected.

Chapter 6. Summary and Conclusions

The summary of design methods, conclusions, contributions, limitations and future works are discussed in this chapter

6.1.Summary

The main motivation of this research was to develop a design method for earthquake resistant steel outrigger braced frame buildings (OBF), to find the optimum outriggers geometry and optimum vertical location among floors. Although outriggers are used in several high-rise buildings since 1980, there are not enough studies leading to a design method for earthquake resistant braced frames with outrigger trusses. This need was underlined in the Guideline for Seismic Based Design of Tall Buildings developed by PEER as part of Tall Building Initiative (PEER, 2010). Meanwhile, buildings located on the Pacific coast of Canada are subjected to crustal and subduction ground motions. The latter are characterized by longer duration and significant Trifunac duration, while the response of multi-storey braced frame buildings subjected to subduction type records is mostly unknown. Furthermore, to emphasize the seismic performance of high-rise OBF buildings proposed herein, these are presented against the seismic performance of high-rise MD-CBF buildings. Therefore, the major design points can be summarized in the following categories

- Characteristics of long-duration subduction ground motions and their selection:
    1) The main contributions to seismic hazard for buildings located in Victoria, B.C. on Site Class C, are moderate-to-large crustal earthquakes of magnitudes M 7.0 – M 7.5 and the potential megathrust subduction earthquake of M 8.0 – M 9.0. Recent studies show that the distance from Victoria to the Cascadia subduction fault is about 50 km and the return period is about 400 years. Therefore, “the big one” is expected to occur anytime around 2100. The proxy subduction records used to analyze the seismic response of buildings in Victoria, B.C. are those selected from the megathrust M9 Tohoku earthquake in Japan (March 2011) that are compatible with geotechnical profile for Site Class C and to the distance to the fault. Using a scale factor of 1.0 for a set of seven selected Tohoku records it is found that the demand is several times greater than the design spectrum (DS) for periods shorter than 0.4 s; between the 0.4 s and 0.6 s, it is slightly above the DS; at 0.6 s,

1.0 s, and 1.8 s - 2.2 s it is equal or comparable to the DS; between 0.6 s and 1.0 s, as well as, between 1.0 s and 1.8 s, it is slightly lower than DS with a lower value of about 0.8 DS at 0.8 s and 1.2 s, respectively. For longer periods than 2.2 s, the mean response spectrum is slightly below the DS.

2) Comparing the subduction records with crustal records it is found that the former shows the total duration and Trifunac duration about seven times larger than the later and in consequence they subject buildings to higher seismic demand due to several loading/unloading cycles.

- The effect of long-duration earthquake versus typical duration on the response of low-rise, middle-rise and high-rise MD-CBF buildings:
  1) The design of MD-CBF buildings followed the NBCC 2010 and CAN/CSA-S16-09 standard provisions. The effect of accidental torsion and P-Δ was considered. The wind load was verified in order to assure elastic response of braced frames. Buildings with first-mode period > 1.0 s are considered dynamically sensitive and the dynamic procedure was employed for wind load calculation. All buildings but the 16-storey one was designed to resist earthquake loads that were greater than the wind loads. However, the wind load controls the design of bottom floors braces (1^{st} to 7^{th} floor) of 16-storey building in N-S direction.
  2) The nonlinear seismic response of studied MD-CBF buildings was conducted using the OpenSees software. The desirable failure mode of MD-CBFs is the failure of braces caused by low-cycle fatigue that occurs within the plastic hinge region. Although the OpenSees model is 2-D, it allows braces to buckle out-of-plane. Each gusset plate brace-to-frame connection resulted from design was simulated using two rotational springs and one torsional spring. The low-cycle fatigue model applied to HSS braces is that proposed by Tirca and Chen (2014). All HSS braces were simulated using the force-based nonlinear beam-column elements with distributed plasticity.
  3) The effect of accidental torsion cannot be simulated using a 2-D model. Hence, it was accounted for artificially by increasing the seismic demand with the ratio between the total base shear including that caused by accidental torsion and the base shear from earthquake loads. In this study, the length-to-width ratio of prototype building is 2.25 and

the shear amplification factor caused by accidental torsion computed with accidental eccentricity $0.1D_n$ is about 1.2.

- Design method for OBF buildings:
  1) A design method for the OBF system is proposed and validated through nonlinear time-history analysis using detailed numerical models developed in OpenSees by considering: i) outrigger truss's geometry, ii) dissipative capacity of diagonal members of outriggers and iii) optimum location of outrigger trusses among the building floors.
  2) The stiffness of outrigger truss geometry shall be controlled in order to avoid the introduction of vertical stiffness irregularity, known as Type 1 in NBCC. Using two diagonal members per a truss bay instead of one it leads to larger storey stiffness. Thus, the truss geometry with minimum number of diagonal members is recommended.
  3) In this study, outriggers were designed similar to conventional construction braced frame with R_d = 1.5 and R_0 = 1.3, while the core system of outrigger braced frame, OBF, was designed similar to MD-CBF with R_d = 3 and R_0 = 1.3. Concerning the design of outrigger system, the far end columns were proportioned to carry the tributary gravity loads in addition to axial forces triggered from outriggers by applying the capacity design principle. However, it was observed that axial forces in these exterior columns did not increase much. The same principles as those required for the MD-CBF system in NBCC and CSA/S16 standard were used.

6.2. Conclusions

From the present study of low-rise, medium-rise and high-rise MD-CBF buildings and high-rise OBF buildings subjected to crustal and subduction ground motions, the following conclusions are drawn.

- For the low-rise, middle-rise and high-rise MD-CBF buildings:
  1) From OpenSees analysis, it is found that all studied MD-CBF buildings experienced lower peak of mean interstorey drift than 2.5% h_s and lower peak of mean residual interstorey drift than 0.5% h_s which is considered acceptable for buildings to be reparable after an earthquake event. The effect of subduction records characterized by several

loading-unloading cycles increases the accumulation of compression strain in the outermost compression fiber of critical cross-section of HSS braces. The floor level where the peak interstorey drift occurred starts deflecting one side under a small increase in demand. Meanwhile, braces of this critical floor are driven to failure caused by low-cyclic fatigue. When an upper floor of a building taller than 8-storey starts losing its stiffness, the lateral deflection migrates and concentrates at a lower floor. Thus, to increase the safety level, it is recommended to concentrate the energy dissipation at upper floors. In addition, it is believed that $0.1D_n$ accidental eccentricity is too conservative.

- For the high-rise OBF buildings:
  1) The recommended optimum vertical location for the one floor outrigger system may be selected either at the floor where storey shear reaches half of the base shear or at the floor experiencing maximum interstorey drift. The former scenario leads to the floor reference at 2/3 h_n measured from the ground, where h_n is the building height. However, both scenarios should be considered in order to select that providing reduced peak interstorey drift and a uniform distribution of damage along the building height.
  2) The high-rise OBF buildings show better seismic performance than traditional CBF buildings. The nonlinear seismic response shows a substantial reduction of interstorey drift at the floor where outriggers are located, as well as, at all floors above the outriggers location. The peak of mean inter-storey drift of 12-storey and 16-storey OBF buildings is within the code limit and the peak of mean residual interstorey drift is lower than 0.5% h_s.

- Seismic performance of OBF buildings versus MD-CBF buildings according to FEMA P695 procedure:
  1) The low-rise (2-storey and 4-storey) MD-CBF buildings and middle-rise (8-storey) MD-CBF buildings are able to pass the collapse safety acceptance criteria ACMR $\geq$ $ACMR_{10\%}$ when subjected to both sets of crustal and subduction ground motions. The $S_a(T_1)$ value involved in the assessment corresponds to the first-mode period of design spectrum. When $S_a(T_1)$ value was artificially increased to account for the effect of accidental torsion due to accidental eccentricity $0.1D_n$, the collapse safety acceptance criteria is verified only for the 2-storey building. When the 4-storey and 8-storey

buildings were subjected to amplified crustal records the collapse safety acceptance criteria was also verified but it fails under the set of subduction records.

2) The 12-storey and 16-storey MD-CBF buildings are able to pass the collapse safety acceptance criteria ACMR $\geq$ $ACMR_{10\%}$ when subjected to crustal ground motions and fails under the subduction ground motion sets. Similarly, when $S_a(T_1)$ value was artificially increased to account for additional shear caused by accidental torsion, the collapse safety acceptance criteria did not pass when subduction records were considered. Therefore, the effect of accidental torsion is a concern in design.
3) In all case study, the collapse margin ration (CMR) computed for MD-CBF buildings is greater when buildings are subjected to crustal than the subduction ground motions.
4) Assessing the seismic performance of 12-storey and 16-storey OBF buildings, it is shown that both buildings are able to pass the collapse safety acceptance criteria ACMR $\geq$ $ACMR_{10\%}$ under both sets of crustal and subduction ground motions. In addition, both buildings subjected to artificial greater demand, $S_a(T_1)$, applied to crustal records, in order to account for the accidental torsion effect, are able to pass the collapse safety acceptance criteria. However, it was not the case when these buildings were subjected to subduction records scaled for increase demand.
5) The OBF buildings provide increase margin safety than MD-CBF buildings when designed for high-risk seismic areas. When buildings are subjected to megathrust M9 Tohoku records, for similar spectral acceleration demand, damage in braces accumulates at higher rates than under crustal ground motions. Hence, special attention should be given when designing buildings in B.C. where both earthquake types are potential mechanism sources.

6.3. Contributions

The contribution of this thesis can be summarizing in the following points:

1) Provide a design method for high-rise OBF building. The use of the outriggers as an additive to get better structural performance was since more than 40 years, but there is not enough literature proving a method to design a structure with added outriggers. In this thesis, a detailed design method was provided for a high-rise OBF building, and its effectiveness was validated through detailed nonlinear dynamic analysis.

2) Determine the characteristic response of high-rise OBF structures under real earthquake accelerations; the normal crustal and the mega-thrust subduction records. The response of the OBF structure provides an added information on the behaviour of theses structure and provides a better understanding on their failure mechanisms.
3) Compare the response of low-rise, middle-rise and high-rise MD-CBF buildings under real earthquake accelerations i.e. crustal and subduction records, the response was measured the inter-storey drift, residual inter-storey drift and the damage index. The comparison in this thesis highlights very important points for the design of MD-CBF buildings under real long-duration earthquake accelerations.
4) Include the effect of accidental torsion in the design of MD-CBF and OBF structures under study. Since the inclusion of accidental torsion by using a 2-D OpenSees model is not possible, an amplification of demand by means of a scaling factor computed as the ratio of the base shear resulted from the consideration of shear including shear caused by accidental torsion to the base shear force resulted only from earthquake loads was used to amplify the design spectrum demand.
5) Provide the collapse safety assessment for the low-rise, middle rise and high-rise MD-CBF buildings and the high-rise OBF buildings under FEMA P695 procedure. The new element in this study is to provide the collapse assessment with and without the consideration of accidental torsion.

6.4.Limitations

The limitations of this study are listed as follow:

1) The design of the outrigger braces was limited to be in elastic range, while they can be used in many different ways and this could be done as a future work.
2) In this study, only the conventional outrigger system was considered. As a future work is proposed to investigate the response of OBF system where virtual outriggers are employed.
3) The number of ground motions per set was limited to seven.

6.5. Future work

The OBFs are cost efficient earthquake resistant systems. In this study it was considered elastic response of outriggers, while the core braced frame system is designed to perform in the nonlinear range. A future research direction may be to consider buckling restrained braces (BRB) for outriggers diagonal members and to assign percentage of earthquake input to be dissipated by outriggers. To preserve the stability of OBF system with dissipative outriggers, it is proposed to keep the core system braces within the outrigger system floor to perform in the elastic range. In addition, another research direction may be to consider energy dissipation devices to be installed in-line with outrigger truss diagonal members.

For tall buildings, it is recommended to use virtual belt trusses located on one or several perimeter floors in order to belt all perimeter gravity columns. This virtual belt trusses system can be added to the proposed OBF system with conventional or dissipative outrigger trusses.

The OBF systems with or without virtual belt trusses can be developed in a modular version of prefabricated 4-storey systems. Special connection types can be developed to reduce the building construction time.

To simulate the effect of accidental torsion, there are some research directions that can be developed: i) consider a 3-D model in OpenSees and study in detail the effect of accidental torsion considering the accidental eccentricity $0.05D_n$, as allowed by code ii) using the 2-D OpenSees model study the seismic performance of buildings when the demand is amplified by a lower factor equivalent to accidental eccentricity $0.05D_n$ and investigate the difference between the building response resulted from 2-D versus 3-D model iii) reduce the shear caused by accidental torsion by restricting the length-to-width ratio for buildings located in high-risk seismic area. It is believed that for the length-to-width ratio an upper limit of 2.0 - 2.5 should be introduced in the building code. Currently, it is only the Eurocode 8, where a limit of 4 is provided for the length-to-width ratio of buildings.

It is also believed that the proposed UHS for Victoria, BC in the 2015 edition of NBCC is too conservative. It is noted that in the long period range the spectral ordinates are about two times greater which implies to amplify by a factor of 2 the records selected from the megathrust M9 Tohoku event.

References

Aguero, A., Izvernari, C., Tremblay, R. (2006). “Modeling of the Seismic Response of Concentriclly Brace Steel Frames using the OpenSees Analysis Environment” . International Journal of Advanced Steel Construction, 2,3,242-274.

Ahmed, M., Rahee, S., Ahmed, M., G.A. Aly, Sahy A. (2016).”Irregularity Effects on the Seismic Performace of the L Shape Multi Story Buildings.” Journal of engineering Sciences,Vol 44, No 5,PP,513-536.

AIR Worldwide Commissioned by the Insurance Bureau of Canada (2013). “Major Earthquake in British Columbia and Ontario/Québec”.

AISC (2010). “Seismic Provisions for structural Steel Buildings.” ANSI/AISC 341-10. American institute of Steel Construction, inc, IL, USA.

American Society of Civil Engineers (ASCE). (2010). “Minimum design loads for buildings and other structures.” ASCE/SEI 7-10, Reston, Virginia.

ASCE. (2013). “Seismic rehabilitation of existing buildings.” ASCE/Structural Engineering Institute (SEI) 41-13, Reston, VA.

Astanech-ASL, A. (2005). “Design of Shear Tab Connections for Gravity and Seismic Loads.” Steel Type Education.

ASTM. (2003). “ASTM E 1049 - 85: Standard Practices for Cycle Counting in Fatigue Analysis.” West Conshohocken, PA.

Atkinson, G. (2009). “Earthquake time histories compatible with the 2005 National Building Code of Canada uniform hazard spectrum.” Can. Journal of Civil Eng., 36(6), 991-1000.

Baker, J. W., and Cornell, C. A. (2005). “A vector-valued ground motion intensity measure consisting of spectral acceleration and epsilon.” Earthquake Engineering & Structural Dynamics, 34(10), 1193–1217.

Bayati, Z., Ahdikhani, M., (2008). “Optimized Used of Multi-Outriggers System to Stiffen Tall Builings.” The 14th World Cnference on Earthquake Engineering, Beijing, China.

Black, R.G., Wenger, W.A.B., Popov, E.P. (1980), ” Inelastic Buckling of Steel Strut under Cyclic Load Reversals.” Report N. UCB/EERc-80/40, Earthquake Enginering Research Center, University of California, Berkely, CA.

Boore, D.M. (2003), ”Simulation of Ground Motion Using the Stochastic Method.” Pure and Applied Geophysics, 160(3-4), 635-676.

Buyukozturk, O., and Gunes, O. (2004). “High-Rise Buildings: Evolution and Innovations.” CIB2004 World Building Congress. Toronto: Massachusetts Institute of Technology.

Canadian Standard Association. (2009). “CAN/CSA-S16-09 Limit states design of steel structures.” Canadian Standard Association, Toronto, ON.

CEN, EN 1998-1-1: Eurocode 8: Design of Structures for Earthquake Resistance. Part 1: General Rules, Seismic Actions and Rules for Buildings, Comite Europeen de Normalisation, CEN/TC 250,2005.

Choi, H., Ho, G., Joseph, L. and Mathias, N. (2012). “Outrigger Design for High–Rise Buildings.” An output of the CTBUH outrigger working group. Councile on Tall Buildings and Urban Habitat, Chicago.

Choi, H., Ho, G., Joseph, L. and Mathias, N. (2017). “Outrigger Design for High–Rise Buildings 2nd edition.” An output of the CTBUH outrigger working group. Councile on Tall Buildings and Urban Habitat, Chicago.

Choi, H.S. and Leonard, J. (2012). “Outrigger System Design consideration.” International Journal of High-rise Buildings, Vol. 1, No 3, pp 237-246.

Christopolos, C., Pampani, S. (2004). “Towards Performance–Based Seismic Design of MDOF Structures with Explict Consideration of Residual Deformations.” ISET Journal of Earthquake Technology, Vol. 41, No.1, pp 53-73.

Coffin, L.F. (1962), ”Low Cycle Fatigue-A Review.” Applied Material Research, Vol. 1,No, 3, pp. 129-141.

Computers and Structures, Inc., (CSI). (2011). “ETABS Nonlinear- extended 3d analysis of building systems, version 9.7.4 (computer program).” CSI, Berkeley, CA.

Dadris, J. (2017). “Rigger for the Future.” Modern Steel Constructrion, AISC, March 2017, USA.

Dicleli, M., Calik, E., (2008). “Physical Theory Hysteretic Model for Steel Braces.” Journal of Structural Engineering ,Vol. 134, No.7,pp 1215-1228.

Ellingwood, B., Celik, O.C., Kinali, K. (2007). “Fragility Assessment of Building Structural Systems in Mid-America”. Earthquake Eng. and Structural Dynamics, 26:1935-1952.

Fawzia, S., Fatima, T. (2010). “Deflection Control in Composite Building by Using Belt Truss and Outriggers Systems.” International Journal of Structural and Construction Engineering, Vol 4, No 12.

FEMA P695, (2009). “Quantifications of Building Seismic Performace Factors”, Federal Emergency Management Agency, Washington, DC.

Filiatrault, A. (2002). “Elements of Earthquake and Structural Dynamics.” Second edition.

Fisher, J.W., Kulak, G.L., and Smith, I.F.C. (1997). “A Fatigue Primer for Structural Engineers.” *97-11*, Advanced Technologies for Large Structural Systems (ATLSS), Lehigh University; Bethlehem, Pennsylvania, USA.

Glinka, G., and Kam, J.C.P. (1987). “Rainflow counting algorithm for very long stress histories.” International Journal of Fatigue, 9(3), 223–228.

Goman, W.M.Ho. (2016). “The Evolution of Outrigger System in Tall Buildings.” International Journal of High-Rise Buildings, Vol 5, No 1, pp 21-30.

Haddad, M.A. (2004). “Design of Concentrically Braced Steel Frames for Earthquakes,” Ph.D. Thesis, Department of CivilEngineering, University of Calgary, Calgary, AB.

Haghollahi, A., Besharat, M., Ferdous, Kasiri, M. (2012). “Optimization of Outrigger Locations in Steel Tall Buildings Subjected to Earthquake Loads.” 15WCEE, Lisbon, Portugal.

Haukaas, T. and Der Kiureghian, A. (2004).“Finite Element Reliability and Sensitivity Methos for Performance-Based Earthquake Engineering.” Report No. 2003/14, Pacific Earthquake Engineering Research Center (PEER), Univ. of California, Berkeley, CA.

Herath, N., Haritos, N., Ngo, T., Mendis P. (2009).”Behaviour of Outrigger Beams in High – Rise Buildings under Earthquake Loads.” Australian Earthquake Engineering Society.

Hoenderkamp, J.C.D. (2008). “Second Outrigger at Optimum Location on High-Rise shear Wall.” The Structural Design of Tall and Special Builings, 17-619-634.

Hoenderkamp, J.C.D., Bakker, M.C. (2003). “Analysis of high-rise Braced Frames with Outriggers.” The Structural Design of Tall and Special Builings,12-225-350.

Hoenderkamp, J.C.D., Bakker, M.C., Snijder (2003). “Perliminary Design of High-Rise Outrigger Braces Shear Wall Structures on Flexible Foundations.” Heron, Vol.48, No.2.

Hoenderkamp, J.C.D., Snijder (2000). “Simplified Analysis of Facade Rigger Braced for High-rise Structures.” The Structural Design of Tall and Special Builings, 9-309-319.

Hsiao P.C., Lehman D., Roeder C. (2013). “A model to simulate special concentrically braced frames beyond brace fracture”. Earthquake Engineering and Structural Dynamics, 42,183-200.

Hsiao, P.C., Lehman, D., Roeder (2012). “Impooved analytical model for special concentrically braced frames”. Journal of Construction Steel Research,73,80-94.

Hsiao, P.C., Lehman, D., Roeder (2013). “Evaluation of the response modification coefficient and collapse potential of special concentrically braced frames ”. Earthquake Engineering and Structural Dynamics ,42,1547-1564.

Ibarra, L., Medina, R., and Krawinkler, H. (2002). “Collapse assessment of deteriorating SDO Fsystems.” Conf. Proc., 12th European Conference on Earthquake Engineering, London, Elsevier Science Ltd, paper no. 665.

Ikeda, K., Mahin, S.A., Dermizakis, S.N. (1984), ”Phenomenological Modeling of Steel Braces under Cyclic Loading.” Report N. UCB/EERc-84/09, Earthquake Enginering Research Center, University of California, Berkely, CA.

Kamath, K., Divya, N., Rao, A. (2012). “A study on Static and Dynamic Behavior of Outrigger Structural system for Tall Buildings.” Bonfring International Journal of Industrial and Management sceince , Vol 2, No 4.

Kamgar, R., Rahgozar, R. (2015). “Determination of Optimum Location for Flexible Outrigger Systems in Non Uniform Tall Buildings Using Energy Method.” International Journal of Civil Engineering, 433-444

Kamgar, R., Rehgozar, R. (2017).”Determination of Optimum Location for Flexible Outrigger Systems in Tall Buildings with Constant Cross Section Consisting of Framed Tube, Shear Core , Belt Truss and Outrigger System Using Energy Method”. International Journal of Steel Structures 17(1).

Karamachi, E. , Ligons, D., (2012). “Predictive equations for modelling cyclic buckling and fracture of steel braces.” The 10th International Conference on Urban Earthquake Engineering,Tokyo 2013, pp. 105–117.

Kennedy, R.P., Ravindra, M.K. (1984). ”Seismic Fragility for Nuclear Power Plant Risk Studies.” Nuclear Engineering and Design, 79(1), 47-68.

Kian, S., Frits Torang, F. (2001). “The Use of Outrigger and Belt Truss System for High-Rise Concrete Buildings.” Dimensi Teknik Sipil, Vol.3, No.1, Mar. 2001, 3 6-41.

Krem, M., (2012). “Effect of Building Morphology on Energy and Structural Performance of High-Rise Office Buildings.” PhD Thesis , University of Massachusetts – Amherst, USA.

Lacerte, M., Temblay, R. (2006). ”Making Use of Braced Overstrength to Impove the Seismic Response of Multi-Storey Split-X Concentrically Braced Frames.” Can. J. of Civil Engineeing, 33, 8, 1005-1021.

Lai, J.W., Mahin, S. (2014). “Steel Concentrically Braced Frames Using Tubular Structural Sections as Bracing Members.” Design, Full-scale Testing and Numerical Simulation. International Journal of Steel Structures, Vol. 14, No. 1, 43-58.

Lam, A. (2008). “Optimization of Outrigger Structures”. Master of engineering thesis, Massachusetts Institution of Technology, Cambridge, MA.

Lee, K., Bruneau, M. (2005). ”Energy Dissipation of Compression members in Concentricallu Braced Frames Review of Experimental Data.” Journal of Structural Engineering, ASCE, 131 (4), pp 552-559.

Luco, N., and Cornell, C. A. (2007). “Structure-specific scalar intensity measures for near source and ordinary earthquake ground motions.” Earthquake Spectra, 23(2), 357-392.

Manson, S.S., Hirschberg, M.H. (1963), ”Fatigue Behavior in Strain Cycling in the Low – and Intermediate-Cycle Range.” The 10th Sagamore Army Resarch Conference: Fatigue- An Interdisciplinary Approch , New York, pp. 13-16.

Mazzoni, S., McKenna, F., Scott, M., Fenves, G. et al. (2007).“OpenSees User Manual.” “Opensees.berkeley.edu/OpenSees/manuals/usermanual/OpenSeesCommandLanguage Maual.”.

McKenna, F. (1997), ”Seismic Object Oriented Finite Element Analysis: Framrae works for Analysis Alogrithms and Parallel Computing.” Ph.D. Thesis, University of California, Berkely.

McNabb, J.W., Muvdi, B.B. (1975).”Drift Reduction Factors for Belted High-Rise Structures.” Eng. Journal, AISC,.12(3), pp 88-91.

Merczel, D.,Somja, H., Aribert, J., M., Logo, J., (20103). “On the Behavior of Concentrically Braced Frames Subjected to Seismic Loading.” Periodica Polytechnica Civil Engineering, 57(2), 113–122.

Morales, JD. (2011).”Numerical Simulation od Steel Frames Equipped with Friction-Damped Diagonal-Bracing Devices”. MASc thesis, Concordia University, Canada.

Moudarres, F.R., (1984), ”Outrigger- Braced Coupled shear walls.” Journal of Structural Engineering , ASCE, 110: 2876-2890.

Nair, R.S. (1989), “Belt Truss and Basements as Virtual Outriggers for Tall Buildings.” Enginnering Journal, Fourth Quarter- New York , 35(4):140-146.

Nanduri, P.M.B., Suresh, B., Ihtesham Hussain, MD. (2013). “Optimum Position of Outrigger System for High-rise Reinforced Concrete Buildinmgs under Wind and Earthquake Loading.” American Journal of Engineering Research (AJAR), Volume-02, Issue -08, pp-76-89.

National Building Code of Canada (NBCC) 2010. Part 4. Ottawa, ON: National Research Council of Canada; 2010

Opensees Version 2.4.4 [Computer Software]. Beakely, CA, Pacific Earthquake Engineering Reserch Center.

Oyarzo-vera, C., Chouw, N. (2008). ”Comparison of Record scaling method proposed by standards currently applied in different countries”. The 14th World Conference on Earthquake Engineering, Beijing, China.

PEER (2010).”Guidelines for Performance-Based Seismic Design of Tall Buildings.” Report No. 2010/05, College of Engineering University of California, Berkeley,USA.

Poon, D. (2013). “Shanghi Sky.” Modern Steel Constructrion , N34a/b at NASCC ,St Luis, Missouri, USA.

Razvani, F.H., Mohammadi M., Alam S. (2012). “Seismic Progressive Collapse Analysis of Concentrically Braces Frames Through Increamental Dynamic Analysis.” The 15th World Conference on Earthquake Engineering, Lisbon, Portugal.

Remennikov, A.M., Walpole, W.R. (1997), ”Modeling the Inelastic Cyclic Behaviour of a Bracing member of Work-Hardening Material.” International Journal of Solids and Structures, 34 (27),.PP 491-515.

Rutenburg, A., Tal, D. (1987). “Lateral load response of belted tall building structures.” Engineering Structure, 9,53-67.

Sabelli, S., Roeder, C., Hajjar J. (2013).”Seismic design od steel special concentrically braced frame systems.” NEHRP seismic design technical brief No.8, NIST GCR 13-917-24.

Salmanpour, A.H., Arbabi (2008). “Seismic of Concentrically Braced Steel Frames.” The 14th World Conference on Earthquake Engineering, Beijing, China.

Santagati, S. Bolognini, D. Nascimbene, R. (2012). “Strain Life Analysis at low cycle Fatigue on Concentrically Braced Steel Structure with RHS Shape Braces”. Journal of Earthquake Engineering ,16(S1):107-137.

Smith, B., and Coull, A. (1991). “Tall building Structures: Analysis and Design” (1 ed.). New York: John Wiley & Sons Inc.

Stafford Smith B., Salim, I. (1981), ”Parameter Study of Outrigger-Braced Tall Structures.” Journal of the Structural Division, ASCE 107:2001-2013.

Standards New Zealand. (2004a). NZS 1170.5:2004 - Structural design actions. Earthquake actions.,Wellington, New Zealand.

Standards New Zealand. (2004b). NZS 1170.5:2004 - Structural design actions. Earthquake actions. Commentary, Wellington, New Zealand.

Taranath, B. (1974). ”Optimum belt truss location for high rise structures.” Engineering Journal, 18-21.

Taranath, B. (2012).”Structural Analysis and Design of Tall Buildings.” Steel and Composite Construction. Tylor and Francis , CRC Press, New York, N.Y., USA.

Terzic, V. (2013). “Modeling SCB Frames Using Beam-Column Elemnst.” NEES UC Berkeley, USA.

Tirca, L., Chen, L., (2014). “Numerical Simulation of Inelastic Cyclis Response of HSS braces Upon Fracture.” Advanced Steel Construction Journal, Vol 10, No 4, pp 442-462.

Tirca, L., Chen, L., Tremblay, R. (2015). “Assessing Collapse of CBF Buildings Subjected to Crustal and Subduction Earthquakes.” Jornal of Constructional Steel Research, pp 47-61.

Tirca, L., Serban O., Lin, L.,Wang, M., Lin, N. (2015). “Improving the Sesmic Resilience of Existing Braced –Frame Office Buildings.” American Society of Civil Engineers.

Tremblay, R, St-onge, E., Roger, C., Morrison, T., Legeron, F., Dejardins, E., Tirca, L., Gray, M., Christopoulos, C., Packer, J. (2011). “Overview of Ductile Seismic Brace Fuse Systems in Canada.” Eurostee, Budapest, Hungary.

Tremblay, R. (2002). “Inelastic Seismic Response of Steel Bracing Members.” Journal of Constrcutional Steel Research , pp 665-701.

Tremblay, R. Haddad, M., Martinez, G., Richard, J., Moffat, K. (2008). “Inelastic cyclic of large size steel bracing members ,” The 14th World Conference on Earthquake Engineering, Beijing, China.

Tsai, K.C., Lin, C.H., Hsiao, P.C., Lin, M.L., Weng, Y.T., Lin, K.C., Lin, J.L. (2008).”Collaborative Hybrid Experiments on Large Scale Frame Structures at NCREE”. The 14th World Conference on Earthquake Engineering, China.

Uriz, P. and Mahin, S. (2008). “Toward Earthquake Resistant Design of Concentrically Braced Steel Frame Structures”, PEER Report 2008/08.

Uriz, P., (2005). “Towards Earthquake Resistant Design of Concentrically Braced Steel Buildings”, Ph.D. Dissertation, PEER Report 2008/08. Pacific Earthquake Engineering Research Center University of California, Berkeley, CA.

Vamvatsiko, D., Fragiadakis, M. (2008). “Sesmic Performance Uncertainty of a 9-Storey Steel Frame with Non-Deterministic Beam-Hinge Properties.” The 14th World Conference on Earthquake Engineering, Beijing, China.

Vamvatsikos, D. (2002).” Seismic performance capacity and reliability of structures as seen through incremental dynamic analysis”. PhD thesis

Vamvatsikos, D., Cornell, A. (2002). “Increamental Dymanic analysis. Earthquake Engineering and Structural Dynamics.” 31: 491-514.

Vamvatsikos, D., Cornell, A. (2004). ”The Incremental Dynamic Analysis and its application to performance –based earthquake engineeering.” 12th European conference on Earthquake Engineering , Paper reference 479.

Vanmarcke, E.H., Cornell, C.A., Gasparini, D.A., Hou, S. (1990), ”SIMQKE-I: Simulation of Earhquake Ground Motions.” Department of Civil Engineering, Massachusetts Institute of Technology, Cambridge, MA.

Wen, Y.K., Ellingwood, B., and Bracci, J. (2004). “Vulnerability function framework for consequence-based engineering.” MAE Center Project DS-4 Report.

Ziemian, R. (2010), “Guid to Stability Design Criteria for Metal Structures”, J.Wiley & Sons.

Appendix A –Wind Load calculation

Wind laod on 12 storey building

The wind load is calculated according to the current NBCC provisions.

Building height, H = 44.8 m < 60 m –Static procedure can be followed.

Building length is L= 67.5 m and the building width is w =30.0 m.

Height/ width = 44.8 /30.0 =1.49 < 4 Static procedure can be followed.

w/H=30m/44.8m=0.67.

To find the natural frequency, any Finite Element software can be used, as well as the Rayleigh's method expressed by the equation given in NBCC 2010 commentary (I) as follows:

$$f_n = \frac{1}{2\pi}\sqrt{\frac{\sum_{i=1}^{N} F_i \frac{x_i}{x_N}}{x_N \sum_{1}^{N} M_i \left(\frac{x_i}{x_N}\right)\left(\frac{x_i}{x_N}\right)}} \qquad \text{(A1)}$$

where N is the number of vertical levels, each level or floor has an associated wind force, F_i, which may be computed using the Static Procedure. In addition, each floor has an associated mass, M_i, and the horizontal deflections of each floor, x_i is caused by F_i. The lateral force F_i is computed using a static analysis method. The deflection of the top level is x_N.

The first step is to evaluate the wind force distribution along the building height and the base shear using the static procedure given in NBCC. The calculation in N-S direction (perpendicular to longer facade) is showed in Table 1A, where $C_{e\_windward}$ is computed as $0.7(h/12)^{0.3}$ where h is the reference height. Because in the N-S direction the ratio H/D is >1.0 (e.g. 44.8/30 = 1.47) it results $C_{p\_windward} = 0.8$ and $C_{p\_leeward} = 0.5$. The gust factor C_g is 2.0.

The evaluation of natural frequency is given in Table 2A. An ETABS model was built and the applied lateral loads was taken from wind static procedure to find out the lateral floor displacement x_i which was used in Table 2A.

By applying Eq. (A1) the natural frequency is $f_n = \frac{1}{2\pi}\sqrt{\frac{2462}{136x2.82}} = 0.40$Hz < 1.0 Hz. Thus, the dynamic procedure should be followed for the 12-storey building located in rough terrain (exposure B)in Victoria, BC, Canada.

For buildings in rough terrain, the exposure factor C_e is calculated from the following equation and it results 0.94 for h = 44.8 m.

$$C_e = 0.5(\frac{h}{12.7})^{0.5} \rightarrow C_e = 0.5(\frac{44.8}{12.7})^{0.5} = 0.94 \qquad \text{where } 0.5 \leq C_e \leq 2.5$$

The gust factor C_g is calculated as:

$$C_g = 1 + g_p(\sigma/\mu)$$

(A2)

where g_p is the peak factor computed from Eq. (A3) and σ/μ is computed from Eq. (A4).

$$g_p = (2\ln(\nu T))^{0.5} + 0.577/(2\ln(\nu T))^{0.5}$$

(A3)

$$\sigma/\mu = \sqrt{\frac{K}{C_{eH}}(B + \frac{sF}{\beta})} \qquad \text{(A4)}$$

Herein, ν is the average fluctuation rate calculated as:

$$\nu = f_{nD}[(sF/(sF + \beta B)]^{0.5} \qquad \text{(A5)}$$

where B is the background turbulence factor computed as a function of w/H determined from Fig. I-18, β is the damping ratio taken as 0.01 for steel structures and *s* is the size reduction factor

$$s = \frac{\pi}{3}\left[\frac{1}{1+\frac{8f_nH}{3V_H}}\right]\left[\frac{1}{1+\frac{10f_nW}{V_H}}\right] \qquad \text{(A6)}$$

calculated as:

In addition, F is the gust energy ratio calculated as: $F = x_0^2/(1+x_0^2)^{4/3}$ where $x_0 = (1220f_n/V_H)$. In Eq. (A3), T = 3600 s and in Eq. (A4), for rough terrain K= 0.1.

In Eq. (A5), f_{nD} is the natural frequency of vibration of the building in the along-wind direction, in Hz. In Eq. (A6), f_n is the natural frequency of the building in Hz, V_H is the mean wind speed at the top of the structure in m/s, calculated as $\bar{V}(C_{eH})^{0.5}$, where $\bar{V}$ is the reference wind speed at a height of 10 m, in m/s, calculated as $(2I_w q C_{eH}/\rho)^{0.5}$; I_w is the importance factor, C_{eH} is the exposure factor at the top of the building with the height, H, q is the velocity pressure, in Pa, and ρ is the air density (ρ = 1.2929 kg/m^3).

For the 12-storey building, C_{eH} = 0.94. The reference speed at the height of 10 m is $\bar{V}=39.2\sqrt{I_w q} = 39.2\sqrt{1x0.63}$= 31.11m/s

$V_H = \bar{V}\sqrt{C_{eH}}$ = 31.11 x √0.94 = 30.15m/s

w/H=67.5/44.8=1.51

From Figure I-18 from NBCC Commentary, considering the height H and ratio w/H, the background turbulence factor is B = 0.68.

To calculate F, the value of x_0 is $x_0 = (1220f_n/V_H)$ = (1220x0.4/30.15) = 16.186 and $F = x_0^2/(1+x_0^2)^{4/3} = 16.186^2/(1+16.186^2)^{4/3}$ = 0.994

From Eq. (A6) it results s = 0.041 and $\nu = f_{nD}[(sF/(sF + \beta B)]^{0.5}$ = 0.4[(0.041x0.994/(0.041x0.994 +0.01x0.68)]$^{0.5}$ = 0.37

From Eq. (A3):

$g_p = (2\ln(\nu T))^{0.5} + 0.577/(2\ln(\nu T))^{0.5}$ = 8.68

$$\sigma/\mu = \sqrt{\frac{K}{C_{eH}}(B + \frac{sF}{\beta})} = \sqrt{\frac{0.1}{0.94}(0.68 + \frac{0.041x0.181}{0.01})}= 0.152$$

Thus, $C_g = 1 + g_p(\sigma/\mu)$ = 1 + 8.68*0.152 = 2.32

The wind forces resulted from dynamic procedure are provided in Table 3A.

From calculation it resulted that the base shear from seismic design is bigger than the base shear resultant from wind load per dynamic procedure showed in Table 3A.

Wind load calculation on 16-storey building

A similar design procedure as above is used.

Building height, H = 59.6m < 60 m. Thus, the Static procedure can be followed.

Building length, L= 67.5 m

Building width, w = 30.0 m

Height /width=59.6/30.0 =1.99 < 4. Thus, the Static procedure can be followed. Because this ratio is > 1.0, in the N-S direction, $C_{p\_windward}$ = 0.8 and $C_{p\_leeward}$ = 0.5. The building is located on rough terrain. Wind load from the static procedure is given in Table 4A.

To calculate the natural frequency, Eq. (1A) is used and the natural frequency calculation is shown in Table 5A. An ETABS model was built and the applied lateral loads are taken from wind static procedure to find out the lateral floor displacement x_i which was used in Table 5A.

From Eq. (A1) it results $f_n = \frac{1}{2\pi}\sqrt{\frac{3466}{246x3.55}}$ =0.32Hz < 1.0Hz, therefore, the dynamic procedure should be followed.

The building location is at Victoria, BC, Canada, and then the exposure is exposure B.

$C_e = 0.5(\frac{h}{12.7})^{0.5} \rightarrow C_e = 0.5(\frac{59.6}{12.7})^{0.5} = 1.083$ $\qquad 0.5 \leq C_e \leq 2.5$

The same equations as above are used. The reference speed at the height of 10 m is $\bar{V}$=39.2$\sqrt{I_w q} = 39.2\sqrt{1x0.63}$= 31.11m/s and $V_H = \bar{V}\sqrt{C_{eH=}}$31.11x√1.083=32.38 m/s

In N-S direction, the ratio w/H is 67.5/59.6 =1.13. From Figure I-18 and for height H = 59.6 m and w/H, the background turbulence factor is B = 0.71.

From Eq. (A4) it results:

$$\sigma/\mu = \sqrt{\frac{K}{C_{eH}}(B + \frac{sF}{\beta})} = \sqrt{\frac{0.1}{1.083}(0.71 + \frac{0.053x0.181}{0.01})} = 0.392$$

From equation 15 in NBCC 2010 commentary I:

$v = f_n\sqrt{\frac{sF}{sF+\beta B}} = 0.32x\sqrt{\frac{0.053x0.188}{0.053x0.188+0.015x0.71}}$= 0.222 m/s

From figure I-21 the peak factor is g_p= 3.81

From Eq. (A2) it results: $C_g = 1 + g_p(\sigma/\mu)$=1+3.81 x (0.392) = 2.495

The wind forces resulted from dynamic procedure are provided in Table 6A.

The design of the braces cross section in the 16-storey building used the larger shear between the wind and the seismic forces. Comparing the shear forces at each floor of the 16-storey building it resulted that in the N-S direction, the wind loads given in Table 6A controls the design of the braces in the lower floors while the seismic force controls the design of the braces in the upper floors.

Level	Wind area (m)	Elevation (m)	$C_{e\_winward}$	$C_{e\_leeward}$	$C_{p\ winward}$	$C_{p\_leeeward}$	P (kPa)	1.4W (kN)	Shear force (kN)	Shear per 1 MD-CBF (kN)	Force in brace (kN)
12	124.875	44.8	1.039	0.844	0.8	0.5	1.579	276	276	138	77
11	249.75	41.1	1.013	0.844	0.8	0.5	1.553	543	819	410	228
10	249.75	37.4	0.984	0.844	0.8	0.5	1.524	533	1352	676	377
9	249.75	33.7	0.954	0.844	0.8	0.5	1.494	522	1874	937	522
8	249.75	30	0.921	0.844	0.8	0.5	1.461	511	2385	1192	665
7	249.75	26.3	0.886	0.844	0.8	0.5	1.425	498	2883	1442	804
6	249.75	22.6	0.846	0.844	0.8	0.5	1.385	484	3367	1684	939
5	249.75	18.9	0.802	0.844	0.8	0.5	1.340	469	3836	1918	1069
4	249.75	15.2	0.751	0.844	0.8	0.5	1.289	451	4287	2143	1195
3	249.75	11.5	0.700	0.844	0.8	0.5	1.237	433	4719	2360	1316
2	249.75	7.8	0.700	0.844	0.8	0.5	1.237	433	5152	2576	1436
1	263.25	4.1	0.700	0.844	0.8	0.5	1.237	456	5608	2804	1598

Table 1A. Wind load distribution (N-S direction) using static procedure for the 12-storey building

Level	M_i	Mass/ floor	x_i (mm)	x_i/x_N	$(x_i/x_n)^2$	$F_i (x_i/x_N)$ (kN)	$M_i (x_i/x_N)^2$
12	0.467	473	136	1	1.00	197.23	0.47
11	0.523	529	132	0.967	0.94	375.01	0.49
10	0.525	532	124	0.911	0.83	346.88	0.44
9	0.526	533	115	0.845	0.71	315.34	0.38
8	0.528	534	105	0.768	0.59	280.23	0.31
7	0.529	536	92	0.679	0.46	241.74	0.24
6	0.531	538	81	0.596	0.35	206.03	0.19
5	0.534	540	69	0.504	0.25	168.85	0.14
4	0.535	542	56	0.411	0.17	132.24	0.09
3	0.538	544	42	0.311	0.10	96.08	0.05
2	0.542	549	28	0.208	0.04	64.31	0.02
1	0.550	557	16	0.117	0.01	38.24	0.01
					Σ	2462	2.82

Table 02A. Lowest natural frequency parameters computed for the 12-storey building

Level	Wind area (m)	Elevation (m)	$C_{e\_winward}$	$C_{e\_leeward}$	$C_{p\ winward}$	$C_{p\_leeeward}$	P (kPa)	1.4W (kN)	Shear force (kN)	Shear per 1 MD-CBF (kN)	Force in brace (kN)
12	124.875	44.8	0.939	0.664	0.8	0.5	1.582	277	277	138	77
11	249.75	41.1	0.899	0.664	0.8	0.5	1.536	537	814	407	227
10	249.75	37.4	0.858	0.664	0.8	0.5	1.487	520	1334	667	372
9	249.75	33.7	0.814	0.664	0.8	0.5	1.436	502	1836	918	512
8	249.75	30	0.768	0.664	0.8	0.5	1.383	483	2319	1160	647
7	249.75	26.3	0.720	0.664	0.8	0.5	1.325	463	2783	1391	776
6	249.75	22.6	0.667	0.664	0.8	0.5	1.264	442	3225	1612	899
5	249.75	18.9	0.610	0.664	0.8	0.5	1.197	419	3643	1822	1016
4	249.75	15.2	0.547	0.664	0.8	0.5	1.124	393	4036	2018	1125
3	249.75	11.5	0.500	0.664	0.8	0.5	1.069	374	4410	2205	1229
2	249.75	7.8	0.500	0.664	0.8	0.5	1.069	374	4784	2392	1334
1	263.25	4.1	0.500	0.664	0.8	0.5	1.069	394	5178	2589	1475

Table 3A. Wind load distribution (N-S direction) using dynamic procedure for the 12-storey building

Level	Wind area (m)	Elevation (m)	$C_{e\_winward}$	$C_{e\_leeward}$	$C_{p\ winward}$	$C_{p\_leeward}$	P (kPa)	1.4W (kN)	Shear force (kN)	Shear per 1 MD-CBF (kN)	Force in brace (kN)
16	124.875	59.6	1.132	0.920	0.8	0.5	1.721	301	301	150	84
15	249.75	55.9	1.111	0.920	0.8	0.5	1.699	594	895	447	249
14	249.75	52.2	1.088	0.920	0.8	0.5	1.676	586	1481	740	413
13	249.75	48.5	1.064	0.920	0.8	0.5	1.652	578	2059	1029	574
12	249.75	44.8	1.039	0.920	0.8	0.5	1.627	569	2627	1314	732
11	249.75	41.1	1.013	0.920	0.8	0.5	1.600	560	3187	1593	888
10	249.75	37.4	0.984	0.920	0.8	0.5	1.572	550	3736	1868	1042
9	249.75	33.7	0.954	0.920	0.8	0.5	1.541	539	4275	2138	1192
8	249.75	30.0	0.921	0.920	0.8	0.5	1.508	527	4803	2401	1339
7	249.75	26.3	0.886	0.920	0.8	0.5	1.472	515	5317	2659	1482
6	249.75	22.6	0.846	0.920	0.8	0.5	1.433	501	5818	2909	1622
5	249.75	18.9	0.802	0.920	0.8	0.5	1.388	485	6304	3152	1757
4	249.75	15.2	0.751	0.920	0.8	0.5	1.337	467	6771	3386	1888
3	249.75	11.5	0.700	0.920	0.8	0.5	1.285	449	7220	3610	2013
2	249.75	7.8	0.700	0.920	0.8	0.5	1.285	449	7670	3835	2138
1	263.25	4.1	0.700	0.920	0.8	0.5	1.285	474	8143	4072	2270

Table 4A. Wind load distribution (N-S direction) using static procedure for the 16-storey building

Level	M_i	Mass/ floor	x_i (mm)	x_i/x_n	$(x_i/x_n)^2$	$F_i (x_i/x_n)$ (kN)	$M_i (x_i/x_n)^2$
16	0.467	473	246	1	1	215	0.467
15	0.524	531	240	0.973	0.947	413	0.496
14	0.525	532	229	0.930	0.865	389	0.455
13	0.526	533	218	0.884	0.781	365	0.411
12	0.528	534	204	0.827	0.684	336	0.361
11	0.529	536	189	0.768	0.589	307	0.312
10	0.532	539	172	0.698	0.487	274	0.259
9	0.535	541	157	0.637	0.406	245	0.217
8	0.536	543	140	0.568	0.323	214	0.173
7	0.539	545	124	0.503	0.253	185	0.137
6	0.541	548	106	0.432	0.187	155	0.101
5	0.543	550	90	0.364	0.133	126	0.072
4	0.546	553	71	0.289	0.083	96	0.046
3	0.549	556	54	0.219	0.048	70	0.026
2	0.552	559	36	0.147	0.022	47	0.012
1	0.558	565	21	0.084	0.007	29	0.004
						3466	3.55

Table 05A. Lowest natural frequency parameters computed for the 16-storey building

Level	Wind area (m)	Elevation (m)	$C_{e\_winward}$	$C_{e\_leeward}$	$C_{p\ winward}$	$C_{p\_leeeward}$	P (kPa)	1.4W (kN)	Shear force (kN)	Shear per 1 MD-CBF (kN)	Force in brace (kN)
16	124.875	59.6	1.083	0.766	0.8	0.5	1.853	324	324	162	90
15	249.75	55.9	1.049	0.766	0.8	0.5	1.812	634	957	479	267
14	249.75	52.2	1.014	0.766	0.8	0.5	1.770	619	1576	788	439
13	249.75	48.5	0.977	0.766	0.8	0.5	1.727	604	2180	1090	608
12	249.75	44.8	0.939	0.766	0.8	0.5	1.682	588	2768	1384	772
11	249.75	41.1	0.899	0.766	0.8	0.5	1.635	572	3340	1670	931
10	249.75	37.4	0.858	0.766	0.8	0.5	1.586	554	3894	1947	1086
9	249.75	33.7	0.814	0.766	0.8	0.5	1.534	536	4431	2215	1235
8	249.75	30.0	0.768	0.766	0.8	0.5	1.479	517	4948	2474	1379
7	249.75	26.3	0.720	0.766	0.8	0.5	1.421	497	5445	2722	1518
6	249.75	22.6	0.667	0.766	0.8	0.5	1.359	475	5920	2960	1650
5	249.75	18.9	0.610	0.766	0.8	0.5	1.291	452	6372	3186	1776
4	249.75	15.2	0.547	0.766	0.8	0.5	1.217	425	6797	3398	1895
3	249.75	11.5	0.500	0.766	0.8	0.5	1.161	406	7203	3601	2008
2	249.75	7.8	0.500	0.766	0.8	0.5	1.161	406	7609	3804	2121
1	263.25	4.1	0.500	0.766	0.8	0.5	1.161	428	8037	4018	2240

Table 6A. Wind load distribution (N-S direction) using dynamic procedure for the 16-storey building

Appendix B – Ground motion details

Below is the acceleration and velocity of crustal ground motions NG for Northrige and LP for loma preita earthquakes.

Ground motion	Acceleration	Velocity
C1 NR(963-90)	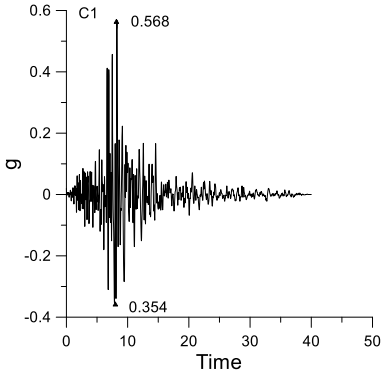	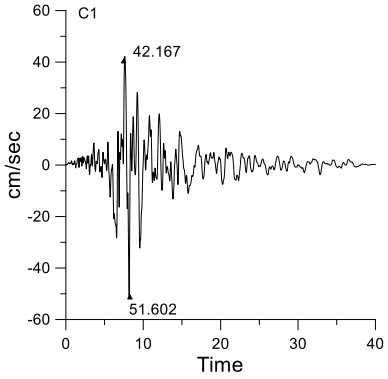
C2 NR(1006-90)	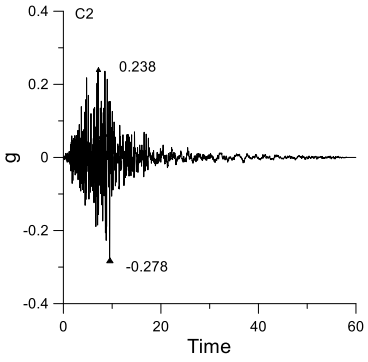	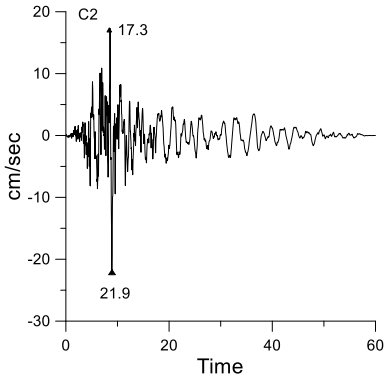
C3 NR(1039-180)	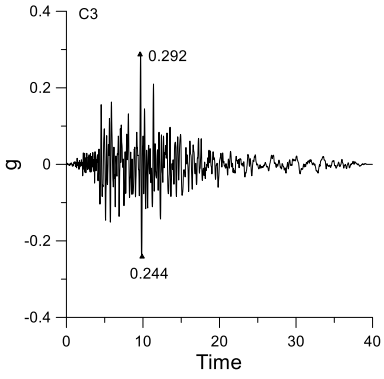	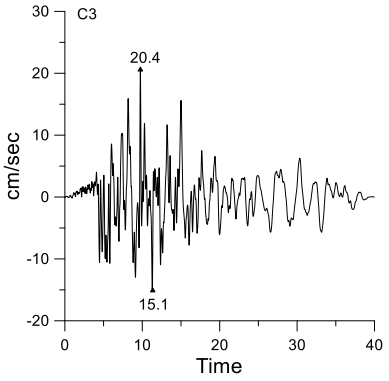

C4
(767-0)

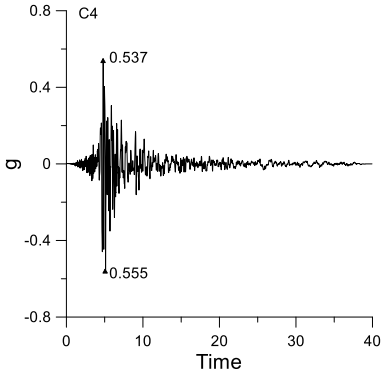

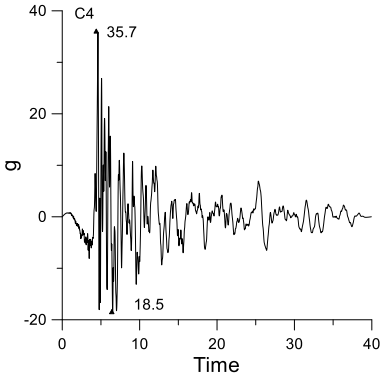

C5
LP(787-360)

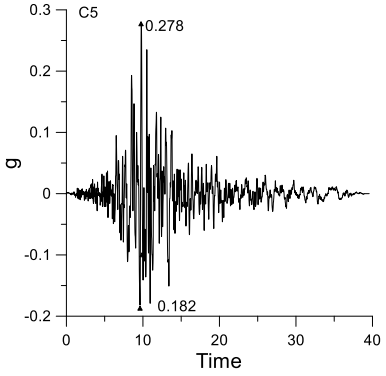

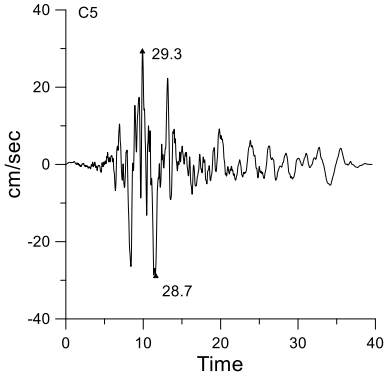

C6
LP(736-227)

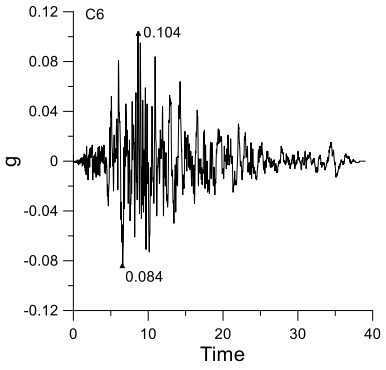

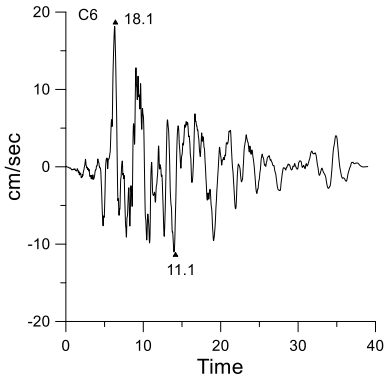

C7
LP(739-250)

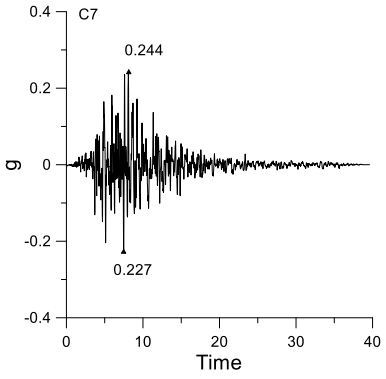

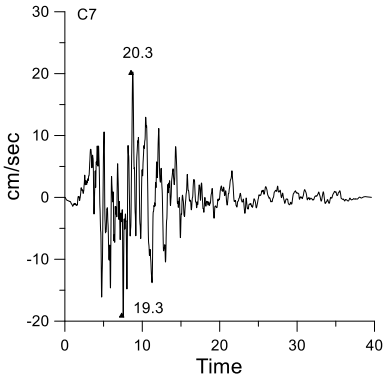

Below is the acceleration and velocity of subduction ground motions all to Tohoku earthquake.

Ground motion	Acceleration	Velocity
S1 (MGY001EW)	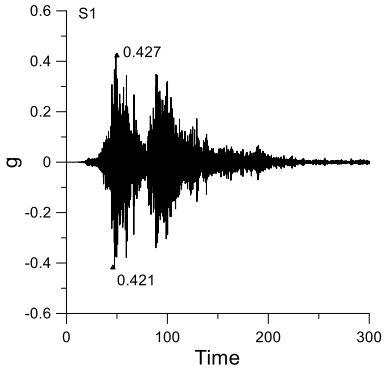	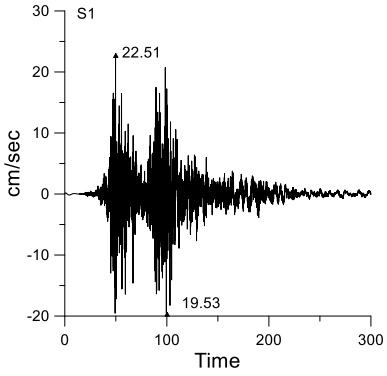
S2 (MGY004EW)	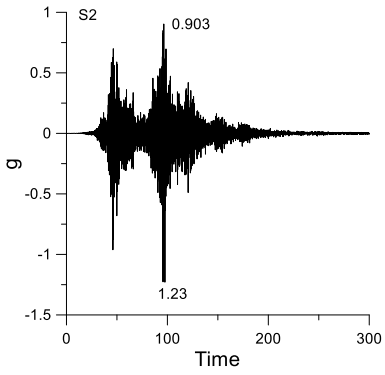	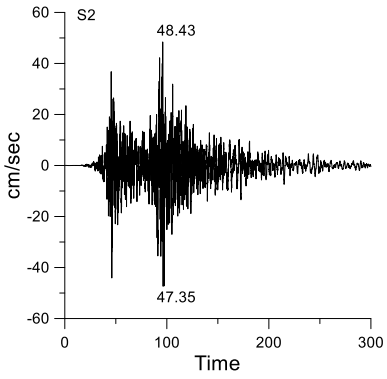
S3 (FKS005EW)	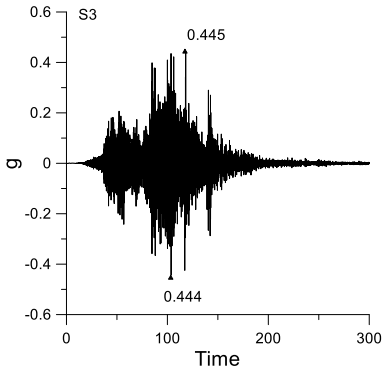	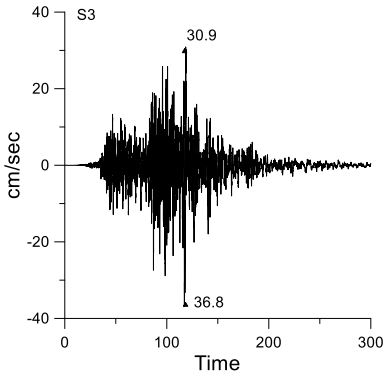

S4
(FKS010EW)

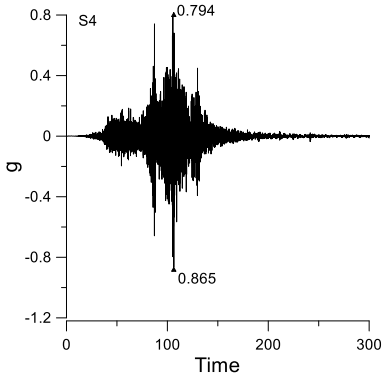

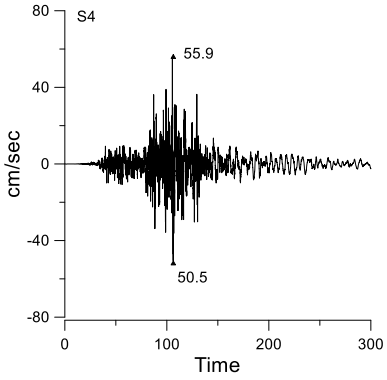

S5
(FKS009EW)

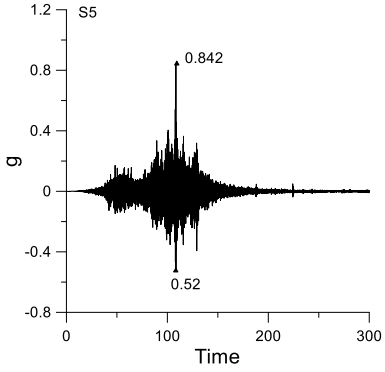

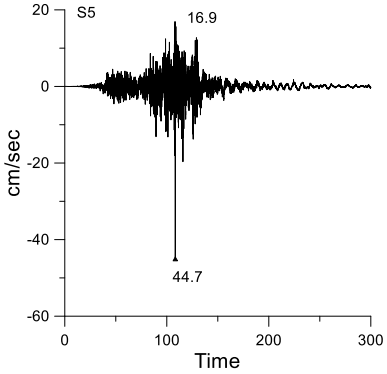

S6
(IBR004EW)

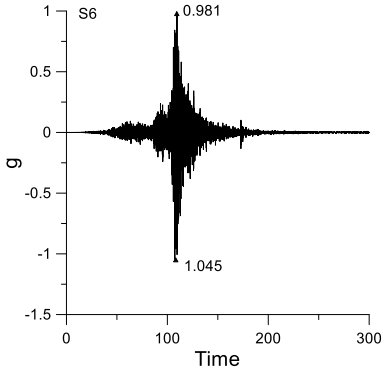

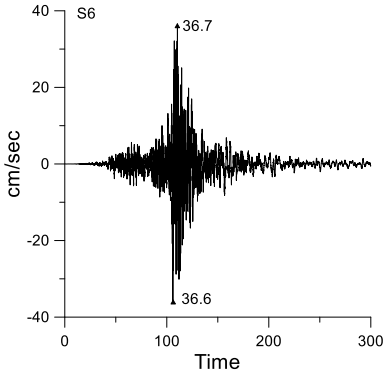

S7
(IBR006EW)